A comprehensive analysis of PP1c leads to the identification and characterization of a novel family of regulators for the Mypt1/PP1β phosphatase.

Virja Mehta

A thesis submitted to the Faculty of Graduate and Postdoctoral Studies in partial fulfillment of the requirements for the PhD degree in Cellular and Molecular Medicine

Department of Cellular and Molecular Medicine
Faculty of Medicine
University of Ottawa

TABLE OF CONTENTS

LIST OF TABLES

CHAPTER 1

CHAPTER 4

CHAPTER 5

APPENDIX I and II

LIST OF FIGURES

CHAPTER 1

CHAPTER 3

CHAPTER 4

CHAPTER 5

APPENDIX II

LIST OF ABBREVIATIONS/ LEGEND

Abbreviation	Meaning
AD	Alzeimer's Disease
ANK	Ankyrin
AP	Affinity Purification
AP/MS	Affinity-Purification/Mass Spectrometry
ASPP1	Apoptosis-Stimulating Of P53 Protein 1
ASPP2	Apoptosis-Stimulating Of P53 Protein 2
ATCC	American Type Culture Collection
ATP	Adenosine Triphosphate
BAC	Bacterial Artificial Chromosome
BiFC	Bimolecular Fluorescence Complementation
BioID	Biotin Identification
BirA	Biotin Ligase
C-term	C-Terminus
Ca^{2+}	Calcium Ion
CC	Coiled-Coil
CCD	Coiled Coil Domain
CDC42	Cell Division Cycle 42
cDNA	Complementary DNA
CH	Calponin Homology
CHD	Calponin Homology Domain
CMV	Cytomegalovirus
CNCC	Cranial Neural Crest Cells
CP	Cytoplasmic
CSK	Cytoskeletal
DMEM	Dulbecco's Modified Eagle Medium
DNA	Deoxyribonucleic Acid
DTT	Dithiothreitol
EDTA	Ethylenediaminetetraacetic Acid
eGFP	Enhanced Green Fluorescent Protein
EGTA	Ethylene Glycol-Bis(B-Aminoethyl Ether)-N,N,N',N'-Tetraacetic Acid
ER	Endoplasmic Reticulum
F2H	Fluorescence Two-Hybrid
FP	Florophore
FRAP	Fluorescence Recovery After Photobleaching
G418	Geneticin
GFP	Green Fluorescent Protein

GL	Hepatic-Type G Subunit
GM	Muscle Type G Subunit
gRNA	Guide RNA
GSK3	Glycogen Synthase Kinase 3
GST	Glutathione S-Transferase
H:L	Heavy:Light
HDAC6	Histone Deacetylase 6
HEK293T	Human Embryonic Kidney Cells Expressing SV40 Large T Antigen
HeLa	Human cervical cancer cell line derived from Henrietta Lacks
HEPES	4-(2-Hydroxyethyl)-1-Piperazineethanesulfonic acid
His	Histidine
hPP1	Hyperpigmentation Progressive 1
iASPP	Inhibitor of Apoptosis-Stimulating Protein of p53
ILK	Integrin-Linked Kinase
Inh2	Inhibitor 2
Inh3	Inhibitor 3
IP	Immunoprecipitation
KCl	Potassium Chloride
KD	Knock-Down
KO	Knock-Out
LAT	Latrunculin
LC-MS/MS	Liquid Chromatography-Tandem Mass Spectrometry
MAP	Microtubule Associated Protein
MBS	Myosin-Binding Subunit
MCF7	Michigan Cancer Foundation 7
Mg^{2+}	Magnesium Ion
$MgCl_2$	Magnesium Chloride
MLCK	Myosin Light Chain Kinase
Mn^{2+}	Manganese Ion
MP/MLCP	Myosin Light Chain Phosphatase
mPP1	Membrane Palmitoylated Protein 1
MPS1	Mono-Polar Spindle Kinase 1
MRCKalpha	Cdc42 Binding Kinase Alpha
MS	Mass Spectrometry
MT	Microtubule
MTOC	Microtubule-Organizing Center
MyPhoNE	Myosin Phosphatase N-Terminal Element
MYPT	Myosin Phosphatase Targeting Protein
N-term	N-Terminus
NaCl	Sodium Chloride
NIPP1	Nuclear Inhibitor Of Protein Phosphatase Type 1
NM II	Non – Muscle Myosin II

No	Nucleolar
NOC	Nocodazole
NP	Nucleoplasmic/Nucleoplasm
NUC	Nuclear
ObFC	Oblique Facial Clefts
PAGE	Polyacrylamide Gel Electrophoresis
PARD3	Partitioning Defective 3 Homolog
PBS	Phosphate Buffered Saline
PCR	Polymerase Chain Reaction
PFA	Paraformaldehyde
PFD	Prefoldin
PHEM	PIPES HEPES EGTA Magnesium Sulfate
pHis	Phospho Histidine
PIPES	Piperazine-N,N′-Bis
PKA	Protein Kinase A
PLK1	Polo Like Kinase 1
PMSF	Phenylmethylsulfonyl Fluoride
PNUTS	Protein Phosphatase 1 Nuclear-Targeting Subunit
polyP	Polyphosphate
PP1	Protein Phosphatase 1
PP1c	PP1 Catalytic Subunit
PPM	Mg^{2+} or Mn^{2+} Protein Phosphatase
PPP	Phosphoprotein Phosphatase
PTP	Tyrosine Phosphatase
RE	Restriction Enzymes
RIF1	Rap1-Interacting Factor 1
RIPA	Radioimmunoprecipitation Assay
RLC	Regulatory Light Chains
RNA	Ribonucleic Acid
RNA Pol I	RNA Polymerase 1
ROI	Region Of Interest
ROK	Rho Associated Kinase
SDS	Sodium Dodecyl Sulfate
Ser	Serine
SILAC	Stable Isotope Labeling by Amino Acids In Cell Culture
siRNA	Small Interfering RNA
SOD1	Superoxide Dismutase 1
SPECC1	Sperm Antigen With Calponin Homology And Coiled-Coil Domains 1

SPECC1L	Sperm Antigen With Calponin Homology And Coiled-Coil Domains 1 Like
STLC	S-Trityl-L-Cysteine
STRING	Search Tool For The Retrieval Of Interacting Genes/Proteins
Thr	Threonine
TPRN	Taperin
Tyr	Tyrosine
U2OS	U-2 Osteosarcoma
UPR	Unfolded Protein Response
WB	Western Blot
ZIPK	Zipper-Interacting Protein Kinase

ABSTRACT

Reversible protein phosphorylation, the best studied post-translational modification, regulates most cellular processes, including signaling, migration, cell cycle progression, DNA damage repair, stress response and modulaton of the activities of metabolic enzymes. Therefore, it has emerged as a key therapeutic target in diseases in which these processes are deregulated. Unlike kinases, protein phosphatase 1 (PP1) is a promiscuous enzyme that gains its substrate specificity from a large group of “regulatory subunits” with which it associates to form a range of holoenzyme complexes targeted to specific subcellular localizations and substrates. Inhibition of a specific dephosphorylation event therefore relies on targeting the regulatory rather than the catalytic subunit. The present study uses GFP as a molecular reporter to assess the localization of PP1c and identify the underlying binding events that govern it via a combination of fluorescence imaging, cellular fractionation, affinity purification and quantitative mass spectrometry.

While there is some overlap in their targeting and intracellular roles, the three PP1 isoforms show distinct localizations based on relative preferences for particular regulatory subunits. In this study we assembled a comprehensive map of isoform- and compartment- specific phosphatase complexes in three different cultured human cell lines, using the data to extrapolate, with confidence, the distribution of each PP1 isoform between a large pool of known/predicted and novel regulatory subunits. Network analysis also highlighted key multiprotein complexes to which PP1 is targeted by these regulatory subunits, and identified a novel regulatory subunit that links phosphatase activity to regulation of protein degradation.

Our work confirmed that Mypt1, the regulatory subunit that targets PP1 activity to the myosin light chain, preferentially associates with the beta isoform of PP1c. We further demonstrated that they are in complex in both the cytoplasm and nucleus, and represent ~30% of the total PP1β holoenzyme complexes in both interaphase and mitotic cells. Further investigation of these complexes led to the discovery of Specc1 and Specc1L, which associate with Mypt1/PP1β via direct binding to Mypt1. Specc1/1L are microtubule binding proteins that can also associate with actin filaments, and we demonstrated that they mediate the distribution of Mypt1/PP1β complexes between these two cytoskeletal networks. Given that disruption of this balance has been implicated in disease states including cancer and hypertension, the Specc1/L family represents a novel therapeutic target for the regulation of Mypt1/PP1 activity.

With PP1 now emerging as a promising therapeutic target and the first PP1-targeted therapeutic drug, Sephin 1, in clinical trials, a better understanding of PP1's *in vivo* distribution between holoenzyme complexes is essential. Our work establishes an initial "snapshot" of this distribution against which changes can be assessed, as we demonstrated here by showing its re-distribution in mitotic cells. Dynamic redistributions during specific cell processes such as differentiation or in response to perturbations or disease states can be assessed in a similar fashion in future, facilitating both identification of the relevant complexes and the design of specific strategies to target them therapeutically.

ACKNOWLEDGEMENTS

I owe thanks to each and every person who has contributed to this thesis, both directly and indirectly.

I would like to express my deepest gratitude to Dr. Laura Trinkle-Mulcahy for all her help and support. Additionally I would like to thank my thesis advisory members for all their help and guidance over the years.

For Chapter 3, I would like to acknowledge the various research technicians who carried out AP/MS experiments that were not carried out by me, including Delphine Chamousset, Jennifer Law and Sarah Ooi. The technicians also cloned the majority of the interactome hits and performed some of the Western blot analyses. The c20orf27 mutagenesis and imaging experiments were carried out by a technician (Sadia Iqbal) and an undergraduate student (Vincent Nguyen), under my supervision.

For Chapter 4, I would like to thank Priyam Maini, who under my supervision carried out the cloning for Specc1. Furthermore, I would like to thank Dr. Nathalie Decan for cloning the Mypt1 fragments and Jennifer Law for helping with the Lentivirus purifications.

Lastly, I would like to thank my parents and my family for always supporting me, and providing me with unconditional love and encouragement. A special thanks to my husband Rajen for being patient and always encouraging me to do my best.

COPYRIGHTED CONTENTS

ELSEVIER LICENSE
TERMS AND CONDITIONS

Apr 25, 2017

This Agreement between University of Ottawa -- Virja Mehta ("You") and Elsevier ("Elsevier") consists of your license details and the terms and conditions provided by Elsevier and Copyright Clearance Center.

License Number	4095071347947
License date	Apr 23, 2017
Licensed Content Publisher	Elsevier
Licensed Content Publication	Trends in Endocrinology & Metabolism
Licensed Content Title	Protein Phosphorylation: A Major Switch Mechanism for Metabolic Regulation
Licensed Content Author	Sean J. Humphrey,David E. James,Matthias Mann
Licensed Content Date	December 2015
Licensed Content Volume	26
Licensed Content Issue	12
Licensed Content Pages	12
Start Page	676
End Page	687
Type of Use	reuse in a thesis/dissertation
Portion	figures/tables/illustrations
Number of figures/tables/illustrations	1
Format	both print and electronic
Are you the author of this Elsevier article?	No
Will you be translating?	No
Order reference number	
Original figure numbers	Figure 1
Title of your thesis/dissertation	A comprehensive analysis of PP1c leads to the identification and characterization of a novel family of regulators for the Mypt1/PP1β phosphatase
Expected completion date	Jul 2017
Estimated size (number of pages)	250
Elsevier VAT number	GB 494 6272 12
Requestor Location	University of Ottawa 451 Smyth Road Ottawa, ON k1h8m5 Canada Attn: Virja Mehta
Total	**0.00 CAD**

ELSEVIER LICENSE
TERMS AND CONDITIONS

Apr 25, 2017

This Agreement between University of Ottawa -- Virja Mehta ("You") and Elsevier ("Elsevier") consists of your license details and the terms and conditions provided by Elsevier and Copyright Clearance Center.

License Number	4095080093721
License date	Apr 23, 2017
Licensed Content Publisher	Elsevier
Licensed Content Publication	Translational Research
Licensed Content Title	Protein phosphatase 1 catalytic isoforms: specificity toward interacting proteins
Licensed Content Author	Luís Korrodi-Gregório,Sara L.C. Esteves,Margarida Fardilha
Licensed Content Date	November 2014
Licensed Content Volume	164
Licensed Content Issue	5
Licensed Content Pages	26
Start Page	366
End Page	391
Type of Use	reuse in a thesis/dissertation
Intended publisher of new work	other
Portion	figures/tables/illustrations
Number of figures/tables/illustrations	2
Format	both print and electronic
Are you the author of this Elsevier article?	No
Will you be translating?	No
Order reference number	
Original figure numbers	Figures 1, 2
Title of your thesis/dissertation	A comprehensive analysis of PP1c leads to the identification and characterization of a novel family of regulators for the Mypt1/PP1β phosphatase
Expected completion date	Jul 2017
Estimated size (number of pages)	250
Elsevier VAT number	GB 494 6272 12
Requestor Location	University of Ottawa 451 Smyth Road Ottawa, ON k1h8m5 Canada Attn: Virja Mehta
Total	**0.00 CAD**

ELSEVIER LICENSE
TERMS AND CONDITIONS

Apr 25, 2017

This Agreement between University of Ottawa -- Virja Mehta ("You") and Elsevier ("Elsevier") consists of your license details and the terms and conditions provided by Elsevier and Copyright Clearance Center.

License Number	4095090097369
License date	Apr 23, 2017
Licensed Content Publisher	Elsevier
Licensed Content Publication	Archives of Biochemistry and Biophysics
Licensed Content Title	The myosin phosphatase targeting protein (MYPT) family: A regulated mechanism for achieving substrate specificity of the catalytic subunit of protein phosphatase type 1δ
Licensed Content Author	Michael E. Grassie,Lori D. Moffat,Michael P. Walsh,Justin A. MacDonald
Licensed Content Date	15 June 2011
Licensed Content Volume	510
Licensed Content Issue	2
Licensed Content Pages	13
Start Page	147
End Page	159
Type of Use	reuse in a thesis/dissertation
Intended publisher of new work	other
Portion	figures/tables/illustrations
Number of figures/tables/illustrations	1
Format	both print and electronic
Are you the author of this Elsevier article?	No
Will you be translating?	No
Order reference number	
Original figure numbers	Figure 1
Title of your thesis/dissertation	A comprehensive analysis of PP1c leads to the identification and characterization of a novel family of regulators for the Mypt1/PP1β phosphatase
Expected completion date	Jul 2017
Estimated size (number of pages)	250
Elsevier VAT number	GB 494 6272 12
Requestor Location	University of Ottawa 451 Smyth Road Ottawa, ON k1h8m5 Canada Attn: Virja Mehta
Total	**0.00 USD**

ELSEVIER LICENSE
TERMS AND CONDITIONS

Apr 26, 2017

This Agreement between University of Ottawa -- Virja Mehta ("You") and Elsevier ("Elsevier") consists of your license details and the terms and conditions provided by Elsevier and Copyright Clearance Center.

License Number	4096231170296
License date	Apr 25, 2017
Licensed Content Publisher	Elsevier
Licensed Content Publication	Cellular Signalling
Licensed Content Title	Role of extracellular matrix and YAP/TAZ in cell fate determination
Licensed Content Author	Jin Hao,Yueling Zhang,Yating Wang,Rui Ye,Jingyi Qiu,Zhihe Zhao,Juan Li
Licensed Content Date	February 2014
Licensed Content Volume	26
Licensed Content Issue	2
Licensed Content Pages	6
Start Page	186
End Page	191
Type of Use	reuse in a thesis/dissertation
Intended publisher of new work	other
Portion	figures/tables/illustrations
Number of figures/tables/illustrations	1
Format	both print and electronic
Are you the author of this Elsevier article?	No
Will you be translating?	No
Order reference number	
Original figure numbers	Figure 1
Title of your thesis/dissertation	A comprehensive analysis of PP1c leads to the identification and characterization of a novel family of regulators for the Mypt1/PP1β phosphatase
Expected completion date	Jul 2017
Estimated size (number of pages)	250
Elsevier VAT number	GB 494 6272 12
Requestor Location	University of Ottawa 451 Smyth Road Ottawa, ON k1h8m5 Canada Attn: Virja Mehta
Total	**0.00 USD**

Terms and Conditions

INTRODUCTION

1. The publisher for this copyrighted material is Elsevier. By clicking "accept" in connection with completing this licensing transaction, you agree that the following terms and conditions apply to this transaction (along with the Billing and Payment terms and conditions established by Copyright Clearance Center, Inc. ("CCC"), at the time that you opened your Rightslink account and that are available at any time at http://myaccount.copyright.com).

GENERAL TERMS

2. Elsevier hereby grants you permission to reproduce the aforementioned material subject to the terms and conditions indicated.
3. Acknowledgement: If any part of the material to be used (for example, figures) has appeared in our publication with credit or acknowledgement to another source, permission must also be sought from that source. If such permission is not obtained then that material may not be included in your publication/copies. Suitable acknowledgement to the source must be made, either as a footnote or in a reference list at the end of your publication, as follows:
"Reprinted from Publication title, Vol /edition number, Author(s), Title of article / title of chapter, Pages No., Copyright (Year), with permission from Elsevier [OR APPLICABLE SOCIETY COPYRIGHT OWNER]." Also Lancet special credit - "Reprinted from The Lancet, Vol. number, Author(s), Title of article, Pages No., Copyright (Year), with permission from Elsevier."
4. Reproduction of this material is confined to the purpose and/or media for which permission is hereby given.
5. Altering/Modifying Material: Not Permitted. However figures and illustrations may be altered/adapted minimally to serve your work. Any other abbreviations, additions, deletions and/or any other alterations shall be made only with prior written authorization of Elsevier Ltd. (Please contact Elsevier at permissions@elsevier.com). No modifications can be made to any Lancet figures/tables and they must be reproduced in full.
6. If the permission fee for the requested use of our material is waived in this instance, please be advised that your future requests for Elsevier materials may attract a fee.
7. Reservation of Rights: Publisher reserves all rights not specifically granted in the combination of (i) the license details provided by you and accepted in the course of this licensing transaction, (ii) these terms and conditions and (iii) CCC's Billing and Payment terms and conditions.
8. License Contingent Upon Payment: While you may exercise the rights licensed immediately upon issuance of the license at the end of the licensing process for the transaction, provided that you have disclosed complete and accurate details of your proposed use, no license is finally effective unless and until full payment is received from you (either by publisher or by CCC) as provided in CCC's Billing and Payment terms and conditions. If full payment is not received on a timely basis, then any license preliminarily granted shall be deemed automatically revoked and shall be void as if never granted. Further, in the event that you breach any of these terms and conditions or any of CCC's Billing and Payment terms and conditions, the license is automatically revoked and shall be void as if never granted. Use of materials as described in a revoked license, as well as any use of the materials beyond the scope of an unrevoked license, may constitute copyright infringement and publisher reserves the right to take any and all action to protect its copyright in the materials.
9. Warranties: Publisher makes no representations or warranties with respect to the licensed material.
10. Indemnity: You hereby indemnify and agree to hold harmless publisher and CCC, and their respective officers, directors, employees and agents, from and against any and all claims arising out of your use of the licensed material other than as specifically authorized pursuant to this license.
11. No Transfer of License: This license is personal to you and may not be sublicensed, assigned, or transferred by you to any other person without publisher's written permission.
12. No Amendment Except in Writing: This license may not be amended except in a writing signed by both parties (or, in the case of publisher, by CCC on publisher's behalf).
13. Objection to Contrary Terms: Publisher hereby objects to any terms contained in any purchase order, acknowledgment, check endorsement or other writing prepared by you, which terms are inconsistent with these terms and conditions or CCC's Billing and Payment terms and conditions. These terms and conditions, together with CCC's Billing and Payment terms and conditions (which are incorporated herein), comprise the entire agreement between you and publisher (and CCC) concerning this licensing transaction. In the event of any conflict between your obligations established by these terms and conditions and those established by CCC's Billing and Payment terms and conditions, these terms and conditions shall control.
14. Revocation: Elsevier or Copyright Clearance Center may deny the permissions described in this License at their sole discretion, for any reason or no reason, with a full refund payable to you. Notice of such denial will be made using the contact information provided by you. Failure to receive such notice will not alter or invalidate the denial. In no event will Elsevier or Copyright Clearance Center be responsible or liable for any costs, expenses or damage incurred by you as a result of a denial of your permission request, other than a refund of the amount(s) paid by you to Elsevier and/or Copyright Clearance Center for denied permissions.

LIMITED LICENSE

The following terms and conditions apply only to specific license types:
15. **Translation**: This permission is granted for non-exclusive world **English** rights only unless your license was granted for translation rights. If you licensed translation rights you may only translate this content into the languages you requested. A professional translator must perform all translations and reproduce the content word for word preserving the integrity of the article.
16. **Posting licensed content on any Website**: The following terms and conditions apply as follows: Licensing material from an Elsevier journal: All content posted to the web site must maintain the copyright information line on the bottom of each image; A hyper-text must be included to the Homepage of the journal from which you are licensing at http://www.sciencedirect.com/science/journal/xxxxx or the Elsevier homepage for books at http://www.elsevier.com; Central Storage: This license does not include permission for a scanned version of the material to be stored in a central repository such as that provided by Heron/XanEdu.
Licensing material from an Elsevier book: A hyper-text link must be included to the Elsevier homepage at http://www.elsevier.com . All content posted to the web site must maintain the copyright information line on the bottom of each image.

Posting licensed content on Electronic reserve: In addition to the above the following clauses are applicable: The web site must be password-protected and made available only to bona fide students registered on a relevant course. This permission is granted for 1 year only. You may obtain a new license for future website posting.
17. **For journal authors:** the following clauses are applicable in addition to the above:
Preprints:
A preprint is an author's own write-up of research results and analysis, it has not been peer-reviewed, nor has it had any other value added to it by a publisher (such as formatting, copyright, technical enhancement etc.).
Authors can share their preprints anywhere at any time. Preprints should not be added to or enhanced in any way in order to appear more like, or to substitute for, the final versions of articles however authors can update their preprints on arXiv or RePEc with their Accepted Author Manuscript (see below).
If accepted for publication, we encourage authors to link from the preprint to their formal publication via its DOI. Millions of researchers have access to the formal publications on ScienceDirect, and so links will help users to find, access, cite and use the best available version. Please note that Cell Press, The Lancet and some society-owned have different preprint policies. Information on these policies is available on the journal homepage.
Accepted Author Manuscripts: An accepted author manuscript is the manuscript of an article that has been accepted for publication and which typically includes author-incorporated changes suggested during submission, peer review and editor-author communications.
Authors can share their accepted author manuscript:

- immediately
    - via their non-commercial person homepage or blog
    - by updating a preprint in arXiv or RePEc with the accepted manuscript
    - via their research institute or institutional repository for internal institutional uses or as part of an invitation-only research collaboration work-group
    - directly by providing copies to their students or to research collaborators for their personal use
    - for private scholarly sharing as part of an invitation-only work group on commercial sites with which Elsevier has an agreement
- After the embargo period
    - via non-commercial hosting platforms such as their institutional repository
    - via commercial sites with which Elsevier has an agreement

In all cases accepted manuscripts should:

- link to the formal publication via its DOI
- bear a CC-BY-NC-ND license - this is easy to do
- if aggregated with other manuscripts, for example in a repository or other site, be shared in alignment with our hosting policy not be added to or enhanced in any way to appear more like, or to substitute for, the published journal article.

Published journal article (JPA): A published journal article (PJA) is the definitive final record of published research that appears or will appear in the journal and embodies all value-adding publishing activities including peer review co-ordination, copy-editing, formatting, (if relevant) pagination and online enrichment.
Policies for sharing publishing journal articles differ for subscription and gold open access articles:
Subscription Articles: If you are an author, please share a link to your article rather than the full-text. Millions of researchers

have access to the formal publications on ScienceDirect, and so links will help your users to find, access, cite, and use the best available version.
Theses and dissertations which contain embedded PJAs as part of the formal submission can be posted publicly by the awarding institution with DOI links back to the formal publications on ScienceDirect.
If you are affiliated with a library that subscribes to ScienceDirect you have additional private sharing rights for others' research accessed under that agreement. This includes use for classroom teaching and internal training at the institution (including use in course packs and courseware programs), and inclusion of the article for grant funding purposes.
Gold Open Access Articles: May be shared according to the author-selected end-user license and should contain a CrossMark logo, the end user license, and a DOI link to the formal publication on ScienceDirect.
Please refer to Elsevier's posting policy for further information.
18. **For book authors** the following clauses are applicable in addition to the above: Authors are permitted to place a brief summary of their work online only. You are not allowed to download and post the published electronic version of your chapter, nor may you scan the printed edition to create an electronic version. **Posting to a repository:** Authors are permitted to post a summary of their chapter only in their institution's repository.
19. **Thesis/Dissertation**: If your license is for use in a thesis/dissertation your thesis may be submitted to your institution in either print or electronic form. Should your thesis be published commercially, please reapply for permission. These requirements include permission for the Library and Archives of Canada to supply single copies, on demand, of the complete thesis and include permission for Proquest/UMI to supply single copies, on demand, of the complete thesis. Should your thesis be published commercially, please reapply for permission. Theses and dissertations which contain embedded PJAs as part of the formal submission can be posted publicly by the awarding institution with DOI links back to the formal publications on ScienceDirect.

Elsevier Open Access Terms and Conditions
You can publish open access with Elsevier in hundreds of open access journals or in nearly 2000 established subscription journals that support open access publishing. Permitted third party re-use of these open access articles is defined by the author's choice of Creative Commons user license. See our open access license policy for more information.
Terms & Conditions applicable to all Open Access articles published with Elsevier:
Any reuse of the article must not represent the author as endorsing the adaptation of the article nor should the article be modified in such a way as to damage the author's honour or reputation. If any changes have been made, such changes must be clearly indicated.
The author(s) must be appropriately credited and we ask that you include the end user license and a DOI link to the formal publication on ScienceDirect.
If any part of the material to be used (for example, figures) has appeared in our publication with credit or acknowledgement to another source it is the responsibility of the user to ensure their reuse complies with the terms and conditions determined by the rights holder.
Additional Terms & Conditions applicable to each Creative Commons user license:
CC BY: The CC-BY license allows users to copy, to create extracts, abstracts and new works from the Article, to alter and revise the Article and to make commercial use of the Article (including reuse and/or resale of the Article by commercial entities), provided the user gives appropriate credit (with a link to the formal publication through the relevant DOI), provides a link to the license, indicates if changes were made and the licensor is not represented as endorsing the use made of the work. The full details of the license are available at http://creativecommons.org/licenses/by/4.0.
CC BY NC SA: The CC BY-NC-SA license allows users to copy, to create extracts, abstracts and new works from the Article, to alter and revise the Article, provided this is not done for commercial purposes, and that the user gives appropriate credit (with a link to the formal publication through the relevant DOI), provides a link to the license, indicates if changes were made and the licensor is not represented as endorsing the use made of the work. Further, any new works must be made available on the same conditions. The full details of the license are available at http://creativecommons.org/licenses/by-nc-sa/4.0.
CC BY NC ND: The CC BY-NC-ND license allows users to copy and distribute the Article, provided this is not done for commercial purposes and further does not permit distribution of the Article if it is changed or edited in any way, and provided the user gives appropriate credit (with a link to the formal publication through the relevant DOI), provides a link to the license, and that the licensor is not represented as endorsing the use made of the work. The full details of the license are available at http://creativecommons.org/licenses/by-nc-nd/4.0. Any commercial reuse of Open Access articles published with a CC BY NC SA or CC BY NC ND license requires permission from Elsevier and will be subject to a fee.
Commercial reuse includes:

- Associating advertising with the full text of the Article
- Charging fees for document delivery or access
- Article aggregation

- Systematic distribution via e-mail lists or share buttons

Posting or linking by commercial companies for use by customers of those companies.

20. **Other Conditions**:

v1.9

JOHN WILEY AND SONS LICENSE TERMS AND CONDITIONS

Apr 25, 2017

This Agreement between University of Ottawa -- Virja Mehta ("You") and John Wiley and Sons ("John Wiley and Sons") consists of your license details and the terms and conditions provided by John Wiley and Sons and Copyright Clearance Center.

License Number	4095080668559
License date	Apr 23, 2017
Licensed Content Publisher	John Wiley and Sons
Licensed Content Publication	The EMBO Journal
Licensed Content Title	Structural basis for the recognition of regulatory subunits by the catalytic subunit of protein phosphatase 1
Licensed Content Author	Marie-Pierre Egloff,Deborah F. Johnson,Greg Moorhead,Patricia T. W. Cohen,Philip Cohen,David Barford
Licensed Content Date	Apr 15, 1997
Licensed Content Pages	12
Type of Use	Dissertation/Thesis
Requestor type	University/Academic
Format	Print and electronic
Portion	Figure/table
Number of figures/tables	1
Original Wiley figure/table number(s)	Figure 2
Will you be translating?	No
Title of your thesis / dissertation	A comprehensive analysis of PP1c leads to the identification and characterization of a novel family of regulators for the Mypt1/PP1β phosphatase
Expected completion date	Jul 2017
Expected size (number of pages)	250
Requestor Location	University of Ottawa 451 Smyth Road Ottawa, ON k1h8m5 Canada Attn: Virja Mehta
Publisher Tax ID	EU826007151
Billing Type	Invoice
Billing Address	University of Ottawa 451 Smyth Road Ottawa, ON k1h8m5 Canada Attn: Virja Mehta
Total	**0.00 USD**

JOHN WILEY AND SONS LICENSE TERMS AND CONDITIONS

Apr 25, 2017

This Agreement between University of Ottawa -- Virja Mehta ("You") and John Wiley and Sons ("John Wiley and Sons") consists of your license details and the terms and conditions provided by John Wiley and Sons and Copyright Clearance Center.

License Number	4095080872971
License date	Apr 23, 2017
Licensed Content Publisher	John Wiley and Sons
Licensed Content Publication	BioEssays
Licensed Content Title	Regulator-driven functional diversification of protein phosphatase-1 in eukaryotic evolution
Licensed Content Author	Hugo Ceulemans,Willy Stalmans,Mathieu Bollen
Licensed Content Date	Mar 29, 2002
Licensed Content Pages	11
Type of Use	Dissertation/Thesis
Requestor type	University/Academic
Format	Print and electronic
Portion	Figure/table
Number of figures/tables	1
Original Wiley figure/table number(s)	Figure 2
Will you be translating?	No
Title of your thesis / dissertation	A comprehensive analysis of PP1c leads to the identification and characterization of a novel family of regulators for the Mypt1/PP1β phosphatase
Expected completion date	Jul 2017
Expected size (number of pages)	250
Requestor Location	University of Ottawa 451 Smyth Road Ottawa, ON k1h8m5 Canada Attn: Virja Mehta
Publisher Tax ID	EU826007151
Billing Type	Invoice
Billing Address	University of Ottawa 451 Smyth Road Ottawa, ON k1h8m5 Canada Attn: Virja Mehta
Total	**0.00 USD**
Terms and Conditions	

JOHN WILEY AND SONS LICENSE TERMS AND CONDITIONS

Apr 25, 2017

This Agreement between University of Ottawa -- Virja Mehta ("You") and John Wiley and Sons ("John Wiley and Sons") consists of your license details and the terms and conditions provided by John Wiley and Sons and Copyright Clearance Center.

License Number	4095090731566
License date	Apr 23, 2017
Licensed Content Publisher	John Wiley and Sons
Licensed Content Publication	British Journal of Pharmacology
Licensed Content Title	Movers and shakers: cell cytoskeleton in cancer metastasis
Licensed Content Author	C M Fife,J A McCarroll,M Kavallaris
Licensed Content Date	Jul 2, 2014
Licensed Content Pages	17
Type of Use	Dissertation/Thesis
Requestor type	University/Academic
Format	Print and electronic
Portion	Figure/table
Number of figures/tables	1
Original Wiley figure/table number(s)	Figure 2
Will you be translating?	No
Title of your thesis / dissertation	A comprehensive analysis of PP1c leads to the identification and characterization of a novel family of regulators for the Mypt1/PP1β phosphatase
Expected completion date	Jul 2017
Expected size (number of pages)	250
Requestor Location	University of Ottawa 451 Smyth Road Ottawa, ON k1h8m5 Canada Attn: Virja Mehta
Publisher Tax ID	EU826007151
Billing Type	Invoice
Billing Address	University of Ottawa 451 Smyth Road Ottawa, ON k1h8m5 Canada Attn: Virja Mehta
Total	**0.00 USD**

- IN NO EVENT SHALL WILEY OR ITS LICENSORS BE LIABLE TO YOU OR ANY OTHER PARTY OR ANY OTHER PERSON OR ENTITY FOR ANY SPECIAL, CONSEQUENTIAL, INCIDENTAL, INDIRECT, EXEMPLARY OR PUNITIVE DAMAGES, HOWEVER CAUSED, ARISING OUT OF OR IN CONNECTION WITH THE DOWNLOADING, PROVISIONING, VIEWING OR USE OF THE MATERIALS REGARDLESS OF THE FORM OF ACTION, WHETHER FOR BREACH OF CONTRACT, BREACH OF WARRANTY, TORT, NEGLIGENCE, INFRINGEMENT OR OTHERWISE (INCLUDING, WITHOUT LIMITATION, DAMAGES BASED ON LOSS OF PROFITS, DATA, FILES, USE, BUSINESS OPPORTUNITY OR CLAIMS OF THIRD PARTIES), AND WHETHER OR NOT THE PARTY HAS BEEN ADVISED OF THE POSSIBILITY OF SUCH DAMAGES. THIS LIMITATION SHALL APPLY NOTWITHSTANDING ANY FAILURE OF ESSENTIAL PURPOSE OF ANY LIMITED REMEDY PROVIDED HEREIN.

- Should any provision of this Agreement be held by a court of competent jurisdiction to be illegal, invalid, or unenforceable, that provision shall be deemed amended to achieve as nearly as possible the same economic effect as the original provision, and the legality, validity and enforceability of the remaining provisions of this Agreement shall not be affected or impaired thereby.

- The failure of either party to enforce any term or condition of this Agreement shall not constitute a waiver of either party's right to enforce each and every term and condition of this Agreement. No breach under this agreement shall be deemed waived or excused by either party unless such waiver or consent is in writing signed by the party granting such waiver or consent. The waiver by or consent of a party to a breach of any provision of this Agreement shall not operate or be construed as a waiver of or consent to any other or subsequent breach by such other party.

- This Agreement may not be assigned (including by operation of law or otherwise) by you without WILEY's prior written consent.

- Any fee required for this permission shall be non-refundable after thirty (30) days from receipt by the CCC.

- These terms and conditions together with CCC's Billing and Payment terms and conditions (which are incorporated herein) form the entire agreement between you and WILEY concerning this licensing transaction and (in the absence of fraud) supersedes all prior agreements and representations of the parties, oral or written. This Agreement may not be amended except in writing signed by both parties. This Agreement shall be binding upon and inure to the benefit of the parties' successors, legal representatives, and authorized assigns.

- In the event of any conflict between your obligations established by these terms and conditions and those established by CCC's Billing and Payment terms and conditions, these terms and conditions shall prevail.

- WILEY expressly reserves all rights not specifically granted in the combination of (i) the license details provided by you and accepted in the course of this licensing transaction, (ii) these terms and conditions and (iii) CCC's Billing and Payment terms and conditions.

- This Agreement will be void if the Type of Use, Format, Circulation, or Requestor Type was misrepresented during the licensing process.

- This Agreement shall be governed by and construed in accordance with the laws of the State of New York, USA, without regards to such state's conflict of law rules. Any legal action, suit or proceeding arising out of or relating to these Terms and Conditions or the breach thereof shall be instituted in a court of competent jurisdiction in New York County in the State of New York in the United States of America and each party hereby consents and submits to the personal jurisdiction of such court, waives any objection to venue in such court and consents to service of process by registered or certified mail, return receipt requested, at the last known address of such party.

WILEY OPEN ACCESS TERMS AND CONDITIONS

Wiley Publishes Open Access Articles in fully Open Access Journals and in Subscription journals offering Online Open. Although most of the fully Open Access journals publish open access articles under the terms of the Creative Commons Attribution (CC BY) License only, the subscription journals and a few of the Open Access Journals offer a choice of Creative Commons Licenses. The license type is clearly identified on the article.

The Creative Commons Attribution License

The Creative Commons Attribution License (CC-BY) allows users to copy, distribute and transmit an article, adapt the article

NATURE PUBLISHING GROUP LICENSE TERMS AND CONDITIONS

Apr 25, 2017

This Agreement between University of Ottawa -- Virja Mehta ("You") and Nature Publishing Group ("Nature Publishing Group") consists of your license details and the terms and conditions provided by Nature Publishing Group and Copyright Clearance Center.

License Number	4095090513352
License date	Apr 23, 2017
Licensed Content Publisher	Nature Publishing Group
Licensed Content Publication	Nature Reviews Microbiology
Licensed Content Title	Subversion of the actin cytoskeleton during viral infection
Licensed Content Author	Matthew P. Taylor, Orkide O. Koyuncu and Lynn W. Enquist
Licensed Content Date	Apr 27, 2011
Licensed Content Volume	9
Licensed Content Issue	6
Type of Use	reuse in a dissertation / thesis
Requestor type	academic/educational
Format	print and electronic
Portion	figures/tables/illustrations
Number of figures/tables/illustrations	1
High-res required	no
Figures	Figure 3
Author of this NPG article	no
Your reference number	
Title of your thesis / dissertation	A comprehensive analysis of PP1c leads to the identification and characterization of a novel family of regulators for the Mypt1/PP1β phosphatase
Expected completion date	Jul 2017
Estimated size (number of pages)	250
Requestor Location	University of Ottawa 451 Smyth Road Ottawa, ON k1h8m5 Canada Attn: Virja Mehta
Billing Type	Invoice
Billing Address	University of Ottawa 451 Smyth Road Ottawa, ON k1h8m5 Canada

NATURE PUBLISHING GROUP LICENSE
TERMS AND CONDITIONS

Apr 25, 2017

This Agreement between University of Ottawa -- Virja Mehta ("You") and Nature Publishing Group ("Nature Publishing Group") consists of your license details and the terms and conditions provided by Nature Publishing Group and Copyright Clearance Center.

License Number	4096250792955
License date	Apr 25, 2017
Licensed Content Publisher	Nature Publishing Group
Licensed Content Publication	Nature Reviews Molecular Cell Biology
Licensed Content Title	Tracking the ends: a dynamic protein network controls the fate of microtubule tips
Licensed Content Author	Anna Akhmanova and Michel O. Steinmetz
Licensed Content Date	Apr 1, 2008
Licensed Content Volume	9
Licensed Content Issue	4
Type of Use	reuse in a dissertation / thesis
Requestor type	academic/educational
Format	print and electronic
Portion	figures/tables/illustrations
Number of figures/tables/illustrations	1
High-res required	no
Figures	Box 1
Author of this NPG article	no
Your reference number	
Title of your thesis / dissertation	A comprehensive analysis of PP1c leads to the identification and characterization of a novel family of regulators for the Mypt1/PP1β phosphatase
Expected completion date	Jul 2017
Estimated size (number of pages)	250
Requestor Location	University of Ottawa 451 Smyth Road Ottawa, ON k1h8m5 Canada Attn: Virja Mehta
Billing Type	Invoice

Billing Address	University of Ottawa 451 Smyth Road Ottawa, ON k1h8m5 Canada Attn: Virja Mehta
Total	0.00 USD

Terms and Conditions

Terms and Conditions for Permissions

Nature Publishing Group hereby grants you a non-exclusive license to reproduce this material for this purpose, and for no other use,subject to the conditions below:

1. NPG warrants that it has, to the best of its knowledge, the rights to license reuse of this material. However, you should ensure that the material you are requesting is original to Nature Publishing Group and does not carry the copyright of another entity (as credited in the published version). If the credit line on any part of the material you have requested indicates that it was reprinted or adapted by NPG with permission from another source, then you should also seek permission from that source to reuse the material.

2. Permission granted free of charge for material in print is also usually granted for any electronic version of that work, provided that the material is incidental to the work as a whole and that the electronic version is essentially equivalent to, or substitutes for, the print version.Where print permission has been granted for a fee, separate permission must be obtained for any additional, electronic re-use (unless, as in the case of a full paper, this has already been accounted for during your initial request in the calculation of a print run).NB: In all cases, web-based use of full-text articles must be authorized separately through the 'Use on a Web Site' option when requesting permission.

3. Permission granted for a first edition does not apply to second and subsequent editions and for editions in other languages (except for signatories to the STM Permissions Guidelines, or where the first edition permission was granted for free).

4. Nature Publishing Group's permission must be acknowledged next to the figure, table or abstract in print. In electronic form, this acknowledgement must be visible at the same time as the figure/table/abstract, and must be hyperlinked to the journal's homepage.

5. The credit line should read:
   Reprinted by permission from Macmillan Publishers Ltd: [JOURNAL NAME] (reference citation), copyright (year of publication)
   For AOP papers, the credit line should read:
   Reprinted by permission from Macmillan Publishers Ltd: [JOURNAL NAME], advance online publication, day month year (doi: 10.1038/sj.[JOURNAL ACRONYM].XXXXX)

   Note: For republication from the *British Journal of Cancer,* the following credit lines apply.
   Reprinted by permission from Macmillan Publishers Ltd on behalf of Cancer Research UK: [JOURNAL NAME] (reference citation), copyright (year of publication)For AOP papers, the credit line should read:
   Reprinted by permission from Macmillan Publishers Ltd on behalf of Cancer Research UK: [JOURNAL NAME], advance online publication, day month year (doi: 10.1038/sj.[JOURNAL ACRONYM].XXXXX)

6. Adaptations of single figures do not require NPG approval. However, the adaptation should be credited as follows:

Adapted by permission from Macmillan Publishers Ltd: [JOURNAL NAME] (reference citation), copyright (year of publication)

Note: For adaptation from the *British Journal of Cancer,* the following credit line applies.
Adapted by permission from Macmillan Publishers Ltd on behalf of Cancer Research UK: [JOURNAL NAME] (reference citation), copyright (year of publication)

7. Translations of 401 words up to a whole article require NPG approval. Please visit http://www.macmillanmedicalcommunications.com for more information.Translations of up to a 400 words do not require NPG approval. The translation should be credited as follows:

   Translated by permission from Macmillan Publishers Ltd: [JOURNAL NAME] (reference citation), copyright (year of publication).

   Note: For translation from the *British Journal of Cancer,* the following credit line applies.
   Translated by permission from Macmillan Publishers Ltd on behalf of Cancer Research UK: [JOURNAL NAME] (reference citation), copyright (year of publication)

We are certain that all parties will benefit from this agreement and wish you the best in the use of this material. Thank you.
Special Terms:
v1.1

Questions? customercare@copyright.com or +1-855-239-3415 (toll free in the US) or +1-978-646-2777.

CHAPTER 1: Introduction

1.1 Reversible phosphorylation

Post-translational modifications can alter a protein's function, leading to changes in its subcellular behavior and a consequent physiological response. The concept of protein phosphorylation, originally discovered by Edmond Fischer and Edwin Krebs, arose from the observation that both ATP and a "converting enzyme" is needed to convert phosphorylate b to phosphorylase a (Krebs & Fischer 1956; Krebs et al. 1958; Sutherland & Wosilait 1955). More than one third of all eukaryotic cellular proteins undergo reversible phosphorylation, the most common type of post-translational modification in eukaryotic organisms, and are termed phosphoproteins. The phosphorylation state of a protein is dependent on the external stimuli, and on the activities of the protein kinases (add the phosphate group) and phosphatases (remove the phosphate group) that act on a particular amino acid residue (Figure 1.1). The addition of the negatively charged phosphate group to the phosphoprotein can result in a conformational change, affect localization and protein binding, alter its activity, and affect the turnover rates of its targets (Humphrey et al. 2015). As a result, reversible phosphorylation is responsible for modulating a majority of molecular events within a cell, including division, differentiation, signaling and metabolism.

The majority of phosphoproteins are covalently modified on the hydroxyl-containing serine (ser), threonine (thr) and/or tyrosine (tyr) residues, forming stable phosphoester bonds. Based on over 2000 phosphoproteins identified by mass spectrometry (MS), Olsen et al. demonstrate that phosphoserine is the predominant phosphorylated amino acid, accounting for 86.4% of phospho-events, while

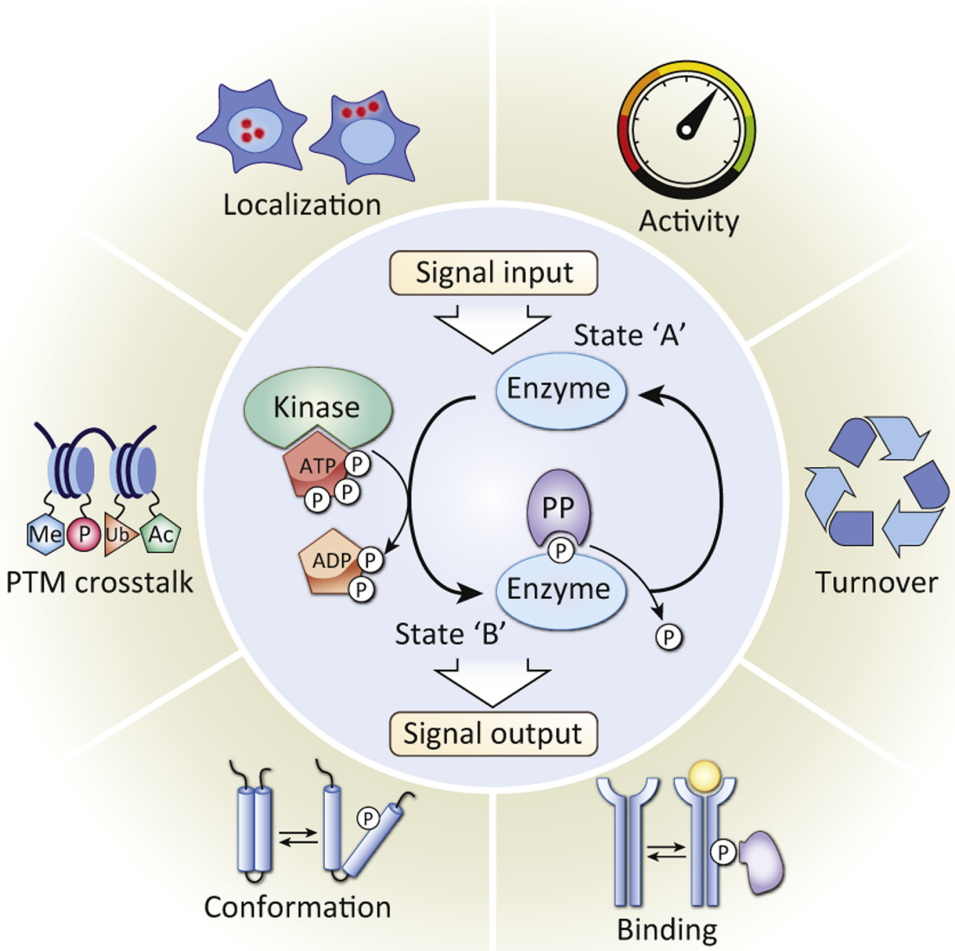

Figure 1.1. Reversible protein phosphorylation functions as a molecular switch. The phosphorylation state of a protein is dependent on the external stimuli, and on the activities of the protein kinase (adds the phosphate group) and phosphatase (removes the phosphate group) that act on the residue of the phosphoprotein. *Reproduced by permission from Elseivier: [Trends in Endocrinology & Metabolism]* (Humphrey et al. 2015)*, copyright (2015).*

phosphothreonine and phosphotyrosine account for 11.8% and 1.8%, respectively (Olsen et al. 2006). The standard biochemical and proteomic procedures used to detect amino acids that form stable phosphoester bonds fail to preserve or detect other known phosphorylated amino acids, such as phosphorylated histidine (pHis) residues. In 1962, Boyer et al. discovered an enzyme intermediate of oxidative phosphorylation that was pHis phosphorylated (Boyer et al. 1962). These phosphoproteins are covalently modified on histidine's imidazole nitrogen atoms, forming a high energy and unstable phosphoramidate bond which is easily hydrolyzed when exposed to heat and low pH (Fuhs & Hunter 2017; Attwood et al. 2007). Most studies have investigated the role of pHis in the prokaryotic two-component signal transduction system and as a reactive enzyme intermediate (Fuhs & Hunter 2017). Recently, with the availability of new reagents (Fuhs et al. 2015) and a better appreciation of pHis in the regulation of protein function, the role of pHis is now being explored. Five other amino acids in eukaryotes are also known to undergo phosphorylation. While arginine and lysine amino acid side chains also form phosphoramidates, aspartate and glutamate form acylphosphates and cysteine residues form thiophosphates (Venerando et al. 2017).

Phosphate is found in the cell as orthophosphate or free phosphate, and as long chains known as polyphosphate (polyp) (Jiménez et al. 2017). While the addition of a single phosphate group, achieved via a kinase, can alter a protein's function, studies have shown that polyP chains are covalently attached to proteins on amino acid residues such as lysine, affecting the localization and function of the phosphoprotein (Azevedo et al. 2015).

There are 428 human genes that encode protein ser/thr kinases (Manning et al. 2002), while 90 encode kinases that modify their substrates on a tyrosine residue. To counteract the tyr kinases, 107 human genes encode protein phosphatases that dephosphorylate phosphotyrosine residues (Alonso et al. 2004; Andersen et al. 2005). Interestingly, there are only 45 established or putative ser/thr phosphatases to counteract the 428 ser/thr kinases. This 10-fold fewer number of ser/thr phosphatases suggests a broader substrate specificity, determined by association with regulatory proteins or by other regulatory mechanisms set in place, such as localization or modifications. The high ratio of ser/thr kinases to phosphatases is evolutionary conserved, where a 6:1 kinase to phosphatase ratio is also observed in Drosophila (Morrison et al. 2000).

1.1.1 Classification of Protein Phosphatases

Initially, the families were divided based on whether they dephosphorylate serine, threonine or tyrosine residues alone, or whether they have dual specificity. However, following the discovery that certain ser/thr-specific enzymes are capable of dephosphorylating tyrosine, and thus most have dual-specificity, the phosphatases were instead classified based on their sequence, structure and catalytic mechanism (Moorhead et al. 2007). Table 1.1 summarizes the families identified to date. The first group comprises the ser/thr phosphatases of the phosphoprotein phosphatase (PPP) and the protein phosphatase, Mg^{2+} or Mn^{2+} dependent (PPM) families. The second and third groups consist, respectively, of the protein Tyrosine phosphatase (PTP) superfamily and the Asp-based protein phosphatase (with a DXDXT/V catalytic signature) family. Lastly, the remaining phosphatase family consists of phosphatases

FAMILY	EXAMPLES OF MEMBERS
Serine/Threonine Phosphatases[1]	
PPP Family	PP1, PP2A, calcineurin, PP4-7
PPM Family	PP2C
Phosphotyrosine Phosphatase (PTP) Super family[1]	
Class I PTPs (Classic)	Transmembrane and non-receptor PTP
Class I PTPs (DSP - Dual Specific Phosphatase)	MAPKP, PTEN, Slingshots, PRLs, Atypical DSPs, CDC14, Myotubularins
Class II PTPs	CDC25s
Class III PTPs	Low molecular weight (LMW) PTP
Asp-based catalysis[1]	
FCP/SCP Family	FCP1, SCP, FCP/SCP-like
HAD Family	Eya, cronophin
Other Amino Acid Phosphatases[2]	
pHis Phosphatases[2]	PHPT1, LHPP
pLys	LHPP

References:
1. Moorhead, G. B. G., Trinkle-Mulcahy, L. & Ulke-Lemée, A. Emerging roles of nuclear protein phosphatases. *Nat. Rev. Mol. Cell Biol.* **8,** 234–244 (2007).
2. Fuhs, S. R. & Hunter, T. pHisphorylation: the emergence of histidine phosphorylation as a reversible regulatory modification. *Curr. Opin. Cell Biol.* **45,** 8–16 (2017).

Table 1.1. The Classification of human protein phosphatases.

responsible for dephosphorylating lysine and/or histidine residues (Fuhs & Hunter 2017).

The two most abundant ser/thr phosphatases are classified as either type 1 (PP1) or type 2 (PP2), defined using biochemical assays, and then further divided based on their requirements for metal ions and substrate specificity. Most ser/thr phosphatases, including PP1 and PP2A, are regulated and achieve their substrate specificity through the association of the catalytic subunit with a range of regulatory subunits. The regulatory subunits have been shown to direct the localization of the endogenously (Brush et al. 2003) and ectopically (Trinkle-Mulcahy et al. 2001; Trinkle-Mulcahy et al. 2003; Lesage et al. 2007) expressed phosphatase, thereby emphasizing the importance of these regulators in defining the subcellular distribution of the phosphatase catalytic subunits. Other Ser/Thr phosphatases, including PP2C and Asp-based phosphatases, contain the regulatory domain within the same polypeptide chain as the catalytic subunit.

1.1.2 Protein Phosphatase 1 (PP1)

PP1 is ubiquitously expressed in all eukaryotic cells and it is estimated that PP1 accounts for 40-70% of ser/thr dephosphorylation events (Roadcap et al. 2007). The PP1 catalytic subunit (PP1c) is involved in the regulation of diverse cellular processes, and its specificity is governed by regulatory proteins (regulatory subunits) that confer the subcellular localization of the phosphatase, bringing it into proximity of its substrates. Evolutionarily, all eukaryotes have more than one PP1 gene, with the exception of *Saccharomyces cerevisiae*, which has only one (GLC7). While *Drosophila*

melanogaster have four PP1 genes, *Arabidopsis thaliana* have eight and *Caenorhabditis elegans* are predicted to have 30 (Shenolikar 1994).

In mammalian cells, PP1c is found primarily as three isoforms (α, β/δ, γ) encoded by three distinct genes (Barker et al. 1993; Barker et al. 1994; Sasaki et al. 1990), and each has the potential for alternative splicing. PP1γ has been shown to undergo tissue-specific splicing, generating the testis-enriched and sperm-specific isoform PP1γ2 (Korrodi-Gregório et al. 2014). These PP1c isoforms have amino acid sequences that are more than 89% identical, varying mostly in their N- and C-termini (Figure 1.2A), and show distinct localization patterns in the cell (Andreassen et al. 1998; Chamousset, De Wever, et al. 2010; Trinkle-Mulcahy 2006). A phylogenetic tree made based on the ClustalW alignment of amino acid sequence of all PP1c isoforms demonstrates that PP1γ is more closely related to PP1α than it is to PP1β (Korrodi-Gregório et al. 2014) (Figure 1.2B). While PP1α and PP1γ1 is more enriched in the brain and heart, PP1β is found in the brain, small intestine, lung and muscle (Korrodi-Gregório et al. 2014). Compensation of one isoform for the other is seen in knockout (KO) experiments, where one isoform may compensate for the other. However, knockout/knockdown experiments demonstrate that compensation may not occur for specific functions, as seen with the KO mice of PP1γ, where the mice are viable with no obvious physical dysfunctions, except that the males are infertile (Varmuza et al. 1999; Korrodi-Gregório et al. 2014); or with morpholino knockdown (KD) of PP1β in zebrafish, where developmental defects are observed (Korrodi-Gregório et al. 2014; Jayashankar et al. 2013). KD of PP1α in cardiomyocytes and HeLa cells shows a slight increase in cell shortening and involvement in cell proliferation, respectively. KD of PP1β in cardiomyocytes shows a

A

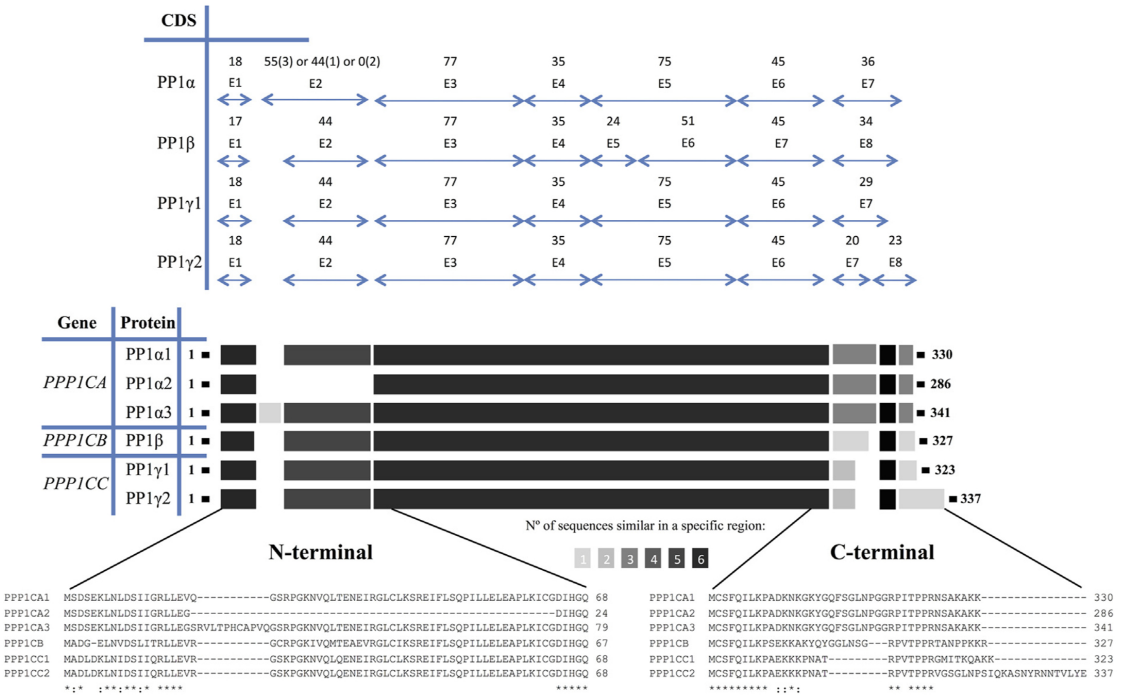

B

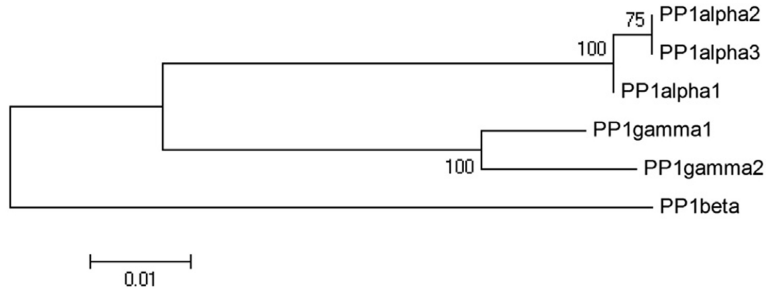

Figure 1.2. Alignment of the three human PP1 genes. A. Schematic representation of human PP1c genes, coding sequences (CDS), and proteins. The variability lies in the N- and C-terminus of the PP1c genes. **B.** Human PP1c isoforms phylogenetic tree. The phylogenetic tree, based on a ClustalW alignment, demonstrates the similarities between the PP1c isoforms based on their primary amino acid sequence. Scale bar represents estimated phylogenetic distance in substitutions per site. *Reproduced by permission from Elseivier: [Translational Research]* (Korrodi-Gregório et al. 2014)*, copyright (2014).*

significant increase in cell shortening, while knockdown in HeLa cells shows its importance during the cell cycle. KD of PP1γ in HeLa cells also leads to the formation of lamellipodia (for review, see (Korrodi-Gregório et al. 2014)).

1.1.3 Functional analysis of PP1

Although the PP1 catalytic subunits are abundant, they are not found as free monomers in eukaryotic cells (Virshup & Shenolikar 2009). This is likely due to the fact that a free subunit would be capable of dephosphorylating a large population of phosphoproteins, as shown *in vitro* (Bollen et al. 2010). Early work done in budding yeast demonstrated that GLC7 controls diverse cellular processes including glycogen metabolism, DNA damage and transcription and cell-cycle progression (Aggen et al. 2000; Virshup & Shenolikar 2009). Collectively the data are in agreement that PP1 interacts with several other proteins to control the diverse cellular processes. In fact, >200 PP1-binding regulatory proteins or putative targeting subunits have been identified to date using proteomic and biochemical approaches, and yeast two-hybrid and bioinformatics screens (Roadcap et al. 2007; Moorhead et al. 2008; Trinkle-Mulcahy et al. 2006; Esteves et al. 2013; Bennett et al. 2006; Fardilha et al. 2011; Flores-Delgado et al. 2007; Hendrickx et al. 2009; Hrabchak & Varmuza 2004). Affinity isolation of PP1 complexes has been carried out using immobilized microcystin-LR, which tightly binds the catalytic site of both PP1 and PP2A-like phosphatases (Roadcap et al. 2007; Moorhead et al. 2008). Similarly, tagged-PP1c has also been employed for pull down assays and identification of PP1 complexes by LC-MS/MS (Hendrickx et al. 2009; Chamousset, Mamane, et al. 2010; Prevost et al. 2013). Potential PP1 interactors have

also been identified using a broad in silico screen based on a stringent definition of the motif known to be bound by PP1, followed by biochemical approaches to validate hits (Hendrickx et al. 2009).

1.1.4 Identification and Evolution of Regulatory Subunits

The cytosolic regulatory subunits that were the first identified and consequently have been the best characterized are those that direct PP1c to glycogen and myosin. The hepatic-type G subunit (G_L) targets PP1c to liver glycogen, while the muscle-type G subunit (G_M) targets PP1c to both glycogen particles and sarcoplasmic reticulum of striated muscles (Sutherland & Wosilait 1955; Bollen 2001; Egloff et al. 1997), The Mypt1 subunit (also known as the M_{110}, MBS or M130 subunit) targets PP1c to myosin (Olsen et al. 2006; Alessi et al. 1992; Shimizu et al. 1994; Shirazi et al. 1994). Studies with G_M (Johnson et al. 1996) and M_{110} (Tanaka et al. 1998) demonstrate that the interaction of the regulatory subunits with PP1c occurs through a short amino acid "RVxF" motif. Egloff et. al. co-crystallized PP1c with a short peptide sequence (residues 63-75) containing the region of the G_M subunit known to bind PP1c (Egloff et al. 1997). X-ray crystallography was used to elucidate the structural basis of the association (Egloff et al. 1997). The structure shows that hydrophobic residues (V and F) within this peptide bind to a hydrophobic groove located near the C-terminal region of PP1c, found on the opposite side of the active site of PP1c (Egloff et al. 1997; Aggen et al. 2000) (Figure 1.3). In contrast, studies with the PP1c inhibitors, I-1 (Endo et al. 1996) and DARPP-32 (H. B. Huang et al. 1999; Kwon, Huang, et al. 1997), show that they bind and block the PP1 catalytic active site, which contain two metal ions required for PP1 activity (Peti et al. 2013).

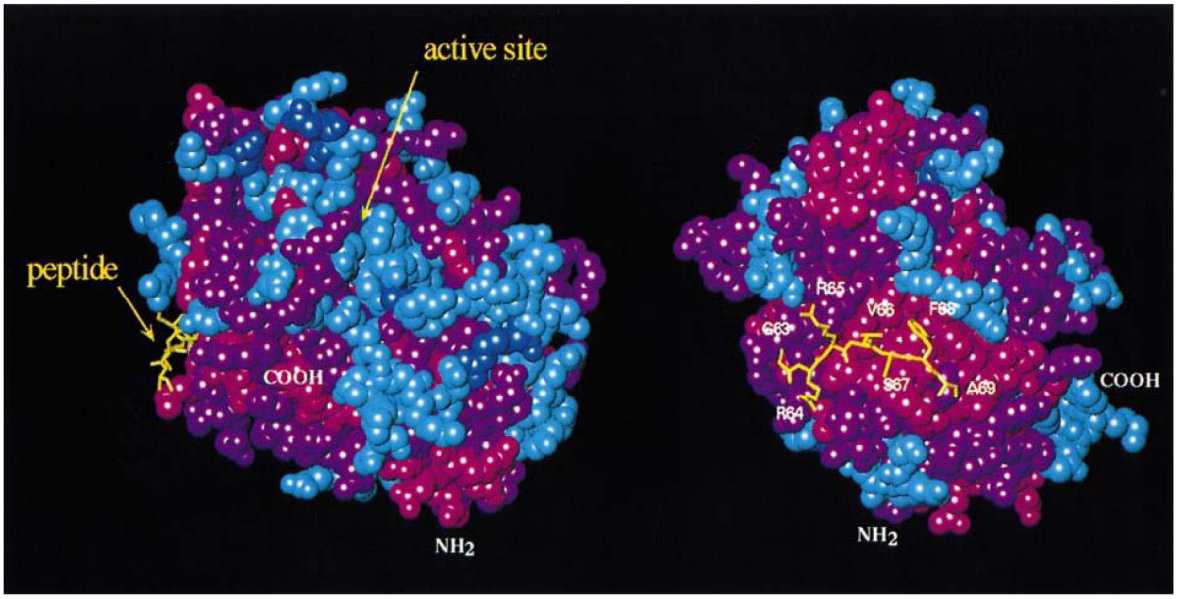

Figure 1.3. Crystal structure of PP1-$G_{M[63-75]}$ peptide complex. The structure shows that residues 64-69 binds to a hydrophobic groove located by the C-terminal region of PP1c, found on the opposite side of the active site of PP1c. Pink: hydrophobic; purple: hydrophilic; cyan: acidic; blue: basic residues. *Reproduced by permission from John Wiley and Sons: [The EMBO Journal]* (Egloff et al. 1997)*, copyright (1997).*

Most regulatory proteins contain an RVxF motif. The full consensus sequence is (R/K)x_1-(V/I)-x_2-(F/W), where x_1 may be absent or any residue except large hydrophobic residues and x_2 can be any amino acid except large hydrophobic residues. This binding motif enables them to bind the hydrophobic channel in PP1c (Manning et al. 2002; Doherty et al. 1995; Johnson et al. 1996; Egloff et al. 1997), and this binding is mutually exclusive (i.e. only one regulatory subunit can bind PP1c at a time via this motif). The RVXF motif is needed for the interaction but does not influence the enzymatic activity of PP1, as the catalytic site is 20 Å away (Peti et al. 2013). More than 10% of all proteins in the human genome contain the degenerate RVxF motif, but not all motifs are accessible and some also contain other PP1-binding sequences that enhance their binding to PP1c (Alonso et al. 2004; Eto et al. 2002; Andersen et al. 2005; Lesage et al. 2007). Experiments also demonstrate that the sequences that flank the RVxF motif can play important roles in the affinity and specificity of these regulatory subunits for PP1c (Morrison et al. 2000; Terry-Lorenzo et al. 2002; Carmody et al. 2004).

The ancient regulatory (R) subunit families, expressed ubiquitously in humans, include Inhibitor-3/Inh3 (PPP1R11), SDS22 (PPP1R7), Inhibitor-2/Inh2 (PPP1R2) and NIPP1 (PPP1R8). While Inh3 and SDS22 were identified in all four taxonomy classes that constitute the eukaryotic crown, Inh2 was identified in at least three, while NIPP1 was identified in two (Figure 1.4) (Ceulemans, Stalmans, et al. 2002). While Inh3 and NIPP1 contain an RVXF motif that mediates their binding to PP1c, they also contain additional binding sites, modules or motifs that account for their inhibitory properties (Ceulemans & Bollen 2004). SDS22 and Inh2 however, do not contain a canonical RVxF-motif. The conserved region of SDS22, which folds into a curved superhelix,

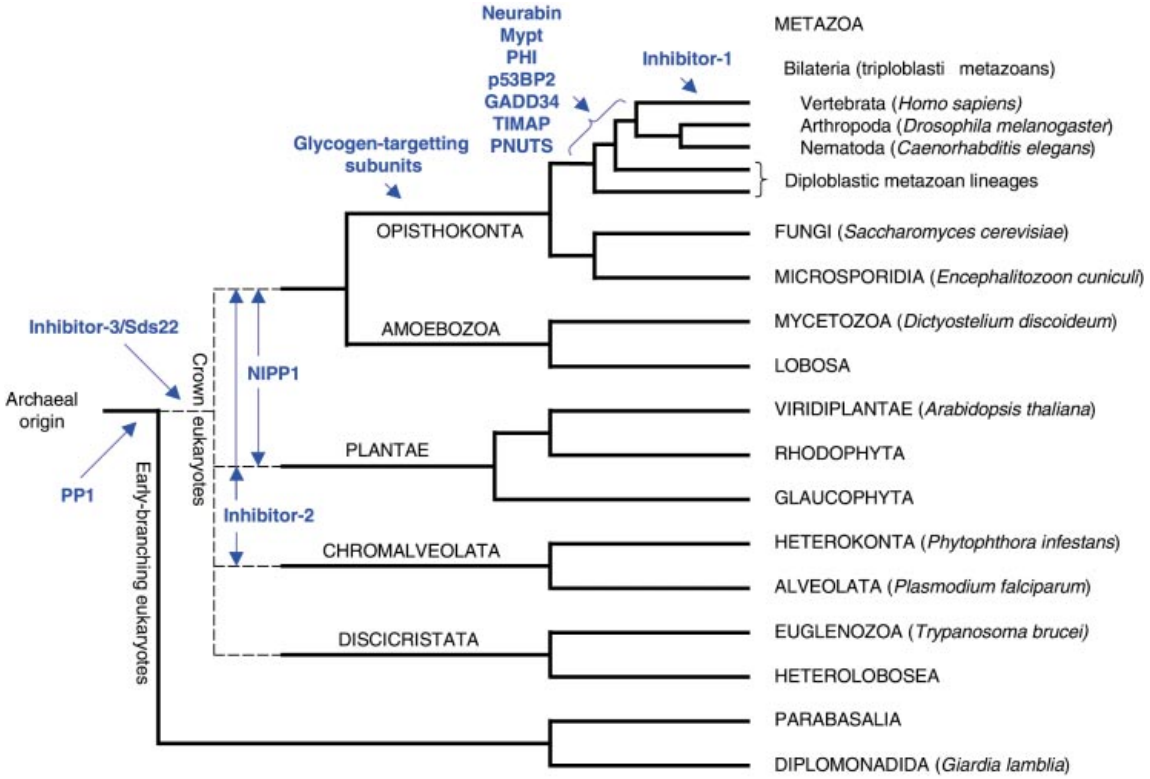

Figure 1.4. The emergence of PP1 and the regulatory subunits in eukaryotic evolution. *Reproduced by permission from John Wiley and Sons: [BioEssays]* (Ceulemans, Stalmans, et al. 2002)*, copyright (2002).*

is important for PP1 binding (Ceulemans, Vulsteke, et al. 2002). Inh2 contains a conserved SILK motif, [GS]IL[RK](H. B. Huang et al. 1999; Wakula et al. 2003; Hendrickx et al. 2009), essential for inhibitory function, in addition to a non-canonical RVxF motif. Interestingly, the glycogen-targeting subunits, which were identified in the later taxonomy class comprising the animal and fungus kingdom, contain conserved RVxF motifs (Ceulemans, Stalmans, et al. 2002). However, other regulatory subunits, identified in the metazoan class, contain the RVxF motif in addition to other motifs, including the SILK and the N-terminal MyPhoNE motif. This is seen with Mypt1, for example, and may contribute to its preferential association with the β isoform of PP1c (Scotto-Lavino et al. 2010).

1.1.5 Phosphatases as therapeutic targets

Work to date has focused primarily on kinases as therapeutic targets in disease states, due to the availability of specific kinase inhibitors. Discrepancy in the number of phosphatases relative to kinases has contributed to the misleading view that phosphatases may be promiscuous and therefore not “drug-targetable”.

Until recently, there have been no selective inhibitors for specific phosphatase complexes, as targeting the catalytic subunit of the phosphatase results in the inactivation of all PP1 holoenzyme complexes within the cell. The first PP1c-targeted therapeutic drug, Sephin1 (selective inhibitor of a holophosphatase), was recently discovered to selectively bind PPP1R15A (GADD34) and disrupt the GADD34-PP1c complex (Barker et al. 1993; Das et al. 2015; Barker et al. 1994; Sasaki et al. 1990). This complex is involved in a cellular stress response in which the accumulation of a misfolded protein in the endoplasmic reticulum (ER) triggers the unfolded protein

response (UPR), which in turn reduces the amount of aberrant protein and restores homeostasis (Schröder & Kaufman 2005; Walter & Ron 2011). ER stress activates PKR-like ER kinase (PERK), which phosphorylates the translation initiation factor 2α (eIF2α) to decrease protein synthesis, but also activates GADD34. When complexed with PP1, GADD34 is responsible for dephosphorylating eIF2α (Novoa et al. 2001). Under stressful conditions the activation of UPR is essential, and Sephin1, through selective inhibition of GADD34-PP1c, prolongs eIF2α phosphorylation to enable an effective stress response (Das et al. 2015). Sephin1 has been tested in mouse models of Charcot-Marie-Tooth1B demyelinating neuropathy (MPZ^{mutant}), where the myelin protein zero (P0 protein) in Schwann cells is misfolded due to a serine 63 amino acid deletion and the mice exhibit motor defects (Pennuto et al. 2008; D'Antonio et al. 2013), and amyotrophic lateral sclerosis (ALS), a motor neuron disease (Nordlund & Oliveberg 2008), where the protein superoxide dismutase 1 (SOD1) blocks degradation of ER proteins causing ER stress, with SOD^{mutant} mice exhibiting loss of motor neurons (Gurney et al. 1994). Sephin1 successfully inhibited motor defects and motor neuron loss in both the MPZ^{mutant} and the $SOD1^{mutant}$ mice (Das et al. 2015). Furthermore, studies in Alzheimer's disease (AD) mouse models, in which the accumulation of amyloid-B and abnormally phosphorylated tau induce ER stress, suggest that levels of GADD34 in neurons and oligodendrocytes are significantly increased in early stages (Honjo et al. 2015). The discovery of Sephin1 and its selectivity for a particular PP1 holoenzyme complex has revolutionized our view of phosphatases as therapeutic targets. It is thus essential to identify the regulatory proteins that associate with the phosphatases and to further characterize the multimeric enzyme complexes as a

strategy to design specific inhibitors.

1.2 Myosin Phosphatase Targeting subunit (MYPT) family

The myosin phosphatase targeting subunit (MYPT) family consists of five gene members, Mypt1 (PPP1R12A), Mypt2 (PPP1R12B), Mypt3 (PPP1R16A), TIMAP (PPP1R16B) and MBS85 (LENG3; PPP1R12C). An amino acid alignment of the Mypt1 family (Grassie et al. 2011) (Figure 1.5B) illustrates the conserved regions found at the ankyrin repeats and Leucine zipper motif (for Mypt1/2 and MBS85/Leng3) (Grassie et al. 2011). The family also shares several structural and functional domains that are similar (Figure 1.5A). The PP1c binding site, RVxF motif, is found near the N-terminus, followed immediately by 7-8 ankyrin repeats (conserved β-hairpin-helix-loop-helix structure). (Chamousset, De Wever, et al. 2010; Andreassen et al. 1998; Sedgwick & Smerdon 1999; Trinkle-Mulcahy 2006). While Mypt1, Mypt2 and MBS85 (LENG3) contain a C-terminal leucine zipper (LZ), allows for dimerization and interaction with other proteins, Mypt3 and TIMAP contain a C-terminal CaaX box that may function to target it to the cell membrane. In addition to the RVxF motif, all MYPT family members contain a conserved N-terminal site with the consensus sequence RxxQV/I/LK/RxY/W, referred to as the MyPhoNE (myosin phosphatase N-terminal element) motif, which contacts the conserved central domain of PP1c (Virshup & Shenolikar 2009; Sedgwick & Smerdon 1999).

Mypt1, a widely distributed 115 kDA protein, is the myosin targeting subunit of myosin light chain phosphatase, defined from its role in smooth muscle contraction and non-muscle motile processes. Although found in many cell types, Mypt1 is abundantly

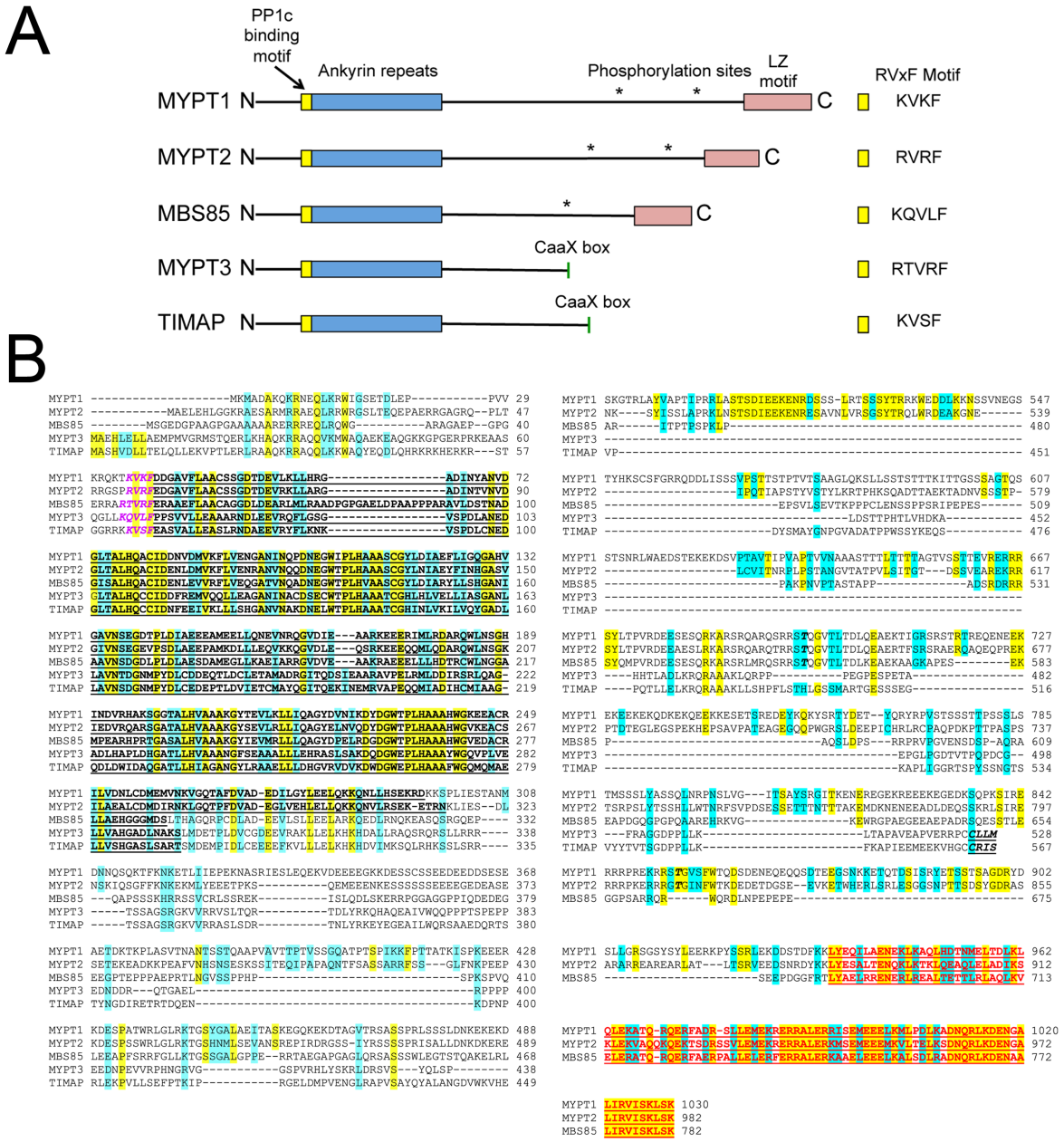

Figure 1.5. Structural features and alignment of the Mypt family members. A. The structural domains of the Mypt family members. **B.** ClustalW was used to align the amino acid sequences of Mypt family members. Identical residues in are indicated in yellow and conservative substitutions in blue. The PP1c-binding motif is highlighted in bold magenta italics. The ankyrin repeat region is indicated in bold black letters underlined. The leucine zipper domain of Mypt1, Mypt2 and MBS85 is indicated in bold red letters underlined. The inhibitory ROK phosphorylation sites (T696 and T853 in Mypt1) are indicated in bold black italics with asterisks. A CaaX box is shown in bold black italics underlined. *Reproduced by permission from Elseivier: [Archives of Biochemistry and Biophysics]* (Grassie et al. 2011)*, copyright (2011).*

expressed in smooth muscle cells (Bollen et al. 2010; Brozovich 2002; Feng et al. 1999). Targeted disruption of the Mypt1 gene in mice results in embryonic lethality, where the mice do not survive beyond e7.5 days (Aggen et al. 2000; Okamoto et al. 2005; Virshup & Shenolikar 2009). Furthermore, loss of Mypt1 in either the zebrafish embryo or *C. elegans,* results in either convergence defects (Weiser et al. 2009) or disruption of cell movements during gastrulation (Piekny et al. 2003). Mypt2 is predominantly found in striated (cardiac and skeletal) muscles and brain, while LENG3, most similar to Mypt2, is ubiquitously expressed and a substrate for myotonic dystrophy kinase-related Cdc42 binding kinase-α (MRCKα) (Tan et al. 2001). Mypt3 is found to be localized to the membrane and is expressed in the heart, brain and kidneys, while TIMAP is localized to the plasma membrane of endothelial cells (Grassie et al. 2011).

1.2.1 Mypt1

Figure 1.6 illustrates the structural features of the Mypt1 protein (Hartshorne et al. 1998). The ankyrin repeat region of Mypt1 interacts with the c-terminal region of PP1δ/β (Terrak et al. 2004). Studies suggest it is the central region of PP1δ/β that confers isoform-specific binding to Mypt1 (Scotto-Lavino et al. 2010). Binding to the C-terminus of PP1δ/β may account for specificity of Mypt1 towards the β/δ isoform, as the three PP1c isoforms vary mostly at their N- and C-termini (Grassie et al. 2011).

Mypt1 is regulated through phosphorylation within its central domain by a variety of ser/thr kinases including ROK (Rho-associated kinase), ZIPK (zipper-interacting protein kinase) and ILK (integrin-linked kinase). All of these kinases phosphorylate the T696 residue (Ito et al. 2004; Matsumura & Hartshorne 2008; Ulke-Lemée & Macdonald 2010), while ROK appears to account for the majority of Thr853 phosphorylation in

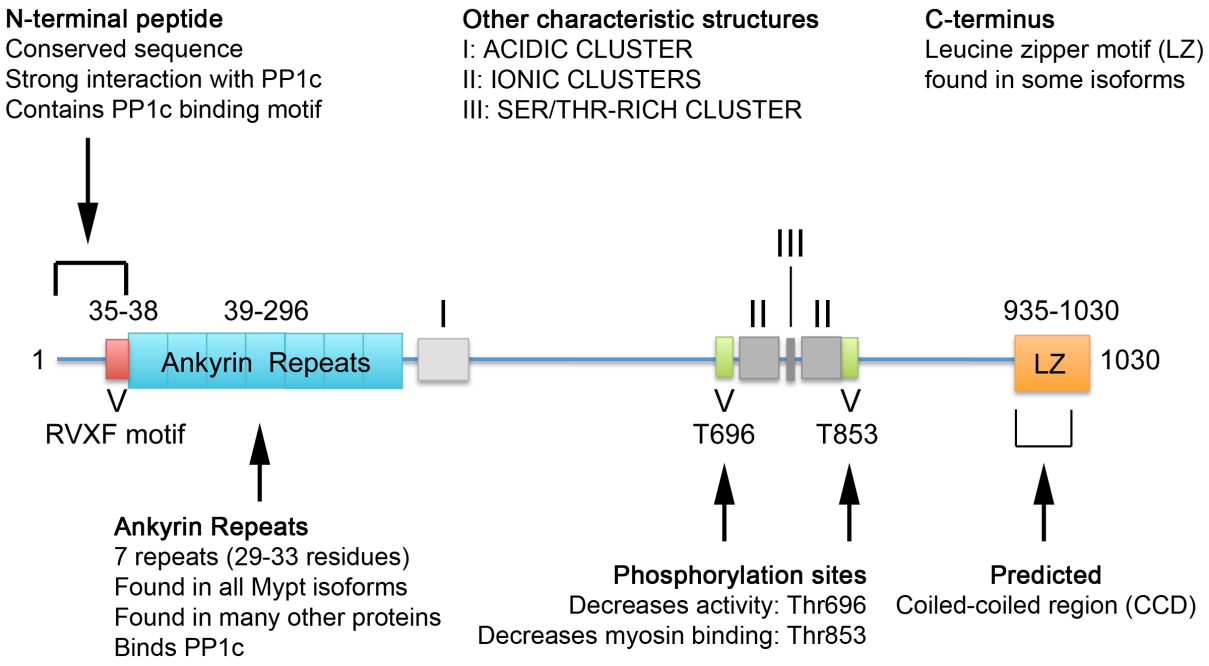

Figure 1.6. Schematic representation of the Mypt1 protein identifying important structural domains. The coiled-coiled domain (CCD) is predicted.

human Mypt1 (Kimura et al. 1996). Both sites are found to be conserved in Mypt2, but neither are conserved in TIMAP or Mypt3, whereas only T696 is conserved in MBS85 (LENG3). It is thought that Mypt1 is localized mainly in the cytoplasm when bound to PP1c (Eto et al. 2005), but its subcellular localization may vary depending on its interactions with other proteins (Grassie et al. 2011). One study suggested that unbound Mypt1 localizes to the nucleus due to a nuclear localization signal (NLS) found in the N-terminus, located at P27-K33 (Y. Wu et al. 2005), although an additional NLS is also found in the C-terminus, located at R843-S852. The complex containing Mypt1, bound to PP1δ/β at its N-terminus and M20 at its C-terminus (Hirano et al. 1997; Johnson et al. 1997; Shimizu et al. 1994), is referred to as the myosin light chain phosphatase (MP/MLCP).

1.2.2 Role of MP in smooth muscle contraction

Smooth muscle contraction occurs when myosins move along actin filaments hydrolyzing ATP (Engelhardt 1939), functioning as molecular motors. Dephosphorylation of myosin II by MP is necessary for the relaxation of the actomyosin fibers in the cells. The two phosphorylation sites of Mypt1, Thr696 and Thr853, catalyzed by Rho-associated kinase (ROK) (Kimura et al. 1996), are important for the association of Mypt1 with myosin II. Phosphorylation of T696 or T853 results in a decrease of MP activity (Ichikawa et al. 1996; Velasco et al. 2002; Muranyi et al. 2005). While phosphorylation of Mypt1 at Thr696 inhibits the activity of MP for myosin II, phosphorylation at Thr853 causes the dissociation of Mypt1 from myosin II and decrease in MP activity (Macdonald et al. 2001; Velasco et al. 2002; Muranyi et al. 2005; Ichikawa et al. 1996). The sequence that surrounds Thr696 and Thr853

resembles the site on myosin that is phosphorylated, which is consistent with a pseudo-substrate mechanism of inhibition where phosphorylation of Thr696 and Thr853 results in the docking of this region to the PP1c active site, blocking its access to its substrate, myosin (Khromov et al. 2009).

1.2.3 Role of MP in non-muscle cells

In addition to its traditional role in regulating muscle contraction, the MP complex plays a key role in the regulation of actomyosin in non-muscle cells, affecting cell migration and adhesion (Xia et al. 2005). For effective cell motility, two regulatory light chain subunits (LC_{20}) of myosin II are regulated through reversible phosphorylation (Figure 1.7). The balance is achieved by the predominant Ca2+/calmodulin-dependent myosin light chain kinase (MLCK) and MP (Grassie et al. 2011). Xia et al. illustrate that Mypt1 KD leads to an enhanced LC_{20} phosphorylation, resulting in an accumulation of active myosin and subsequently affecting stress fibers and focal adhesion, thereby inhibiting cell migration (Xia et al. 2005).

Mypt1 is found to interact with several other proteins, including Tau, MAP2, Moesin and GTP-RhoA (Hartshorne et al. 1998; Amano et al. 2003; Amano et al. 2000; Surks et al. 1999). Recently, a nuclear interactome of Flag-Mypt1 was mapped and 22 potential Mypt1 interacting proteins identified (Sipos et al. 2017). Non-myosin Mypt1/PP1β substrates have also been identified, including polo-like kinase 1 (PLK1) and histone deacetylase 6 (HDAC6). PLK1 is involved in a variety of mitotic events including centrosome maturation and separation, kinetochore-microtubule attachment and cleavage furrow ingression (Petronczki et al. 2008; Bruinsma et al. 2012; Zitouni et al. 2014). Yamashiro et al. demonstrated that Mypt1 contributes to mitotic regulation via

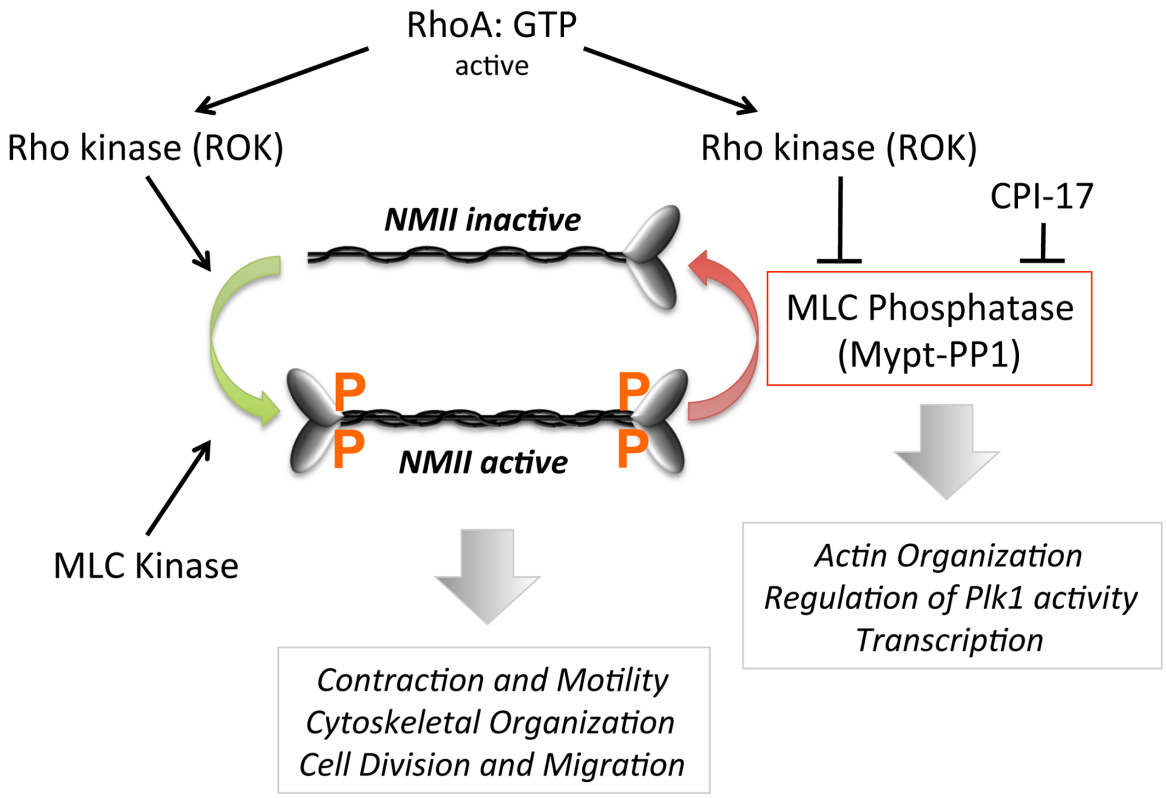

Figure 1.7. Acto-myosin regulation in non-muscle cells. Mypt1-PP1 regulates both non-muscle myosin II (NMII)-dependent and -independent cellular pathways.

its interaction with PLK1, colocalizing with PLK1 on centrosomes (Yamashiro et al. 2008). Joo et al. have shown that HDAC6, which plays an important role in microtubule deacetylation, is a substrate for the Mypt1/PP1β complex (Joo & Yamada 2014). They suggest that the complex balances contractility and microtubule acetylation by either interacting with myosin light chain or HDAC6 (Joo & Yamada 2014).

1.2.4 Mypt1 and Disease

Mypt1 has diverse cellular functions within a cell. Its involvement in smooth muscle contraction links it to several disease states when dysfunctional, including hypertension and congestive heart failure (Grassie et al. 2011). The inhibition of Mypt1, via the phosphorylation of T696 or T853 by upstream kinases, decreases MP activity (Ichikawa et al. 1996; Velasco et al. 2002; Muranyi et al. 2005) and thus contributes to disease development. Furthermore, downregulation of Mypt1 is found in patients with Parkinson's disease (E. S. Wang et al. 2010) and Mypt1 is indirectly implicated in chronic gastritis caused by *Helicobacter* pylori. In chronic gastritis, MLCK has been implicated in disrupting claudin4/5 and thus increasing the permeability of epithelial cells (Fedwick et al. 2005). Lastly, Mypt1 has been implicated in playing a role in cancer (Kaneko et al. 2002), regulating myosin II activity and thus affecting migration, adhesion and the cell cycle.

1.3 Sperm Antigen With Calponin Homology And Coiled-Coil Domains 1 and 1-Like (Specc1/1L) Family

Sperm antigen with calponin homology and coiled-coil domains 1 (Specc1), also known as CYTSB, shares 42.6% identity with Sperm antigen with calponin homology and coiled-coil domains 1 Like (Specc1L), also known as CYTSA. The Specc1/1L gene

encodes three coiled-coil (CC) domains, four in the case of Specc1, and a C- terminal calponin homology (CH) domain, where the CC domains may be involved in key protein interactions while the latter domain is believed to facilitate actin binding (Gimona et al. 2002) (Figure 1.8A). The highest conservation between the two family members is found in their CH domain, which are 83.5% identical (Figure 1.8B). Mattison et al. illustrate that the CH domain shows moderate homology to those found in α-actinin, Smoothelin, Macrophin and Beta-Spectrin (Mattison et al. 2011).

The presence of a CH domain suggests that Specc1L may be a potential actin binding protein (Gimona et al. 2002). Functionally, however, two tandem CH domains are normally required to bind actin, while Specc1L, like EB1, contains only one (Kanaba et al. 2013). Previous studies showed that Specc1L localizes predominantly to the actin cytoskeleton (CSK) in interphase cells (Saadi et al. 2011; Mattison et al. 2011). Treatment with ionomycin (increases intracellular calcium and reorganizes the actin CSK by translocating F-actin fibers to the cell membrane) resulted in a translocation of Specc1L to the cell membrane, co-localizing with the F-actin fibers as shown by phalloidin staining (Saadi et al. 2011). Interestingly, when transiently overexpressed, Specc1L was observed to relocalize to the MT network and co-localize with acetylated tubulin, a marker for stabilized microtubules (Saadi et al. 2011). Endogenous Specc1L relocalizes to the mitotic spindle (Saadi et al. 2011) in early mitosis, and was observed at the cleavage furrow during cytokinesis (Mattison et al. 2011). Mattison et al. found that the mid region of Specc1L, containing two CC domains, interacts with mono-polar spindle kinase 1 (MPS1), which is required to ensure proper spindle positioning during the onset of anaphase (Mattison et al. 2011). While they claim to observe a transient association of Specc1L with the centrosome (although the data was not shown) (Mattison et al. 2011),

A

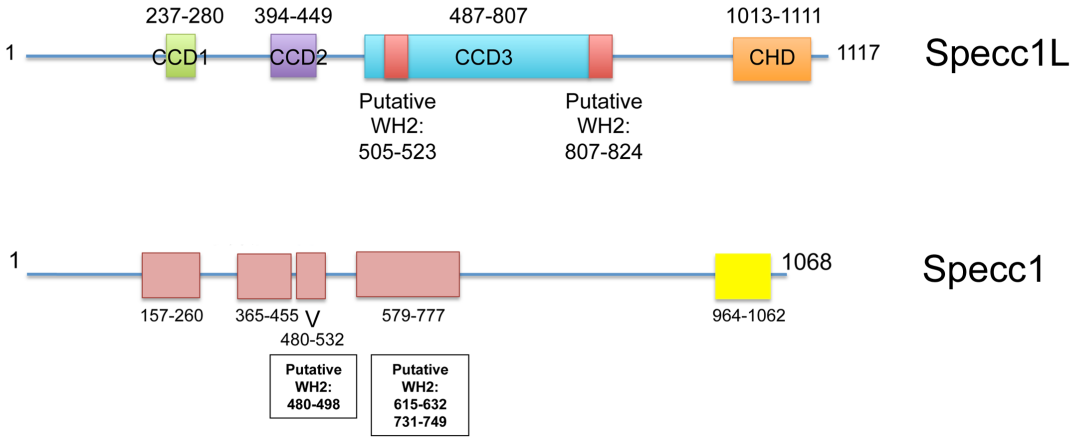

B

```
Specc1L     MKKAS-------RSVGS-------VPKVSAISK---TQT--AEKIKPENSSSASTGGKLV   41   VASDQIEMNRLKAQLENEKQKVAELYSIHNSGDKSDIQDLLESVRLDKEKAETLASSLQE   628
Specc1      MRSAAKPWNPAIRAGGHGPDRVRPLPAASSGMKSSKSSTSLAFESRLSRLKRASSEDTLN   60   LEGLKMENGSLKSHLQGEKQKATEASAVEQTAESCEVQEMLKVARAEKDLLELSCNELRQ   603
            *:.*:       *: *        :* .*:  *   :.*  * : : .. . **: ..*          : . ::* . **::*:.****.:*  ::.::.:..::*::*: .* :*:  *  ...*::

Specc1L     KPGTAASLSKTKSSDDLLAGMAGGVTVTNGVKGKKSTCPSAAPSASAPAMTT-VENKSKI   100  DLAHTRNDANRLQDAIAKVEDEYRAFQEEAKKQIEDLNMTLEKLRSDLDEKETERSDMKE   688
Specc1      KPGSTAA----------------------SGVVRLKKTATA-------GAISELTESRLRS   92   ELLKANGEIKHVSSLLAKVEKDYSYLKEICDHQAEQLSRTSLKLQEKASESDAEIKDMKE   663
            ***::*:                      .**   *.*. :        *::  .*.: :          :* ::..: :::.. :****.:*  ::* ..:* *:*. *  **:.. .*.::* .****

Specc1L     STGTASSTKRSTSTGNKESSST--RERLRERTRLNQSKKLPSAGQGANDMALAKRSRSRT   158  TIFELEDEVEQHRAVKLHDNLIISDLENTVKKLQDQKHDMEREIKTLHRRLREESAEWRQ   748
Specc1      GTGAFTTTKRTGIPAPREFSVTVSRERSVPRGPSNPRKSVSSPT-SSNT--------PTP   143  TIFELEDQVEQHRAVKLHNNQLISELESSVIKLEEQKSDLERQLKTLTKQMKEETEEWRR   723
            .**: ::***:   . :* * *  ***   *   *  *.: *   .:*          *******:**********:* :**:**.:* **::** *:**::*** ::::**: ***:

Specc1L     ATECDVRMSKSKSDNQISDRAALEAKVKDLLTLAKTKDVEILHLRNELRDMRAQLGINED   218  FQADLQTAVVIANDIKSEAQEEIGDLKRRLHEAQEKNEKLTKELEEIKSRKQEEERG---   805
Specc1      TKHLRTPSTKPKQENEGGEKAALESQVRELLAEAKAKDSEINRLRSELKKYKEKRTLNAE   203  FQADLQTAVVVANDIKCEAQQELRTVKRKLLEEEEKNARLQKELGDVQGHGRVVTSRAAP   783
            :..  .  :* *.:*: .::****::*::**: **:** ** :**.**:. : :  :* :          **********:*****.***:*:  :**:* * :*** :* *** :::.: :

Specc1L     HSEGDEKSEKETIMAHQPTDVESTLLQLQEQNTAIREELNQLKNENRMLKDRLNALGFSL   278  -RVYNYMNAVERDLAALRQGMGLSRRSSTSSEPTPTVKTLIKSFDSASQV---PNPAAAA   861
Specc1      GTDALGPN--VDGTSVSPGDTEPMIRALEEKNKNFQKELSDLEEENRVLKEKLIYLEHSP   261  PPVDEEPESSEVDAAGRWPGVCVSRTSPTPPESATTVKSLIKSFDLGRPGGAGQNISVHK   843
             ::.   .      : .* *.*  :  *:*:*. :::**.:*::***:**::*  * .*          * :  :: * * *.   *: :** * *  * : ***:****** .       * :.

Specc1L     EQRLDNSEKLFGYQSLSPEITPGNQSDGGGTLTSSVEGSAPGSVEDLLSQDENTLMDHQH   338  IPRTPLSPSPMKTPPAAAVSPMQRHSISGPISTSKPLTALSDKRPNYGEIPVQEHLLRTS   921
Specc1      NSEGAA--SHTGDSSCPTSITQ----------ESSFGSPTG---NQMSSDIDEYKKNIH   305  TPRSPLSGIPVRTAPAAAVSPMQRHSTYSSVRPA---SRGVTQRLDLPDLPLSDILKGRT   900
            :..     .  * .*   .**             .*  **  *   : :*.* :   .: *          **:*** *::* ************  . :  :   :    :* :  ::*:.: *   :

Specc1L     SNSMDNLDSECSEVYQPLTSSD---------DALDAPSSSESEGIPSIERSRK-GSSGNA   388  SASRPAS-LPRVPAMESAKTLSVSRRSSEEMKRDISAQEGASPASLMAMGTTSPQLSLSS   980
Specc1      GNALRTSGSSSSDVTKASLSPDASDFEHITAETPSRPLSSTSNPFKSSKCSTAGSSPNSV   365  ETLKPDPHLRKSPSLESL----------------------SRPP-SLGFGDTR----LLS   933
            .*:: . .*..*:* :   * *          :: . * ** *: : * : *   .* ...          .: :*   * : *::**                        : *   :.:* *     * *

Specc1L     SEVSVACLTERIHQMEENQHSTSEELQATLQELADLQQITQELNSENERLGEEKVILMES   448  SPTASVTPTTRSRIREERKDPLSALAREYGGSKRNALLKWCQKKTEGYQNIDITNFSSSW   1040
Specc1      SELSLASLTEKIQKMEENHHSTAEELQATLQELSDQQQMVQELTAENEKLVDEKTILETS   425  ASTR--AWKPQSKLSVERKDPLAALAREYGGSKRNALLKWCQKKTQGYANIDITNFSSSW   991
            **:*:*.***:*::****:***:*********:* **:.***.:***:* :**.**  *          : *   : . :*::  ******:**********************:** **********

Specc1L     LCQQSDKLEHFSRQIEYFRSLLDEHHISYVIDEDVKSGRYMELEQRYMDLAENARFEREQ   508  NDGLAFCALLHTYLPAHIPYQELNSQDKRRNFMLAFQAAESVGIKSTLDINEMVRTERPD   1100
Specc1      FHQHRERAEQLSQENEKLMNLLQERVK--NEEPTTQEGKIIELEQKCTGILEQGRFEREK   483  SDGLAFCALLHTYLPAHIPYQELNSQEKKRNLLLAFEAAESVGIKPSLELSEMLYTDRPD   1051
            : *: :: *::*:: * : .**:*:       :  .:.*: :*****:  .: *:.*****:          .************************:*:**::***:******** :*::.**: *:***

Specc1L     LLGVQQHLSNTLKMAEQDNKEAQEMIGALKERSHHMERIIESEQKGKAALAATLEEYKAT   568  WQNVMLYVTAIYKYFET  1117
Specc1      LLNIQQQLTCSLRKVEEENQGALEMIKRLKEENEKLNEFLELERHNNNMMAKTLEECRVT   543  WQSVMQYVAQIYKYFET  1068
            **.:**:*: :*: .*::*: * ***  ***...:::.::* *::.:  :* **** :.*          **.** **: *******
```

Figure 1.8. Clustal Omega Alignment of human Specc1L (aa 1-1117) and Specc1 (aa 1-1068) reveals that the highest conserved region is in their CH domain (CHD). A. Schematic showing the location of the coiled coil domains (CCDs) within the C-terminal halves of Specc1L and Specc1. **B.** Alignment of Specc1L with Specc1 identified a region (highlighted in yellow) that shows an 83.5% identity. This region corresponds to aa 997-1117 in Specc1L and aa 948-1068 in Specc1. Mutations in Specc1L found in patients with developmental diseases are highlighted in orange. The amino acids threonine (T397) and glutamine (Q415) are found to be mutated into proline (P) in patients with Opitz G/BBB Syndrome and Tessier IV Clefting, respectively. The amino acid glycine (G1083) is mutated to a serine (S) in patients with Opitz G/BBB Syndrome. The amino acid glutamic acid (E420) is mutated to aspartic acid (D) in patients with Teebi Hypertelorism.

Saadi et al. showed punctate Specc1L expression that localized in a ring around γ-tubulin labeled centrioles. The removal of the CH domain from full length Specc1L abolished the formation of stabilized microtubules, suggesting that Specc1L may stabilize microtubules via an interaction with the actin CSK (Saadi et al. 2011).

Although Specc1L may associate with microtubules, a direct interaction has not been established. Furthermore, no studies to date have shown whether Specc1 behaves in a similar fashion to Specc1L as a novel "cross-linking" protein with the capacity to interact with both microtubules and the actin CSK. Also, while several cytoskeletal proteins have been deposited as putative Specc1/L binding partners in the BioGrid dataset, from high-throughput AP/MS screens, their interactomes have not yet been mapped and it remains unclear how they carry out their proposed physiological roles.

Specc1L KD in Drosophila results in an integrin knockout phenotype where both cell migration and adhesion is affected (Saadi et al. 2011). Similarly, KD of Specc1L affects the migration of cranial neural crest cells (CNCC) in zebrafish, producing a craniofacial "faceless" phenotype (Saadi et al. 2011; Gfrerer et al. 2014). Migration and adhesion defects were also observed in HEK293T and U2OS Specc1L KD stable cell lines (levels reduced 60-70%) (Saadi et al. 2011). HEK293T Specc1L KD cells failed to remain adherent once they reached confluency, compared to the parental control, while U2OS Specc1L KD cells demonstrated a reduced ability to close the gap in a wound repair assay (Saadi et al. 2011). *In vivo*, similar to the CNCC migration defects seen in zebrafish, CNCC migration was affected in Specc1L deficient mice (Wilson et al. 2016), resulting in neural tube closure failure. Wilson et al. demonstrated that the failure of CNCC migration and neural tube closure failure was due to reduced P13K-AKT levels

subsequently increasing E-cadherin expression, leading to increased apico-basal density of adherens junctions at the neural folds that affected delamination.

1.3.1 Specc1/1L and Disease

While Specc1 is highly overexpressed in several cancer cell lines and is being explored as a potential therapeutic target in head and neck cancers (D'Agostino & Giordano 2011; D'Agostino & Giordano 2008), Specc1L is found to be mutated in developmental diseases including Oblique facial Clefts (ObFC), also known as Tessier IV clefts (Saadi et al. 2011), that result in congenital malformations.

ObFC are complex orofacial clefts, which are the most common congenital malformations, affecting one in every 700 to 1000 births (Tolarová & Cervenka 1998; Genisca et al. 2009). The discovery of Specc1L mutations in patients with ObFC can aid in a genetic diagnosis of this developmental disease and allow potential advances in the treatment of the disease, as current treatments such as surgery are costly and not every effective at treating the malformations (Versnel et al. 2011; Pidgeon et al. 2014) (Deleyiannis et al. 2013). Patients with ObFC have a missense mutation c.1244A>C (p.Gly415Pro) (Saadi et al. 2011). The identified mutation is predicted by PolyPhen, SIFT, and pMUT mutation evaluation algorithms (Thusberg & Vihinen 2009) to have a deleterious effect on protein function (Saadi et al. 2011). When transiently overexpressed, the G415P Specc1L mutant severely impairs the formation of stabilized MTs as monitored by acetyl α-tubulin staining (Saadi et al. 2011). Furthermore, lymphoblastoid cells (immortalized from an ObFC patient) failed to form large clumps with increased adhesion and were marked by a reduced number of F-actin microspikes and filopodia (both linked to reduced adhesion and motility) (Kislauskis et al. 1997; Webb et

al. 2003).

Since its original discovery in ObFC, Specc1L mutations have been found in patients with Optiz G/BBB syndrome, genetically heterogeneous with variable expression in both X-linked and autosomal dominant families (Kruszka et al. 2015), and Teebi hypertelorism syndrome (Bhoj et al. 2015), a rare autosomal dominant disorder. Both syndromes are characterized by hypertelorism, the abnormally increased distance between two organs or bodily parts, with slight differences in the facial features affected and the mutations in Specc1L identified. In patients with Optiz G/BBB, two missense mutations were discovered in Specc1L: c.1189A>C (p.Thr397Pro) and c.3247>A (p.Gly1083Ser). Similar to the G415P Specc1L mutation, the T397P and G1083S Specc1L mutants did not induce formation of stabilized MTs (Kruszka et al. 2015). In patients with Teebi Hypertelorism one mutation, c.1260G>C (p.Glu420Asp), was observed (Bhoj et al. 2015).

1.4 Actin Cytoskeleton

The actin cytoskeleton, required for cell motility (in non-muscle cells) and muscle contraction, is composed of polymers of actin and actin-binding and associated proteins (Stossel 1993; Winsor & Schiebel 1997; Schmidt & M. N. Hall 1998). Actin is found in the cell in a monomeric (G-actin) or polymeric (F-actin; composed of G-actin monomers) form. The polymers are capable of forming spontaneously and are highly dynamic structures that assemble and disassemble at both ends. However, it is the plus (barbed) end, which gets capped to prevent the addition or loss of actin subunits (Casella et al. 1987; Caldwell et al. 1989), that grows quicker than the minus (pointed end). The first step in actin polymerization, known as actin nucleation, occurs at membrane-associated

complexes such as focal adhesions and adherens junctions. These also serve as cross-linkers between the exterior of the cell, the plasma membrane and the actin cytoskeleton (Yamada & Geiger 1997). The site of nucleation consists of multimolecular complexes. Focal adhesions mediate cell substrate adhesion via integrin-type receptors that attach to the extracellular matrix and associate with protein complexes containing talin, vinculin, α-actinin, paxillin, tensin, zyxin and focal adhesion kinase (FAK) (Schmidt & M. N. Hall 1998). Intercellularly, adherens junctions mediate cell-cell interaction that are complexed with vinculin, α-actinin, catenin, ERM proteins, and filamin (Geiger et al. 1990). Although adhesions are important to initiate actin polymerization, the organization of actin polymers into a filamentous network is achieved by cross-linking proteins that include α-actinin, filamin, fimbrin, and villin (Schmidt & M. N. Hall 1998). The RhoA, Rac and Cdc42 families of GTPases play an important role in organizing the actin cytoskeleton to induce morphological changes. While Rac controls the formation of lamellipodia and membrane ruffles at the leading edge of the cell, Cdc42 is involved in the formation of actin microspikes including filopodia, which are finger-like protrusion consisting of bundles of actin filaments (Schmidt & M. N. Hall 1998). The generation of stress fibers, bundles of actin filaments that help with cell migration, focal adhesions and cortical actin, are controlled by RhoA activation. Furthermore, myosins are responsible for the movement of actin filaments within the cell. The localization of the actin structures can be seen in Figure 1.9.

1.5 Myosins

Myosins constitute a large family of F-actin based motor proteins, playing an important role in eukaryotic motility (Sellers 1999). All myosins to date share a common

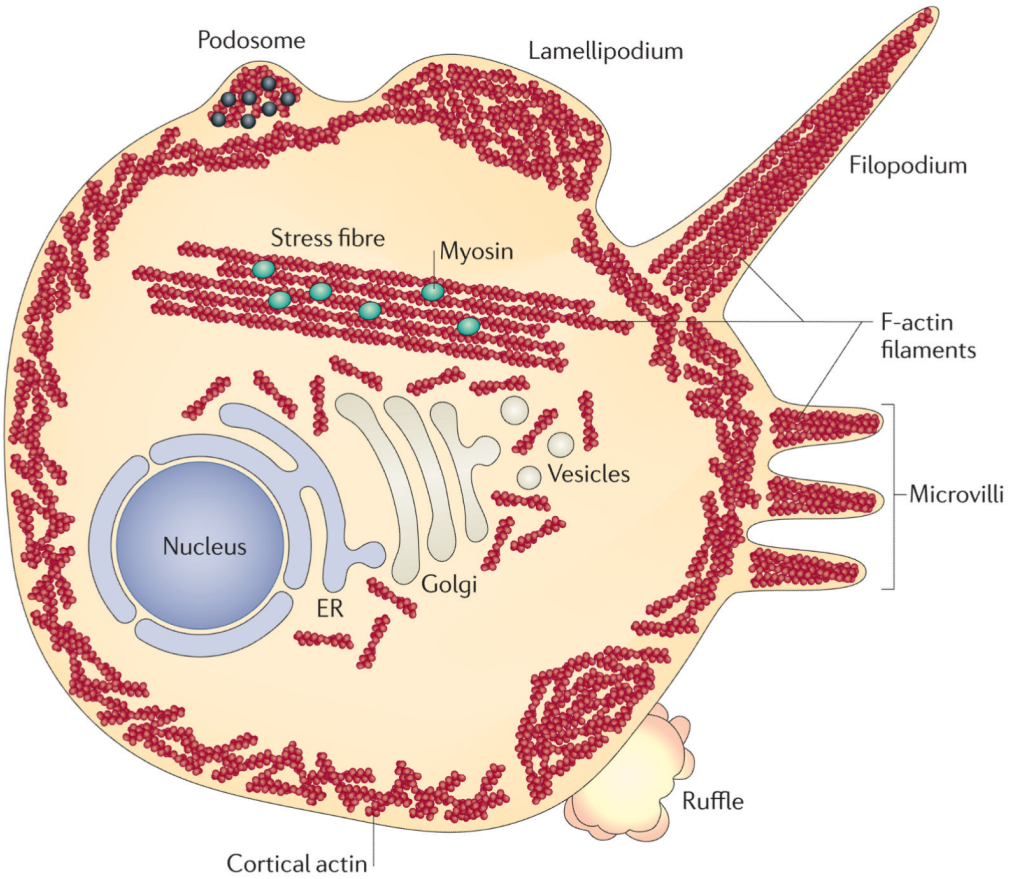

Figure 1.9. Arrangements of Actin filaments within the cell. Actin filaments can be arranged to form multiple structures, including stress fibres, filopodium, lamellipodium, membrane ruffles and cortical actin. *Reproduced by permission from Nature Publishing Group: [Nature Reviews Microbiology]* (Taylor et al. 2011)*, copyright (2011).*

domain, the conserved head domain, which interacts with actin and binds ATP to produce movement in most cases. This is followed by a neck domain, which consists of one or more helical motifs, termed an IQ motif, (consensus sequence of IQXXXRGXXXR (Cheney & Mooseker 1992)) capable of binding the regulatory light chains (RLC). Finally, the presence of a C-terminal tail domain anchors and positions the motor domain, allowing it to interact with actin. The most diversity amongst the myosins occurs in the tail domain, as they vary in length and sequence, contain functional motifs, and can have coiled-coil forming regions that allow the myosin to dimerize and produce two-headed molecules. Phylogenetic analysis classifies myosins using the head domains (Goodson & Spudich 1993; Cheney et al. 1993; Hodge & Cope 2000), grouping them into 18 distinct classes (Furusawa et al. 2000), although there are a few that do not fall in any of the classes (Berg et al. 2001). Each class has a distinct function. Class I, known as the unconventional myosins, cannot form filaments and plays a role in endocytic and exocytic membrane trafficking (Thompson & Langford 2002). Class II, known as the conventional myosins, can form filaments and constitutes and important component of the sarcomere in muscle cells. It is also known to be a component of the contractile ring in dividing cells (Thompson & Langford 2002). Most myosins belong to Class II and help make up the contractile proteins of cardiac, skeletal and smooth muscle. There are also myosin II molecules in non-muscle cells, referred to as non-muscle myosin (NM) II, that resemble their muscle counterparts in both structure and function (Clark et al. 2007; Conti & Adelstein 2008; Krendel & Mooseker 2005).

1.5.1 Non – muscle myosin II (NM II)

Similar to muscle myosin II, NM II is composed of two heavy, light and essential

light chains (Vicente-Manzanares et al. 2009). There are three isoforms of NM II: IIA, B and C. In mammalian cells, three genes encode the NM II heavy chain (NMHC II), myosin heavy chain 9, 10 and 14 (MYH9,10,14), which represent NMIIA, B and C. It is the presence of the heavy chain isoform that determines the NM II isoform (Vicente-Manzanares et al. 2009). NM II isoforms vary in two kinetic properties, the rate of ATP hydrolysis (Mg^{2+} - ATPase activity) and the time that myosin is bound to actin in a force generating state (duty ratio). While NM IIA has the highest rate of ATP hydrolysis out of the three isoforms, NM IIB has a higher duty ratio. Reversible phosphorylation of the light chain and heavy chains regulates the Mg^{2+} - ATP hydrolysis and filament formation of NM II. Phosphorylation on serine (Ser) 19 of the regulatory light chain (RLC) increases the Mg^{2+} - ATPase activity of myosin (A. P. Somlyo & A. V. Somlyo 2003) without having any effect on the affinity for actin (Sellers et al. 1982). Threonine (Thr) 18 can also be phosphorylated, and phosphorylation on both Thr 18 and Ser 19 increases the Mg^{2+} - ATPase activity (Umemoto et al. 1989). While several kinases are found to phosphorylate the RLC of NM II, including MLCK, Rho-associated, coiled coil-containing kinase (ROCK) and many others (Vicente-Manzanares et al. 2009), dephosphorylation of RLC of NM II, similar to muscle myosin II, is accomplished by the major myosin phosphatase, Mypt1/PP1β (Matsumura & Hartshorne 2008) (Figure 1.7).

1.5.2 NM II and migration

NM II plays an important role in both the formation of cellular protrusions and the maturation of adhesions, both required for effective cell migration, with the four steps of migration being protrusion, adhesion, contraction and retraction (Fife et al. 2014) (Figure 1.10). At the leading edge of a migrating cell, the adhesions formed are small, while the

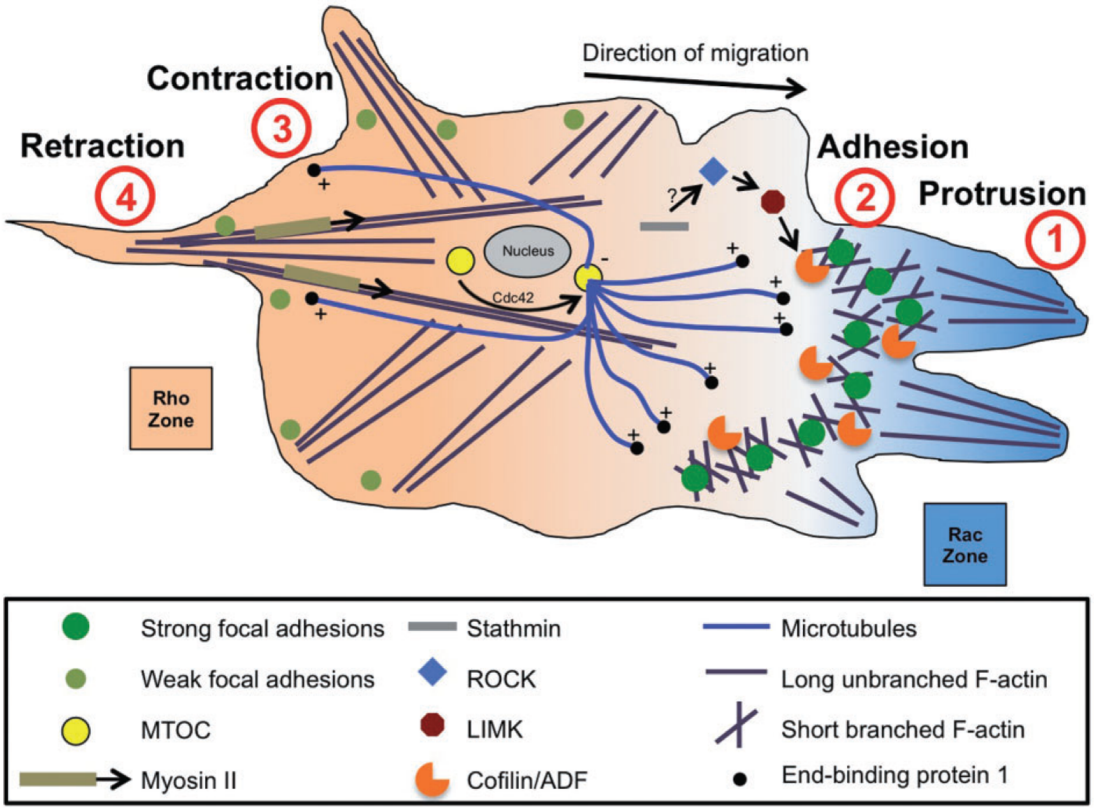

Figure 1.10. A schematic illustrating the steps of a migrating cell. Four steps of cell migration involve protrusion, adhesion, contraction and retraction. *Reproduced by permission from John Wiley and Sons: [British Journal of Pharmacology]* (Fife et al. 2014)*, copyright (2014).*

rear has more stable mature adhesions, which are supported by the presence of larger actin filament bundles. Mature adhesions are also found at the transition zone between the lamellum and lamellipodium, where traditionally it was proposed that the latter is positioned anteriorly to the former (Yui et al. 1998; Heath & Holifield 1991). Adhesions are associated with actin bundles (Vicente-Manzanares et al. 2009), and actin bundling requires NM II, as knocking down or inhibiting NM II results in a loss of actin bundles (Ponti et al. 2004). Adhesion maturation, mediated by NM II, is thought to occur in two ways. First, NM II bundles actin filaments, bringing together the adhesion proteins found at the end of the actin filaments. Second, the force generated by NM II causes a conformational change that now exposes the activation and binding sites of important adhesion components (Sawada et al. 2006; del Rio et al. 2009; Friedland et al. 2009). It is thought that NM II affects protrusions by decreasing the rate of actin retrograde flow in the lamellum, where it is already slow to begin with, subsequently affecting the transition zone between the lamellum and lamellipodium (Anderson et al. 2008; Nemethova et al. 2008). When NM II is inhibited or deleted protrusiveness increases (Vicente-Manzanares et al. 2009). In summary, activation of NM II results in large actin bundles, stable adhesions and decreased protrusion.

1.6 Microtubules

Microtubules (MTs) are composed of polymers of α and β-tubulin dimers, which associate with each other to form hollow tubes. Assembly of MTs occurs from one or several microtubule organizing centers (MTOCs). The centrosome is a major MTOC in most cell types (Etienne-Manneville 2013). Although the centrosome is the primary MTOC, many cell types have MT assembly occur both at the centrosome and other

structures, such as the Golgi complex, that can also contribute to organization of the microtubule network (Vinogradova et al. 2009). MTs are dynamic and undergo episodes of growth and shrinkage, which usually occurs from the plus (+) end located away from the MTOC (Figure 1.11) (Akhmanova & Steinmetz 2008; Gardner et al. 2008). The functions of MTs depend largely on the MT-associated motors, such as kinesins and dyneins, and microtubule-associated proteins (MAPs) (Etienne-Manneville 2010). Most MAPs associate with the MT network to help with their stability, thereby greatly influencing MT dynamics. MTs are important in a number of cellular processes, including maintaining the structure of the cell, movement of organelles and vesicles, chromosome segregation and migration.

1.6.1 Microtubules and Migration

Migration in various cell types is affected during both drug-induced depolymerization and stabilization of microtubules (Etienne-Manneville 2004; Liao et al. 1995; Vasiliev et al. 1970). Cellular protrusion, particularly the formation of the lamellipodium, is an important step needed for effective migration, along with adhesion, contraction and retraction. While actin polymerization is solely responsible for membrane protrusions in small cells such as fish keratocytes or leukocytes, microtubules are primarily responsible for cell protrusion in astrocytes and neurons (Euteneuer & Schliwa 1984; Keren et al. 2008). In most cell types, including epithelial and endothelial cells, cellular protrusions require the presence of both actin microfilaments and microtubules, although most MTs do not enter the lamellipodium (Etienne-Manneville 2013). MTs may effect protrusions through microtubule polymerization towards the leading edge, stabilization via association with MAPs, such as MAP4, or through tubulin acetylation or

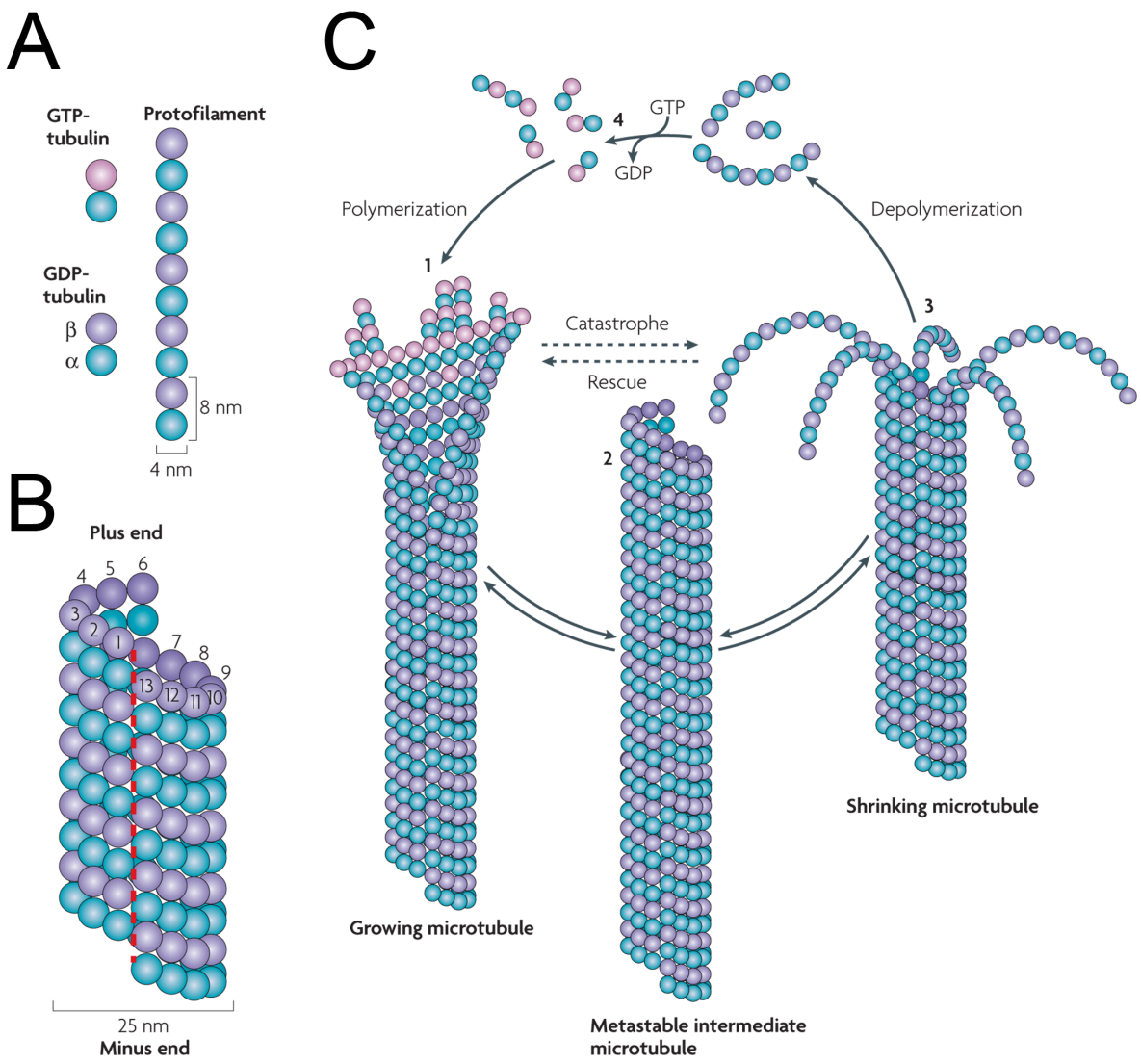

Figure 1.11. Microtubule dynamics. A. MTs are composed of a/b-tubulin heterodimers that assemble to form a protofilament. **B.** The helical microtubule wall typically consists of 13 parallel protofilaments. **C.** Assembly (polymerization) and disassembly (depolymerization) of microtubules is acheived by the binding, hydorlysis and exchange of GTP on the b-tubulin monomer. GTP is needed for the switching between catastrophe and rescue. *Reproduced by permission from Nature Publishing Group: [Nature Reviews Molecular Cell Biology]* (Akhmanova & Steinmetz 2008)*, copyright (2008).*

crosslinking with other cytoskeletal structures (Etienne-Manneville 2004). The targeted delivery of membranes and associated proteins may also contribute to migration. Additionally, MTs may contribute indirectly to cellular migration by interacting with and regulating signaling molecules such as the RhoGTPases (Waterman-Storer & Salmon 1999), which are important for actin polymerization. Lastly, MTs affect focal adhesions by regulating their formation, via their activation of Rac (Rooney et al. 2010), their maturation, by modulating actomyosin contractility (Ren et al. 1999; Waterman-Storer & Salmon 1999) and their disassembly (Kaverina et al. 1998; Krylyshkina et al. 2003).

1.7 Rationale

It is now generally agreed that regulated protein phosphatases play equally essential roles in the control of key cellular processes as their kinase counterparts. One of the major cellular serine/threonine phosphatases is PP1, which gains its substrate specificity from regulatory subunits with which it associates in heteromeric complexes. Although >200 regulatory subunits have been identified to date, we still do not have a clear overview of the dynamic subcellular distribution of PP1, nor a full understanding of its contribution to the wide range of signaling events to which its activity has been linked.

With PP1 now emerging as a promising therapeutic target, it is essential to gain a better understanding of how its' diverse family of regulatory subunits target its catalytic activity throughout the cell. This will in turn help us to design strategies to inhibit specific pools of phosphatase activity while minimizing off-target effects. Although there is evidence of overlap in their targeting and intracellular roles, the three PP1 isoforms also show distinct targeting based on relative preferences and affinities for particular regulatory subunits. Given the overlap of regulatory subunits, it is not surprising that

some compensation has been observed in single isoform knockout experiments. However, for certain functions, this compensation does not occur, which may be attributed to specialized regulatory subunits with PP1c isoform preferences that have evolved to control specific events in higher eukaryotes.

Using GFP-tagged PP1c isoforms stably expressed in a range of cell lines as molecular reporters for the endogenous proteins, we combined fluorescence imaging and cellular fractionation with quantitative AP-MS/MS to characterize their subcellular distributions. The goal was to assemble a comprehensive map of isoform- and compartment-specific phosphatase complexes in interphase and mitotic cells and assign, with confidence, their distribution between known, predicted and novel regulatory subunits. This map, in addition to identifying novel PP1 complexes, will also serve as a baseline for comparing changes in PP1c distribution between these complexes in perturbed cells or disease conditions, to highlight potential therapeutic targets.

1.8 Hypothesis

The combination of a quantitative AP-MS strategy with cellular fractionation, to reduce sample complexity and increase coverage of the regulatory networks to which PP1c is targeted will enable the identification of novel regulatory factors that contribute to the subcellular distribution and physiological function of PP1.

1.9 Aims/Objectives

i) Assemble comprehensive interactome maps for the three PP1 isoforms in human cell lines during interphase and mitosis.

ii) Characterize a novel trimeric complex identified for the beta isoform of PP1 that regulates it distribution between the actin cytoskeleton and the microtubule network.

CHAPTER 2: Materials and Methods

2.1 Cloning and Plasmid Constructs

Most fluorophore (FP) tagged-PP1 constructs were described previously (Trinkle-Mulcahy et al. 2001; Trinkle-Mulcahy et al. 2003), while the PP1β-EGFP was prepared by subcloning human PP1β cDNA into the EGFP-N3 vector.

Full-length Mypt1 and Mypt1 fragments were amplified using specific primers by PCR from human cDNA (Open BioSystems). The PCR products were digested using restriction enzymes (RE) and inserted into the pEGFP/mCherry-C1, pEGFP N3, and pGEX-4-T3 vector. Primers and RE used are listed in Table A1. Similarly, full-length Specc1L and Specc1L fragments were amplified using specific primers by PCR from human Specc1L cDNA (OpenBioSystems). The PCR products were digested using the appropriate RE. Primers and RE used are listed in Table A2. Full length Specc1L and Specc1L fragments were amplified using specific primers and inserted into BioID-HA pcDNA 3.1 and pET-47b (+) vector, respectively, following digestion with the appropriate RE (Table A3). Specc1 (Iso1 and Iso4) was cloned into the pEGFP-N3 vector (Table A4) after amplification by PCR from human cDNA (Open BioSystems) and digestion. Full-length Mypt3, Leng3, PEAK1 (gift from the Klemke Lab) and C20orf27 were amplified using specific primers (Table A5) by PCR from human cDNA (Mypt3-Openbiosystems; Leng3-Addgene; C20orf27-Addgene). The PCR products were digested using the RE listed in Table A5 and inserted into the pEGFP-N3 and/or mCherry-C1 vectors and/or pECYFP-C1 vectors. The Val and Phe residues of the PP1 binding motif in C20orf27 (V55 and F57) were changed to Ala (primers listed in Table A6) using the QuickChange

site directed mutagenesis kit. ASPP2 was a gift from the Holmes Lab, and subcloned into our pEGFP-C1 vector.

2.2 Cell Culture and Transfection Assays

HeLa, MCF7 and U2OS cells, obtained from ATCC, were grown in Dulbecco's modified Eagles' medium supplemented with 10% fetal calf serum and 100 U/mL penicillin and streptomycin (Wisent Bioproducts Inc, St. Bruno, QC). Cells were transfected with either polyethylenimine/PEI (Polysciences, Inc., Warrington, PA) for Immunoprecipitation assays, or Effectene transfection reagent (Qiagen, Valencia, CA) for immunofluorescence (IF) assays. Transfection using PEI was carried out according to Table A10, while transfection with Effectene was carried out according to manufacturers' protocol. For mitotic arrest experiments, cells were treated with either 3.3 μM nocodazole (NOC), or 5 μM S-trityl-L-cysteine (STLC) for 18 h before harvesting by mitotic shake-off. For MT destabilization and disruption of actin polymerization experiments, cells were treated with either 8.3 μM NOC or 2 μM Latrunculin (LAT) for 2 hrs, respectively.

2.3 Stable Cell Lines

Stable cell lines were generated by transfecting U2OS/MCF7/HeLa cells, using the Effectene transfection reagent, with GFP-tagged Specc1L/Leng3/PP1 specific isoforms. Since the pEGFP vector encodes resistance to Neomycin in mammalian cells, cells transfected with GFP-tagged constructs were selected for using a final concentration of 0.8μg/ml of G418 for 10 days. Colonies were picked and expanded further using media containing G418. Mouse Mypt1-GFP Bacterial Artificial Chromosome (BAC) HeLa cell

line, where 2% of the cell line express GFP-tagged mouse Mypt1, was provided by Tony Hyman's lab (Dresden, Germany).

2.4 Lentivirus Production and Infection

HEK293T cells were seeded in 2 x 15 cm dishes and grown to confluence. A 3:1 volume of PEI was added to a 5:3:1 DNA mix containing 27.78 mg of shuttle vector plasmid (lentiviral construct PLVX-Mypt1), 16.66 mg of packaging plasmid psPAX2, and 5.56 mg of pMD2G (broad range VSV-G envelope) in 2.3 mL of serum free media and allowed to incubate at room temperature for 30 minutes to prepare the transfection. The confluent cells were trypsinized, resuspended in 2.5 mL of media, and pelleted at 1000 x g for four minutes. The pellet was resuspended in 2.5 mL serum-free DMEM and the transfection mixture was added in a 1:1 ratio to the cell mix. The 5 mL transfection/cell mix was distributed between 5 x 15 cm dishes and brought up to final volume of 15 mL of DMEM media. The media was changed 6-8 hrs later. The following day transfection efficiency was monitored to ensure > 50% transfection efficiency. On day 3, the supernatant was collected using the Virus Precipitation Kit (Benchmark Biosciences) as per protocol to purify competent lentivirus in high yield. Infections were performed by adding lentiviral-containing supernatant (10μl/1mL media) to cells along with 8 mg of polybrene.

2.5 CRISPR/Cas9 Cloning and Stable Cell line

The target sequences to be used as guide RNAs (gRNA) were designed using the Zhang Lab's online generator (http://crispr.mit.edu/). Oligonucleotides, 5'gRNA CACC-GGAGGCAAACTTGTAAAACC and 3'gRNA AAAC-GGTTTTACAAGTTTGCCTCC specific for the first exon of the Specc1L gene were annealed and phosphorylated in a

thermocycler, and cloned into the Bbs1-digested pSpCas9(BB)-2A-PURO (PX459), a gift from Dr. Ryan Russell (University of Ottawa). For the backbone vector digestion, 1μg of DNA was digested with BbsI for 30 min at 37 °C. The digested PX459 was gel purified using Qiagen Gel Extraction Kit (QIAGEN). The plasmid was transformed into DH5-alpha competent cells and a few of the colonies were picked for screening by sequencing.

U2OS cells were cultured at 37°C, 5% CO2, in Dulbecco's modified eagle medium, supplemented with 10% foetal bovine serum and 1 mM penicillin/streptomycin. Transient transfections of the plasmids sgRNA/Cas9 and control were performed in six-well plates (5 × 105 cells) using PEI.

Cells transfected with the PX459 control plasmid or with the gRNA/Cas9 constructs were placed under selection with Puromycin 1 μg/mL at 24 h of transfection. After three days, the antibiotic selection was removed and all selected cells were left on the plate to recover. After 10-14 days, clonies were then FACs sorted for surviving cells into 96 well plates. We also attempted to pick single colonies from plates treated with puromycin and allowed to recover. The cells were seeded in 96-well plates for expansion and screened by western blot.

2.6 Immunostaining, Fluorescence Imaging and co-localization analysis

For tubulin staining, cells on coverslips (Fisher, CAT# 12-542; Ted Pella, CAT# 260377-15) were washed in PBS, fixed for 10 min in 3.7% (wt/vol) PFA in PHEM buffer, (60mM PIPES pH 6.8, 27 mM HEPES, 20mM EGTA, 16mM $MgSO_4$), pH 7.0 with 10M KOH, at room temperature, or 5 min in ice-cold Methanol. PFA fixed cells were then permeabilized with 1% Triton X-100 in PBS for 10min before staining. For all other fixed cell imaging, cells were washed in PBS, fixed for 5min in 3.7% (wt/vol) paraformaldehyde

(PFA) in CSK buffer (1mM PIPES pH 6.8, 100mM NaCl, 300mM sucrose, 3mM $MgCl_2$, 2mM EDTA) at room temperature, and permeabilized with 1% Triton X-100 in PBS (Blocking Buffer) for 10min. DNA was detected with DAPI (Sigma Aldrich, CAT# D9542).

Following fixation and permeabilization, cells were blocked with 1% Donkey serum (Sigma, CAT# D9663) in 0.2% PBS/tween. Cells were then incubated with appropriate primary (Table A7) and secondary antibodies or dyes (Table A8/A9), diluted in blocking buffer, for 45min at room temperature. Primary antibodies were detected with Alexa-Fluor 488/568/649-conjugated goat anti-mouse/rabbit secondary antibodies (Jackson ImmunoResearch). Blocking and staining of cells with AlexaFluor® 488/568 streptavidin (ThermoFisher Scientific, CAT# S-11223/s-11226) was done in (1%BSA/2%Triton X-100 in PBS). Coverslips were mounted using Vectashield (Vector Labs, CAT# H-1000).

All images were taken using a wide-field deconvolution-based fluorescence microscope (DeltaVision CORE; Applied Precision, Issaquah, WA) equipped with a three-dimensional motorized stage, temperature- and gas-controlled environmental chamber, Xenon light source, and quantifiable laser module (for photobleaching EGFP). Images were collected using either a 40X or 60X NA 1.4 Plan- Apochromat objective and recorded with a CoolSNAP coupled-charge device (CCD) camera (Roper Scientific, Trenton, NJ). The microscope was controlled by SoftWorX acquisition and deconvolution software (Applied Precision).

2.7 Live Cell Imaging and Fluorescence Recovery after Photobleaching (FRAP) experiments

For live cell imaging, cells were cultured in plastic-bottomed dishes (Ibidi, CAT#81156), and DNA was stained by incubating the cells for 20 min in medium

containing 0.25 μg/ml Hoechst No. 33342 (Sigma-Aldrich, CAT# H1399). All images were taken using the DeltaVision CORE microscope (previously mentioned), using a 40X objective.

For FRAP experiments, cells were cultured in glass-bottomed dishes (WilCo Wells, CAT# HBSt-3522). Three single sections were imaged before photobleaching, a region of interest (ROI) was then bleached to ~50% of its original intensity using the 488-nm laser, and a rapid series of images was acquired after the photobleaching period. Recovery curves were plotted and the mobile fraction and half time of recovery were determined using Microsoft Excel and SoftWorX, respectively.

2.8 Super-resolution imaging – direct stochastic optical reconstruction microscopy (dSTORM)

U2OS cells seeded on 18x18 mm coverslips (size 1.5) were transfected for 18 hrs to drive transient over expression of Specc1L-GFP. The cells were PFA-fixed and permeabilized as usual, and then stained with anti-acetylated-alpha-tubulin and anti-mouse-Alexa647. The coverslips were mounted in a 40% Vectashield, 60% Tris/glycerol solution that has been shown to support efficient blinking of Alexa647(Olivier et al. 2013).

Images were acquired on a Quorum spinning disk confocal system (Quorum Technologies) using a 63X/1.4NA objective, a Hamamatsu EM-CCD ImagEM camera and the appropriate laser lines and filter sets. Initially, widefield and spinning disk confocal images were acquired for both the Specc1L-GFP signal (490 nm laser and FITC emission filter set) and the anti-acetylated-alpha-tubulin-Alexa647 signal (639 nm laser and Cy5 emission filter set) using low laser power. A region of interest was then chosen for super-resolution imaging, using the MetaMorph Single Molecule Resolution real time

acquisition and analysis module (Molecular Devices LLC).

Stochastic activation of the Alexa647 fluorophores was achieved by firing the 639 nm laser at full power, which causes them to blink as they cycled through their ON/OFF states. A series of 10,000 images was acquired, and a super-resolved image reconstructed from the individual x-y localizations mapped in each image. This imaging was carried out in the Cell Biology and Image Analysis Core Facility at the University of Ottawa, under the guidance of imaging specialist Tong Zhang.

2.9 Preparation of Cell Extracts

Whole cell lysates were prepared by solubilizing cells with ice-cold RIPA buffer (50mM Tris-HCl pH 7.5; 0.15 M NaCl; 1% (vol/vol) Nonidet P-40; 0.5% (wt/vol) sodium deoxycholate; and protease inhibitor cocktail (Roche, Indianapolis, IN) directly after washing it twice with PBS. Samples lysed in >500µl was sonicated for 1min and 30 sec at 25% amplitude, 10sec on/ 10sec off. Samples lysed in <500µl was passed through a Qiashredder column (Qiagen) to shear DNA. In both cases lysates were cleared by centrifugation at 2,800 x g for 10 min at 4°C. Lysates were separated on 4–12% Novex Nu-PAGE bis-Tris polyacrylamine gels (Invitrogen, Carlsbad, CA) and transferred to nitrocellulose membranes for immunoblotting.

For preparation of cytoplasmic and nuclear fractions, 5-10 x 15cm dishes of cells were trypsinized, pelleted and washed with 1x PBS. Briefly, HeLa cells are resuspended in 4mL of ice-cold swelling buffer (10mM Hepes pH 7.7, 1.5mM $MgCl_2$, 10mM KCl, 0.5mM DTT) and incubated on ice for 5min. Cells are broken open to release nuclei using a pre-chilled Dounce homogenizer (20 strokes with a tight pestle). Lysed cells are centrifuged at 228 x g for 5min at 4°C to pellet the nuclei and other fragments. U2OS

cells are less amenable to douncing and require a different approach to release nuclei. Pelleted U2OS cells are resuspended in ice-cold mild detergent buffer (20mM Tris pH7.4, 10mM KCl, 3mM $MgCl_2$, 0.1% NP40, 10% Glycerol) for 10 min and centrifuged at 1350 x g for 10 min at 4°C to break open cells, in order to release and pellet nuclei and other fragments, with the supernatant retained as the cytoplasmic fraction. The supernatant is retained as the cytoplasmic fraction, where 1mL of 5x ice-cold RIPA buffer is added and cleared by centrifugation. The nuclear pellet, resuspended in 3mL of 0.25M sucrose/10mM $MgCl_2$, was layered over a 3mL cushion of 0.88M sucrose/0.5mM $MgCl_2$) and centrifuged at 2,800 x g for 10min at 4°C to obtain a cleaner nuclear pellet. The nuclear pellet was resuspended in 5mL of RIPA buffer, sonicated and cleared as described above.

In cases where we needed to fractionate our nuclear fraction further, the cleaner nuclear pellet is resuspended in 0.35 M sucrose/0.5 mM $MgCl_2$ and sonicated 6 x 10 sec on ice (10 sec rest between pulses) to disrupt nuclei and release nucleoli, which are visible as dense, refractile bodies. Additional sonication steps may be necessary. The sonicate is layered over a 3 ml cushion of 0.88 M sucrose/0.5 mM $MgCl_2$ and centrifuged at 2800 g for 10 min at 4°C to pellet nucleoli and the supernatant was retained as the nucleoplasmic fraction.

All solutions used in the fractionation, extraction and IP protocols are supplemented with EDTA-free COMPLETE protease inhibitors (Roche) to minimize protein degradation. As a divalent cation, in this case Mg^{2+}, is required to maintain the integrity of nucleoli during sonication, we use a chelator (EDTA)-free protease inhibitor mixture (Muramatsu & Onishi 1978). Total protein concentrations are measured using a Bradford Assay.

2.10 Immunoblotting

For immunoblotting, nitrocellulose membranes were incubated in 5% milk/0.01%Tween 20 in PBS blocking buffer, unless otherwise stated, for 1 hr at room temperature on a shaking platform. The membrane was then incubated for 1hr at room temperature on a shaking platform with the appropriate primary antibody, diluted in the blocking buffer. The membrane was washed 3x for 5min each with PBS-0.01%Tween, after which the membrane was incubated for 1 hr at room temperature on a shaking platform with the appropriate secondary antibody. A full list of primary and secondary antibodies, with the appropriate dilutions can be found in Table A7/A8.

2.11 Immunoaffinity purification of GFP-tagged and endogenous proteins

GFP immunoaffinity experiments were carried out on cells either stably or transiently expressing FP-tagged protein. Cells were lysed in RIPA buffer and first precleared with Sepharose beads. For affinity purification of GFP- and mCh-tagged proteins, extracts were incubated for 1 hr with end-over-end rotation at 4°C with either GFP-Trap_A^{TM} or RFP-Trap_A^{TM}, respectively (Chromotek, Martinsried, Germany). The beads were washed 3x with PBS before use. For immunoprecipitation (IP) of endogenous Mypt1 protein, Mypt1 antibody (Bethyl Lab, A300-888A) was covalently conjugated to protein A Dynabeads (Invitrogen, 100.02D) at a concentration of 12.5 mg/50μl Dynabead slurry. Covalently-conjugated affinity purified IgG (Sigma Aldrich, I8140) from the same species (Rabbit) was used for the control IP. Following the 1 hr IP, the affinity matrix was washed 3x with 1 mL of RIPA buffer/20 μl of beads. For efficient elution of bound proteins, bead equivalent volume of RIPA buffer was added before the addition of 4x

Laemmli sample buffer. The sample was then boiled at 95°C for 10 min before loading the sample onto a pre-casted 4-12% acrylamide gel (Invitrogen).

2.12 Streptavidin affinity purification of biotinylated proteins from cells overexpressing BioID fusion proteins

Cells transiently transfected with the Myc-BioID or BioID-HA pcDNA3.1 constructs were treated at the same time with 50μM biotin overnight. After 16 h the cells were washed twice with PBS and lysed in ice-cold high salt RIPA buffer (50mM Tris-HCl pH 7.5; 0.5 M NaCl; 1% (vol/vol) Nonidet P-40; 0.5% (wt/vol) sodium deoxycholate; and protease inhibitor cocktail (Roche, Indianapolis, IN)). Samples lysed in >500 μl was sonicated for 1 min and 30 sec at a 25% amplitude, 10sec on/ 10sec off. Samples lysed in <500 μl was passed through a Qiashredder column (Qiagen) to shear DNA. In both cases lysates were cleared by centrifugation at 14,000 x g for 10 min at 4°C. For streptavidin affinity purification (AP), extracts were incubated for 4 hrs with end-over-end rotation at 4°C with 40 μl/15 cm dish of Streptavidin agarose beads (Thermo Fisher, CAT# 20359). The beads were washed with 3x with PBS before use. Following the 4 h AP, the affinity matrix was washed 3x with 1mL of high salt RIPA buffer/40μl of beads. For efficient elution of bound proteins, bead equivalent volume of 2x Laemmli sample buffer containing 30 μM excess biotin was added to the beads. The sample was then boiled at 95°C for 10 min before loading the sample onto a pre-casted 4-12% acrylamide gel (Invitrogen).

2.13 Metabolic Labeling for Quantitative Interactome Mapping

Quantitative stable isotope labeling with amino acids in cell culture (SILAC) based affinity purification experiments were carried out as previously described (Trinkle-Mulcahy et al. 2008). For double encoding experiment, cells were encoded in media containing either "light" media containing 12C-isotopes of L-arginine (84 μg/mL) and L- lysine (146 μg/mL) (Sigma-Aldrich, Oakville, ON) and "medium" media containing L-arginine^{13C} and L-lysine 4,4,5,5-D4/ or "heavy" media containing L-arginine$^{13C/15N}$ and L-lysine$^{13C/15N}$ (Cambridge Isotope Laboratories, Andover, MA). For triple encoding experiments, all three medias were utilized. The amino acid concentrations are based on the formula for normal DMEM (Invitrogen). Once prepared, the SILAC media was mixed well, filtered through a 0.22 μm filter (Millipore) using a suction pump, and stored at 4°C.

Protein purifications were carried out separately. The extracts were incubated with their affinity matrix, after which they were removed and washed once with ice-cold RIPA buffer. Following the first wash, the control and experimental beads were carefully combined and washed an additional three times with ice-cold RIPA buffer. To ensure efficient elution of bound proteins, a bead equivalent volume of 1% SDS (or 2% SDS with 30 μM biotin, in the case of BioID-SILAC experiments) was added. The matrix was then boiled for 10 min followed by adding a 4x volume of dH_2O and boiled for an additional 10 min. The samples were vortexed and the solution removed and reduced to the original bead-equivalent volume (and 1% SDS concentration) using a speedvac. Proteins in solution were then reduced, by the addition of 10 mM DTT (boiled for 10 min), and alkylated, with the addition of 50 mM iodoacetamide (incubated at room temperature in the dark for 30 min). A small aliquot of Laemmli sample buffer was added to protein

solution, boiled for 10 min and separated by running halfway down NuPAGE 10% Bis-Tris gels. Gels were coomassie stained (Invitrogen), as per manufactures protocol, and destained overnight before excision of gel slices. The gel slices were further destained and peptides were extracted from the gel slices after an overnight digestion using 10 μg/ml trypsin solution (enough to cover the gel pieces), and prepared for mass spectrometry (MS) analysis.

2.14 Mass Spectrometry and Data Analysis

An aliquot of the tryptic digest (prepared in 1% Formic Acid) was analyzed by LC-MS/MS (liquid chromatography – tandem mass spectrometry) on an UltiMate 3000 RSLC nano HPLC (Dionex) and an LTQ-Orbitrap XL hybrid mass spectrometer with nanospray ionization source (Thermo Scientific) at the OHRI Proteomics Core Facility (Ottawa, Canada). The system was controlled by Xcalibur software version 2.0.7 (Thermo Scientific). Peptides were loaded onto a C18 CapTrap column (Michrom) for 5 min at a flow rate of 15 μL/min and then eluted over a 60 min gradient of 3%-5% acetonitrile with 0.1% formic acid at a flow rate of 0.3 microlitres per minute onto a 10 cm long column with integrated emitter tip (Picofrit PF360-75-15-N-5, New Objective packed with Zorbax SB-C18, 5 micron, Agilent), and nanosprayed into the mass spectrometer. MS scans were acquired in FTMS mode at a resolution setting of 60,000. MS/MS scans were acquired in ion trap CID mode using data-dependent acquisition of the top 5 ions from each MS scan. Database searching (against the human IPI database v3.68; 87,061 entries) and quantitation were performed using MaxQuant software v1.2.7.4 or v1.5.5.1 and the Andromeda search engine(Cox et al. 2009; Cox et al. 2011). The following criteria were used: peptide tolerance = 10 ppm, trypsin as the enzyme (2 missed

cleavages allowed) and carboxyamidomethylation of cysteine as a fixed modification. Variable modifications were oxidation of methionine and N-terminal acetylation. Medium SILAC labels were Arg6 and Lys4 and heavy SILAC labels were Arg10 and Lys8. Minimum ratio count was 2 and quantitation was based on razor and unique peptides. Peptide and protein FDR was 0.01.

2.15 His-tagged Protein Purification

Recombinant 6x His-tagged Specc1L fragments were transformed in BL-21 cells. Briefly, the constructs were mixed with 50µl of bacteria on ice for 20min, heat-shocked for 45sec at 42°C, cooled on ice and incubated at 37°C with 1mL of LB. The transformation was then plated on respective antibiotic resistant plates overnight at 37°C. LB was inoculated with a colony and grown up into a larger culture (500mL) and induced with 0.5mM IPTG once the OD_{600} reached ~0.5. The induced culture was left overnight shaking at 16°C. The following day the culture was pelleted, resuspended in buffer (20 mM Tris pH 7.5, 250 mM NaCl, 10 mM Imidazole). 1 mg/mL of Lyzozyme was added and incubated on ice for 30 min, followed by sonication (30 sec on/off for 2 min) to further lyse the samples. The cell debris was pelleted, and the lysate was incubated with 100 µl of Ni^{2+} -NTA agarose beads (Qiagen, 1018244)/ 5 mL of cell lysate (beads were washed 2x with PBS and 3x with Equilibration buffer (20 mM Tris pH7.5 and 0.5 M NaCl) with 2x the bead volume each time) at 4°C for 1 hr on end-over-end rotation. The beads were pelleted and washed 3x in buffer (20 mM Tris pH7.5, 0.5 M NaCl, and 20 mM Imidazole). The His-tagged proteins were eluted with elution buffer (20mM Tris pH7.5, 0.5M NaCl, and 300mM Imidazole) at 500 µl increments. Eluted proteins were dialyzed in TGEM buffer (20 mM Tris-HCl pH7.9, 0.1 M NaCl, 20% glycerol, 1mM EDTA, 5 mM $MgCl_2$, 0.1%

NP-40, 0.2 mM PMSF) for in test tube IPs. After dialysis 1 mM DTT was added before the IP experiment.

2.16 GST-tagged Protein Purification

GST-tagged Mypt1 (CD) and MyptN98 fragment was transformed in Rosetta™ cells. Briefly, the constructs were mixed with 50 µl of bacteria on ice for 20 min, heat-shocked for 45 sec at 42°C, cooled on ice and incubated at 37°C with 1 mL of LB. The transformation was then plated on respective antibiotic resistant plates overnight at 37°C. LB was inoculated with a colony and grown up into a larger culture (500 mL) and induced with 0.2 mM-0.5 mM IPTG once the OD_{600} reached ~0.5. The induced culture was left overnight shaking at 16°C. The following day the culture was pelleted, resuspended in buffer (50 mM Tris pH 8.0, 2 mM EDTA pH 8.0, 0.1% BME, and protease inhibitor cocktail (ROCHE)), and lysed by sonication (30 secs on/off for 2min). Samples were centrifuged at 40,000 x g and the lysate was incubated with 500 µl of Glutathione sepharose beads (GE Healthcare, CAT#17-0756-01) (beads were pre-washed 2x with PBS and equilibrated 3x with Equilibration buffer (20 mM Tris pH7.5, 0.25 M NaCl, 2 mM EDTA, 2 mM EGTA, 1% Triton X-100) with twice the bead volume each time) at 4°C for 1 hr on end-over-end rotation, after the addition of NaCl at a final concentration of 0.25 M. The beads were pelleted and washed 3x in buffer (20 mM Tris pH7.5, 0.25 M NaCl, 2 mM EDTA, 2 mM EGTA) with 5x the bead volume each time. GST-Mypt1(CD) was eluted using 10 mL of wash buffer containing 61 mg of reduced glutathione and 13 µl of 10 M NaOH (pH 8.0). The eluted protein was dialyzed in TGEM buffer (20 mM Tris-HCl pH 7.9, 0.1 M NaCl, 20% glycerol, 1 mM EDTA, 5 mM $MgCl_2$, 0.1% NP-40, 0.2 mM PMSF) for in test tube IPs. After dialysis 1 mM DTT was added before the IP experiment.

For GST-MyptN98, 50 units of Thrombin (GE Healthcare, CAT# 27-0846-01) was added to ~500 μl of Glutathione sepharose beads (resuspended in 500 μl of Wash buffer) and incubated at 30°C for 45 min on a thermomixer (Eppendorf) shaking at 1300 rpm. To remove the thrombin, the eluted protein lysate was treated with 80ul bead volume of Benzamidine agarose (Sigma, CAT# A7155) for 30 min at room temperature on a thermomixer shaking at 1300rpm. The purified lysate was sent to Medimabs (Montreal, Canada) where the purified MyptN98 was injected into rabbits. Titers of 1:100,000 were obtained in two rabbits, after which they proceeded with boost immunization, production bleeding and final bleeding. Once we received the crude sera, we affinity purified the antibody using our purified MyptN98 antigen coupled to CNBr- Sepharose beads. Briefly, 0.3 μg of Freeze-dried Sepharose (SIGMA) was rehydrated in ice-cold 10 mM HCl (6x 10mL washes). The CNBr-sepharose was washed once in CNBr coupling buffer (0.1 M Na_2CO_3, 0.5 NaCl pH 8.3) After the last wash, the beads were vaccum dried till the column cracked, and incubated with our purified MyptN98 (dialyzed into CNBr coupling buffer) for 2 hrs at room temperature. Remaining active groups on column were blocked by the addition of 6 mL of coupling buffer plus 0.2 M glycine for 2 hrs at room temperature. Excess protein was washed off by 4x washes of alternating coupling buffer (5 mL) and then acetate buffer (5 mL). This was followed by three additional washes of coupling buffer. The beads were then washed with 15 mL of TBST (20 mM Tris, 150 mM NaCl, 0.1% Tween-20, pH 7.5). 10 mL of the final bleed sera was diluted with 40 mL of TBS-T and filtered with a 0.22 μm syringe filter. The Sera was then loaded on the CNBr column (now coupled to the Mypt1N98 protein) and then subsequently washed with 20 mM Tris, 0.4 M NaCl, pH 7.5 to eliminate the non-specifically bound proteins. The

antibody was eluted with 10 mL of 50 mM Glycine, pH 2.5, and collected in 1 mL fractions in eppendorf tubes containing 50 μl of 1.5M Tris, pH 8.8 to bring the pH back up to 7 quickly. The protein concentration was then checked by the Bradford assay. The purified antibody was tested by western blot analysis by pre-incubating the purified antibody with the Mypt1/N98 antigen, before using it on a western blot to detect endogenous Mypt1. The antibody was also tested for immuoprecipitation assays when conjugated to protein A Dynabeads.

2.17 Far Western Blot

Purified recombinant His-tagged Specc1L fragments (6 μg each) were electrophoresed and transferred to nitrocellulose membrane (as previously described). The membrane was incubated overnight with 10% milk (in PBS + 0.5 % Tween) to block nonspecific binding sites and washed 3x with PBS/0.5%Tween, then 1x with PBS, before it was overlaid with 5 μg purified recombinant GST-Mypt (CD) or purified GST in 5 mL of 1mg/mL BSA/PBS solution. Primary anti-GST (Thermo, CAT# PA1-982A), with a secondary mouse-HRP antibody was used to detect the GST and GST-Mypt1 interactions.

2.18 *In vitro* Co-immunoprecipitation

Purified recombinant HisSpecc1LΔCD was combined with immobilized GST and GST-Mypt1(CD) on Glutathione agarose beads in vitro. Briefly, 1.6 μg of GST and GST-Mypt1(CD) was immobilized on 10μl Glutathione Agarose beads (pre-washed in TGEM buffer), where the bead/purified protein was brought up to 80 μl in TGEM buffer and incubated for 2 hrs on the thermomixer at 4°C. The immobilized GST and GST-Mypt1

(CD) was incubated with 1.6 μg of HisSpecc1LΔCD in a pulldown assay separated on a SDS-PAGE gel, transferred to nitrocellulose and detected with an anti-His antibody to detect the Specc1L fragment. The blot was stripped and detected with an anti-GST antibody to confirm the presence of GST and GST-Mypt1(CD).

2.19 Microtubule Binding Protein Spin-down Assay

The Microtubule Binding Protein Spin-down assay was performed according to manufacturers' protocol (Cytoskeleton, CAT# BK029). Briefly, stabilized microtubules were prepared by incubating a 20 μl aliquot of Tubulin protein (5 mg/mL) at 35°C with 2 μl of Cushion Buffer (80 mM PIPES pH7.0, 1 mM $MgCl_2$, 1 mM EGTA, 60 % glycerol) for 20 min on ice. 2 μl of 2 mM Taxol was added to 200 μl of preheated (at 35°C) General Tubulin Buffer (80 mM PIPES pH 7.0, 2 mM $MgCl_2$, 0.5 mM EGTA), which was immediately added to the MTs after the 20 min incubation on ice. The sample was gently and thoroughly mixed and left at room temperature, allowing the MTs to stabilize. 20 μl of the stable microtubules were then mixed with either Bovine serum albumin (BSA), MAP fraction, or our test protein (2-5 μg) according to the manufacturers' protocol. After a 30min incubation the samples were carefully pipetted onto 100 μl of Cushion Buffer (1 mL containing 10 μl of 2 mM Taxol) and centrifuged at 100, 000 x g at room temperature for 40 min. The uppermost supernatant layer (50 μl) was removed and added to 16.7 μl of 4x Laemmli sample buffer. The remaining supernatant was removed and disposed of. The pellet was resuspended in 66.7 μl of 1x Laemmli sample Buffer. 20 μl of the supernatant and pellet sample were run on an SDS- PAGE gel.

CHAPTER 3: Assembly of a comprehensive map of PP1 isoform distribution in holoenzyme complexes reveals overlapping associations and distinct preferences and identifies novel binding partners

Loss of function and biochemical studies of individual PP1 genes in eukaryotic organisms suggest some level of compensation but also highlight distinct phenotypes associated with the disruption of a single gene (Korrodi-Gregório et al. 2014). Although evolutionary conserved in their catalytic domain, the significant variability in their amino- and carboxyl-terminal sequences of the PP1 genes likely determines any unique functions, with certain regulatory subunits showing preferential association with a particular subunit (Scotto-Lavino et al. 2010; Ferrar et al. 2012; Trinkle-Mulcahy et al. 2006; Chamousset, De Wever, et al. 2010). This reinforces the importance of a better understanding of the distribution of the PP1 isoforms between these regulatory subunits, which confer the subcellular localization and function of the phosphatase (Brush et al. 2003; Trinkle-Mulcahy et al. 2001; Trinkle-Mulcahy et al. 2003; Lesage et al. 2007).

Analysis of the individual PP1 isoforms is complicated by the lack of specific and robust reagents. Our lab and others have tested a range of commercial “isoform-specific” antibodies against PP1 isoform fusion proteins and demonstrated varying degrees of cross-reactivity for all of them (Trinkle-Mulcahy et al. 2003; Lesage et al. 2004). In addition, none are sufficiently robust or reliable for immunoprecipitation or immunofluorescence analysis. Having confirmed that GFP-tagged PP1 isoforms are active phosphatases that associate with known regulatory subunits (Trinkle-Mulcahy et al. 2001; Trinkle-Mulcahy et al. 2003), we established a collection of cell lines that stably

express them at very low levels and adapted this as our method of choice for analyzing each one independently, both by imaging and by proteomic analysis. This allows us to define their distinct and dynamic localization patterns and the interaction networks that underlie their subcellular distributions. As presented below, the comprehensive PP1 isoform distribution map that we have assembled in multiple cell lines has enabled the identification of new signaling hubs, confirmed previous results linking PP1 activity to certain cellular structures/pathways, and identified new functional roles for the phosphatase.

3.1 The PP1 isoforms are more equally distributed between the cytoplasm and nucleus than the predominantly cytoplasmic PP2 family phosphatases

Serine/threonine protein phosphatases have been linked to the regulation of signaling pathways throughout the cell, with PP1 believed to play a prominent role in nuclear events (Moorhead et al. 2007). We first assessed its subcellular distribution using a combination of cell fractionation and quantitative mass spectrometry. Specifically, U2OS cells were differentially labeled by passaging for 7-10 days in “Light” and “Heavy” SILAC media, at which point the cells were harvested and fractionated into cytoplasm (CP) and nuclei (NUC) using a detergent-based method that we had previously optimized for this cell type (Chamousset, Mamane, et al. 2010; Fox et al. 2015) (Figure 3.1A). This allowed us to directly compare the distribution of all identified proteins between the two compartments, by combining cell equivalent volumes of Heavy CP and Light NUC extract for LC-MS/MS analysis and MaxQuant-based quantitation of H:L ratios (i.e. CP:NUC distribution). To reduce sample complexity and increase coverage, the combined sample

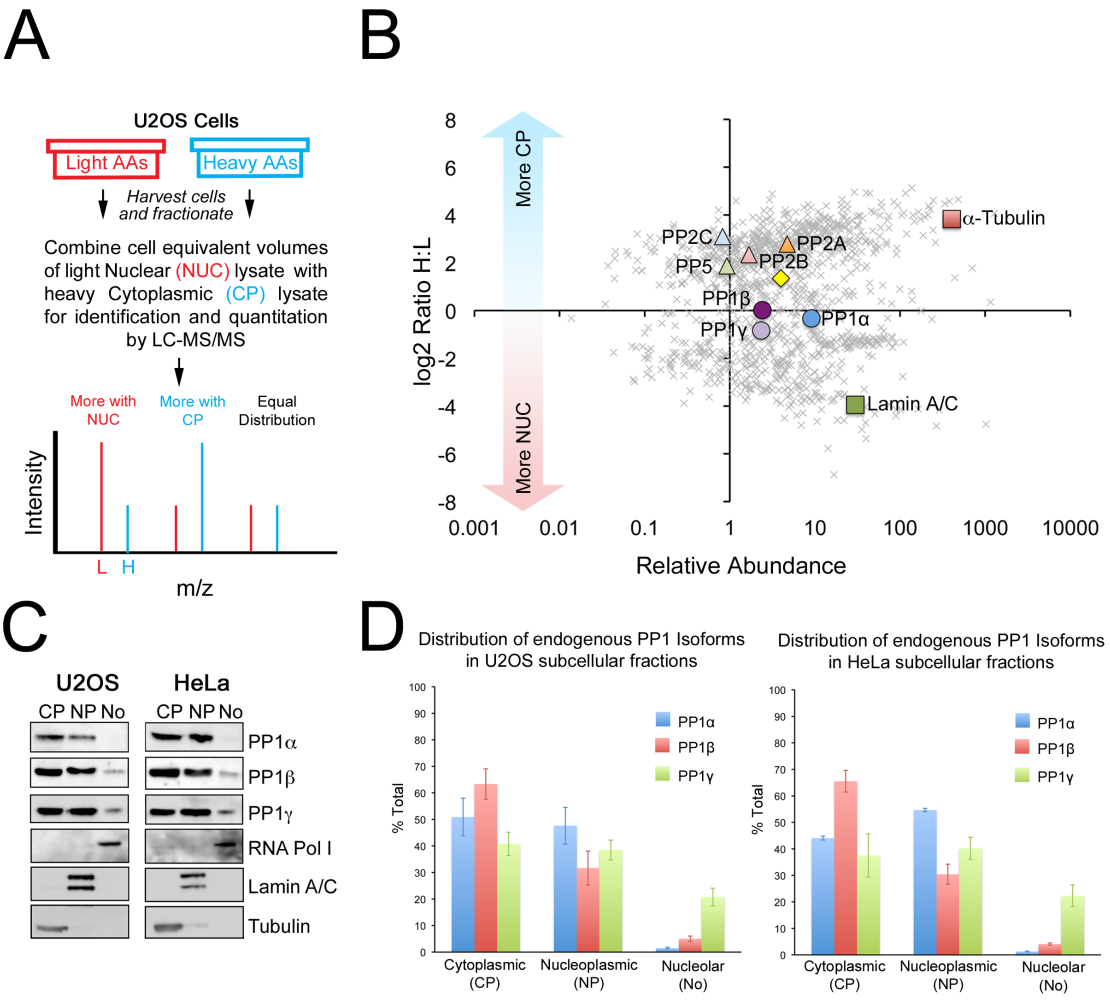

Figure 3.1. PP1 isoforms exhibit a more equal cytoplasmic/nuclear distribution compared to other type 2 serine/threonine phosphatases. A. Design of quantitative subcellular proteome mapping experiment directly comparing the distribution of proteins between cell equivalent volumes of Nuclear (NUC; R0K0) and Cytoplasmic (CP; R6K4) U2OS extracts. **B.** Plotting log2 H:L ratio (CP:NUC distribution) vs. relative abundance (normalized intensities) for each identified protein highlights the distribution of the three PP1 isoforms relative to other type 2 serine/theronine phosphatases. Common CP (α-tubulin) and NUC (Lamin A/C) markers distributed as expected, confirming the extraction efficiency. **C.** Stringently validated PP1 isoform-specific antibodies were utilized for Western blot analysis to assess the distribution of PP1α, β and γ between Cytoplasmic (CP), Nucleoplasmic (NP) and Nucleolar (No) extracts from U2OS and HeLa cells. CP (Tubulin), NP (Lamin A/C) and No (RNA Pol I; A190) markers confirmed the extraction efficiency. **D.** Quantitation of the data in (C), plotted as mean ± SE for three biological replicates.

was first separated by 1D SDS-PAGE and the entire gel lane cut into 5 slices for in-gel trypsin digestion. Aliquots were injected onto a Thermo Orbitrap mass spectrometer, and the resulting raw data files analyzed using MaxQuant 1.2.7.4, for both protein identification (via the Andromeda search engine) and quantitation of H:L ratios and total peptide intensities. All 5 slices were analyzed as a concatenated dataset, and >1100 proteins identified/quantified. Although this is not full coverage of the human cellular proteome, we did identify/quantify all three PP1 isoforms plus several PP2 family members.

The full dataset was plotted as log(2) Ratio H:L vs. Relative Abundance (Figure 3.1B). Given that a log Ratio of 0 represents equal distribution (ratio 1:1) between CP and NUC, we chose a threshold of 1 log above/ below this value (i.e. 2-fold enrichment in either direction) to classify proteins as CP-enriched (53%), NUC-enriched (33%) or equally distributed (14%). As expected, the commonly utilized CP marker, α-tubulin, was strongly CP-enriched (log(2) H:L = 3.82), while the commonly utilized NUC marker, Lamin A/C, was strongly NUC-enriched (log(2) H:L = -3.94). Other protein families were found enriched in the expected fractions, such as the CP myosin/tubulins/filament proteins/GAPDH and the NUC histones/hnRNPs/splicing factors.

The distribution of identified Ser/Thr phosphatases between the two subcellular fractions is highlighted on the graph (Figure 3.1B). In general, PP2 family phosphatases (PP2A, PP2B, PP2C and PP5) were all enriched >2-fold in the CP fraction. We also identified four PP2A regulator subunits in our dataset (PPP2R1A/1B, PPP2R2A and PPP2R4), which were also enriched in the CP fraction. In contrast, the PP1 isoforms were found to be more equally distributed, with log2 H:L ratios of -0.33, 0.015 and -0.84,

for PP1α, PP1β and PP1γ, respectively. Thus, although type 1 and type 2 ser/thr phosphatases have been linked to both cytoplasmic and nuclear roles, PP1 holoenzyme activity is distributed more equally between these subcellular compartments in comparison to the PP2 family members.

At this time, in-house PP1 isoform-specific antibodies became available through a collaborator, Dr. Greg Moorhead, at the University of Calgary. We tested them against expressed fusion proteins and concluded that they showed minimal cross-reactivity in Western blot assays, provided the anti-PP1α antibody was first cross-absorbed with the PP1β immunogenic peptide (Ferrar et al. 2012). Unfortunately, they were not sufficiently robust or reliable for immunoprecipitation or immunofluorescence assays.

They did, however, allow us to compare the distribution of each PP1 isoform between subcellular fractions by Western blotting. For these experiments, we further fractionated the purified nuclei into nucleoplasmic and nucleolar fractions. Previous studies had demonstrated accumulation of PP1β and PP1γ with the nucleolus, a subnuclear organelle implicated in a range of key roles including regulation of ribosome biogenesis, stress sensing and cell cycle progression. It should be noted that PP1α is not excluded from nucleoli, but does not accumulate there to the same extent as the other isoforms (Lesage et al. 2005; Trinkle-Mulcahy et al. 2001; Trinkle-Mulcahy et al. 2006; Chamousset, De Wever, et al. 2010; Andreassen et al. 1998). While α-tubulin remained our CP marker and Lamin A/C our nuclear marker, we added the RNA Pol I subunit A190 as our nucleolar marker.

Figure 3.1C summarizes the distribution of the three PP1 isoforms between CP, NUC and nucleolar (No) fractions prepared from U2OS and HeLa cells. The

fractionations were repeated three times for each cell line and the Western blots imaged and analyzed using a FUJI LAS-4000 chemiluminescence imager and MultiGauge software (GE Healthcare). Briefly, the intensity/area (- background) of the isoform band in each subcellular fraction was measured and represented as a fraction of the summed intensity/area of all the fractions (Figure 3.1D).

We first compared the distribution of the isoforms between the Cytoplasm and Nucleus (in this case, the summed NP and No fractions) in U2OS cells, and found that it was consistent with the pattern observed by MS analysis. Specifically, PP1β is more cytoplasmic (63.3 ± 5.75% CP) and PP1γ more nuclear (40.8 ± 4.38% CP), while PP1α is equally distributed (50.9 ± 7.09% CP). The nucleolar fractions were also consistent with previous observations, representing 1.5 ± 0.35% of total PP1α, 5.0 ± 1.0% of total PP1β and 20.7 ± 3.32% of total PP1γ.

We next tested whether these distribution patterns are cell type- or fractionation method-specific by mapping them in HeLa cell fractions. We chose HeLa cells because they are amenable to an alternate fractionation strategy based on Dounce homogenization to physically break open cells (Fox et al. 2015). Using the same quantitation strategy, a similar trend was observed (Figure 3.1D), with PP1β more cytoplasmic (65.5% ± 4.07% CP), PP1γ more nuclear (37.5 ± 8.15% CP) and PP1α more equally distributed (44.1 ± 0.75% CP). With regard to nucleolar pools, they represent 1.3 ± 0.16% of total PP1α, 4.1 ± 0.45% of total PP1β and 22.3 ± 4.09 % of total PP1γ. This is the first time that a high stringency analysis has been carried out on the distribution of individual PP1 isoforms throughout the cell, confirming that PP1γ likely represents the predominant nucleolar phosphatase activity, as previously suggested (Trinkle-Mulcahy et

al. 2003). Given the importance of a homeostatic balance of phosphatase activity throughout the cell and the consequent potential for overexpression artefacts, it also provides us with a baseline against which the behavior of molecular reporters for these proteins can be measured.

3.2 Stably overexpressed GFP-tagged PP1 isoforms show similar subcellular distribution patterns to their endogenous counterparts.

In order to map isoform-specific interactomes for the three PP1 isoforms, we needed to adopt a fusion protein approach that is compatible with both imaging (to confirm in vivo localization patterns) and affinity purification (for Western blot and AP/MS analysis). We chose the GFP tag, as we had previously validated it as an ideal affinity tag based on the minimal non-specific binding of GFP to cellular proteins and the ability to efficiently deplete GFP-tagged proteins from cell extracts using the high affinity GFP-Trap agarose matrix (Trinkle-Mulcahy et al. 2008). This reagent is based on the GFP binder (Rothbauer et al. 2008), a 13 kD protein derived from a Llama heavy chain antibody that binds with high affinity and specificity to GFP. We had previously used GFP tagging to compare the localization patterns of transiently (Trinkle-Mulcahy et al. 2001) and stably (Trinkle-Mulcahy et al. 2003; Trinkle-Mulcahy et al. 2006) overexpressed PP1 isoforms, and to identify novel nuclear binding partners for PP1α and PP1γ (Trinkle-Mulcahy et al. 2006; Chamousset, De Wever, et al. 2010). Our work confirmed that cells cannot tolerate transient overexpression of high levels of PP1 fusion proteins (Trinkle-Mulcahy et al. 2001), but stable overexpression of full-length and functional tagged PP1 isoforms at very low levels is achievable in certain cell lines (Trinkle-Mulcahy et al. 2003; Trinkle-Mulcahy et al. 2006). It has been suggested that the regulatory subunits are found

in excess of the catalytic subunits in cells, which would explain this ability to adapt to increased phosphatase levels (Heroes et al. 2013).

Our previous work had been limited to the α and γ isoforms, as we found that PP1β was more susceptible to degradation, particularly if the GFP tag is fused to the N-terminus. In order to compare all three directly in an AP/MS experiment, we first obtained GFP-PP1 isoform HeLa stable cell lines from the Hyman Lab (Dresden, Germany) generated using the Bacterial Artificial Chromosome (BAC) strategy (Zhang et al. 1998; Poser et al. 2008). As detailed in Figure. 3.2A(I), the BAC constructs, randomly integrated into the genome by antibiotic selection, drive the expression of GFP-tagged proteins under the control of their endogenous promoters. This minimizes overexpression artefacts, although it is an overexpression as the endogenous protein is still expressed. We screened both N- and C-terminally tagged fusion proteins using the workflow detailed in Figure 3.2A(III), confirming that N-terminally tagged PP1α and γ and C-terminally tagged PP1β are full-length, active phosphatases that associate with known binding partners in their respective stable cell lines. It should be noted that the PP1α and PP1γ BAC constructs contain the human genes, whereas the PP1β BAC construct contains the mouse gene. This is not an issue at the protein level, as mouse and human PP1β share 100% amino acid (94% nucleotide) identity.

Live cell fluorescence imaging was used to assess the localization of the GFP-tagged PP1 isoforms in HeLa/BAC stable cell lines in which the nucleus was stained with the cell permeable dye Hoechst 33342 (Figure 3.2B). The distinct patterns approximated those previously observed for low levels of transient or stable overexpression (Trinkle-Mulcahy et al. 2006; Trinkle-Mulcahy et al. 2001; Trinkle-Mulcahy et al. 2003), and for

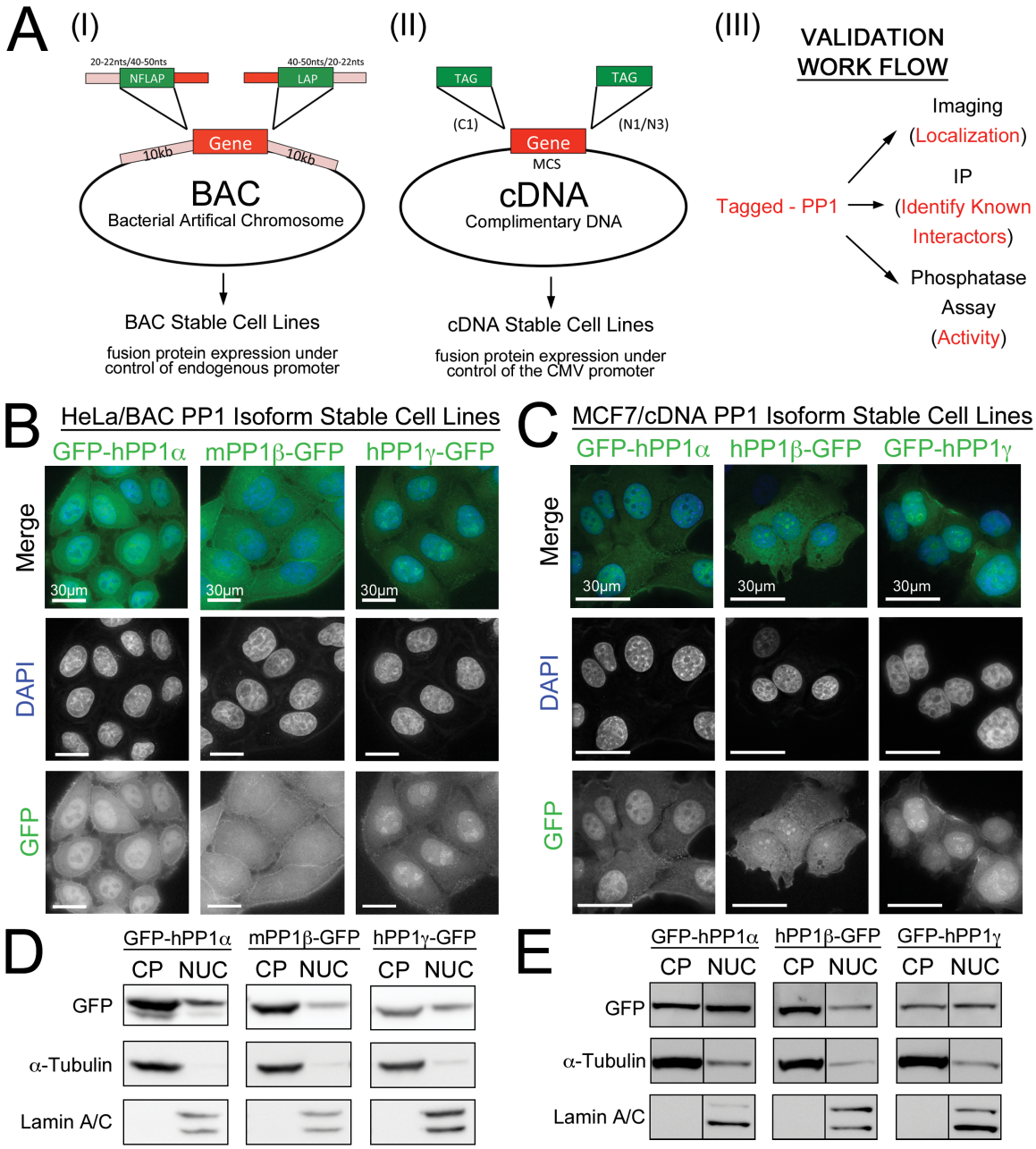

Figure 3.2. Stable cell lines facilitate the direct comparison of GFP-tagged PP1 isoforms. A. Strategies utilized to create HeLa/BAC (I; Hyman lab, Germany) and MCF7 (II) stable lines via random genomic integration of expression constructs. For all stable lines the validation workflow (III) included confirmation of expression of a full-length fusion protein that shows the expected localization, associates with known interactors (by IP/Western blot analysis) and is an active phosphatase (by IP/phosphatase assay). **B.** Localization of GFP-tagged PP1 isoforms (green) in live HeLa/BAC lines stained with Hoechst 33342 (blue). **C.** Localization of GFP-tagged PP1 isoforms (green) in live MCF7/cDNA lines. Western blot analysis mapped the isoforms' distributions between Cytoplasmic (CP) and Nuclear (NUC) extracts in the HeLa (**D**) and MCF7 (**E**) cell lines.

endogenous PP1 isoforms stained with antibodies in fixed cells in an early study (Andreassen et al. 1998). Our first observation was that PP1α is expressed at much higher levels, as we had to increase the exposure time when imaging the PP1β and PP1γ fusion proteins. When acquisition parameters optimized for GFP-PP1α imaging were utilized with the PP1β-GFP and GFP-PP1γ cell lines and the resulting intensities displayed on the same scale, their GFP signals were not detected (Appendix II I, Figure A.1). Given that they are under the control of their endogenous promoters, this suggests that PP1α is the most highly expressed PP1 isoform, at least in HeLa cells. We confirmed this by quantitation of the level of each fusion protein on a Western blot relative to a tubulin loading control (Figure 3.2D). Cells were fractionated for preparation of CP and NUC extracts using our Dounce-based strategy and the fusion proteins monitored with anti-GFP antibodies. The CP and NUC markers were α-tubulin and Lamin A/C, respectively. Quantitation of three biological replicates showed that the total level of GFP-PP1α (CP + NUC) is approximately 1.5x that of PP1β-GFP and 2x that of GFP-PP1γ. Quantitation of their CP/NUC distributions showed that the amount in the CP fraction was higher than normal for all three cell lines, although the trends were maintained (mPP1β-GFP 78.1 ± 5.9% CP, GFP-hPP1α 72.5 ± 1.9% CP and hPP1γ-GFP 65.8 ± 4.2% CP).

We also generated MCF7 cell lines stably overexpressing GFP-tagged PP1α, PP1β and PP1γ (all human genes) by random integration of plasmids in which a CMV promoter drives fusion protein expression (Figure 3.2A(II)). Although unstable in HeLa cells when incorporated in this way, as previously noted, we had found that PP1β-GFP was expressed as a full-length fusion protein in U2OS cells (Chamousset, De Wever, et

al. 2010), and fortunately the same was observed in MCF7 cells. Fluorescence imaging of live Hoechst-stained cells confirmed the expected localization patterns for the individual isoforms (Figure 3.2C), with GFP-tagged PP1β showing a more evident accumulation in nucleoli than it did in the HeLa/BAC stable line.

Cells were next fractionated for preparation of CP and NUC extracts. We tested several methods with this cell line, and although none were ideal, the best was the detergent method that we use for U2OS cells. Carryover of tubulin into the NUC fraction (Figure 3.2E) suggests inefficient cell lysis, however the in vivo localization data supported the expected distribution patterns for the isoforms.

3.3 The three PP1 isoforms show both overlapping and a preference of association with known targeting subunits

The HeLa/BAC and MCF7/cDNA GFP-tagged PP1 stable cell lines provided, for the first time, the opportunity to directly compare the distribution of the isoforms in complexes throughout the cell. We decided to do this by differentially labeling the three isoform cell lines with Light, Medium and Heavy amino acids, to directly compare the L:M:H ratios of all identified interactors (Figure 3.3A). A caveat of this approach is that some genuine interactors that associate with more than one PP1 isoform will end up buried in the cluster of proteins around a ratio of 1:1:1, which includes those that bind non-specifically to the beads. We can, however, annotate the datasets to highlight all known/predicted regulatory subunits and compare their distributions between the isoforms.

To reduce sample complexity and increase coverage, we fractionated the isotopically labeled HeLa/BAC and MCF7 stable cell lines for preparation of CP and NUC

extracts, and performed the pulldown experiments on these extracts. After an initial RIPA wash, the three sets of GFP-Trap beads (Light/PP1α, Medium/PP1β, Heavy/PP1γ) from the same extracts (either CP or NUC) were combined and washed, and all captured proteins eluted using 1% SDS for separation by 1D SDS-PAGE. The entire CP and NUC gel lanes were cut into 5 slices, each for in-gel trypsin digest, and an aliquot of the tryptic digest was sent to the MS facility for analysis on a Thermo Orbitrap System. Using the MaxQuant (Version 1.5.5.1) software, which utilizes a built-in search engine (Andromeda) for protein identification, we assembled CP and NUC datasets for both cell lines with H:L (γ:α), M:L (β:α) and H:M (γ:β) ratios calculated for each protein.

In the BAC/HeLa experiment we identified/quantified 243 CP and 421 NUC proteins, including GFP and the three PP1 isoforms that we pulled down. The GFP distribution confirmed that more PP1α was captured, as expected, given that at least 2-fold more is expressed compared to the other isoforms. We therefore related the distribution of targeting subunits to the amount of GFP captured, as it is the most accurate reflection of the amount of each isoform that was pulled down. In the MCF7/cDNA experiment we identified/quantified 245 CP and 714 NUC proteins, including GFP and the three PP1 isoforms. Similar to our HeLa/BAC experiment, a higher amount of GFP-PP1α was captured compared to the other two isoforms, and we again used GFP as our internal reference.

Annotating the data sets manually allowed us to highlight all known and predicted regulatory subunits identified in both subcellular fractions (Figure 3.3B). Some like Mypt2 and SH2D4A, were identified in only one cell type, which likely indicates differences in their expression levels in the two cell types. For those identified in both cell lines, most

A

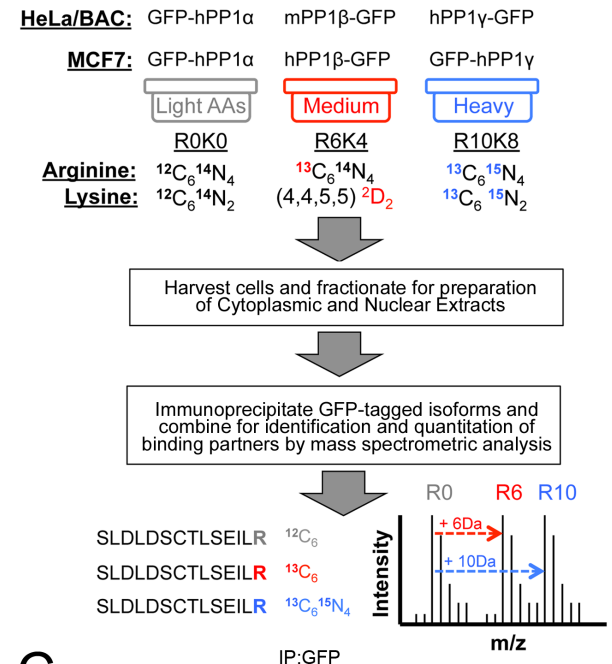

C

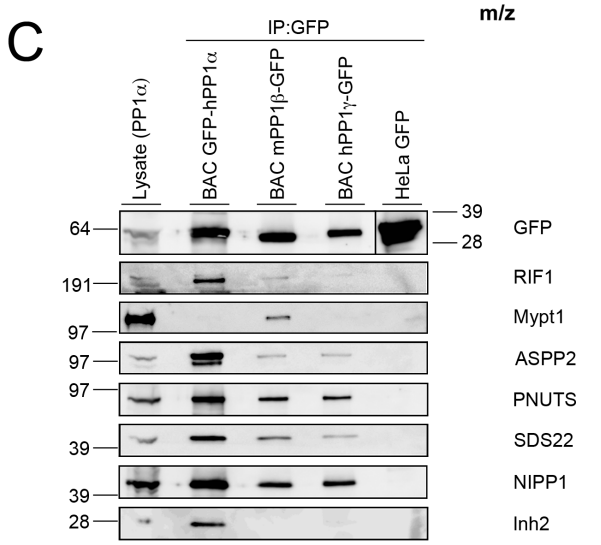

B

PP1α vs PP1β vs PP1γ

Known/Predicted Regulatory Subunits		CYTOPLASMIC INTERACTOME			
		BAC/HeLa cell Lines		MCF7 Cell Lines	
		# Peptides	Preference	# Peptides	Preference
ASPP1	PPP1R13B	9	α	27	
ASPP2	PPP1R13A	25	α > β/γ	17	α > β/γ
DDX21				2	β
HDAC6		7			
iASPP	PPP1R13L	30	α/β	37	α/β > γ
Inh2	PPP1R2	8	α/γ > β	11	
Inh3	PPP1R11	7		7	
LENG3	PPP1R12C	2	β	21	β
LMTK2	PPP1R100	1	γ	3	γ
LRRC68	PPP1R37			27	α > β/γ
MKI67	PPP1R105			7	β
MYPT1	PPP1R12A	37	β	47	β
MYPT2	PPP1R12B	3	β		
MYPT3	PPP1R16A			5	β
Neurabin	PPP1R9A	25	α/γ		
NIPP1	PPP1R8	18		24	α/γ > β
PHACTR4	PPP1R124			21	
Phostensin	PPP1R18	13	α		
PNUTS	PPP1R10	7		2	
PPP1R3B	PPP1R3B			1	α
PPP1R3D	PPP1R3D			8	α
RPL5				3	
SCRIB		12	γ >α/β		
SDS22	PPP1R7	23		21	
SH2D4A	PPP1R38	16	β	16	β
Spinophilin	PPP1R9B	31	α/γ > β	2	α/γ
TPRN		12	α		
URI1	PPP1R19	8			
YWHAG	PPP1R170	3 NQ		3 NQ	
ZAP3	PPP1R169	1	α	8	
ZFYBE9	PPP1R173			2	
ZFYVE16	PPP1R69			2	

PP1α vs PP1β vs PP1γ

Known/Predicted Regulatory Subunits		NUCLEAR INTERACTOME			
		BAC/HeLa cell Lines		MCF7 Cell Lines	
		# Peptides	Preference	# Peptides	Preference
ASPP1	PPP1R13B			5	α
ASPP2	PPP1R13A	7	α	3	α
CHCHD3	PPP1R22	4			
CHCHD3		4		9	
DDX21				19	
HCFC1		4		6	
iASPP	PPP1R13L	10	α		
Inh2	PPP1R2	1		2	α/γ
LTMK2	PPP1R100			1	γ
MCM7		2			
MKI67	PPP1R105	2	γ > α/β	58	γ > α/β
MYPT1	PPP1R12A	15	β	20	β
Neurabin	PPP1R9A	3	α/γ	11	
NIPP1	PPP1R8	17		16	
NONO		3			
ORC5				1	
Phostensin	PPP1R18	7	α		
PNUTS	PPP1R10	23		19	
RepoMan	PPP1R81	1 NQ			
RIF1		36		8	
RPL5				4	
RRP1B	PPP1R136			1	γ
SCRIB				6	
SDS22	PPP1R7	4		2	α/γ
SFPQ		4			
SH2D4A	PPP1R38	2	β		
Spinophilin	PPP1R9B	19	α/γ > β	23	α/γ > β
SRSF10				4	
STAU1	PPP1R150			4	
STAU1				4	
TPRN		2	α	7	α
TRA2B				3	
YWHAG				3	
ZAP3	PPP1R169	37		14	

Figure 3.3. Quantitative AP/MS screen maps the distribution of known PP1 regulatory proteins between the three isoforms. A. Strategy utilized to directly compare the Cytoplasmic (CP) and Nuclear (NUC) interactomes of GFP-tagged PP1α, β and γ stably expressed in HeLa/BAC and MCF7/cDNA cell lines. **B.** Tables summarize known and predicted PP1 regulatory proteins identified in the screens, with number of peptides identified and isoform preferences indicated. **C.** Western blot analysis of GFP-PP1 isoform IPs from HeLa/BAC whole cell extracts, using antibodies against select interactors.

had more peptides found in the MCF7/cDNA experiment, which is consistent with higher levels of GFP-PP1 expression levels increasing the sensitivity of detection of binding partners. Of the regulatory subunits identified, some showed the expected isoform preference (e.g. Mypt1 family (Scotto-Lavino et al. 2010), TPRN (Ferrar et al. 2012)), and some the expected compartment specificity (e.g. URI1 (Djouder et al. 2007), Repo-Man (Trinkle-Mulcahy et al. 2006). The identification of proteins in unpredicted compartments is likely due to fractionation artefacts, which we have observed previously. For example, both tagged and endogenous Taperin are predominantly nuclear in live and fixed cells, yet the majority ends up in the cytoplasmic extract, indicating that it is lost from the nucleus during fractionation (Ferrar et al. 2012). The detection of a particular complex in the CP or NUC is therefore simply a starting point for our analysis, with follow-up experiments required to determine the in vivo localization. As an example, we cloned a large number of the known/predicted targeting subunits for expression in cells as GFP fusions (Figure 3.4). This highlights the diversity of PP1 complexes distributed throughout the CP and NUC of the interphase cell. It also demonstrates that most of these regulatory subunits localize to the subcellular fraction in which they were identified by MS, with the exception of a select few such as TPRN.

With several regulatory subunits showing association with all three isoforms, we carried out follow-up validation experiments by AP/WB. GFP-tagged PP1 isoforms were pulled down from HeLa/BAC whole cell extracts, and a panel of known regulatory subunits assessed using specific antibodies. This confirmed that PNUTS, SDS22 and NIPP1 interact with all three PP1 isoforms, albeit with varying affinities (Figure 3.3C).

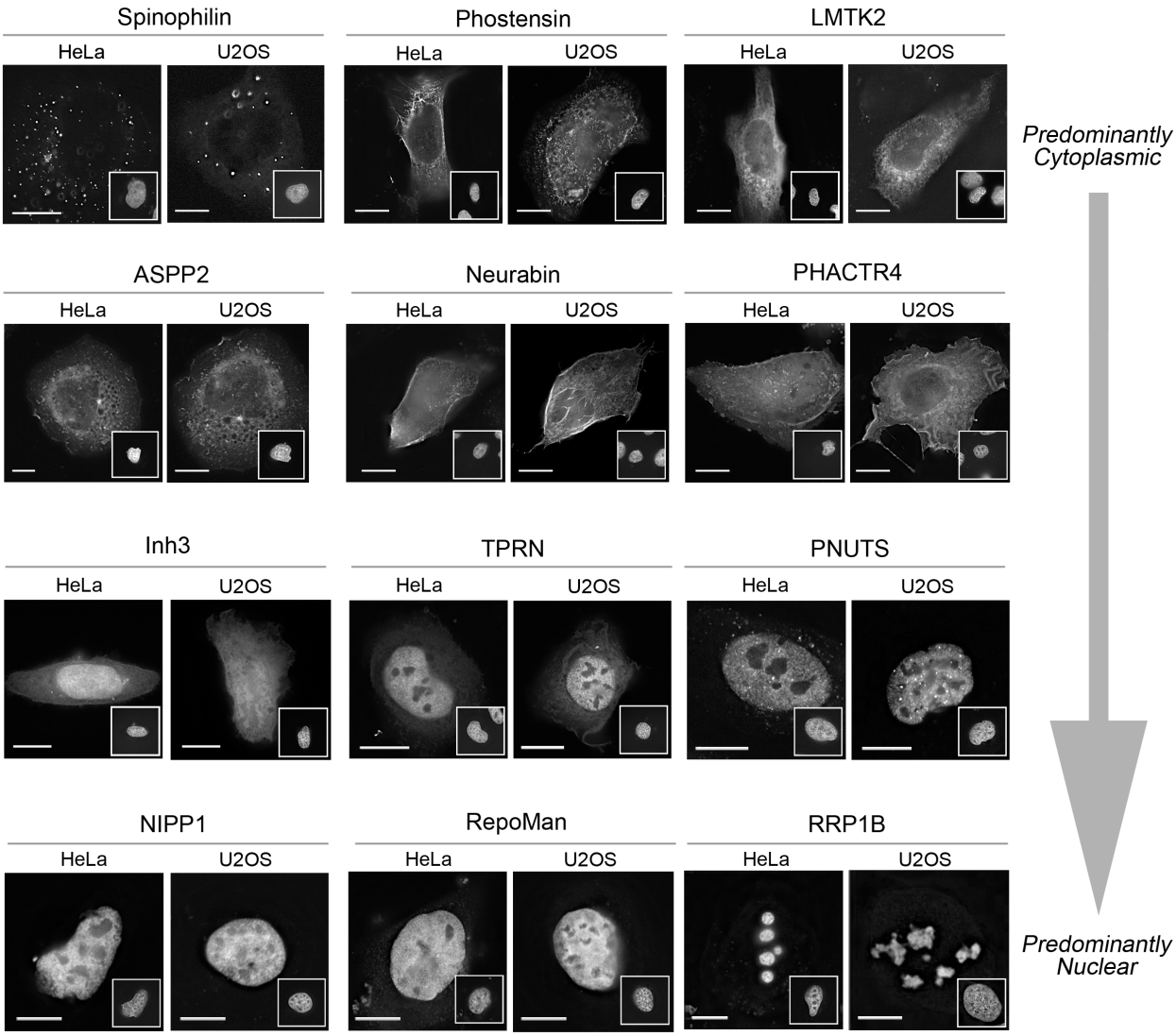

Figure 3.4. PP1 is found in a range of holoenzyme complexes localized throughout the cell. Images show the subcellular localization patterns for a selection GFP-tagged PP1 regulatory subunits transiently overexpressed in HeLa and U2OS cells. The cells were fixed, permeabilized and stained with DAPI to mark the nucleus (inset panels). Scale bars are 5 μm.

The observed preference of Mypt1 for PP1β and ASPP2 for PP1α was also confirmed in this experiment. Although RIF1 and Inh2 did not show a preference for the alpha isoform in the interactome screen, we were only able to detect the interaction with GFP-PP1α in the WB analysis. This may be a detection issue (the antibody is not very robust), or because we did not fractionate the cells to reduce sample complexity.

3.4 Individually focused, fractionation-based AP/MS experiments build a more comprehensive map of the intracellular distribution of each PP1 isoform.

Given the low expression of the GFP fusion proteins in our PP1β and PP1γ HeLa/BAC stable cell lines, and the variability of the CP/NUC fractionation of our MCF7/CMV stable cell lines, we decided to use the HeLa/cDNA stable cell lines that we had previously established for the analysis of GFP-hPP1α and GFP-hPP1γ (Trinkle-Mulcahy et al. 2006; Trinkle-Mulcahy et al. 2003), and our U2OS/cDNA cell lines stably expressing GFP-hPP1α, hPP1β-GFP, and GFP-hPP1γ (Chamousset, De Wever, et al. 2010). Both of these cell types are more amenable to fractionation and expression levels of the isoforms more equivalent, which improved coverage of the PP1β and PP1γ interactomes.

We first assessed the distribution of the GFP-tagged PP1 isoforms by live imaging and WB analysis. As previously noted, and shown in Figure 3.5, GFP-PP1α and GFP-PP1γ show distinct localization patterns when stably overexpressed in HeLa cells. Both are found throughout the cell, with PP1γ showing a more prominent accumulation within the nucleoli. WB analysis (Figure 3.5) of CP, NP and No fractions shows that their

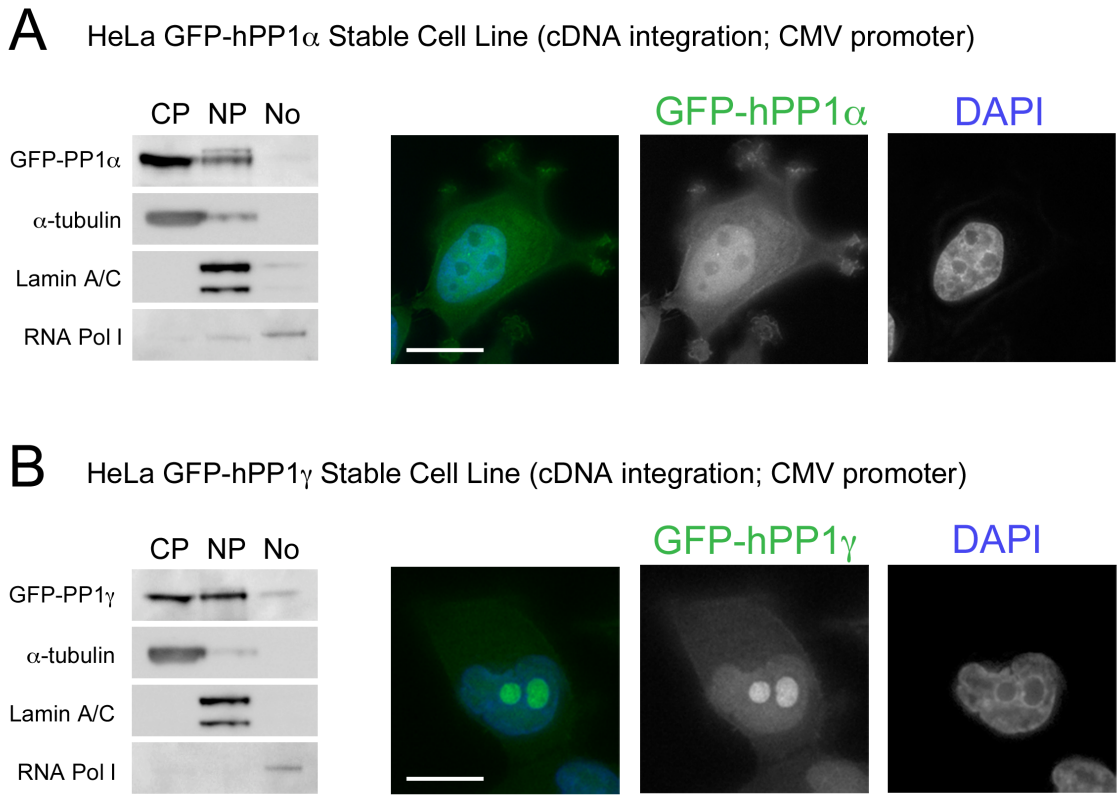

Figure 3.5. GFP-tagged PP1α and PP1γ show the expected localization patterns in HeLa/cDNA stable cell lines. Western blot analysis of Cytoplasmic (CP), Nucleoplasmic (NP) and Nucleolar (No) extracts prepared from GFP-hPP1α (**A**) and GFP-hPP1γ (**B**) stable cell lines confirmed similar distributions to those observed for the endogenous isoforms. Cells were also stained with the cell permeable DNA dye Hoechst 33342 (blue) and imaged live to demonstrate the subcellular localization patterns of the isoforms (green). Scale bars are 15 μm.

distribution between the three approximates that of their endogenous counterparts. Similar results were observed for the U2OS stable cell lines (Figure 3.6). This confirms the validity of these cell lines as markers for the subcellular distribution of the phosphatase.

Next, we designed a strategy to optimally highlight bona fide PP1 isoform interactors above the background of proteins that bind non-specifically to the beads. As shown in Figure 3.7A, this strategy involved differential SILAC labeling of parental cells (LIGHT media) and GFP-PP1 isoform-expressing cells (HEAVY media). Both cell lines were fractionated for preparation of CP, NP and No extracts, and then equivalent total protein amounts of parental (LIGHT) and GFP-PP1 (HEAVY) extracts were incubated with GFP-Trap beads for one hour. Following an initial wash, the beads were carefully combined for all subsequent steps, to minimize sample handling variability.

We specifically chose not to use HeLa and U2OS cell lines stably overexpressing GFP alone as the negative control for these experiments, because we have observed variable upregulation of a number of sticky (i.e. bind non-specifically to affinity matrices) proteins such as chaperones in cell lines stably overexpressing various fusion proteins. This can give the appearance that they are specifically enriched in the experimental pulldown, although they are actually just sticky and more abundant. To highlight them directly, we carried out separate control experiments for HeLa and U2OS CP, NP and No fractions, comparing cells stably overexpressing GFP alone (HEAVY) to the relevant parental line (LIGHT). This identified both cell- and fraction-specific contaminants that are more highly upregulated in overexpressing stable lines (datasets provided in Appendix II), which we could then subtract from our GFP-PP1 isoform datasets.

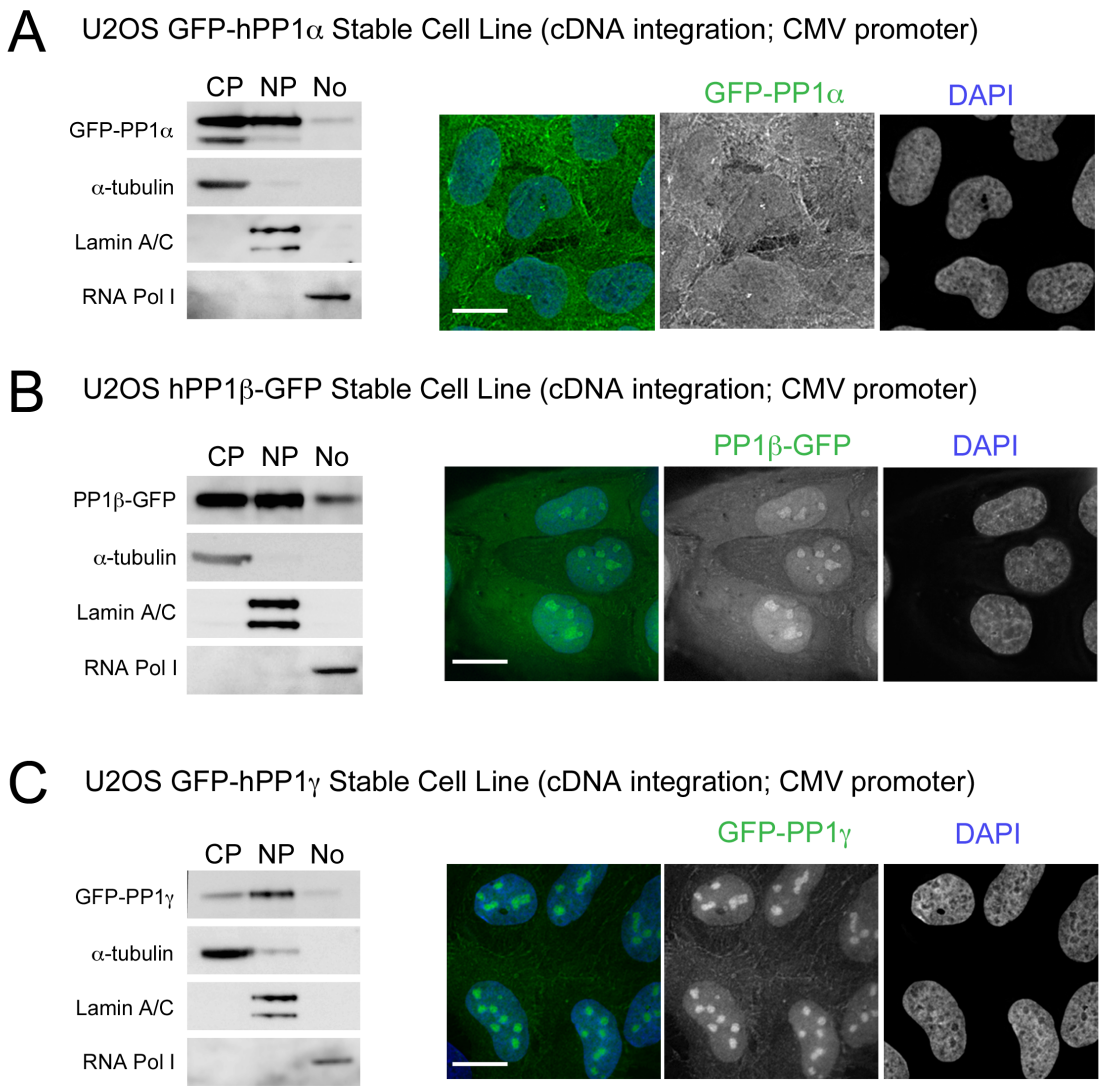

Figure 3.6. GFP-tagged PP1α, PP1β and PP1γ show the expected localization patterns in U2OS/cDNA stable cell lines. Western blot analysis of Cytoplasmic (CP), Nucleoplasmic (NP) and Nucleolar (No) extracts prepared from GFP-hPP1α (**A**), PP1β-GFP (**B**) and GFP-hPP1γ (**C**) stable cell lines confirmed similar distributions to those observed for the endogenous isoforms. Cells were also stained with the cell permeable DNA dye Hoechst 33342 (blue) and imaged live to demonstrate the sub-cellular localization patterns of the isoforms (green). Scale bars are 15 μm.

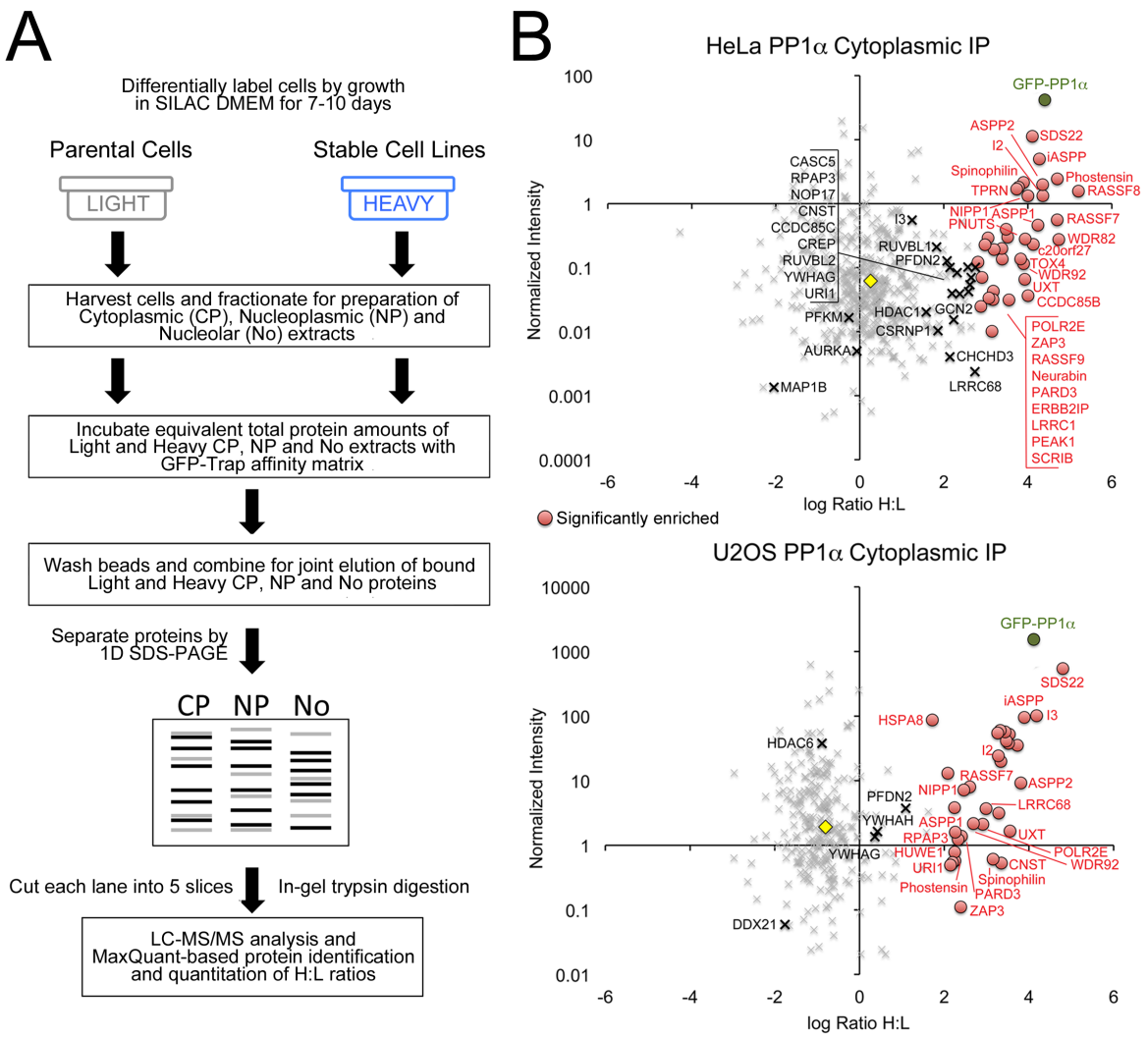

Figure 3.7. The GFP-PP1α cytoplasmic interactome is comparable between HeLa and U2OS cells. **A.** Diagram outlining the quantitative AP/MS strategy used to independently map the Cytoplasmic (CP), Nucleoplasmic (NP) and Nucleolar (No) interactomes for each GFP-tagged PP1 isoform in the HeLa and U2OS cDNA stable cell lines. GFP-Trap pulldowns from equivalent total protein amounts of Parental (Light) and PP1 isoform (Heavy) extracts were combined for analysis for each compartmental experiment, with all bound proteins identified and H:L ratios quantified to highlight those that were specifically enriched with PP1 above the background contaminants that bind non-specifically to the beads. **B.** HeLa and U2OS cytoplasmic PP1α datasets, plotted as Normalized Intensity vs. log(2) Ratio H:L. The proteins cluster around a median (yellow diamond) value, and GFP-PP1α (green circle) is highly enriched. Known/predicted regulatory subunits and common interactors are shown in red (circles) if significantly enriched above median, and in black (X) if not.

3.4.1 Proteins identified in our Cytoplasmic and Nuclear GFP-PP1α Interactome screen

Figure 3.7B summarizes the cytoplasmic interactome of PP1α mapped in the HeLa and U2OS cell lines. In the HeLa experiment, 512 proteins were identified/quantified, 99 of which were enriched more than 2-fold in the GFP-PP1α pulldown (i.e. log2H:L >1 log above median). We also applied the more stringent Significance B analysis, which takes abundance as well as ratio into account and assigns higher confidence to ratios based on larger numbers of peptide identifications (given that proteins with fewer peptide identifications will show higher ratio variability). These values, which are expressed as p values, were calculated using the Perseus module of MaxQuant, and 34 proteins deemed to be significantly enriched ($p < 0.05$) above the mean with GFP-PP1α (shown as red circles on the graph). In the U2OS experiment, 309 proteins were identified/quantified, 57 of which were enriched more than 2-fold in the GFP-PP1α pulldown (i.e. log2H:L >1 log above median) and 33 of which were deemed to be significantly enriched based on Significance B values. Known/predicted regulatory subunits and binding partners commonly enriched in our PP1 datasets or deposited in the BioGrid database as potential PP1 interactors are also labeled.

It is important to note that the Significance B values are calculated with respect to the mean ratio. This is ideal for whole proteome comparisons under different cellular conditions, for example, because the majority of factors do not change while small subsets are enriched or reduced. In a differentially labeled AP/MS experiment, however, the background that does not change is the cluster of proteins that bind non-specifically to the affinity matrix, and a better estimate of this is the median H:L ratio. The mean

often skews toward a higher H:L ratio because there are very few proteins with ratios significantly below 1:1 (typically environmental contaminants such a keratin), and a much larger subset with high H:L ratios, representing the interactome of proteins enriched with the bait protein. This is why we set our 2-fold enrichment threshold above the median. We routinely apply both analyses (Significance B values and 2-fold enrichment) to balance out these differences and to confer different levels of confidence in the results. We anticipate that some interactors may be close to these threshold and occasionally fall below them, so for all our PP1 interactome experiments we also highlighted proteins that were identified in more than one experiment and significantly enriched above mean (or 2-fold enriched above median) in at least one of them. We refer to these in the figures and tables and "commonly enriched interactors". Consistent with our work as mapping them as novel PP1 interactors, several have since been deposited in the BioGrid database as putative PP1 interactors annotated in large-scale interactome screens. Most lack a predicted PP1 binding motif and are thus likely indirect interactors, forming a complex with PP1 via association with a regulatory subunit.

Our next analysis step was the manual elimination of all likely contaminants (i.e. proteins significantly enriched in a pulldown of stably expressed GFP alone compared to the parental cell line from the cytoplasmic fraction of the respective cell type). Examples include chaperones such as HSPA5 and HSPA9, and the U2OS-specific contaminant DHRS2, a short- chain alcohol dehydrogenase that was enriched in nearly all of our CP/NUC/No experiments, both experimental and control. Interestingly, for the 27 DHRS2 interactions deposited in the BioGrid dataset, it was the prey in all cases (i.e. detected in the pulldown of bait proteins) and several of the studies were carried out in U2OS cells (Herr et al. 2015; Deisenroth et al. 2010; Andresen et al. 2014).

We then generated a list of known/predicted PP1 regulatory subunits and commonly enriched interactors that co-precipitated with GFP-PP1α from cytoplasmic extracts of HeLa and U2OS cells (Figure 3.8). We further annotated these tables to note those proteins that were also identified in our BAC and MCF7 cytoplasmic AP/MS experiments (and whether they showed an isoform preference).

In general there is good agreement between the two cell lines, and numerous known regulatory subunits were identified. These include the evolutionarily conserved regulators Inhibitor 2 (Inh2), SDS22, Inh3 and NIPP1. We also identified all three members of the ASPP family (ASPP1, ASPP2 and iASPP). URI1, found in both screens, is an unconventional member of the prefoldin (PFD) family of chaperones found to localize to the mitochondria with PP1 in a stable complex (Djouder et al. 2007). Although that study suggested a specific association with PP1γ, we identified URI1 in both the PP1α and PP1γ interactomes, indicating that isoform "preference" is a better term than isoform "specificity". We had noted this previously for RepoMan, which shows a preference for PP1γ that can be overridden by overexpression of the regulatory subunit (Trinkle-Mulcahy et al. 2006).

Neurabin-I and Spinophilin have been shown to target PP1 activity to actin-rich structures and proposed to play roles in cytoskeletal dynamics (Oliver et al. 2002), while Phostensin and PARD3 target PP1 to the F-actin cytoskeleton (Kao et al. 2007) and tight junctions, respectively. Interestingly, we identified CASC5, which binds PP1 in mitosis and plays an important role in kinetochore microtubule stability (Rosenberg et al. 2011). This may have been detected in the subset of mitotic cells (~10%) present in our asynchronous cell population, the contents of which would end up in the cytoplasmic

Known/predicted TS

Commonly enriched

INTERACTOR		CYTOPLASMIC INTERACTOME					
		Single Isoform Mapping (PP1α)		Comparison to PP1α vs PP1β vs PP1γ datasets			
		HeLa	U2OS	BAC lines HeLa		Stable MCF7	
		# Peptides	# Peptides	# Peptides	Preference	# Peptides	Preference
Inh2	PPP1R2	12	9	8	α/γ > β	11	
SDS22	PPP1R7	25	27	23		21	
NIPP1	PPP1R8	17	5	18		24	α/γ > β
Neurabin	PPP1R9A	25		25	α/γ		
Spinophilin	PPP1R9B	39	4	31	α/γ > β	2	α/γ
PNUTS	PPP1R10	15		7		2	
Inh3	PPP1R11	4	4	7		7	
ASPP2	PPP1R13A	38	14	25	α > β/γ	17	α > β/γ
ASPP1	PPP1R13B	29	8	9	α	27	
iASPP	PPP1R13L	33	27	30	α/β	37	α/β > γ
CREP	PPP1R15B	8					
Phostensin	PPP1R18	24	3	13	α		
URI1	PPP1R19	8	2	8	α/γ > β		
CHCHD3	PPP1R22	3					
LRRC68	PPP1R37	12	10			27	α > β/γ
CASC5	PPP1R55	9					
CNST	PPP1R64	7	3				
PARD3	PPP1R118	31	12				
ZAP3	PPP1R169	59	7	1	α	8	
YWHAG	PPP1R170	4	4	3		3	
LRRC1		5					
SCRIB		13		12	γ >α/β		
TPRN		27		12	α		
C20ORF27		6		6	α	5	α/γ
CCDC85B		5				1 NQ	
CCDC85C		8				1	α
CSRNP1		2					
EIF2AK4/GCN2		13					
ERBB2IP		36		10		2	
HDAC1		2					
PEAK1		34		2	α		
PFDN2		4	3	4			
PIH1D1/NOP17		5		8	α/γ > β	1	α
POLR2E		3	4	3	α		
RASSF7		12	8	7	α		
RASSF8		20		8	α		
RASSF9		8		1	α		
RPAP3		10	6	6			
RUVBL1		6					
RUVBL2		7				8	
TOX4		6		1	α		
UXT		3	2	2		2	α/γ
WDR82		6		5	α	2	
WDR92		8	4	12	α/γ > β	1	α
YWHAH			4				

Significance B value < 0.05

Enriched > 2-fold above median H:L

> median

Figure 3.8. Single isoform interactome mapping identifies a broader range of cytoplasmic interactors for PP1α. Annotation of known/predicted targeting subunits (TS; orange) identified in cytoplasmic PP1α interactomes highlights the distribution of this isoform between holoenzyme complexes in HeLa and U2OS cells, and identifies novel proteins found to be commonly enriched (blue) with PP1 in our repository of interactome screens. Results from the cytoplasmic BAC and MCF7 screens are shown for comparison.

extract.

Some proteins, such as LRRC1, were only detected as binding partners in one experiment. Although this may indicate differences in the distribution of PP1α between regulatory complexes in these cell lines, it may simply reflect differences in the expression levels (and thus detectability) of the proteins. Another example is the commonly enriched interactor c20orf27, which was detected in the HeLa/cDNA, HeLa/BAC and MCF7/cDNA AP/MS experiments (and also in the PP1γ HeLa/cDNA interactome) but not any of the U2OS/cDNA experiments. Follow-up analysis confirmed that c20orf27 and PP1 can interact in U2OS cells, and given that ProteomicsDB annotates higher levels of c20orf27 in U2OS compared to HeLa cells, this could indicate that a larger fraction of PP1 is associated with this particular complex in certain cell lines.

Figure 3.9A summarizes the nucleoplasmic interactome of PP1α mapped in the HeLa and U2OS cell lines. In the HeLa experiment, 734 proteins were identified/quantified, 109 of which were enriched more than 2-fold in the GFP-PP1α pulldown. Using the more stringent Significance B analysis, 17 proteins were deemed to be significantly enriched with GFP-PP1α. In the U2OS experiment, 502 proteins were identified/quantified, 24 of which were enriched more than 2-fold in the GFP-PP1α pulldown and 27 of which were deemed to be significantly enriched based on Significance B values. As describe above, we generated a list of the known/predicted regulatory subunits and commonly enriched interactors that co-precipitate with GFP-PP1α from nucleoplasmic extracts of HeLa and U2OS cells, further annotated to show those also identified in our BAC and MCF7 nuclear AP/MS experiments (and whether they showed an isoform preference) (Figure 3.9B).

A

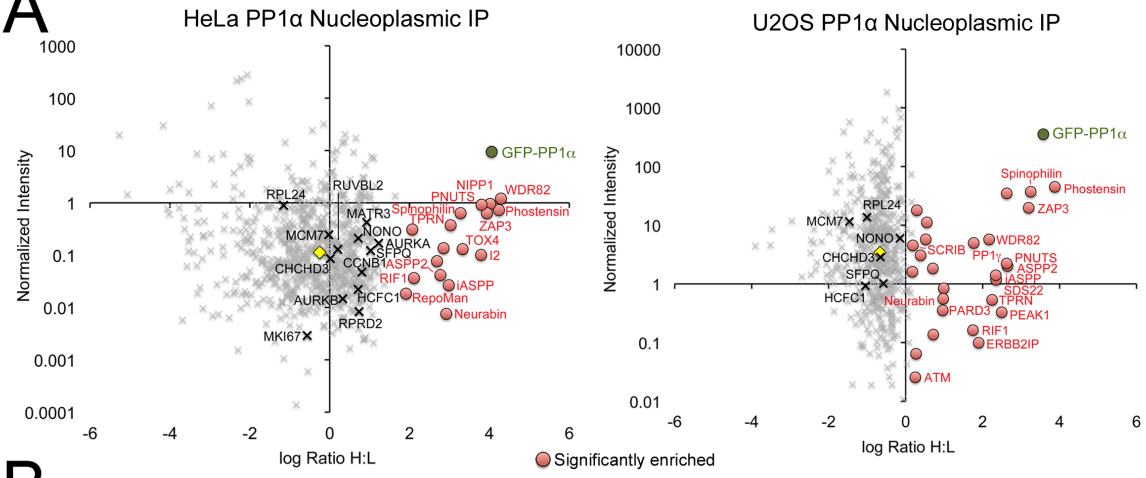

B

Known/predicted TS

Commonly enriched

		NUCLEOPLASMIC INTERACTOME					
		Single Isoform Mapping (PP1α)		Comparison to PP1α vs PP1β vs PP1γ datasets			
		HeLa	U2OS	BAC lines HeLa		Stable MCF7	
INTERACTOR		# Peptides	# Peptides	# Peptides	Preference	# Peptides	Preference
Inh2	PPP1R2	5		1		2	α/γ
SDS22	PPP1R7		2	4		2	α/γ
NIPP1	PPP1R8	16		17		16	
Neurabin	PPP1R9A	4	7	3	α/γ	11	
Spinophilin	PPP1R9B	24	20	19	α/γ > β	23	α/γ > β
PNUTS	PPP1R10	29	8	23		19	
ASPP2	PPP1R13A	8	7	7	α	3	α
iASPP	PPP1R13L	6	5	10	α		
Phostensin	PPP1R18	16	14	7	α		
AURKA	PPP1R47	5					
AURKB	PPP1R48	2					
RepoMan	RRR1R81	3		1 NQ			
PARD3	PPP1R118		3				
ZAP3	PPP1R169	72	55	37		14	
RIF1		24	5	36		8	
TPRN		16	2	2	α	7	α
ATM			2				
CCNB1		2					
ERBB2IP			2			2	α > β/γ
KIF2C		4		3		5	
PEAK1			3			1	γ
RPRD2		3				2	
RUVBL2		7				8	
TOX4		8		6		2	α/γ
WDR82		13	4	10		7	α/γ > β

Significance B value < 0.05

Enriched > 2-fold above median H:L

> median

Figure 3.9. Single isoform interactome mapping identifies a broader range of nucleoplasmic interactors for PP1α. A. HeLa and U2OS nucleoplasmic PP1α datasets, plotted as Normalized Intensity vs. log(2) Ratio H:L. The proteins cluster around a median (yellow diamond) value, and GFP-PP1α (green circle) is highly enriched. Known/predicted regulatory subunits and common interactors are shown in red (circles) if significantly enriched above median, and in black (X) if not. **B.** Data annotated as in Figure 8, to highlight known/predicted targeting subunits (TS) and common interactors.

Several known regulatory subunits that localize to the nucleus and bind PP1 were identified. They include the first identified nuclear PP1 targeting subunits NIPP1 and PNUTS (Kreivi et al. 1997; Trinkle-Mulcahy et al. 1999; Allen et al. 1998; Boudrez et al. 1999) which have since been linked to regulatory roles in transcription, pre-mRNA splicing, chromatin decompaction at mitotic exit and DNA damage repair (Nuytten et al. 2008; Boudrez et al. 2000; Ciurciu et al. 2013; Landsverk et al. 2005). Also found were other nuclear targeting subunits identified in our previous studies (Trinkle-Mulcahy et al. 2006), such as the putative nucleoside kinase ZAP3 that has been linked to RNA modification (Ulke-Lemée et al. 2007; Trinkle-Mulcahy et al. 2006); TPRN, which is recruited to sites of DNA damage (Ferrar et al. 2012); Repo-Man, which recruits PP1 to chromatin and plays roles in DNA damage sensing and of chromatin organization (Vagnarelli et al. 2006; Trinkle-Mulcahy et al. 2006); and RIF1, originally identified as a yeast telomeric chromatin component (Hardy et al. 1992), which functions in controlling replication through PP1 (Hiraga et al. 2017; Hiraga et al. 2014; Mattarocci et al. 2014; Davé et al. 2014). The Aurora kinases, AURKA and AURKB, were also mapped here, and have been shown to regulate kinetochore assembly/disassembly during the cell cycle in conjunction with PP1 (Kim et al. 2010; Emanuele et al. 2008).

Lastly, to gain an overview of the distribution of PP1α in the HeLa and U2OS cell lines, we combined the CP and NP fraction datasets to include all identified proteins enriched >2-fold above median and not detected in the respective control GFP AP/MS experiment. Using the STRING (search tool for the Retrieval of Interacting Genes/Proteins) biological database (Szklarczyk et al. 2015), we generated a network map for these combined datasets that highlights connections based on curated,

experimentally determined, published and predicted protein-protein associations. The known/predicted regulatory subunits identified in these screens would be expected to serve as network "hubs", recruiting PP1 to larger complexes, and are highlighted in yellow on the network maps.

As expected, more (and larger) complexes were mapped in the HeLa dataset (Figure 3.10) compared to the U2OS dataset (Figure 3.11), likely due to the increased number of proteins identified overall. The two complexes that were identified in both screens would thus be predicted to represent a relatively large fraction of cellular PP1α compared to other complexes. One is mediated via the regulatory subunit URI1, which forms a network with the commonly enriched interactors HDAC1/2, RUVBL1/2, PIHID1, RPAP3/, WDR92, UXT, POLR2E and PFDN2. The members identified in this network are linked to regulating the assembly of multisubunit complexes, including the RNA Pol II transcription complex. The other network mapped in both the HeLa and U2OS screen is mediated by the ASSP family of regulatory subunits, which have been shown to network with RASSF7/ RASSF8/ RASSF9/ CCDC85B/ and CCDC85C. The sole homologue of human RASSF7/8/9 in drosophila, dRASSF8, has been linked to the sole homologue of ASPP in drosophila, dASPP, and the complex contributes to regulation of cell-cell adhesion during Drosophila retinal morphogenesis (Langton et al. 2009).

As previously noted, the regulatory subunit CASC5, which recruits PP1 to kinetochores in mitosis, was detected in the HeLa screen, along with other proteins that have been linked to kinetochore regulation such as NSL1, ZWINT, KIF2C, RPRD1B, AURKA and the regulatory subunit PPP1R5B. A complex linked to mitochondria was also identified in the HeLa screen, involving ATP5C1, VDAC2, PRDX3 and UQCRC1/2. It is

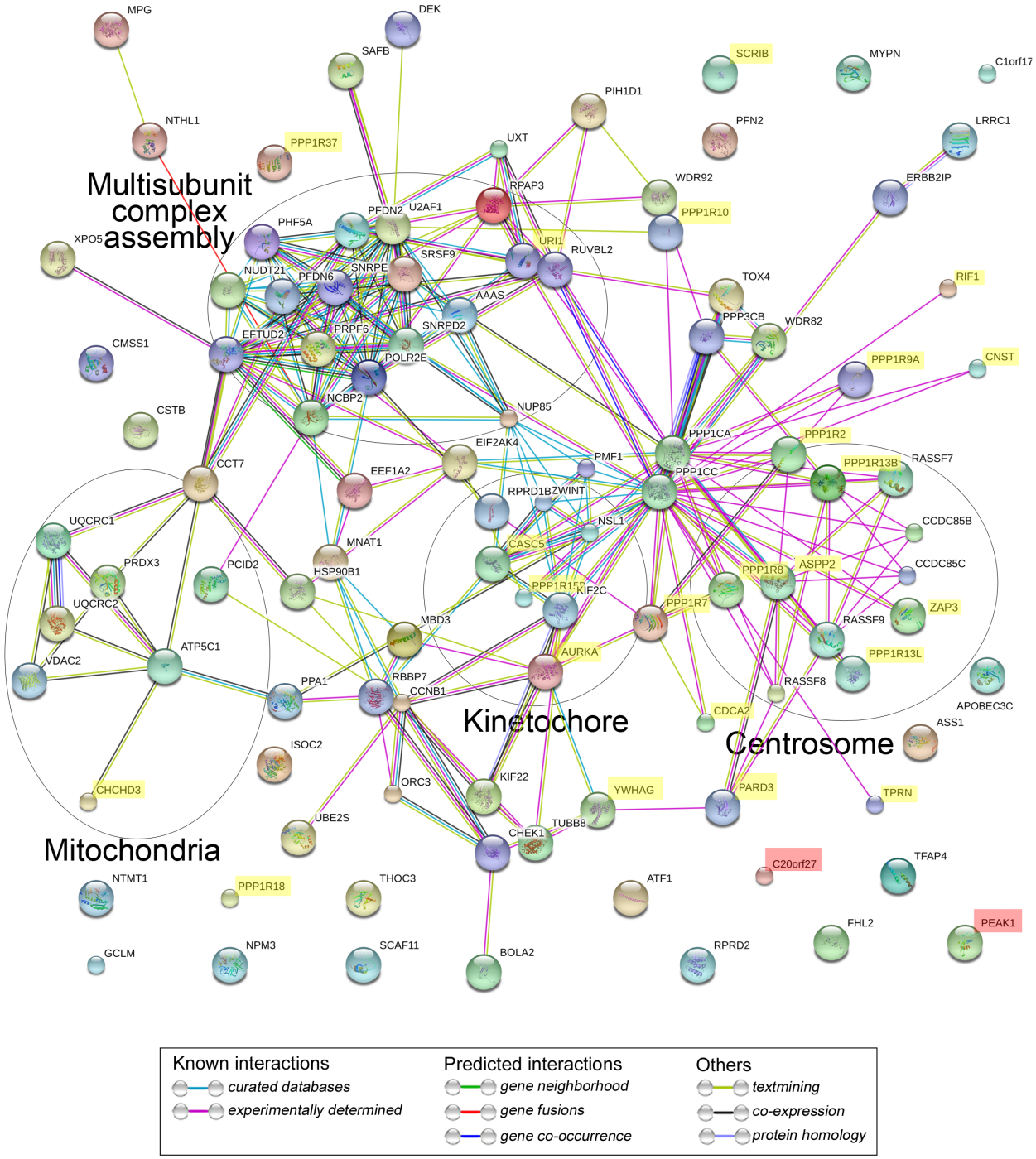

Figure 3.10. STRING analysis identifies key cellular complexes represented in the PP1α interactome in the HeLa stable cell line. STRING-based network mapping for a stringent subset of interactors enriched > 2-fold with GFP-PP1α in the combined CP and NP experiments and not detected in the respective control GFP AP/MS experiments. Known/predicted targeting subunits are highlighted (yellow), as is the novel targeting subunit (c20orf27 and PEAK1; red) that we identified and validated (c20orf27 as a targeting subunit; PEAK1 as an interactor).

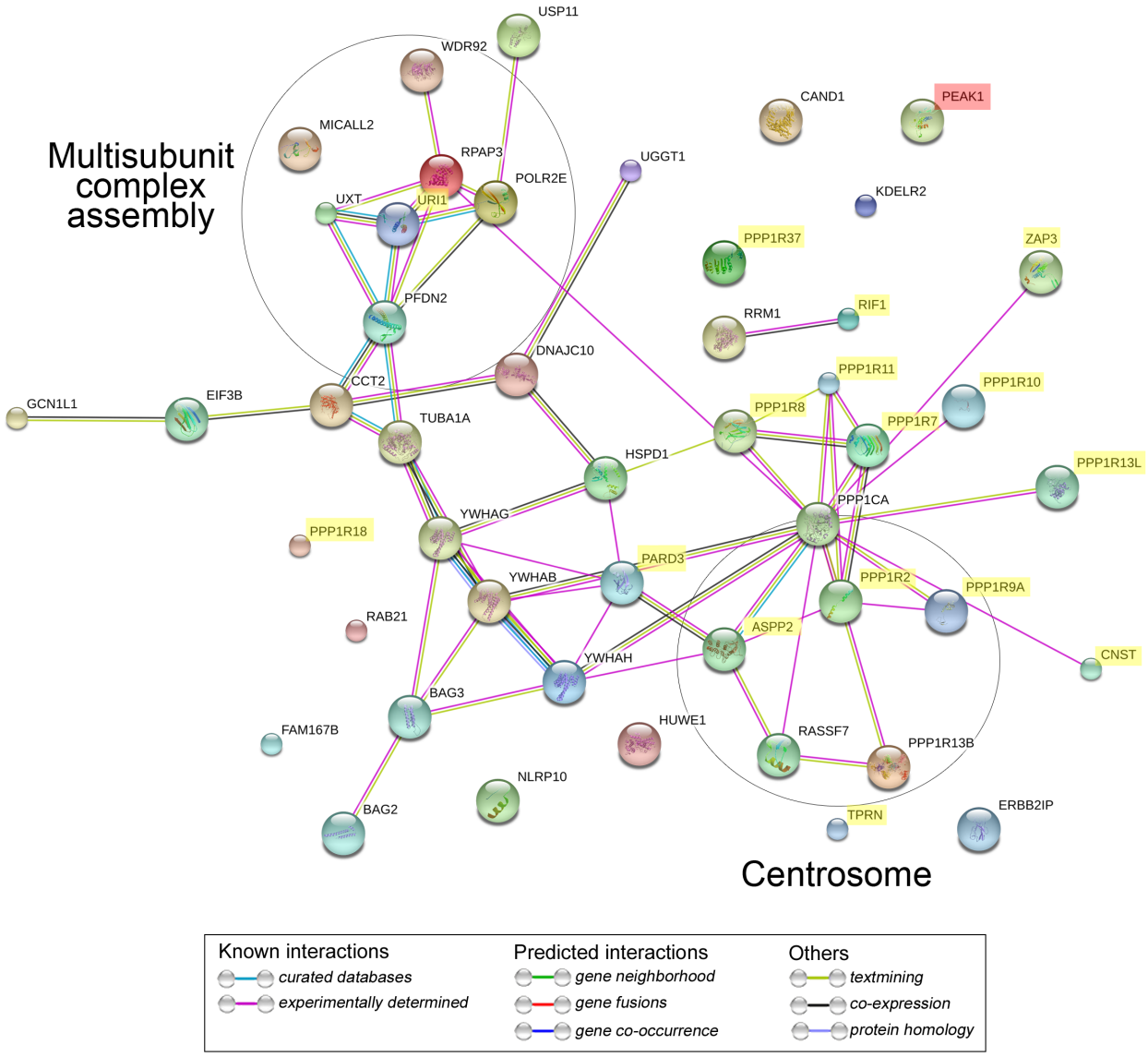

Figure 3.11. STRING analysis identifies key cellular complexes represented in the PP1α interactome in the U2OS stable cell line. STRING-based network mapping for a stringent subset of interactors enriched > 2-fold with GFP-PP1α in the combined CP and NP experiments and not detected in the respective control GFP AP/MS experiments. Known/predicted targeting subunits are highlighted (yellow), as is the novel targeting subunit (PEAK1; red) that we identified as an interactor.

possible that association of PP1 with this complex is mediated via the regulatory subunit CHCHD3, a member of the mitochondrial contact site and cristae organizing system (MICOS) in the inner mitochondrial membrane that is essential for the formation and maintenance of cristae structure (Kozjak-Pavlovic 2017).

3.4.2 Proteins identified in our Cytoplasmic and Nuclear GFP-PP1γ Interactome screen

Similar to our GFP-PP1α interactome analyses, Figure 3.12A summarizes the cytoplasmic interactome of PP1γ mapped in the HeLa and U2OS cell lines. In the HeLa experiment, 254 proteins were identified/quantified, 42 of which were enriched more than 2-fold and 12 deemed to be significantly enriched with GFP-PP1γ. In the U2OS experiment, 365 proteins were identified/quantified, 19 of which were enriched more than 2-fold and deemed to be significantly enriched based on Significance B values. As before, we manually eliminated all likely contaminants and generated a list of the regulatory subunits and commonly enriched interactors, identified above median, that co-precipitate with GFP-PP1γ from cytoplasmic extracts of HeLa and U2OS cells (Figure 3.12B). The table was annotated with those proteins that were also identified in our BAC and MCF7 cytoplasmic AP/MS experiments (and whether they showed an isoform preference). Most of the regulatory subunits that we identified were also identified in our PP1α cytoplasmic dataset. However, we did identify a unique enrichment of PHACTR4, a PP1 interacting protein that regulates dephosphorylation of cofilin in response to decreased actin monomer binding to its RPEL domain (Huet et al. 2013). Also unique to the gamma isoform was LMTK, a novel transmembrane protein shown to associate with PP1γ and Inh2 (H. Wang & Brautigan 2002).

A

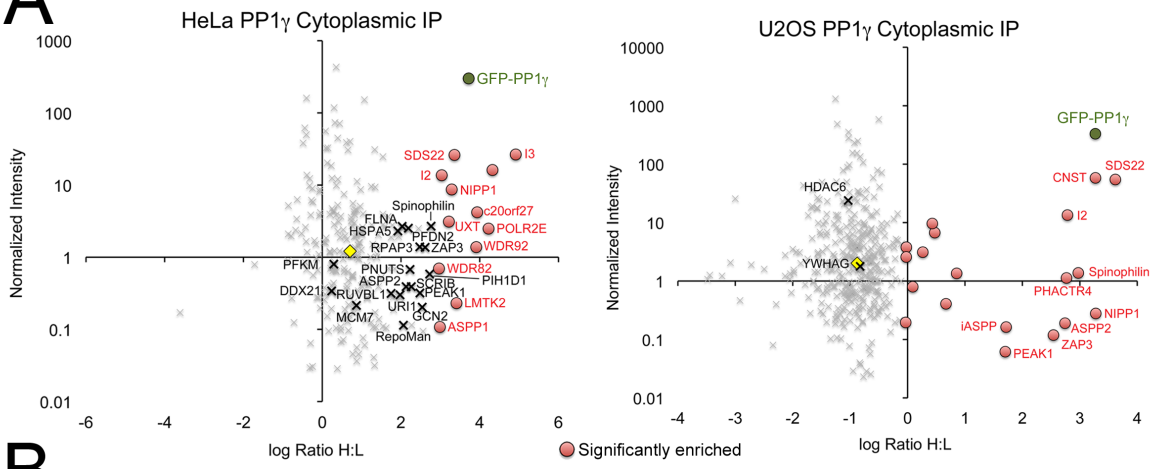

B

Known/predicted TS

Commonly enriched

		CYTOPLASMIC INTERACTOME					
		Single Isoform Mapping (PP1γ)		Comparison to PP1α vs PP1β vs PP1γ datasets			
		HeLa	U2OS	BAC lines HeLa		Stable MCF7	
INTERACTOR		# Peptides	# Peptides	# Peptides	Preference	# Peptides	Preference
Inh2	PPP1R2	9	7	8	α/γ > β	11	
SDS22	PPP1R7	16	21	23		21	
NIPP1	PPP1R8	12	18	18		24	α/γ > β
Spinophilin	PPP1R9B	7	3	31	α/γ > β	2	α/γ
PNUTS	PPP1R10	7		7		2	
Inh3	PPP1R11	5		7		7	
ASPP2	PPP1R13A	7	2	25	α > β/γ	17	α > β/γ
ASPP1	PPP1R13B	4		9	α	27	
iASPP	PPP1R13L		2	30	α/β	37	α/β > γ
URI1	PPP1R19	3		8			
CNST	PPP1R64		2				
RepoMan	PPP1R81	2					
LMTK2	PPP1R100	5		1	γ	3	γ
PHACTR4	PPP1R124		4			21	
ZAP3	PPP1R169	24	3	1	α	8	
YWHAG	PPP1R170		7	3		3 NQ	
SCRIB		11		12	γ >α/β		
C20ORF27		2		6	α	5	α/γ
EIF2AK4/GCN2		9					
PEAK1		11	2	2	α		
PFDN2		4		4			
PIH1D1/NOP17		2		8	α/γ > β	1	α
POLR2E		3		3	α		
RPAP3		8		6			
RUVBL1		2					
UXT		5		2		2	α/γ
WDR82		3		5	α	2	
WDR92		5		12	α/γ > β	1	α

Significance B value < 0.05 | Enriched > 2-fold above median H:L | > median

Figure 3.12. Single isoform interactome mapping identifies a broader range of cytoplasmic interactors for PP1γ. A. HeLa and U2OS cytoplasmic PP1γ datasets, plotted as Normalized Intensity vs. log(2) Ratio H:L. The proteins cluster around a median (yellow diamond) value, and GFP-PP1γ (green circle) is highly enriched. Known/predicted regulatory subunits and common interactors are shown in red (circles) if significantly enriched above median, and in black (X) if not. **B.** Data annotated as in Figure 3.8, to highlight known/predicted targeting subunits (TS) and common interactors.

Figure 3.13A summarizes the nucleoplasmic interactome of PP1γ mapped in the HeLa and U2OS cell lines. In the HeLa experiment, 425 proteins were identified/quantified, 21 of which were enriched more than 2-fold and 15 deemed to be significantly enriched with GFP-PP1γ. In the U2OS experiment, 472 proteins were identified/quantified, 19 of which were enriched more than 2-fold and 21 deemed to be significantly enriched based on Significance B values. As before, after removing contaminants, we generated a list of the regulatory subunits and commonly enriched interactors that co-precipitated with GFP-PP1γ from nucleoplasmic extracts of HeLa and U2OS cells (Figure 3.13B). We further annotated these tables to note those proteins that were also identified in our BAC and MCF7 cytoplasmic AP/MS experiments (and whether they showed an isoform preference). As for PP1α, we identified several known nuclear regulatory subunits, including NIPP1, PNUTS, Repo-Man, ZAP3 and RIF1. Interestingly we also identified the regulatory subunit SCRIB in the NP compartment. SCRIB is a cell polarity-related protein commonly detected at the cell membrane, but also annotated as nucleoplasmic in the ProteinAtlas database. Future studies will address its potential role in recruiting PP1 to nuclear substrates.

Using the STRING biological database to probe for associations between our annotated list of combined CP/NP proteins enriched 2-fold with PP1γ and not detected in the respective control datasets, we again found association with the multisubunit complex assembly hub (Figure 3.14). This is likely mediated via the URI1 regulatory subunit and containing the commonly enriched factors RUVBL1, PIHID1, RPAP3, WDR92, UXT, POLR2E, and PFDN2.

A

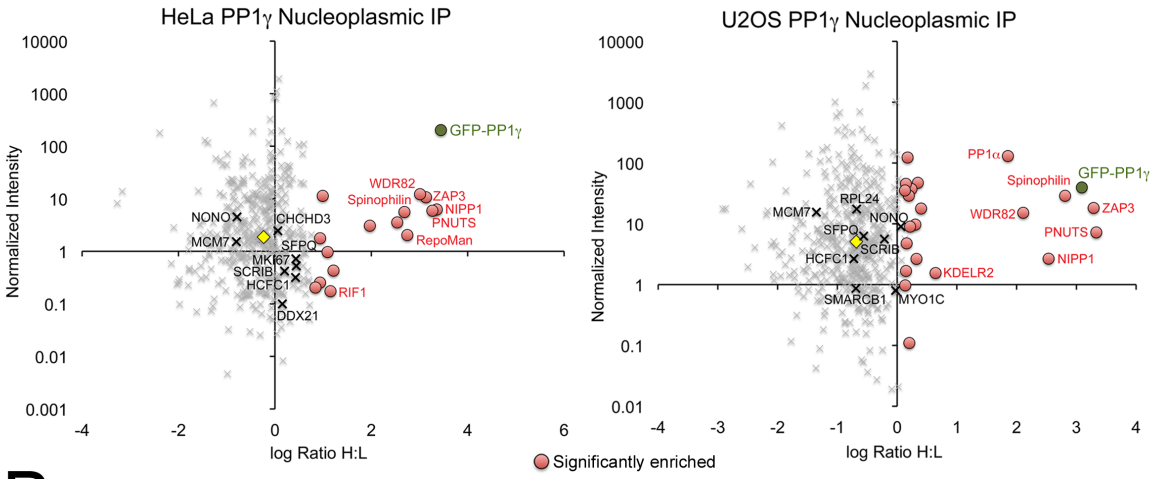

B

Known/predicted TS

Commonly enriched

		NUCLEOPLASMIC INTERACTOME					
		Single Isoform Mapping (PP1γ)		Comparison to PP1α vs PP1β vs PP1γ datasets			
		HeLa	U2OS	BAC lines HeLa		Stable MCF7	
INTERACTOR		# Peptides	# Peptides	# Peptides	Preference	# Peptides	Preference
NIPP1	PPP1R8	4	3	17		16	
Spinophilin	PPP1R9B	12	15	19	α/γ > β	23	α/γ > β
PNUTS	PPP1R10	20	9	23		19	
RepoMan	PPP1R81	9		1 NQ			
ZAP3	PPP1R169	48	46	37		14	
RIF1		8		36		8	
SCRIB		6	17			6	
MYO1C			3				
WDR82		4	4	10		7	α/γ > β

Significance B value < 0.05

Enriched > 2-fold above median H:L

> median

Figure 3.13. Single isoform interactome mapping identifies a broader range of nucleoplasmic interactors for PP1γ. A. HeLa and U2OS nucleoplasmic PP1γ datasets, plotted as Normalized Intensity vs. log(2) Ratio H:L. The proteins cluster around a median (yellow diamond) value, and GFP-PP1γ (green circles) is highly enriched. Known/predicted regulatory subunits and common interactors are shown in red (circles) if significantly enriched above median (yellow diamond), and in black (X) if not. **B.** Data annotated as in Figure 3.8, to highlight known/predicted targeting subunits (TS) and common interactors.

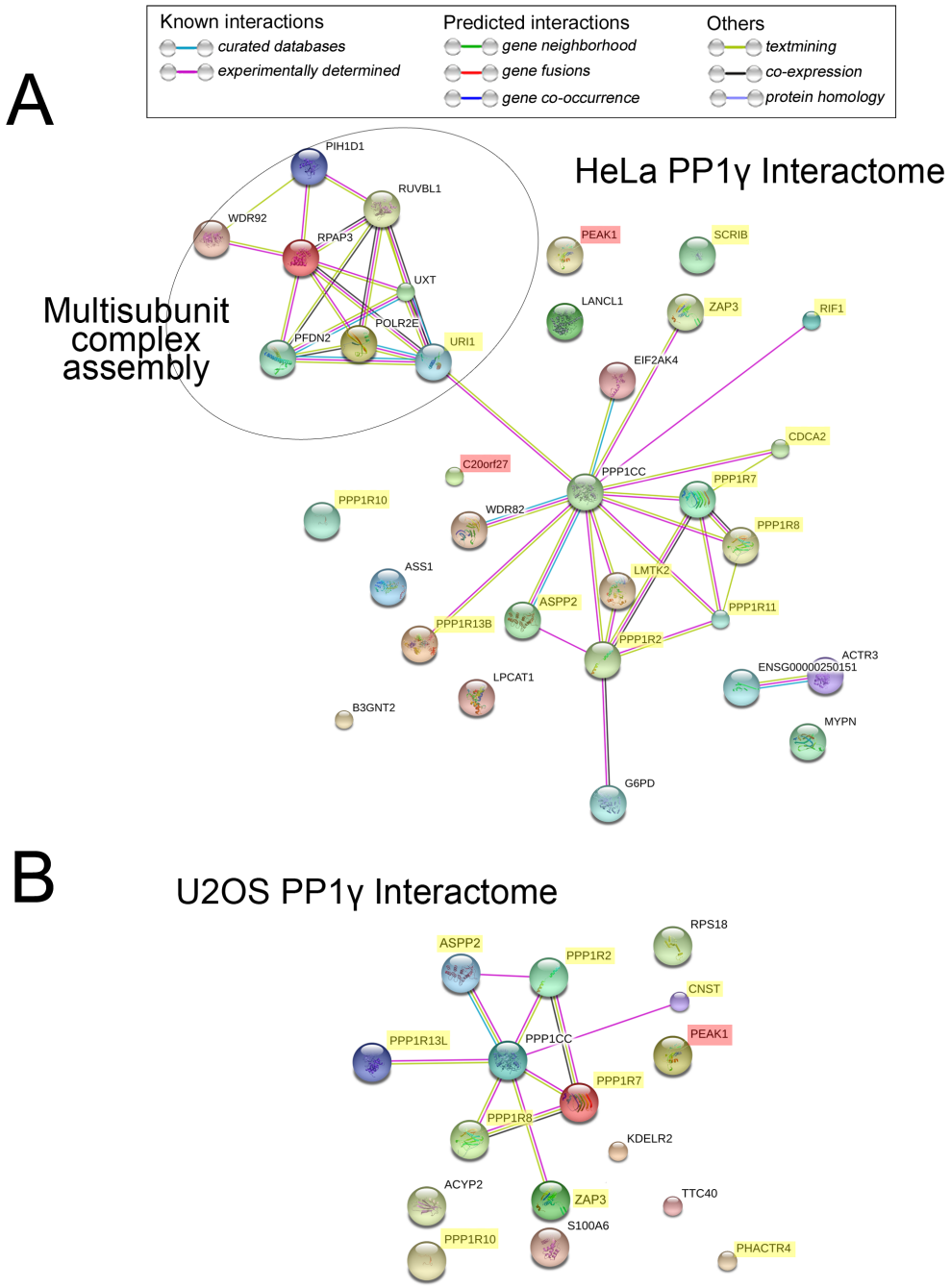

Figure 3.14. STRING analysis identifies a key complex represented in the PP1γ interactome. STRING-based network mapping for all interactors enriched > 2-fold with GFP-PP1γ in the combined NP and CP experiements in the HeLa (**A**) and U2OS (**B**) interactomes and not found in the respective GFP control AP/MS experiments. Known/predicted targeting subunits are highlighted (yellow), as are the novel hits (c20orf27 and PEAK1; red) that we identified and validated (c20orf27 as a targeting subunit; PEAK1 as an interactor).

3.4.3 Proteins identified in our Cytoplasmic and Nuclear GFP-PP1β Interactome screen

Figure 3.15A summarizes the cytoplasmic and nucleoplasmic interactomes of PP1β mapped in the U2OS cell line. In the cytoplasmic fraction, 310 proteins were identified/quantified, 27 of which were enriched more than 2-fold and 20 deemed to be significantly enriched in the GFP-PP1β pulldown. In the nucleoplasmic fraction, 387 proteins were identified/quantified, 49 of which were enriched more than 2-fold and 17 deemed to be significantly enriched in the GFP-PP1β pulldown. As before, we generated a list of the known/predicted regulatory subunits and commonly enriched interactors (Figure 3.15B), and noted those proteins that were also identified in our BAC and MCF7 cytoplasmic AP/MS experiments (and whether they showed an isoform preference).

Many of the regulatory subunits that we identified in both fractions were similar to those identified in our GFP-PP1α/γ cytoplasmic and nucleoplasmic dataset, confirming the overlap that we've observed previously for the three isoforms. We did, however, identify the MYPT family in the PP1β interactome, including Mypt1, LENG3 and Mypt3. In our cytoplasmic fraction we also identified ZFYVE9 and ZFYVE16, which bind PP1 (Shi et al. 2007; Bennett & Alphey 2002) and localize to endosomal structures (Tsukazaki et al. 1998; Seet & Hong 2001). In our nucleoplasmic fraction we identified MKI67, a nuclear protein in proliferating cells that is localized in the nucleolus during interphase (Kill 1996; MacCallum & P. A. Hall 2000) and has been shown to bind PP1 and play a role in the assembly of the perichromosomal compartment (Booth et al. 2014). In addition, we identified Stau1, a PP1 interacting protein (Brendel et al. 2004) found to localize to the rough endoplasmic reticulum and microtubules, and also demonstrated to be an RNA

A

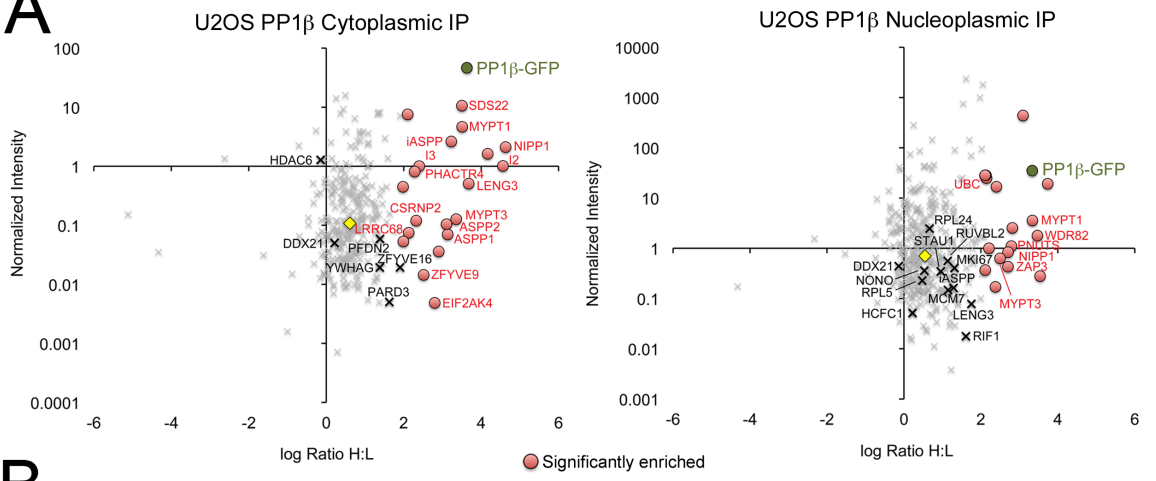

B

Known/predicted TS

Commonly enriched

		CYTOPLASMIC INTERACTOME				
		Single Isoform Mapping PP1β	Comparison to PP1α vs PP1β vs PP1γ datasets			
		U2OS	BAC lines HeLa		Stable MCF7	
INTERACTOR		# Peptides	# Peptides	Preference	# Peptides	Preference
Inh2	PPP1R2	9	8	α/γ > β	11	
SDS22	PPP1R7	19	23		21	
NIPP1	PPP1R8	19	18		24	α/γ > β
Inh3	PPP1R11	3	7		7	
MYPT1	PPP1R12A	62	37	β	47	β
LENG3	PPP1R12C	18	2	β	21	β
ASPP2	PPP1R13A	12	25	α > β/γ	17	α > β/γ
ASPP1	PPP1R13B	11	9	α	27	
iASPP	PPP1R13L	29	30	α/β	37	α/β > γ
MYPT3	PPP1R16A	4			5	β
LRRC68	PPP1R37	9			27	α > β/γ
ZFYVE16	PPP1R69	7			2	
CSRNP2	PPP1R72	7				
PARD3	PPP1R118	2				
PHACTR4	PPP1R124	21			21	
YWHAG	PPP1R170	5	3 NQ		3 NQ	
ZFYVE9	PPP1R173	3			2	
EIF2AK4		2				
PFDN2		4	4			

		NUCLEOPLASMIC INTERACTOME				
		Single Isoform Mapping PP1β	Comparison to PP1α vs PP1β vs PP1γ datasets			
		U2OS	BAC lines HeLa		Stable MCF7	
INTERACTOR		# Peptides	# Peptides	Preference	# Peptides	Preference
NIPP1	PPP1R8	7	17		16	
PNUTS	PPP1R10	11	23		19	
MYPT1	PPP1R12A	26	15	β	20	β
LENG3	PPP1R12C	5				
iASPP	PPP1R13L	5	10	α		
MYPT3	PPP1R16A	5				
MKI67	PPP1R105	46	2	γ > α/β	58	β/γ > α
STAU1	PPP1R150	5			4	
ZAP3	PPP1R169	21	37		14	
RIF1		3	36		8	
RUVBL2		7			8	
UBC		5	4			

Significance B value < 0.05 | Enriched > 2-fold above median H:L | > median

Figure 3.15. Single isoform interactome mapping identifies a broader range of interactors for PP1β. A. U2OS cytoplasmic and nucleoplasmic PP1β datasets, plotted as Normalized Intensity vs. log(2) Ratio H:L. The proteins cluster around a median (yellow diamond) value, and PP1β-GFP (green circle) is highly enriched. Known/predicted regulatory subunits and common interactors are shown in red (circles) if significantly enriched above median, and in black (X) if not. **B.** Data annotated as in Figure 8, to highlight known/predicted targeting subunits (TS) and common interactors.

binding protein both in vitro and in vivo (Kiebler et al. 1999; Wickham et al. 1999; Marión et al. 1999).

Using the STRING biological database to probe for associations between our annotated list of combined CP/NP proteins enriched 2-fold with PP1β and not detected in the respective control datasets (Figure 3.16), we uncovered a cluster of chromatin-related proteins including several histones, the heterochromatin binding proteins CB1 and CBX5, the nucleosome organizing protein SSRP1 and the regulatory subunit RIF1, which has been linked to regulation of telomere replication and repair as previously noted. We also identified a cluster of cell surface proteoglycans (Glypicans 1/4/6 and Syndecans 1/2).

3.4.4 Nucleolar regulatory subunits identified in the nucleolar GFP-tagged PP1 interactome screens

We have spent a significant time attempting to optimize the mapping of nucleolar interactomes, but the datasets are complicated by two factors. First, more stringent conditions are required to efficiently extract proteins from purified nucleoli. Second, there are a large number of nucleolar proteins that bind non-specifically to affinity matrices (Chamousset, Mamane, et al. 2010). The high salt extraction that we developed has the potential to disrupt complexes, which may or may not re-form when the salt concentration is dropped prior to AP. Furthermore, the high background signal provides a large amount of noise that reduces the signal-to-noise ratio, making it difficult to detect proteins that are enriched above background.

To summarize our nucleolar interactome datasets, we did not recover a detectable amount of GFP-PP1α or GFP-PP1γ from U2OS nucleoli. Although both were detected in their respective HeLa nucleolar datasets, no proteins were significantly enriched and only

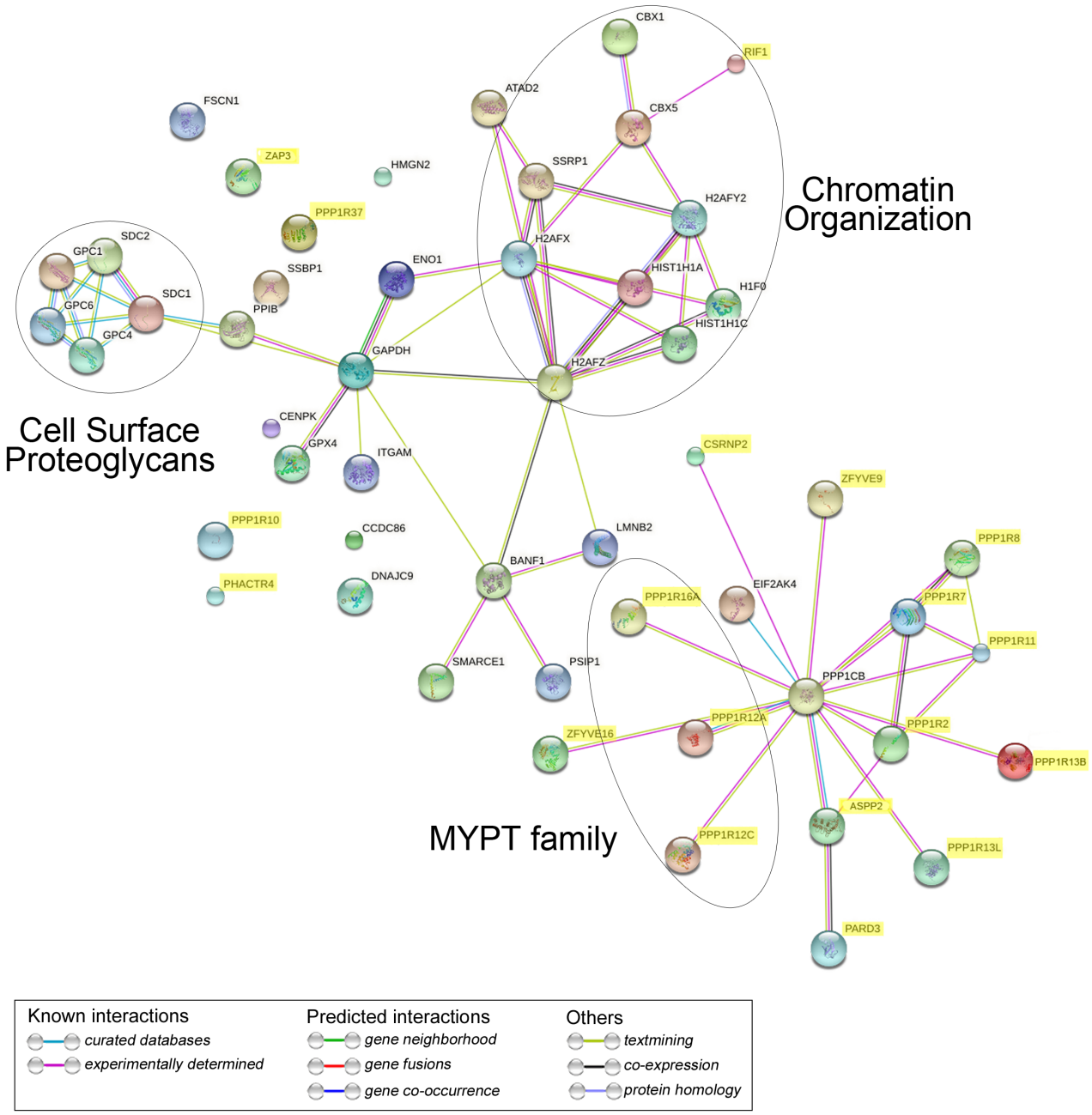

Figure 3.16. STRING analysis identifies key complexes represented in the cytoplasmic PP1β interactome. STRING-based network mapping for a stringent subset of interactors that were significantly enriched with PP1β-GFP in the combined CP and NP experiments and not detected in the respective control GFP AP/MS experiments. Known/predicted targeting subunits are highlighted (yellow).

a few were enriched >2-fold above the median. PP1α was below this threshold, and although PP1γ was above it, only one other protein was enriched >2-fold (the regulatory subunit ZAP3). Similarly, in the U2OS/PP1β-GFP nucleolar dataset, we saw no significant protein enrichment and only PP1β and three other proteins (a histone, a chromatin organizing factor and a scaffolding protein). Given that we originally identified the nucleolar regulatory subunit RRP1B in the PP1γ nucleolar interactome by scaling up our input (Chamousset, De Wever, et al. 2010), we did the same here with our HeLa/GFP-PP1γ cell line. Although this greatly increased our background contaminants (and consequently did not improve the signal-to-noise ratio), we did identify a number of nucleolar regulatory subunits that we and others had previously identified by a variety of strategies. They include RRP1B, MPHOSPH10 and NOM1, which have all been linked to regulation of ribosome biogenesis (Gunawardena et al. 2008; Chamousset, De Wever, et al. 2010; Westendorf et al. 1998; Booth et al. 2014), and MKI67, which has been linked to regulation of nucleolar reorganization at mitotic exit (Booth et al. 2014).

We confirmed the nucleolar localization of GFP-tagged RRP1B, MPHOSPH10 and NOM1 transiently overexpressed in U2OS cells and validated their association with PP1 in vivo using a Fluorescence Two-Hybrid (F2H) strategy (Figure 3.17). This involved tethering mCherry-Lac Repressor (LacR)-tagged PP1γ to a lac Operator (LacO) array stably integrated into the U2OS genome and co-expressing GFP-tagged regulatory subunits to evaluate their accumulation at this engineered gene locus (which indicates association). As shown in Figure 3.17, all three regulatory subunits accumulate within the nucleoli, and an additional pool is recruited to the tethered PP1γ. Mutation of their PP1

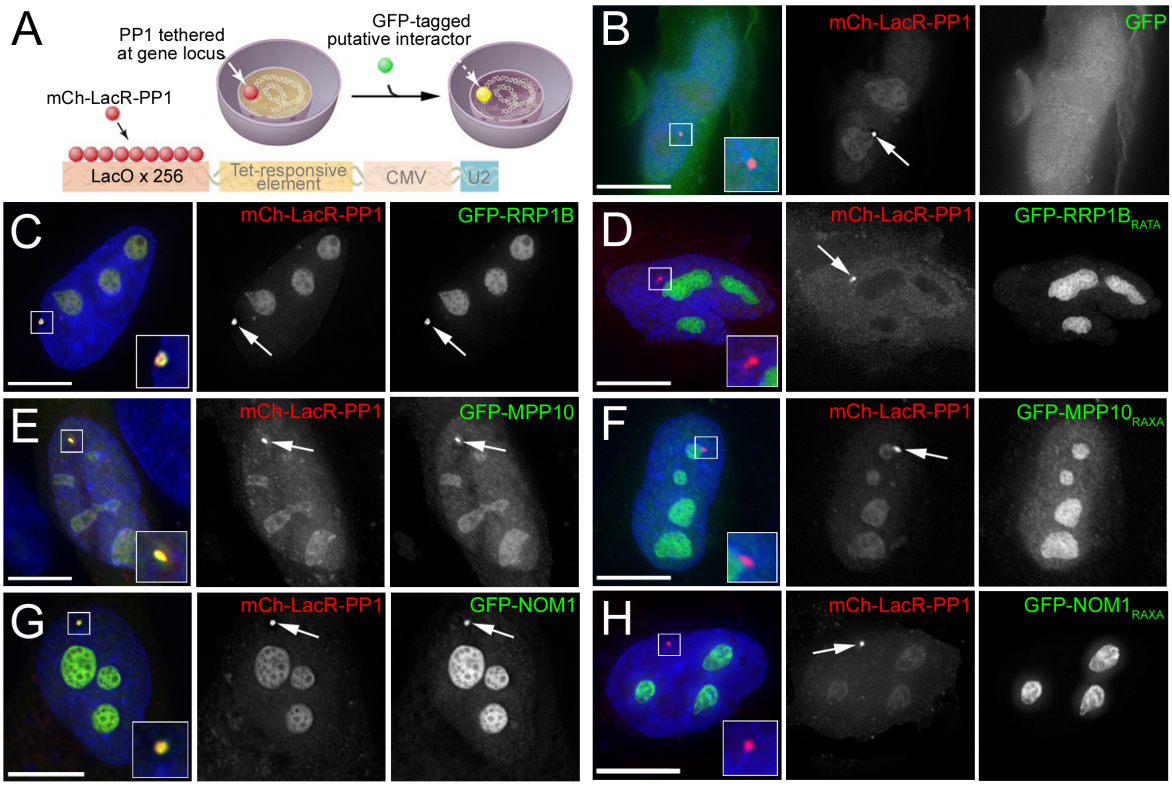

Figure 3.17. Fluorescence Two-Hybrid (F2H) analysis confirms in vivo association of nucleolar regulatory subunits with PP1 via RVXF motifs. A. Design of the F2H screen, based on random integration of an engineered gene locus containing an array of Lac Operator (LacO) repeats into HeLa cells. Although the locus contains an inducible U2 transgene, no doxycycline is provided to the cells; the cell line is used to tether transiently overexpressed mCherry-LacRepressor (LacR)-tagged PP1γ to the locus via association with the LacO array. **B.** Negative control confirming that GFP alone, co-expressed with mCh-LacR-PP1, does not accumulate at the gene locus (arrow). This region is enlarged in the inset image. A pool of GFP-RRP1B co-localizes with mCh-LacR-PP1 at the gene locus (**C**), unless its RVTF motif is mutated to prevent PP1 binding (**D**). A pool of GFP-MPP10 B co-localizes with mCh-LacR-PP1 at the gene locus (**E**), unless its RVXF motif is mutated to prevent PP1 binding (**F**). A pool of GFP-NOM1 co-localizes with mCh-LacR-PP1 at the gene locus (**G**), unless its RVXF motif is mutated to prevent PP1 binding (**H**). Scale bars are 5 μm.

binding “RVxF” motifs abolished this co-localization at the engineered gene locus. It is also interesting to note that, as previously demonstrated, overexpression of RRP1B recruits excess PP1 to the nucleolus (compare localization of mCh-lacR-PP1 in GFP vs. GFP-RRP1B expressing cells), whereas overexpression of the RRP1B that cannot bind PP1 acts as a dominant-negative mutant displacing a significant amount of the nucleolar pool of PP1 (compare localization of mCh-lacR-PP1 in GFP vs. GFP-RRP1B$_{RATA}$ expressing cells) (Chamousset, De Wever, et al. 2010). It also suggests that RRP1B has a higher affinity for PP1 than MPHOSP10 and NOM1, neither of which affected its localization to the same extent.

For future analysis of sub-nucleolar targeting of PP1 and identification of any remaining novel nucleolar regulatory subunits, we will employ a near neighbour labeling strategy such as BioID, to avoid some of the complications inherent in an AP/MS strategy.

3.5 Distribution of regulatory subunits between holoenzyme complexes in interphase and mitosis.

Given that the PP1 regulatory subunits are believed to function as network hubs that recruit PP1 to specific subcellular localizations/complexes/substrates, we mined our datasets for information about the relative distribution of each isoform between its pool of regulatory complexes. To do this, we first reanalyzed our fractionation-based AP/MS experiments for the U2OS and HeLa stable cell lines as a whole cell interactome, by concatenating the CP, NP and No raw data files. We did not eliminate any of the regulatory subunits identified in our control (GFP) interactome data set, but only highlighted those for which the summed Heavy peptides intensities were higher than the

summed Light peptide intensities (indicating some degree of specific enrichment with PP1). This eliminates those that are likely contaminants, binding non-specifically to the beads. Indeed, we detect some of these proteins, such as SFPQ, NONO and HCFC1 in most of our AP/MS experiments, including those not related to PP1. This indicates that care should be taken to when assessing their involvement in PP1 targeting within the cell.

For the remaining regulatory subunits, their specific enrichment relative to total PP1 captured on the beads was quantified by dividing their normalized (by molecular weight) Heavy peptide intensities (minus any Light peptide intensities detected, which represent any non-specific binding to the beads) by that calculated for GFP. This value is represented by the size of the bubbles in the Normalized Intensity vs. log(2) Ratio H:L graphs shown in Figures 3.18-20. These figures thus not only illustrate the regulatory subunits identified, their enrichment and abundance, but also demonstrate visually how much PP1 complexes with each. In theory the amount of GFP-PP1 identified should approximate the sum of all the regulatory subunits identified, however it is almost certain that we have not identified all of the regulatory subunits in each experiment. Also, although this type of analysis can provide some approximation of the distribution of PP1 between its regulatory subunits, it cannot provide absolute stoichiometry, as tryptic patterns and the number of identifiable peptides vary for each protein.

Having already eliminated the regulatory subunits that were below median in each experiment (i.e. higher in the Light AP), we next applied our “>2-fold enrichment with PP1” threshold to generate a high confidence list of PP1 holoenzyme complexes. The relative distribution of PP1 between this group is illustrated in the pie graphs in Figures 3.18-20.

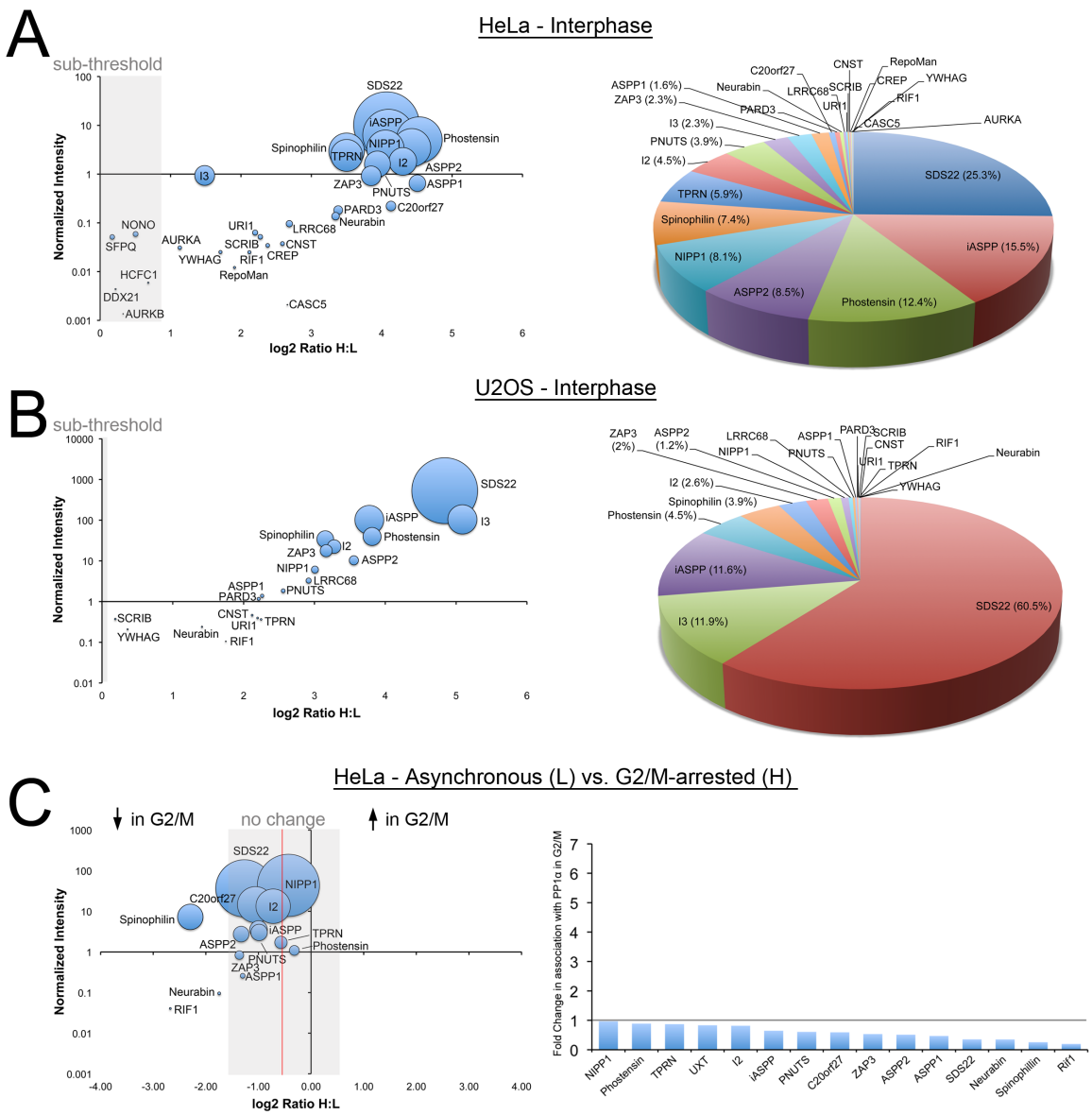

Figure 3.18. Subcellular Distribution of PP1α in Holoenzyme Complexes. A. Known/predicted PP1 regulatory subunits identified in the HeLa/cDNA GFP-PP1α screen, plotted as Normalized Intensity vs. log2 Ratio H:L. The gray box highlights those not enriched above background. For those enriched >2-fold above background, the pie chart summarizes the relative fraction of each associated with PP1 in the AP. Where a % is not indicated, it is < 1. **B.** Similar analysis for the U2OS/cDNA GFP-PP1α screen. **C.** Assessment of the change in the distribution of PP1α between regulatory complexes when the asynchronous HeLa/cDNA GFP-PP1α cell line (Light-encoded) was arrested at G2/M by 16 hr treatment with Nocodazole (Heavy-encoded). the gray box highlights those that show no change, while ratios above this threshold indicate >2-fold increase in enrichment with PP1α in G2/M cells and ratios below this threshold indicate >2-fold reduction in enrichment with PP1α in G2/M cells. The bar chart reports the relative amounts of all regulatory subunits co-precipitated with PP1 in the two conditions as fold-change with G2/M arrest.

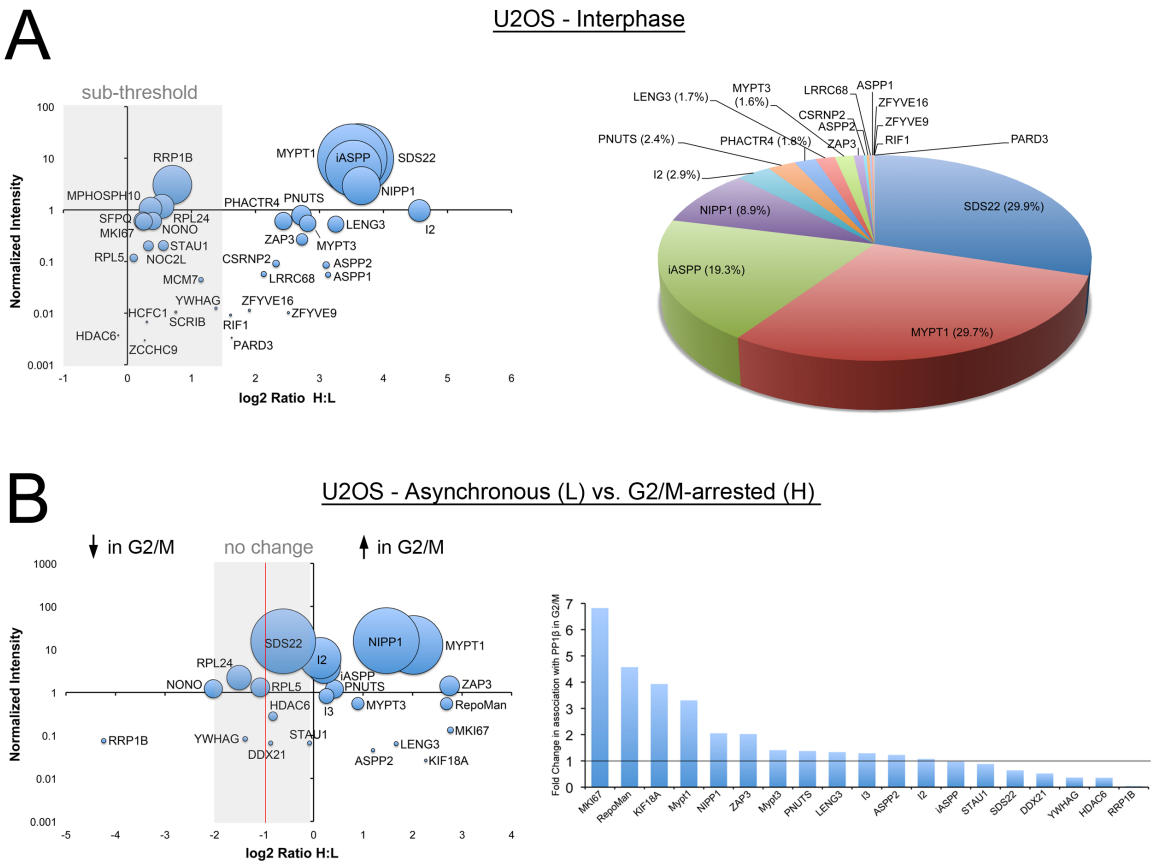

Figure 3.19. Subcellular Distribution of PP1β in Holoenzyme Complexes. A. Known/predicted PP1 regulatory subunits identified in the U2OS/cDNA PP1β-GFP screen, plotted as Normalized Intensity vs. log2 Ratio H:L. The gray box highlights those not enriched above background. For those enriched >2-fold above background, the pie chart summarizes the relative fraction of each associated with PP1 in the AP. Where a % is not indicated, it is < 1. **B.** Assessment of the change in the distribution of PP1β between regulatory complexes when the asynchronous U2OS/cDNA PP1β-GFP cell line (Light-encoded) was arrested at G2/M by 16 hr treatment with Nocodazole (Heavy-encoded). The grey box highlights those that show no change, while ratios above this threshold indicate >2-fold increase in enrichment with PP1β in G2/M cells and ratios below this threshold indicate >2-fold reduction in enrichment with PP1β in G2/M cells. The bar chart reports the relative amounts of all regulatory subunits co-precipitated with PP1 in the two conditions as fold-change with G2/M arrest.

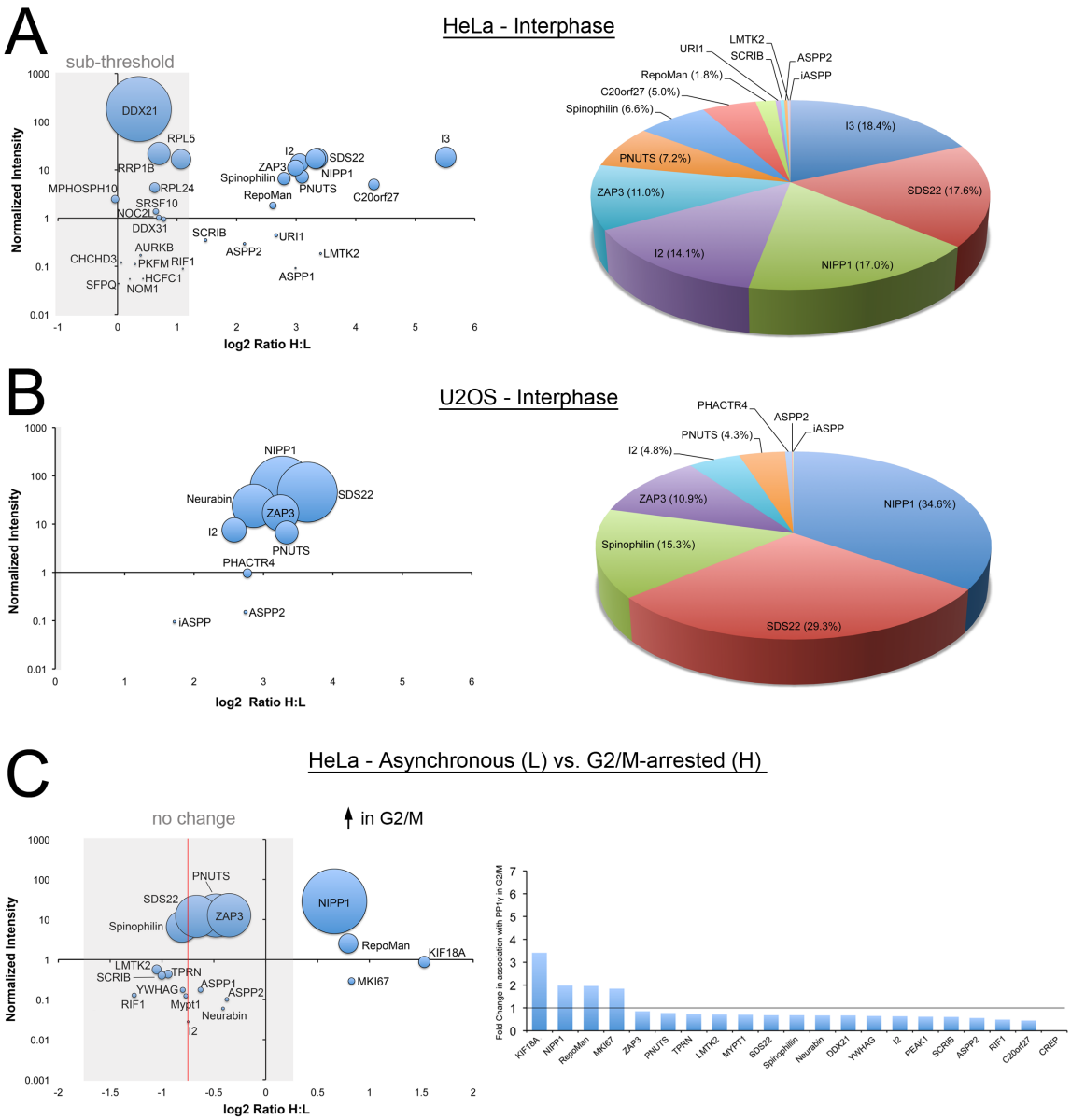

Figure 3.20. Subcellular Distribution of PP1γ in Holoenzyme Complexes. A. Known/predicted PP1 regulatory subunits identified in the HeLa/cDNA GFP-PP1γ screen, plotted as Normalized Intensity vs. log2 Ratio H:L. The gray box highlights those not enriched above background. For those enriched >2-fold above background, the pie chart summarizes the relative fraction of each associated with PP1 in the AP. Where a % is not indicated, it is < 1. **B.** Similar analysis for the U2OS/cDNA GFP-PP1γ screen. **C.** Assessment of the change in the distribution of PP1γ between regulatory complexes when the asynchronous HeLa/cDNA GFP-PP1γ cell line (Light-encoded) was arrested at G2/M by 16 hr treatment with Nocodazole (Heavy-encoded). the gray box highlights those that show no change, while ratios above this threshold indicate >2-fold increase in enrichment with PP1γ in G2/M cells and ratios below this threshold indicate >2-fold reduction in enrichment with PP1γ in G2/M cells. The bar chart reports the relative amounts of all regulatory subunits co-precipitated with PP1 in the two conditions as fold-change with G2/M arrest.

Our results indicate that for most of the cell lines, large fractions of each PP1 isoform are found in complex with the ancient regulatory subunits SDS22, Inh3 and NIPP1, whereas the more specialized (evolutionarily and likely functionally) regulatory subunits make up a much smaller fraction of the holoenzyme complexes. The ASPP family members are strongly represented in the PP1α interactome, particularly the inhibitory member iASPP, which interacts with PP1 via a non-canonical motif (RNYF) (Llanos et al. 2011). The other two isoforms are also found in complex with iASPP, and although it represents a similar fraction of the PP1β interactome, it is only a relatively minor complex for PP1γ. With the exception of Mypt1, which represents 30% of the pool of regulatory subunits associated with PP1β, and Phostensin, which accounts for 12% of complexed PP1α in HeLa cells and 4.5% in U2OS cells, most of the regulatory subunits that isoform preferences were found were in much lower amounts, such as LMTK2 with PP1γ and LRRC68 with PP1α. Overall, however, there is significant overlap between the isoform interactomes, suggesting that compensation could occur if, for example, one was knocked down/out.

The observation that a large fraction of each isoform is found in complexes considered to be inhibitory suggests that they may act, at least in part, as a "sink" for the catalytic subunit, to ensure that there is no unregulated PP1 phosphatase activity in the cell. The ability of overexpressed regulatory subunits to recruit PP1 away from other complexes demonstrates their dynamic nature, which provides the cell with the ability to maintain a homeostatic balance of phosphatase activity by targeting it to specific substrates at specific times or during specific circumstances. Our hypothesis is that regulatory subunits such as SDS22, NIPP1 and Inh3, although postulated to play specific

targeting roles (H.-S. Huang et al. 2005; Rodrigues et al. 2015; Nuytten et al. 2008), also function to maintain pools of inhibited PP1 that can exchange with other, more specialized targeting subunits as required (Lesage et al. 2007). In our U2OS CP vs NUC proteome, we only identified SDS22, which indicates that it is the highest in abundance.

If the distribution of PP1 is dynamic, as we predict, then it would be expected to change in response to cell perturbations or at different stages of the cell cycle, when distinct dephosphorylation events are required. Dynamic association with mitotic regulators such as RepoMan and CASC5 had already been observed, and the spindle-associated regulatory subunit KIF18A was identified specifically in mitotic extracts (De Wever et al. 2014). We compared the whole cell interactomes for the three isoforms in nocodazole-arrested (at G2/M) vs. asynchronous cells, using the HeLa/cDNA lines for PP1α and PP1γ and the U2OS/cDNA line for PP1β that gave us the best coverage in our fractionation experiments. Briefly the stable cell lines were cultured in Light or Heavy media for 7 days, after which the cells in Heavy media were arrested at G2/M by 16 hr treatment with 3.3 μM nocodazole (NOC). The untreated cells (Asynchronous) were harvested by trypsinization while the NOC treated cells were harvested by mitotic shake off. Whole cell extracts were prepared and GFP-PP1 captured on the GFP-Trap_A™ affinity matrix. The samples were processed as previously described and the resulting datasets annotated to highlight known/predicted regulatory subunits.

The data were first plotted (in Figures 18-20) as Normalized Intensity vs. log2 Ratio H:L (with bubble size representing enrichment relative to PP1 captured on the beads), to highlight both the amount detected and whether there was a shift toward more or less association with PP1 in the arrested cells. Where this was the case, the proteins

fell outside the gray box on each graph, which indicates the threshold. This is also visualized in a bar graph in each figure that shows the fold-change in association with PP1 in arrested vs. asynchronous cells, on the same scale (0-7) for each isoform. There was no obvious shift in PP1α complexes in the mitotic cells, except for a reduced association with a few regulatory subunits such as Spinophilin and RIF1. This may indicate a limited role for this isoform in mitosis, which would be consistent with the inhibitory Thr-320 phosphorylation by the mitotic kinase cdc2 that has been observed for this isoform (Kwon, Lee, et al. 1997).

PP1β and PP1γ showed a more dramatic redistribution, with a strong increase in association with KIF18A, RepoMan, MKI67 and NIPP1 in the arrested cells. PP1β also showed an increased association with Mypt1 under these conditions. Although these whole cell interactomes were not as comprehensive as those mapped by fractionation AP/MS, they confirmed that these isoforms undergo a redistribution between holoenzyme complexes at mitotic entry, increasing their association with regulatory subunits known to play mitotic roles (e.g. KIF18A, RepoMan) and reducing their association with those whose specific activity would not be required until the following G1 (e.g. RRP1B, RIF1), when processes such as ribosome biogenesis and transcription resume.

3.6 Validation of a novel centrosomal PP1α complex.

Imaging the various cell lines demonstrated that PP1α is the only isoform that accumulates at the centrosome in interphase cells, as confirmed by counter-staining for the centrosomal marker pericentrin (Figure. 3.21A). Although an association with the centrosomal ser/thr kinase Nek2 (Mi et al. 2007) had been previously identified, and linked to regulation of centrosome splitting (Mi et al. 2007; Meraldi & Nigg 2001),

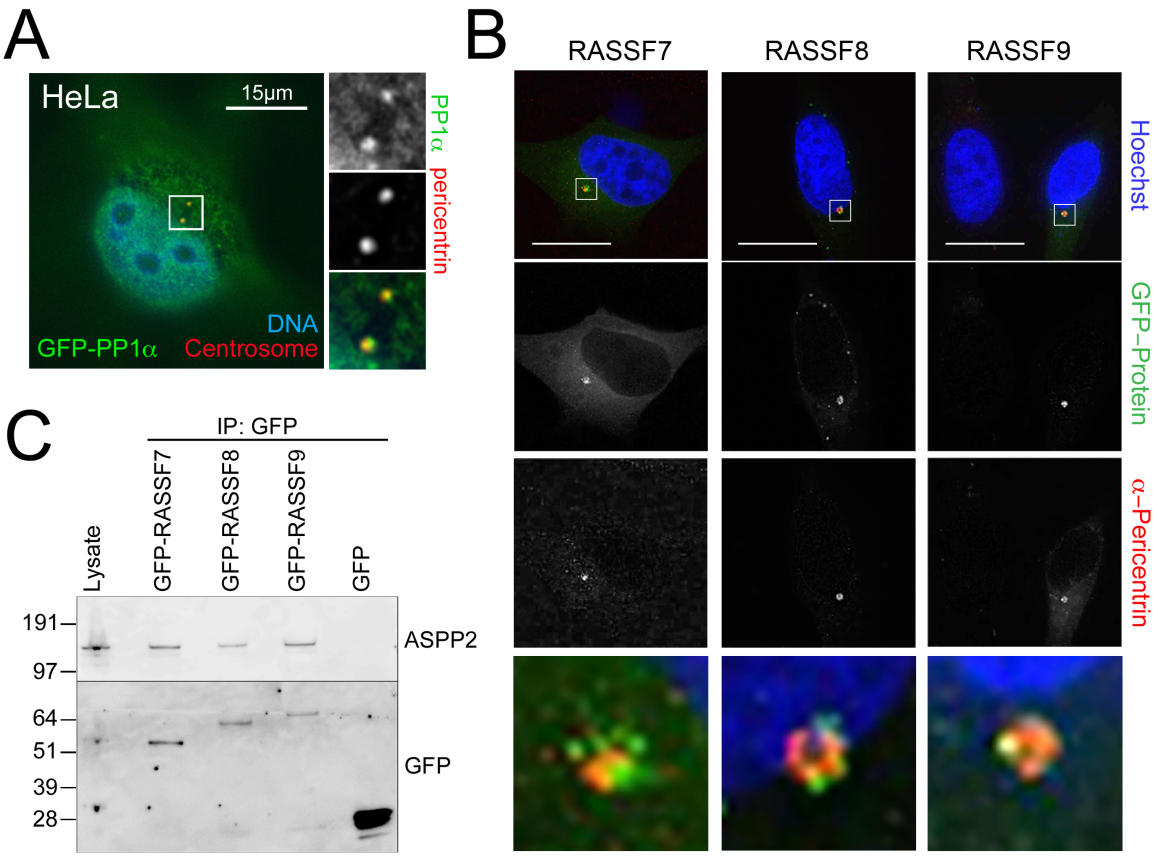

Figure 3.21. ASPP2 likely mediates the association of RASSF7/8/9 with PP1α at the centrosome. A. Accumulation of GFP-PP1α (green) at centrosomes in the HeLa/cDNA cell line, as confirmed by counter-staining with anti-pericentrin (red) and DAPI (blue). The boxed region is shown enlarged to the right. **B.** Accumulation of GFP-tagged RASSF7, RASSF8 and RASSF9 (green) at centrosomes when transiently expressed in HeLa cells, as confirmed by counter-staining with anti-pericentrin (red) and DAPI (blue). The boxed regions are shown enlarged at the bottom. Scale bars are 15 μm. **C.** Western blot analysis of GFP-Trap pulldowns of GFP-tagged RASSF7, RASSF8 and RASSF9 from HeLa whole cell lysates. Endogenous ASPP2 was detected using anti-ASPP2, and the GFP-tagged proteins (or the control GFP alone) using anti-GFP. The lysate lane is an aliquot of the GFP-RASSF7 lysate prior to AP.

we did not detect Nek2 in any of our PP1α interactomes. This may be due to the transient nature of the complex or its low abundance.

We noticed, however, that the regulatory subunit ASPP2 also showed a centrosomal localization pattern when transiently expressed as a GFP fusion (Figure 3.4), and that this subunit, although detected with all three isoforms, represented a much higher fraction of PP1α complexes (8.5%) compared to PP1β and PP1γ (<1% for each). This could explain, in part, the increased centrosomal accumulation of PP1α. Furthermore, Zhang et. al demonstrated that the ASPP proteins can recruit PP1α to dephosphorylate the centrosomal protein C-Nap1 that plays a key role in centrosomal cohesion during interphase (Zhang et al. 2015).

Interestingly, our STRING network analysis (Figure 3.10) highlighted interactions between ASPP2 and three RASS family proteins (RASSF7-9) that were only detected in our PP1α interactome. The link was based on a study in Drosophila that linked dRASSF8 and dASPP, the sole homologues for ASPP1/2, to the regulation of cell-cell adhesion during Drosophila retinal morphogenesis (Langton et al. 2009) We cloned RASSF7/8/9 and showed that all three proteins accumulate at centrosomes (Figure 3.21B). Furthermore, we demonstrated that all three co-purify endogenous ASPP2 (Figure 3.21C), confirming that their association with PP1 occurs via this regulatory subunit.

3.7 c20orf27 is a novel PP1 regulatory subunit that links the phosphatase to an E3 ubiquitin ligase complex.

Our comprehensive interactome analysis provides us with a platform to investigate potential new regulatory subunits. Of particular interest were PEAK1 and C20orf27, both

detected in multiple screens with PP1α and PP1γ. PEAK1 is a non-receptor tyrosine kinase enriched in the pseudopodia of migrating cells. It associates with the actin cytoskeleton and is found to be upregulated in aggressive epithelial cancers (Kelber & Klemke 2010; Y. Wang et al. 2010). Furthermore, it is thought to induce epithelial to mesenchymal transition (EMT) and metastasis by mediating signaling cross talk between TGFβ receptors and the ITGB3/SRC/Grb2/MAPK pathway (Galliher-Beckley & Schiemann 2008; Galliher & Schiemann 2007). A link to PP1 suggests a possible mechanism for metastatic control. We confirmed by AP/Western blot that endogenous PEAK1 co-precipitates with GFP-tagged PP1 (Figure 3.22). We also used a near neighbor labeling approach to demonstrate that PP1, when fused to a biotin ligase, can biotinylate PEAK1 and permit its capture on Streptavidin-agarose beads. The next step will be to test whether or not the association of PEAK1 with PP1 is direct (which would indicate that it is a bona fide PP1 regulatory subunit). This can be done using in vivo protein-protein interaction assays such as Bimolecular Fluorescence Complementation (BiFC) to test association of both the wild type and mutant (hydrophobic residues in the predicted PP1 binding RVxF motif at aa922-929 converted to Ala residues) protein with PP1.

This is the type of approach that we used to validate c20orf27 as a novel PP1 regulatory subunit. Due to the lack of a commercial antibody that recognizes this protein on a Western blot, we first cloned c20orf27 and expressed it as an mCherry-tagged protein. The fusion protein distributed throughout the cell when transiently overexpressed (Figure 3.23A), and Western blot analysis confirmed co-precipitation with GFP-PP1α in the HeLa/cDNA cell line (Figure 3.23C). Using the F2H assay, we demonstrated

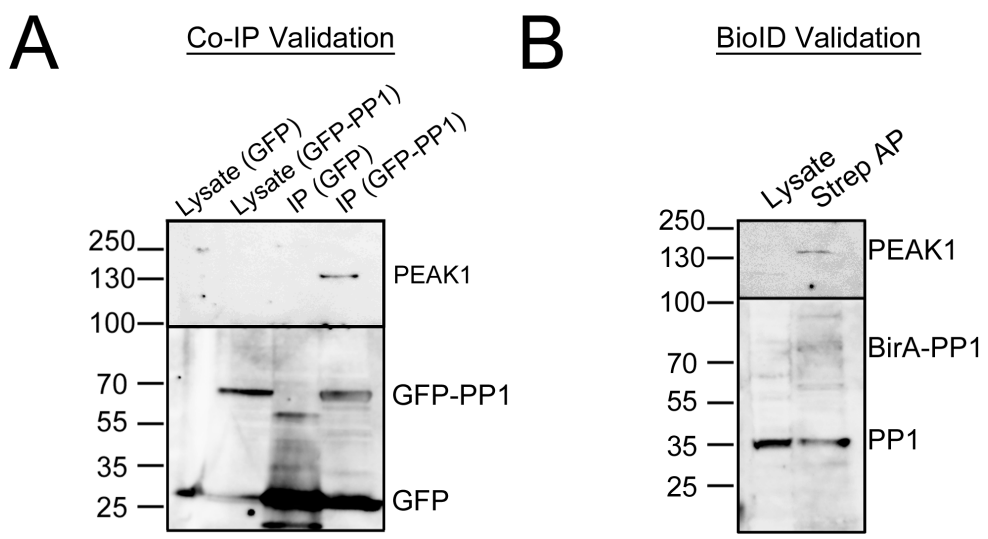

Figure 3.22. Association of PP1 with endogenous PEAK1 confirmed by co-precipitation and BioID assays. A. The co-precipitation of endogenous PEAK1 with GFP-PP1 detected by AP/MS was independently confirmed by IP/Western blot analysis. GFP-PP1γ in the HeLa/cDNA cell line was captured on GFP-Trap beads and endogenous PEAK1 detected with anti-PEAK1 on a Western blot. IP of GFP alone, transiently expressed in HeLa cells, served as a negative control. **B.** Proximity labeling also confirmed the in vivo association of PP1 and PEAK1, in this case by demonstrating that fusion of a biotin ligase (BirA) to PP1 and transient expression in HeLa cells results in the biotinylation (and resulting capture on Streptavidin-agarose beads) of endogenous PEAK1, detected here using anti-PEAK1.

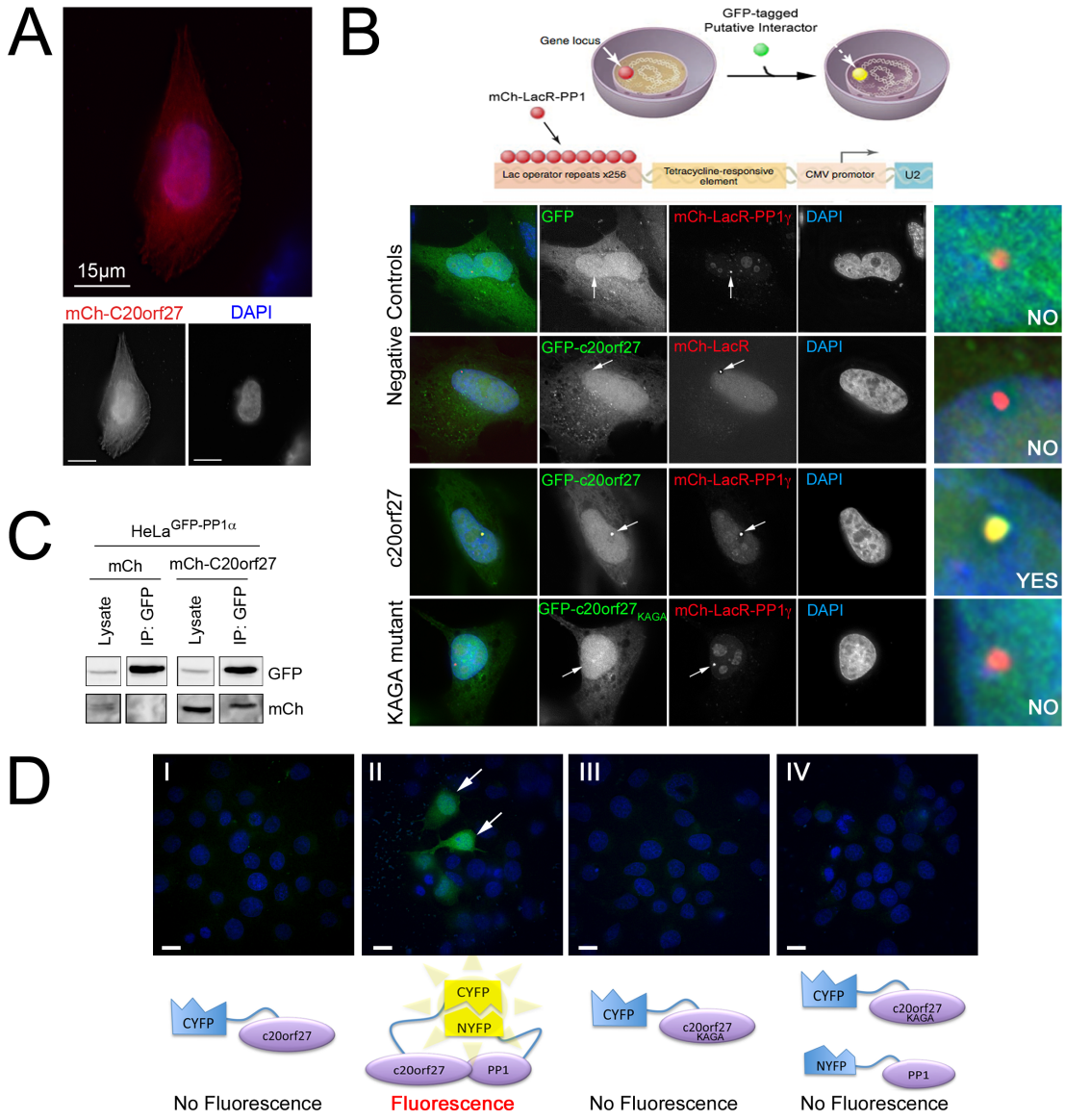

Figure 3.23. c20orf27 is a novel PP1 regulatory subunit that associates with the phosphatase via a classic RVXF-type binding domain. A. When transiently expressed in HeLa cells mCherry-c20orf27 (red) distributes throughout the cytoplasm and nucleus (blue; DAPI). **B.** F2H screen confirms association of c20orf27 with PP1 in vivo. Negative controls confirm that free GFP is not recruited to the engineered LacO array (arrow) at which mCh-LacR-PP1 accumulates, nor does GFP-c20orf27 accumulate at the array when mCh-LacR alone is tethered there. GFP-c20orf27 specifically accumulates at loci to which mCh-LacR-PP1 is tetherered, and this association is lost when the RVXF motif is mutated (KVGF to KAGA). Far right panels enlarge the locus region. **C.** GFP-PP1α (captured on GFP-Trap beads from HeLa/cDNA stable cell lysates) co-precipitates transiently expressed mCh-c20orf27 (visualized with anti-mCherry). **D.** Bimolecular Fluorescence Complementation (BiFC) assay confirms that direct binding (and subsequence fluorescence) of the split fluorophore is observed only when wild type YFP(C-terminal half; CYFP)-c20orf27 is co-expressed with YFP(N-terminal half; NYFP)-PP1 (II). The mutant does not associate with PP1 (IV) and the C-terminal halves alone are not fluorescence (I, III).

that GFP-c20orf27 accumulates at the engineered gene locus when mCh-LacR-PP1γ is tethered there (Figure 3.23B). Mutation of the putative PP1 binding RVxF motif (KVGF > KAGA mutant; V55A/F57A) obviated their association.

To further confirm direct interaction with PP1 via the $_{54}$KVGF$_{57}$ region of the protein, we cloned wild type and KAGA mutant c20orf27 into a BiFC plasmid that fuses them to the C-terminal half of EYFP, and PP1γ into a BiFC plasmid that fuses it to the N-terminal half of EYFP. When co-expressed, the two halves will only re-form a functional (fluorescent) EYFP molecule when in close proximity (< 10 nm), which occurs when the proteins to which they are tagged bind directly. As shown in Figure 3.23D, this occurs when wild type c20orf27 is co-expressed with PP1γ , confirming their direct association.

Given that our STRING network analysis did not identify links between c20orf27 and any other proteins in the datasets (Figures 10 and 14), we set out to map its interactome to gain functional clues to its role in the cell. Using our SILAC AP/MS methodology, we compared GFP-Trap pulldowns of transiently overexpressed GFP-c20orf27 (Heavy) vs. GFP alone (Light) in both HeLa (Figure 3.24A) and MCF7 (Figure 3.24B) cells. Both datasets confirmed the significant enrichment of PP1 with c20orf27, and also highlighted association with APPBP2, first identified as an Amyloid Precursor Protein (APP) binding protein potentially involved in transport of APP on the microtubule network (Zheng et al. 1998). The MCF7 dataset also identified, albeit by a single peptide, enrichment of the protein TCEB1, also known as Elongin C, which is involved in regulation of both transcription and E3 ubiquitin ligase substrate specification (Okumura et al. 2012). In order to increase our interactome coverage for c20orf27, we repeated the HeLa experiment but this time fractionated the cells into CP and NUC. The raw datasets were

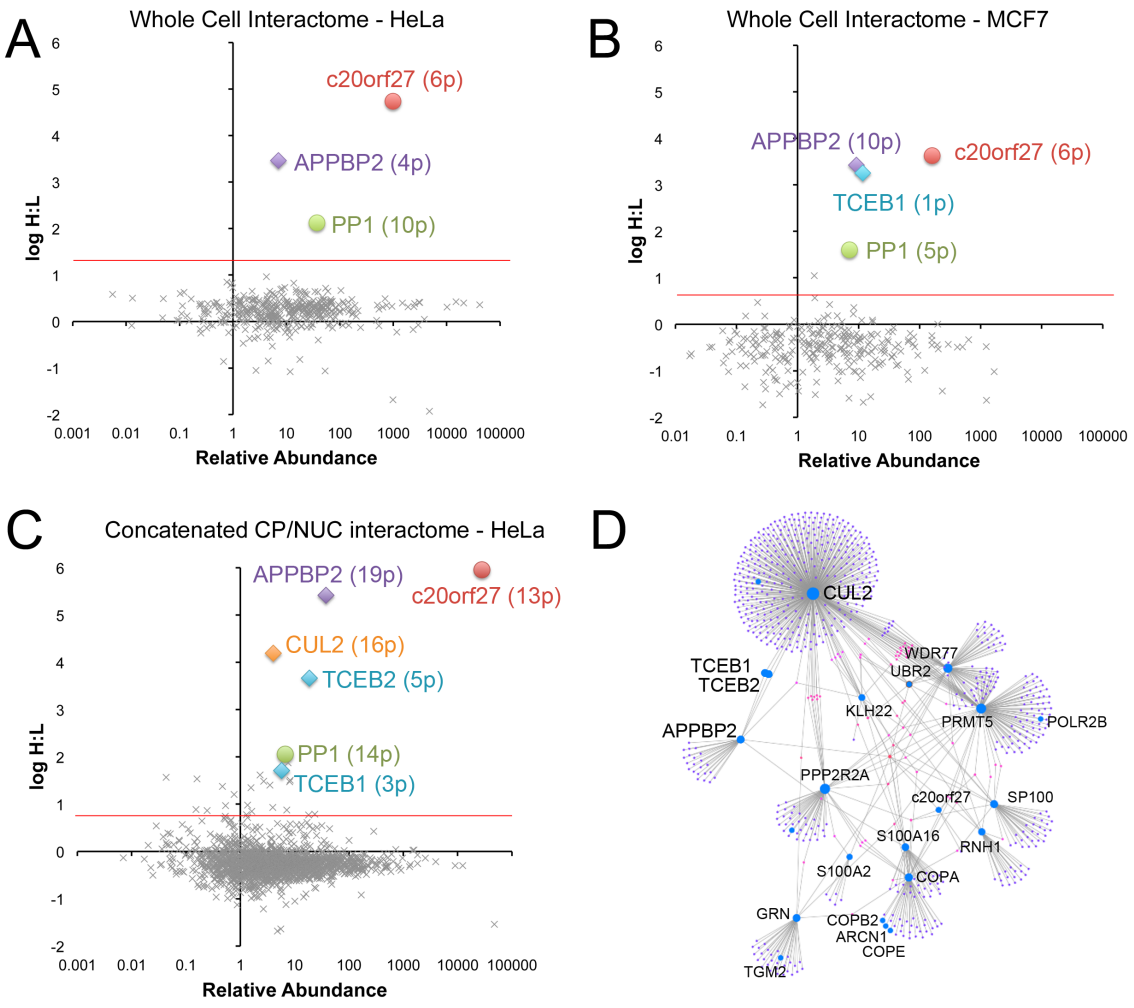

Figure 3.24. c20orf27 complexes with PP1 and APPBP2 and is associated with ubiquitin ligase complex members. PP1γ and APPBP2 were the top hits in c20orf27 interactome screens in HeLa (**A**) and MCF7 (**B**) cells, with the APPBP1 interactor TCEB1 (Elongin C) also identified (p = number of peptides detected for each). More comprehensive coverage was obtained in HeLa cells by fractionation (**C**), identifying the same factors but also TCEB2 (Elongin B) and CUL2. **D.** For the top hits in C (blue circles), interaction hubs were identified using NetworkAnalyst and the IMEx database. They include the APPBP2-TCEB1/2-CUL2 E3 ubiquitin ligase axis and a cluster of COPI (retrograde vesicle transport) coatomer proteins (COPA-COPB2/ARCN1/COPE).

concatenated for analysis, and log(2) H:L ratios vs. relative abundance plotted for all identified proteins. As shown in Figure 3.24C, association with PP1 and APPBP2 was again confirmed, as was enrichment of TCEB1 and its binding partner TCEB2 (aka Elongin B). Although a STRING-based network analysis did not highlight known associations between these proteins, screening the dataset against the IMEx interaction database using NetworkAnalyst indicated direct links between APPBP2 and TCEB1/2, and between TCEB1/2 and CUL2 (Figure 3.24D), which was also enriched in our screen (Figure 3.24C). These associations had been deposited as part of a 2008 study that identified APPBP2 as a new member of the BC box-type CUL2 (Cullin 2) binding protein family (Mahrour et al. 2008). Future studies will include mapping the region in APPBP2 that mediates association with c20orf27/PP1 and determining the downstream functional effects of preventing their association.

CHAPTER 4: Specc1 and Specc1L can form trimeric complexes with Mypt1/ PP1β to regulate its subcellular localization

4.1 Identification of Specc1/1L in the PP1β interactome.

In our BAC/HeLa and MCF7 interactome screens for the three human PP1 isoforms we identified several novel proteins not previously defined as phosphatase complex members. Of interest, was the identification of the Specc1 protein, identified in both screens as being preferentially associated with PP1β yet possessing no obvious PP1 binding motif. Furthermore, we identified the related family member Specc1L in our U2OS PP1β focused spatial AP/MS experiment. Given that only a handful of proteins were PP1β specific, and that the Specc1 family proteins have been linked to cytoskeletal roles, we speculated that the association of Specc1/1L with the catalytic subunit may be mediated by the regulatory subunit Mypt1.

To test this, we cloned both family members for insertion into pEGFP expression plasmids, transiently expressed them in HeLa cells and demonstrated that both GFP-tagged Specc1 and Specc1L co-precipitate endogenous Mypt1 (Figure 4.1A). Furthermore, we demonstrated that GFP-tagged Mypt1, when transiently expressed in HeLa cells, co-precipitates endogenous Specc1L (Figure 4.1B).

In order to identify other putative interactors enriched with this complex, we attempted to map the interactome of GFP-Mypt1 using our quantitative SILAC-based AP/MS approach. U2OS cells were labeled with either Light (R0K0) or Heavy (R6K4) media for 7 days and then transiently transfected with pEGFP or pEGFP-Mypt1, respectively. The following day cells were harvested and fractionated for preparation of

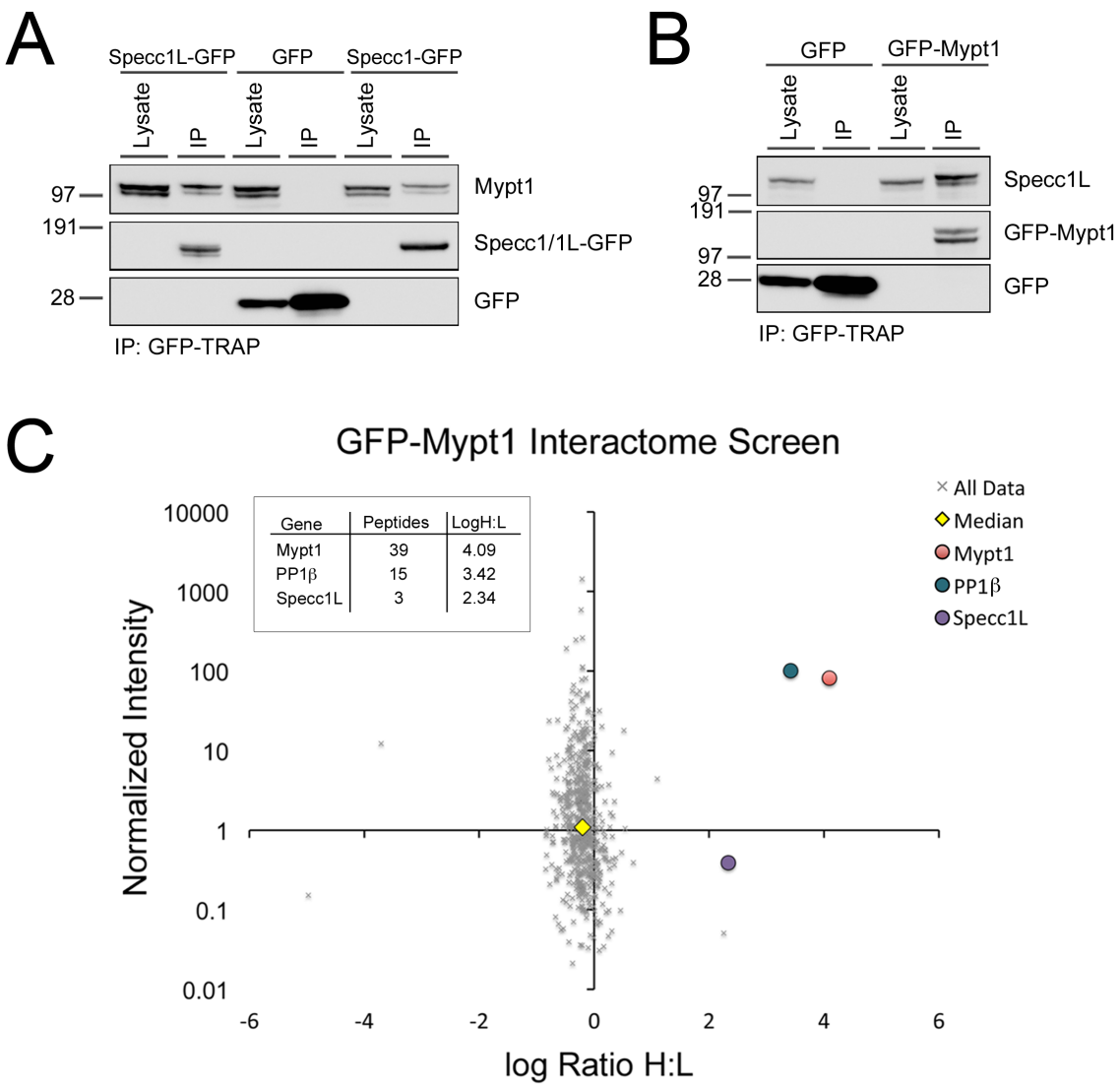

Figure 4.1. Specc1/1L associates with Mypt1. **A**. Western blot analysis demonstrating the co-purification of endogenous Mypt1 (α-Mypt1, Bethyl Lab.) with GFP-tagged Specc1L and Specc1 (α-GFP). **B.** Western blot analysis demonstrating the co-purification of endogenous Specc1L (α-Mypt1) with GFP-tagged Mypt1(α-GFP). **C.** Quantitative AP-MS combined with cellular fractionation identifies proteins that co-purify with GFP-Mypt1. Datasets were concatenated and proteins identified and quanitified using MaxQuant. Data plotted as Normalized Intensity (Intensity/MW) vs. log (2) Ratio H:L (median value -0.20). Mypt1, PP1β and Specc1L are highlighted, and the inset table notes the number of peptides identified and log (2) Ratio H:L for each.

cytoplasmic (CP) and nuclear (NUC) extracts. The data were analyzed both separately (as CP and NUC datasets) and concatenated. In the concatenated analysis we identified and quantified 523 proteins. Surprisingly, only Mypt1 itself and four associated proteins were enriched more than 2-fold above the median H:L ratio (Figure 4.1C), and the top hits in this select group were PP1β and Specc1L (dataset provided as Appendix II). These results suggest that transient overexpression of Mypt1 precludes its proper localization (and association with known substrates such as myosin), likely due to saturation of endogenous binding sites. Association with both PP1β and Specc1L under these conditions may indicate the preservation of a core trimeric complex.

4.2 Endogenous Mypt1 interactome screen confirms association with the Specc1/1L family of proteins.

In order to map the interactome of Mypt1 under non-perturbed conditions, we tested various commercial antibodies and optimized one of them (rabbit anti-Mypt1; Bethyl Laboratories) for use in IP experiments. We then combined this IP with our SILAC-based differential labeling approach to carry out an endogenous Mypt1 interactome screen. U2OS cells were labeled with either Light (R0K0) or Heavy (R6K4) media, harvested and fractionated for preparation of CP and NUC extracts. Equivalent total protein amounts of Light and Heavy extracts were incubated with either rabbit IgG (Control; Light) or anti-Mypt1 antibodies (Experimental; Heavy) covalently conjugated to Protein G sepharose beads. The beads were combined after pulldown, and all proteins eluted for separation by 1D SDS-PAGE and in-gel tryptic digestion. Aliquots of the tryptic peptides were analyzed on a Thermo Orbitrap mass spectrometer and the raw data analyzed using MaxQuant v1.2.7.4.

The data were analyzed both separately (as CP and NUC datasets) and concatenated. In the concatenated analysis we identified and quantified 511 proteins, 97 of which were enriched more than 2-fold above the median H:L ratio (Figure 4.2A). As expected, PP1β was one of the top hits, as was Specc1L. Specc1 was detected, albeit below threshold. It is not a common contaminant in our AP/MS experiments, however, so we believe that it was enriched with Mypt1. Consistent with its well-characterized role in actomyosin regulation, we saw enrichment of several members of the myosin, tropomyosin and troponin families with Mypt1. Surprisingly, we also saw enrichment of LENG3, another MYPT family member. This observation, which we validated by showing co-precipitation of endogenous Mypt1 with LENG3-GFP (Appendix III, Figure A.2), suggests that they may show some functional overlap in shared complexes. We also saw enrichment of histones with Mypt1, which would be consistent with its suggested roles in nuclear events such as transcriptional regulation. This association was confirmed by co-precipitation of histone H3 with Mypt1 from U2OS and HeLa NUC extracts (Figure 2B). Although histones are common bead contaminants that bind non-specifically to affinity matrices (Trinkle-Mulcahy et al. 2008), this IP/WB analysis confirmed the >2-fold enrichment of histone H3 on anti-MYPT1 beads above this background, as quantified in the AP/MS screen.

More surprising was our observation that endogenous Mypt1 co-precipitated known actomyosin associates such as the myosin heavy chain, MyH9, and myosin light Chain, Myl12B, almost exclusively from nuclear extracts of both HeLa and U2OS cells (AP/MS screen and Figure 4.2B), although their association would be predicted to be more readily detected in cytoplasmic extracts. This could suggest inefficient lysis (i.e. a

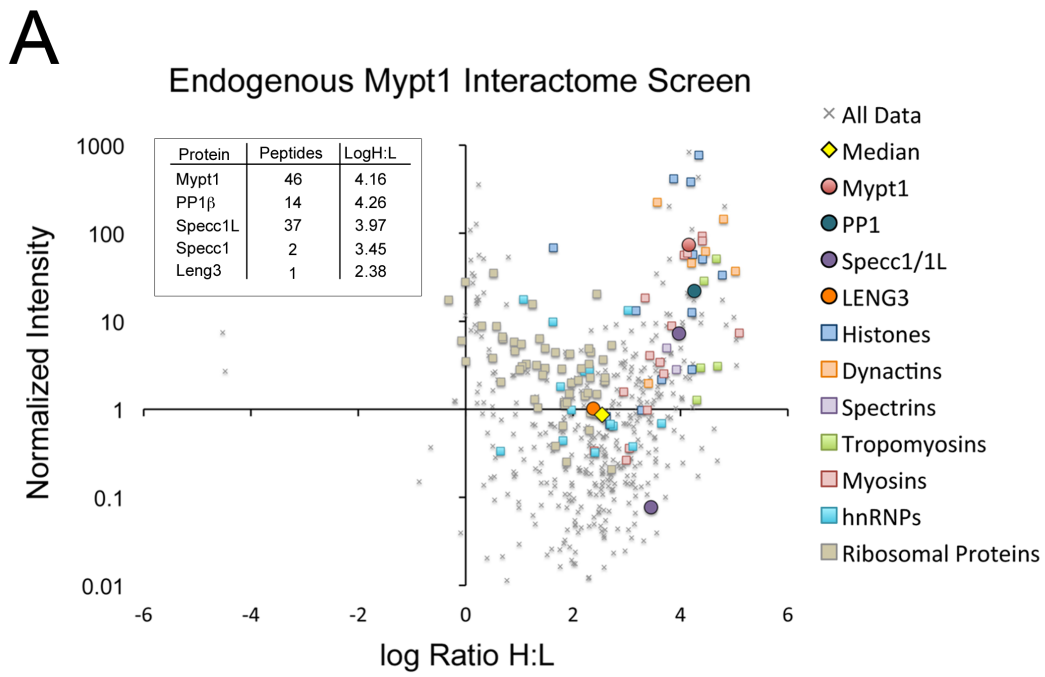

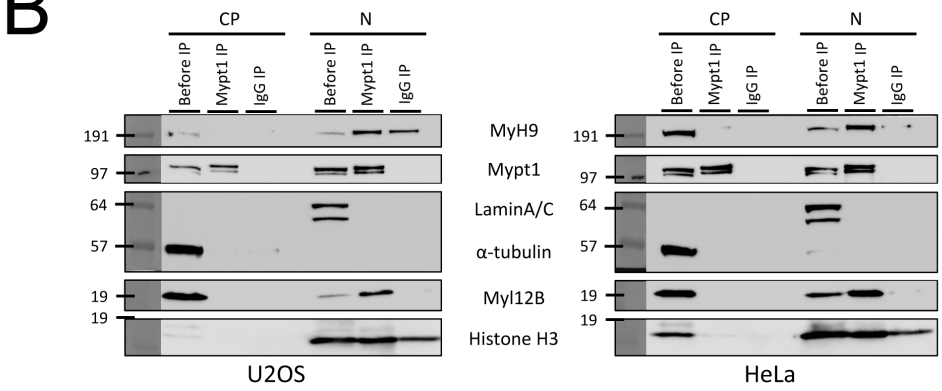

Figure 4.2. Endogenous Mypt1 interactome screen identifies multiple known and novel interactors, including Specc1/L. A. Quantitative AP-MS combined with cellular fractionation highlights proteins that co-purified with endogenous Mypt1 (α-Mypt1, Bethyl Lab). Datasets were concatenated and proteins identified and quanitified using Max-Quant. Data plotted as Normalized Intensity (Intensity/MW) vs. log (2) Ratio H:L (median value 2.54). Specific protein families are highlighted on the graph, while the inset table notes the number of peptides identified and the log Ratio H:L for Mypt1, PP1β, Specc1/L and Leng3. **B.** IP/Western blot analysis of U2OS and HeLa extracts validating the co-purification of the myosin heavy chain MyH9 and light chain Myl12B with Mypt1. Histone H3 also co-precipitates with Mypt1 (two-fold higher enrichment on anti-Mypt1 vs. IgG beads). For these experiments, a different α-Mypt1/ antibody was used for the IP. Markers for CP (α-tubulin) and NUC (Lamin A/C) are shown.

high proportion of whole cells ending up in the nuclear pellet). However, we had previously confirmed the efficiency of our fractionation by direct quantitative whole proteome analysis (See Figure 1A in Ch. 3.1). In that analysis, protein families such as myosins, actins and tropomyosins are predominantly cytoplasmic, whether we used a Dounce-based fractionation method (HeLa cells) or a detergent-based fractionation method (U2OS cells). The fact that the majority of myosin is detected in the CP extract but co-precipitates with Mypt1 primarily from the NUC extract suggests that an abundant pool of soluble myosin ends up in the CP extract as expected, while a smaller pool of filamentous myosin (which is in complex with actin, Mypt1, etc.) ends up in the NUC extract. We attempted to confirm this association by fluorescence imaging of phalloidin-stained actin filaments on purified, Hoechst-stained nuclei, but the results were inconclusive.

Moving forward, we decided to concatenate the CP and NUC data for analysis and presentation as a whole cell interactome. As discussed in Ch 3.1, we had already demonstrated that cellular fractionation increased interactome coverage significantly, as shown by direct comparison of HeLa/GFP-PP1α whole cell vs. concatenated CP/NP/No analyses. The whole cell Mypt1 interactome that we mapped with two biological replicates (see Appendix II for the datasets) confirmed association of the protein with PP1β and Specc1/1L in cell extracts, while also highlighting multiple known (e.g. myosins) and novel (e.g. dynactins) interactions.

4.3 Specc1 and Specc1L both associate with the actin cytoskeleton and the MT network

Consistent with previous reports in the literature, staining of endogenous Specc1L

revealed a predominantly cytoskeletal (CSK) pattern in interphase cells, as confirmed by colocalization with phalloidin-stained filamentous actin (Figure 4.3A). When transiently overexpressed at low levels, GFP-tagged Specc1L shows a similar localization pattern. Expression of increasingly higher levels, however, results in aberrant accumulation on the MT network, which reorganizes into thicker MT structures (Figure 4.3B). These thicker MT structures counter-stain with antibodies raised against both alpha-tubulin and acetylated alpha-tubulin (Figure 4.3C). Given that the latter is a commonly accepted marker for stabilized MTs, we decided to use Alexa647-conjugated secondary antibodies to image the acetylated alpha-tubulin staining pattern in Specc1L-GFP overexpressing cells by dSTORM (direct Stochastic Optical Reconstruction Microscopy) super-resolution imaging, which allows us to observe these structures in more detail. This approach clearly highlighted that the structures appear to be bundles of MTs lying in parallel (Figure 4.3D).

In order to minimize overexpression artefacts while allowing us to assess the dynamic localization of GFP-tagged Specc1L in live cells, we established U2OS cell lines that stably overexpress the fusion protein at very low levels. Western blot analysis confirmed that two of the clonal lines we established, E8 and E16, express low levels of full-length Specc1L-GFP (Figure 4.4A), and that the fusion protein co-purifies endogenous Mypt1 (Figure 4.4B). For both lines, a predominantly cytoplasmic localization was observed for Specc1L-GFP during interphase (Figure 4.4C), and counter-staining with phalloidin confirmed that the filamentous pattern represented actin filaments (Figure 4.4E), consistent with the observed localization of the endogenous protein (Figure 4.3A). The fusion protein was expressed at levels ~5-fold that of the endogenous protein, as

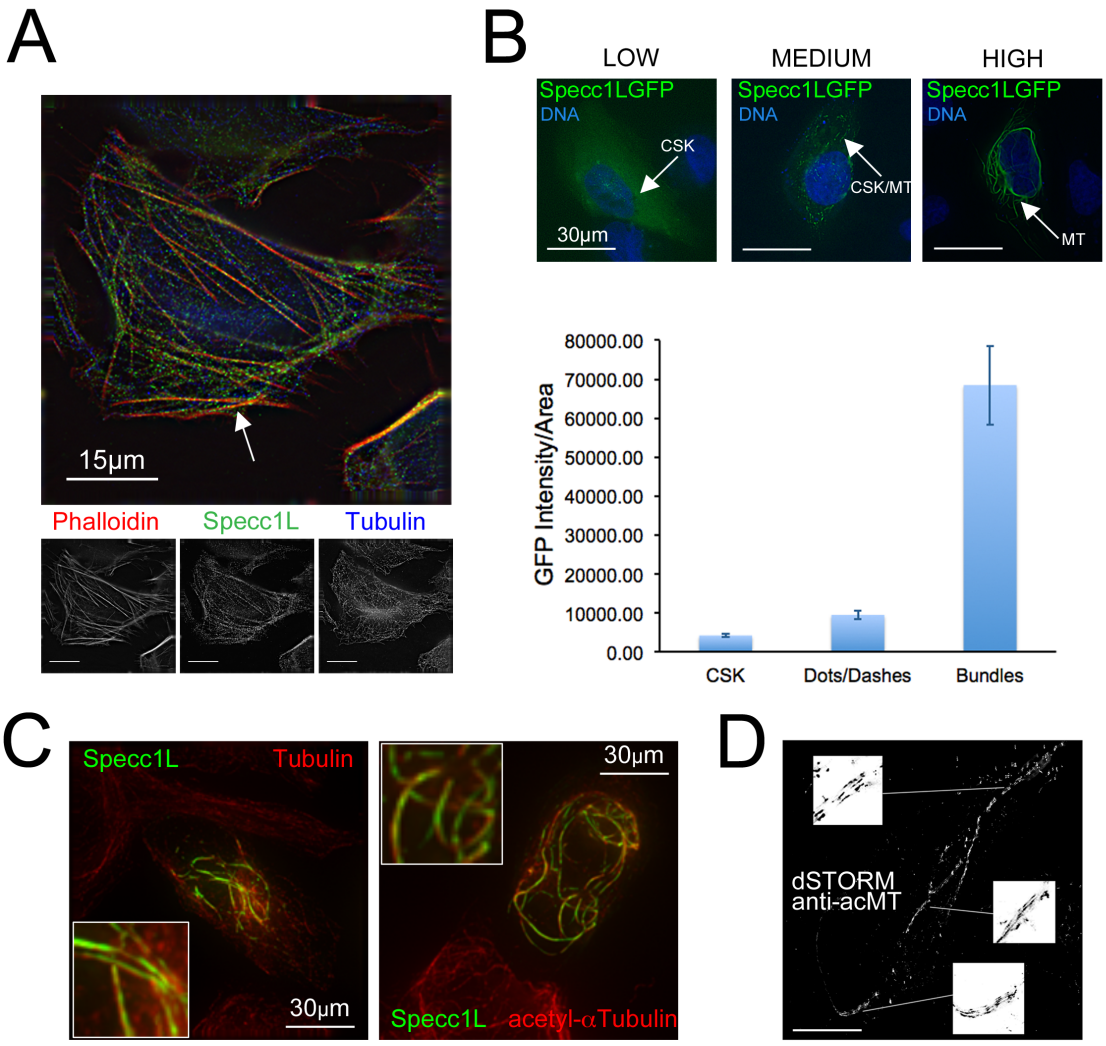

Figure 4.3. Overexpression of Specc1L induces MT stabilization. A. Localization of endogenous Specc1L (green) detected by anti-Specc1L antibody in U2OS cells, actin filaments detected by Phalloidin (Red) and Microtubules detected by anti-αTubulin (blue). Cells were PFA fixed at 37°C for 10 min to preserve the MT network. Arrow points to the phalloidin-stained actin filaments. **B.** U2OS cells transiently overexpressing Specc1L-GFP (green) and stained with Hoechst 33342 (blue) were imaged live to collect 3D Z-stacks and annotate the predominant Specc1L-GFP localization pattern. GFP intensity/area for each cell was calculated from summed intensity projections and plotted as mean +/-SE for >20 cells (n = 3). **C.** Localization of Specc1L-GFP (green) when overexpressed at high levels in HeLa cells. Cells were fixed with PFA at 37°C for 10 min and stained with anti-α-tubulin (left panel; red) or anti-acetylated-α–tubulin (right panel; red) antibodies. **D.** Super resolution imaging of the acetylated microtubule pattern detected by anti-acMT-Alexa647 antibodies in Specc1L-GFP overexpressing cells demonstrates the bundled MT structure (for clarity, regions of interest are shown inverted and enlarged in inset boxes). Scale bar represents 10 μm.

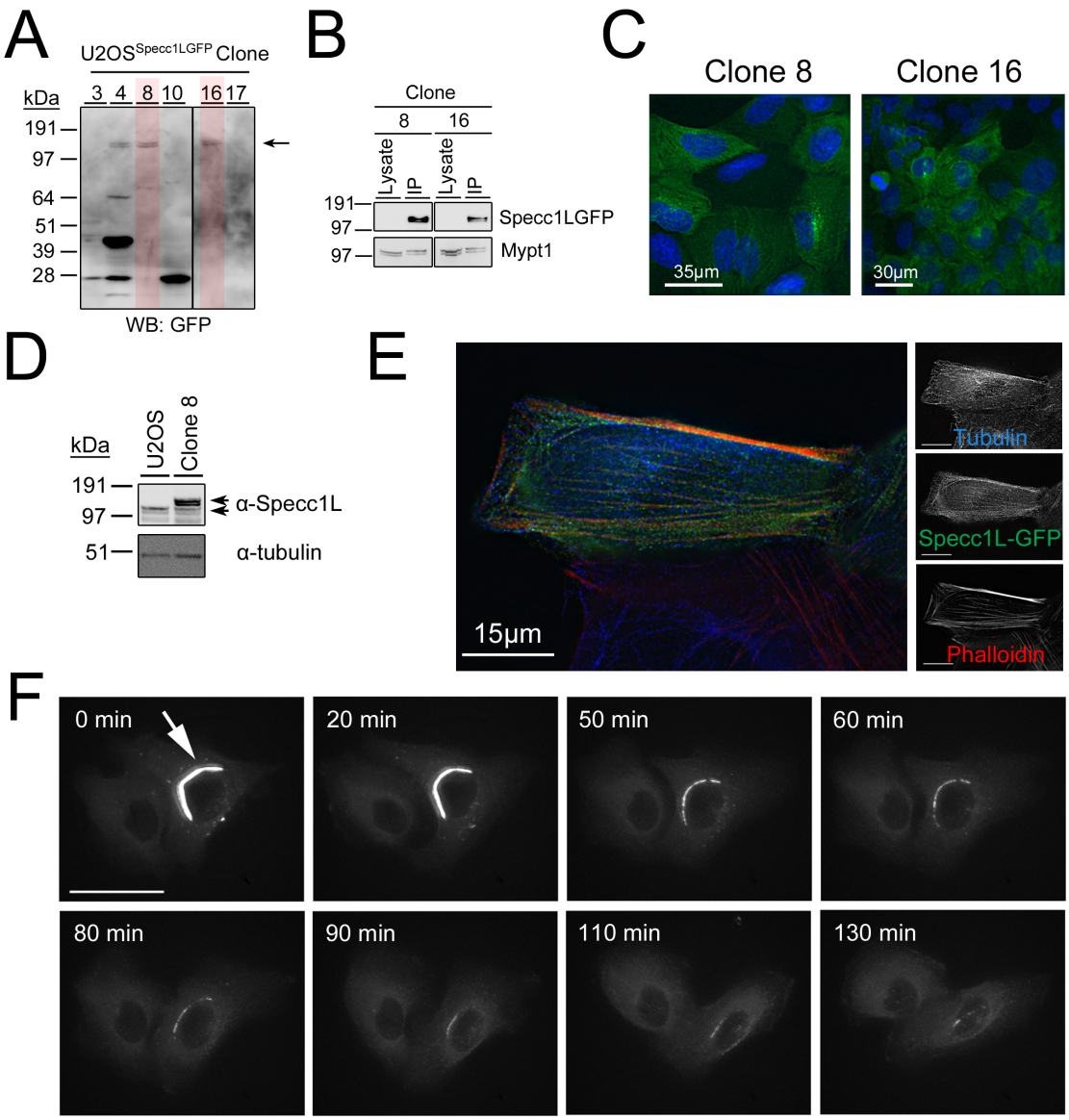

Figure 4.4. Stable expression of GFP-tagged Specc1L validates the Mypt1 interaction and steady-state actin CSK localization. A. WB analysis of U2OS cells stably expressing Specc1L-GFP (black arrow), highlighting clones 8 and 16 which contain mininal degradation products. **B.** WB analysis validating the co-purification of endogenous Mypt1 (detected using anti-Mypt1; Bethyl Labs) with GFP-tagged Specc1L (detected using anti-GFP) from clone 8 and 16 stable cell lines. **C.** Localization of stably expressed Specc1L-GFP (green) in clone 8 and 16 stable cell lines PFA-fixed and stained with DAPI (blue). **D.** WB analysis of parental U2OS and Specc1L-GFP clone 8 cell lysates probed with anti-Specc1L to detect both the endogenous (lower arrow) and fusion (upper arrow) proteins. **E.** Localization of Specc1L-GFP in the U2OS$^{Specc1L\text{-}GFP}$ clone 8 stable cell line, with filamentous actin detected by phalloidin (red) and microtubules by anti-α-tubulin (blue). Cells were PFA-fixed at 37°C for 10 min. **F.** Live imaging of Specc1L-GFP in the clone 8 stable cell line. Images were taken every 10 min. Arrow indicates bundled MTs. Scale bar is 50 μm.

demonstrated by Western blot analysis of clone 8 with anti-Specc1L antibodies (Figure 4.4D).

Interestingly, although the clonal lines had been chosen based on low expression levels of the GFP-tagged fusion protein and the absence of overexpression artefacts, we did observe accumulation of Specc1L-GFP at MT bundles in a small percentage of cells. Live imaging demonstrated that this phenotype is dynamic, with MT bundles observed to assemble and disassemble over time in a subset of cells (Figure 4.4F). This suggests that even a low overexpression of Specc1L, which can associate with both the actin CSK and the microtubule network, has the potential to affect their homeostatic balance.

This ability to monitor dynamic localization patterns in live cells is a major benefit of the U2OS$^{Specc1L\text{-}GFP}$ stable cell line, and we next turned our attention to the behavior of the protein throughout the cell cycle. Upon entry into mitosis, Specc1L-GFP was observed to relocalize to the mitotic spindle in metaphase, and then to the cleavage furrow and contractile ring during late anaphase/early telophase (Figure 4.5A-B). WB analysis confirmed that the Mypt1-Specc1L association continues in mitosis (Figure 4.5C), both in the presence (STLC-arrested cell extracts) and absence (NOC-arrested cell extracts) of the mitotic spindle. Live imaging also confirmed a transient association of GFP-tagged Specc1L with centrosomes prior to the onset of mitosis (Figure 4.5D). This transient recruitment to centrosomes had been suggested, but not demonstrated, in a previous study (Mattison et al. 2011), and suggests a role in spindle assembly. Although our focus here will be on interphase roles, it is important to note that the proteins remain in complex throughout the cell cycle, which suggests additional mitotic roles.

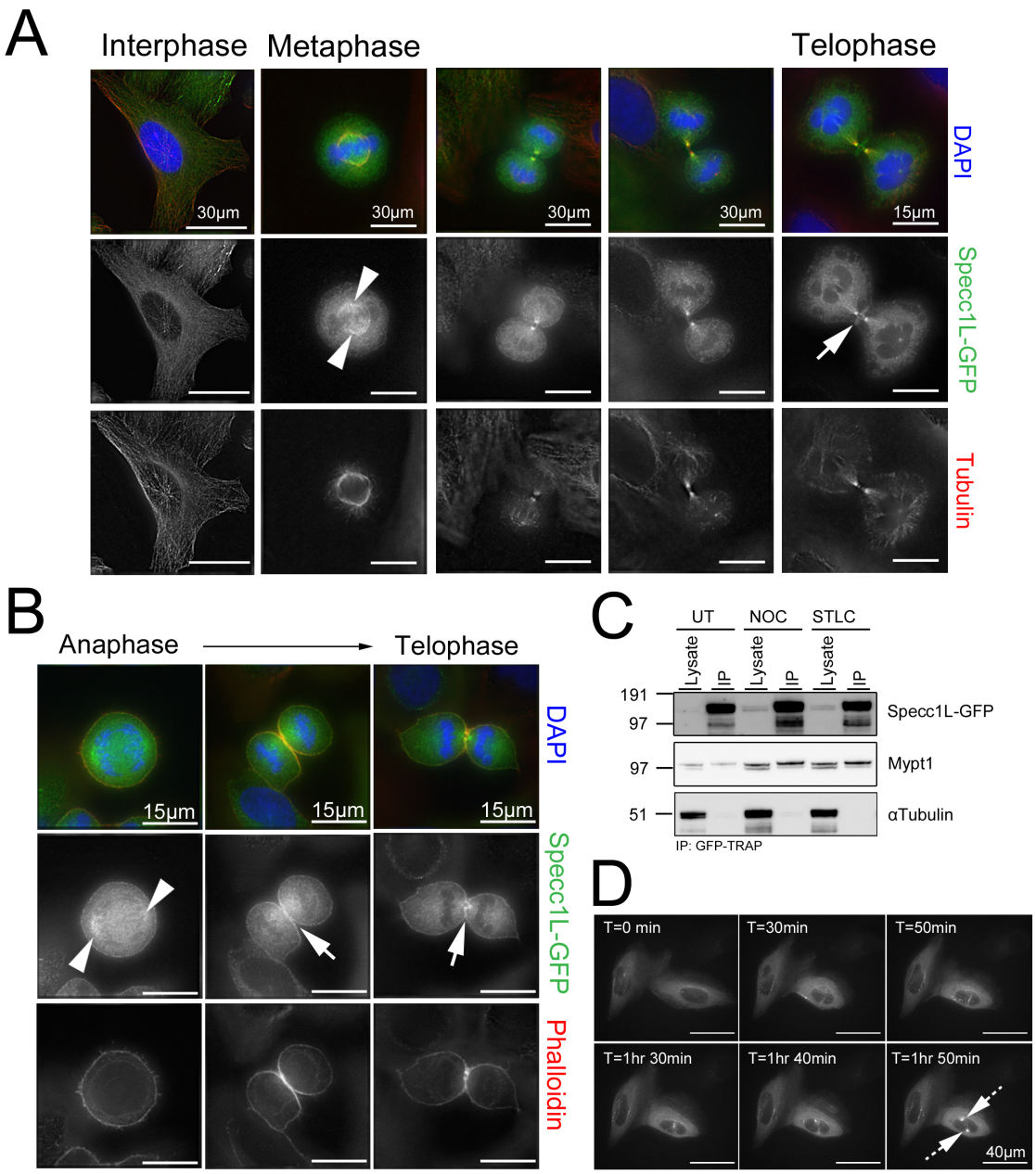

Figure 4.5. Specc1L-GFP associates with MTs, Actin and Mypt1 during mitosis. A-B. Specc1L-GFP (Green) in the U2OS^{Specc1LGFP} stable cell line localizes to the mitotic spindle in metaphase (arrowhead) and the cleavage furrow (arrow) in anaphase and telophase. Cells were PFA-fixed at 37°C for 10 min and stained to detect either MTs (anti-α-tubulin; red in A) or actin (Phalloidin; red in B). DNA was stained with DAPI (blue). **C.** Western blot analysis demonstrating co-purification of endogenous Mypt1 (anti-Mypt1; Bethyl Labs) with Specc1L-GFP (anti-GFP) from extracts of untreated (UT) cells and cells arrested using Nocodazole (NOC) or STLC. Alpha-tubulin was the loading control. **D.** Live imaging of the U2OS^{Specc1LGFP} stable cell line captured a previously proposed transient association of the protein with centrosomes (hashed arrows).

To assess whether the related family member Specc1 behaves similarly to Specc1L, we cloned and transiently overexpressed GFP-tagged Specc1 in U2OS cells. This is a more complex protein in that four isoforms are predicted, specifically splice variants that differ at either the N- or C-terminus, or both (Figure 4.6A). We chose to focus on isoforms 1 and 4 because they contain the full C-terminus of the protein, the region that contains the calponin homology (CH) domain, and thus are most similar to Specc1L. These isoforms differ at their N-termini, with first 94 amino acids of isoform (Iso) 1 replaced by a different 13 amino acid region in isoform (Iso) 4 (Figure 4.6A). Our interactome analyses could not confirm which of the isoforms co-precipitated with Mypt1, as no unique peptides were detected. Although both Specc1/Iso1 and Specc1/Iso4 are predominantly cytoplasmic, Iso1 was observed to accumulate at MTs even at low levels of expression, and induced the bundled/acetylated phenotype as expression levels increased (Figure 4.6B, left panel). Iso4 accumulated at the actin CSK at both low and high levels of expression (Figure 4.6B, right panel). This suggests that different isoforms of Specc1 may mediate its MT and CSK roles, and that the N-terminus is involved in MT association.

It is interesting to note that Specc1L, in contrast to Specc1, only has one additional predicted isoform, which is missing 38 amino acids at the C-terminus. This is consistent with the isoform that we cloned (Specc1L/Iso1) mediating both MT and CSK association. We therefore decided to focus our analysis on this protein in order to determine its overlap with the Mypt1/PP1β complex.

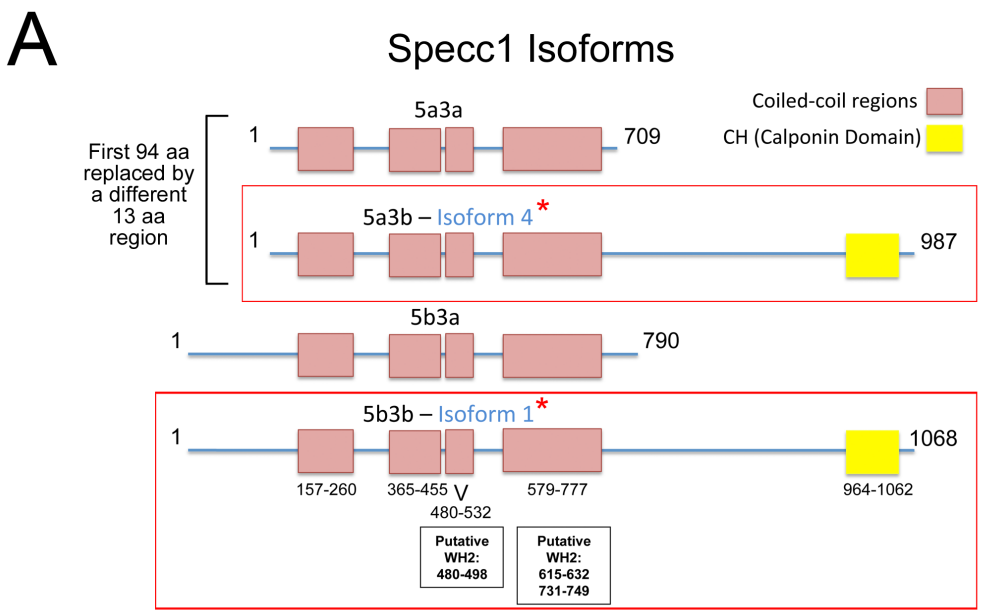

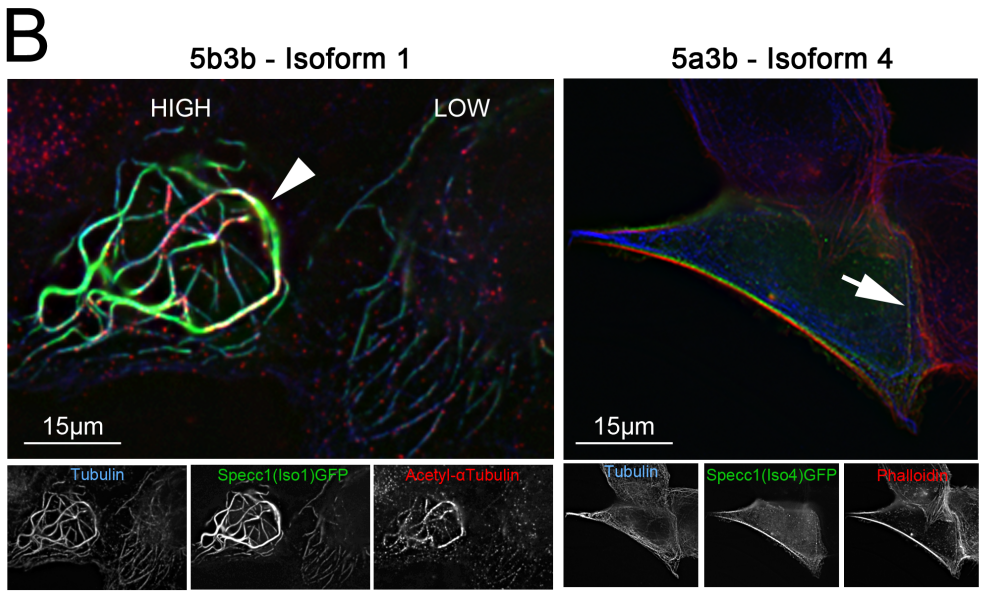

Figure 4.6. Specc1 isoforms show differences in their subcellular localization patterns when transiently overexpressed in cells. A. Schematic showing the four splice variant isoforms of Specc1, with the two that we cloned (Iso1 and Iso4) highlighted in red boxes. **B.** Specc1/Iso1-GFP (green) accumulates predominantly at MTs, with the bundled phenotype (arrowhead) induced with higher expression levels. Specc1/Iso4-GFP shows a predominantly actin CSK localization (arrow) even when overexpressed at high levels. Cells were PFA-fixed at 37°C for 10 min and stained with anti-α-tubulin (blue) and either anti-acetyl-α–tubulin (Iso1; red) or Phalloidin (Iso4; red). Scale bars at 15 μm.

4.4 Mypt1 and Specc1L interactomes show significant overlap

In the absence of robust/reliable antibodies that specifically immunoprecipitate endogenous Specc1L, we decided to use our U2OS$^{Specc1L\text{-}GFP}$ cell line to map the protein's interactome in a quantitative AP-MS experiment, with our U2OS^{GFP} cell line as the built-in negative control. Cells were harvested and fractionated to reduce complexity. Pull-down experiments were performed on CP and NUC extracts using the GFP-Trap_A™ affinity matrix. The beads were combined after pulldown, and all proteins eluted for separation by 1D SDS-PAGE and in-gel tryptic digestion. Aliquots of the tryptic peptides were analyzed on a Thermo Orbitrap mass spectrometer and the raw data analyzed using MaxQuant v1.2.7.4. The data were analyzed both separately (as CP and NUC datasets) and concatenated (datasets included in Appendix II).

We identified numerous proteins that were specifically enriched with Specc1L-GFP, and compared this list to the endogenous Mypt1 interactome (Figure 4.2A) to determine their overlap. In our Specc1L-GFP concatenated analysis we identified and quantified 693 proteins, 67 of which were enriched more than 2-fold above the median H:L ratio. Comparison of the high-confidence Mypt1 and Specc1L interactor datasets revealed that 29 proteins were enriched with both >2-fold above background (Figure 4.7A). This overlap represents 76% of the Specc1L interactome and 43% of the Mypt1 interactome, and includes shared association with several cytoskeletal proteins, including myosin, actins and intermediate filament factors (Figure 4.7B). Examples of unique associations include the specific enrichment of several members of the dynactin family with Mypt1 (DCTN1-5) and the nuclear pore complex member (NUP205) with Specc1L, which will be followed up on in future work. Importantly, the high degree of overlap of

A

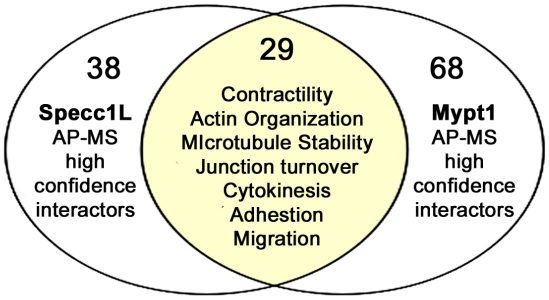

B

Proteins enriched in Screens		Log Ratio H:L		Normalized Intensity	
Description	Gene Name	Specc1LGFP	Mypt1	Specc1LGFP	Mypt1
Phosphatase complex	Mypt1	3.52	4.16	12.99	73.77
	PPP1CB	1.15	4.26	30.74	22.03
Actin and Tubulin binding	SPECC1L	4.34	3.97	471.95	7.27
Myosins, Heavy Chains	MYH10	3.15	3.84	53.20	8.90
	MYH9	4.26	4.07	1228.89	56.59
Myosins, Light Chains	MYL12B	4.52	4.40	810.00	92.81
	MYL3	4.95	5.10	184.78	7.39
	MYL6	4.61	4.41	931.70	81.72
Unconventional Myosins	MYO1C	3.40	4.13	218.66	59.22
	MYO1D	3.14	3.62	15.17	3.42
	MYO6	2.45	3.69	7.12	2.54
Actin Binding	SPTAN1	1.64	3.74	42.20	4.98
	SPTBN1	1.74	3.92	24.81	2.83
	TMOD3	3.40	4.40	63.51	12.05
	TPM1	1.93	4.38	15.13	2.96
	TPM1	3.16	4.44	45.63	28.57
	TPM2	3.73	4.30	145.83	1.27
	TPM4	1.67	4.69	53.55	3.09
	ACTN1	1.62	3.54	62.09	9.51
	ACTN4	1.89	3.80	15.47	11.94
Actin Related	ARPC5	1.57	5.05	9.52	3.15
Actin Crosslinking/ Scaffolding Proteins	SPTAN1	1.64	3.74	42.20	4.98
	SPTBN1	1.74	3.92	24.81	2.83
Constituents of Intermediate Filaments	KRT18	1.95	4.21	116.16	111.01
	KRT8	1.82	3.79	85.29	203.24
	VIM	2.20	4.16	2695.57	836.01
Calcium Binding subunit	CALM2	1.46	4.25	17.56	11.52
Cell surface glycoproteins	CD44	3.50	4.38	3.71	9.62
	CD59	3.96	4.99	127.85	11.16
	THY1	3.59	4.41	130.47	47.50
Subunit of G proteins	GNAI2	1.51	4.03	34.54	9.80
Tight Junction Protein	TJP1	1.86	3.64	1.96	1.49
		Median = 0.135	Median = 2.53		

Figure 4.7. Mypt1 and Specc1L interactomes show a significant overlap of proteins associated with the actin cytoskeletal network. A. Venn Diagram illustrating the number of high confidence interactors (>2-fold enrichment) in our Mypt1 and Specc1L-GFP interactomes that significantly overlap, and a summary of their subcellular roles. **B.** Full list of shared interactors showing their log(2) H:L ratios and normalized intensities in both datasets (median ratios noted below table). Note that although PP1β was sub-threshold in the Specc1L interactome (grey), their association has been confirmed by IP/WB.

their interactomes supports our hypothesis that Specc1L and Mypt1 are both found in similar cytoplasmic complexes and predominantly associated with the actin cytoskeleton in interphase cells. The association of PP1β with Specc1L, although found below the threshold in the Specc1L interactome, was confirmed by IP/western blot analysis done from the NUC extract of the stable cell line (Appendix III, Figure A.3)

4.5 The C-terminal half of Specc1/1L mediates association with the actin cytoskeleton

The presence of a CH domain at the C-terminus of Specc1L has been suggested to facilitate actin binding(Gimona et al. 2002). We first tested whether the C-terminal half of the protein, which contains this region, mediates association of Specc1L with actin. To do this, we created truncation mutants consisting of either the N-terminal (aa 1-462) or C-terminal (aa 462-1117) half of Specc1L fused to GFP (Figure 4.8A, 4.10A). We demonstrated a filamentous localization pattern for the C-terminal half of Specc1L, and confirmed its specific colocalization with phalloidin-stained actin filaments (Figure 4.8B). The C-terminal fragment of Specc1, which is conserved in Iso1 and Iso4, shows a similar filamentous localization pattern (Figure 4.8C) to that of full-length Specc1/Iso4 (Figure 4.6B, right panel).

Association with the actin cytoskeleton was further confirmed by demonstrating the loss of the filamentous localization pattern when cells were treated with 2 μM Latrunculin (LAT) for two hours to disrupt filamentous actin. Conversely, short-term treatment with the MT destabilizing drug Nocodazole had no effect on the localization pattern of the GFP-tagged C-terminal half of Specc1L (Figure 4.8D), which would be expected as it does not colocalize with MTs (see inset, which shows an untreated cell).

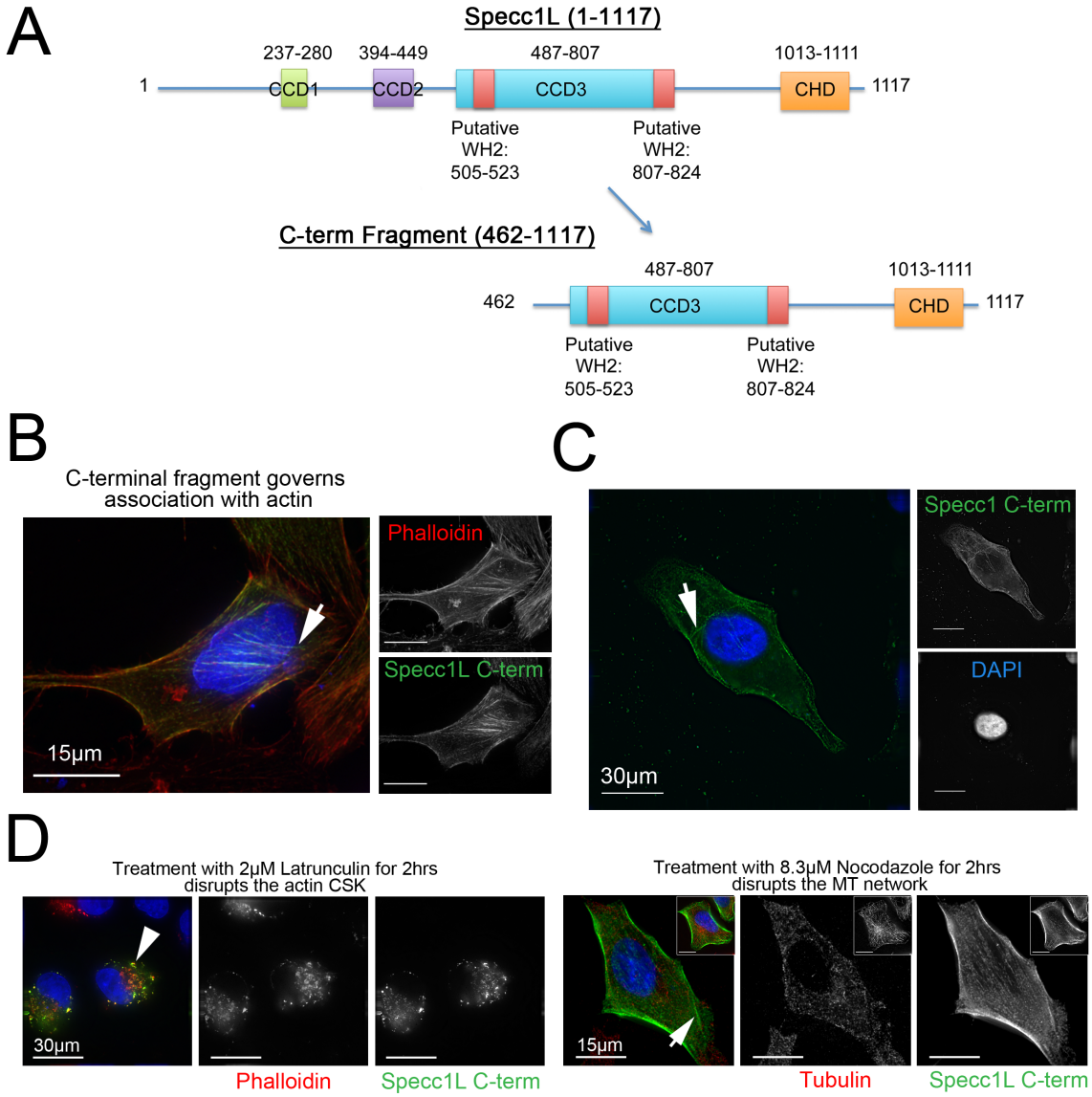

Figure 4.8. The C-terminal (462-1117) half of Specc1L co-localizes with the actin CSK. A. Schematic illustrating the domains that are included in the 462-1117 Specc1L Fragment. **B/C.** GFP-tagged Specc1/1L C-term (green) shows a filamentous pattern that colocalizes with phalloidin-stained filamentous actin (red). Cells were fixed with PHEM/PFA at 37°C for 10min, where the DNA was stained with DAPI (Blue). **D.** Disruption of filamentous actin with 2 µM Latrunculin for two hours disrupted the localization of the C-term half, whereas disruption of the MT network, seen by tubulin staining (red) with 8.3 µM Nocodazole had no affect on the localization, where GFP-Specc1L C-term (green) retained its CSK localization pattern. The inset demonstrates that the localization of GFP-Specc1L C-term does not overlap with the MT network. It also demonstrates the localization pattern of the MTs, seen by staining of tubulin (red), before NOC treatment. Cells were fixed with PHEM/PFA at 37°C for 10min, where the DNA was stained with DAPI (blue).

With both Specc1L and Specc1 able to associate with the actin CSK, and the fact that their C-terminal halves show the highest conservation in the CH domain (83.5% identical; see Figure 1.8B in the Introduction), it is reasonable to assume that this region governs actin association. However, analysis using the ELM (eukaryotic linear motif) online resource identified two putative WH2 actin-binding domains in the C-terminal half of Specc1L, upstream of the CH domain (aa 505-523 and aa 807-824; Figure 4.9A), and 3 in a similar region in Specc1 (aa 480-498, aa 615-632 and aa 731-749; Figure 4.6A). We therefore further divided our Specc1L C-terminal half into two truncation mutants (Figure 9A), one lacking the CH domain (aa 462-890) and the other including this domain plus ~100 aa upstream of it (aa 891-1117).

Removal of the CH domain from the C-terminal half of Specc1L did not obviate actin association (Figure 4.9B), although the pattern appears to be somewhat different to that observed for the CH domain-containing fragment (Figure 4.9C). While the latter distributes along straight stretches of a filamentous network, as observed for phalloidin staining of non-transfected cells, overexpression of the 462-890 truncation mutant appears to induce a “whorled” pattern of actin filaments in the center of the cell. This suggests that both regions play roles in the targeting of Specc1L to the actin network, perhaps by mediating association with particular actin structures, and that certain truncated fragments of the protein may act as dominant-negative mutants that disrupt normal filament architecture.

4.6 The N-terminal half of Specc1/1L associates with MTs

We and others have shown that Specc1L accumulates at the mitotic spindle during mitosis, and can override its predominant actin CSK association pattern in interphase by

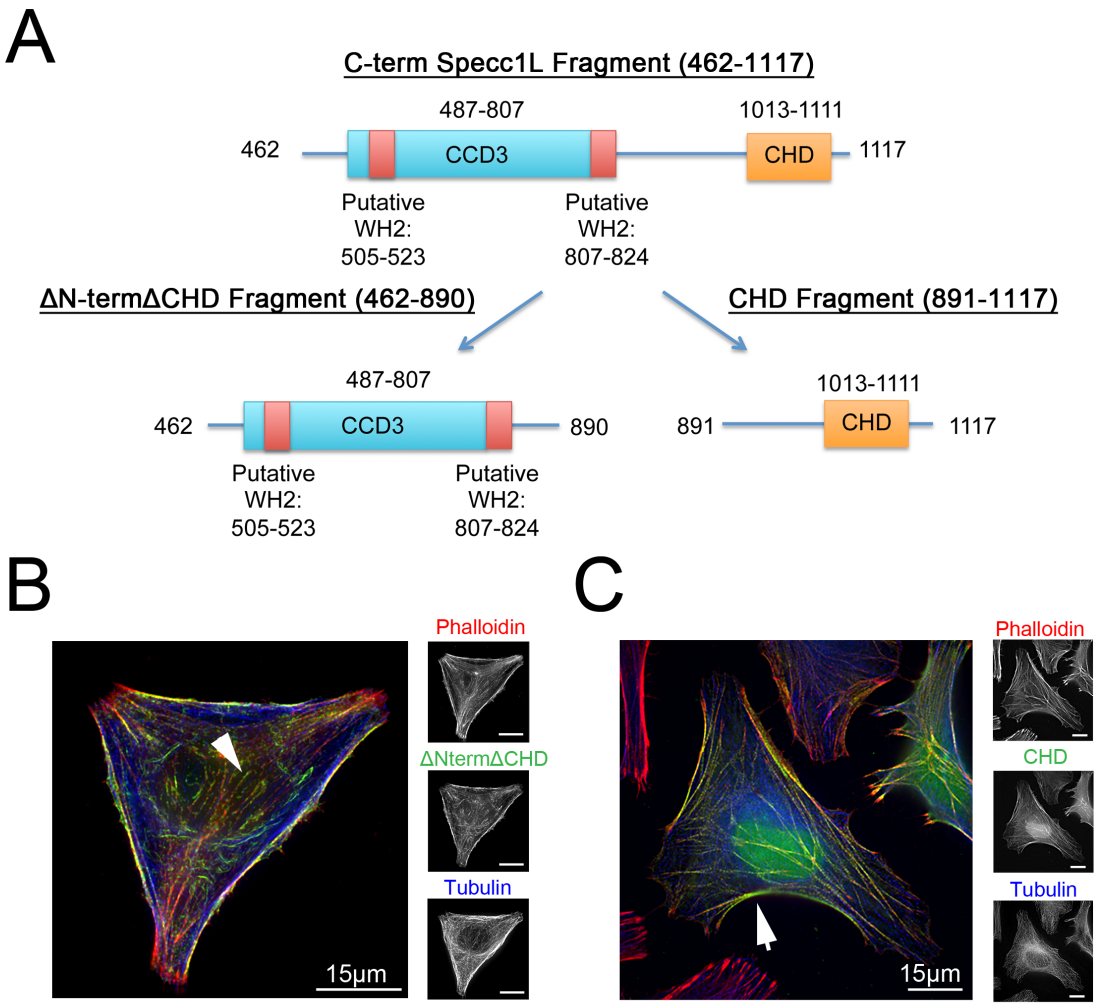

Figure 4.9. Removal of the CH domain (CHD), from the C-terminal (462-1117) half of Specc1L, does not abolish the association with the actin CSK. A. Schematic illustrating how the C-terminal fragment of Specc1L was split, demonstrating the domains that remained with the ΔN-termΔCHD (462-890) and the CHD (891-1117) fragment. **B.** GFP-tagged Specc1LΔN-termΔ CHD (green), shows regions of overlap with phalloidin-stained filamentous actin (red) and less so with the tubulin-stained MTs (blue). **C.** GFP-tagged Specc1L CHD (Green) has a more filamentous actin localization pattern that overlaps with phalloidin-stained filamentous actin (red) and not with the tubulin stained MTs (blue).

accumulating at MT bundles when overexpressed at high levels (Saadi et al. 2011; Mattison et al. 2011). Both observations suggest that Specc1L can associate with the MT network, although it has no obvious MT binding domains. Given that the C-terminal half of the protein mediates association with actin, we speculated that the N-terminal half may mediate MT association.

When transiently expressed in cells, the N-terminal half (aa 1-461; Figure 4.10B) of Specc1L was observed to accumulate at MTs counter-stained with anti-α-tubulin. This localization pattern was lost when cells were treated with 8.3 μM Nocodozole (NOC) for two hours, which disrupts the MT network by destabilizing the MTs (Figure 4.10C). Similarly, the N-terminal half of Specc1/Iso1 (aa 1-461) also accumulates at the MT network (Figure 4.10D). Furthermore, analysis of the localization of this fragment throughout the cell cycle confirmed that it also mediates association with the mitotic spindle (Figure 4.10E).

Unlike full length Specc1L and Specc1/Iso1, overexpression of the truncation mutants does not induce MT bundling/acetylation, suggesting that additional regions of the protein are required for this phenotype. Figure 4.11 shows a CLUSTAL alignment of the N-terminal halves of Specc1/Iso1 and Specc1L, which highlights a stretch of ~50 aa (yellow box) that is 70% identical. Interestingly, this region contains amino acid mutations found in the Specc1L gene of patients with genetic malformations. It is also just downstream of two serine residues in Specc1L (S384, S385) that we have identified as being phosphorylated in interphase and potentially regulated by Mypt1 (discussed below). It is tempting to speculate that domain is involved in the MT association of Specc1/L, and future work will test the functional effect of mutations within and near this region

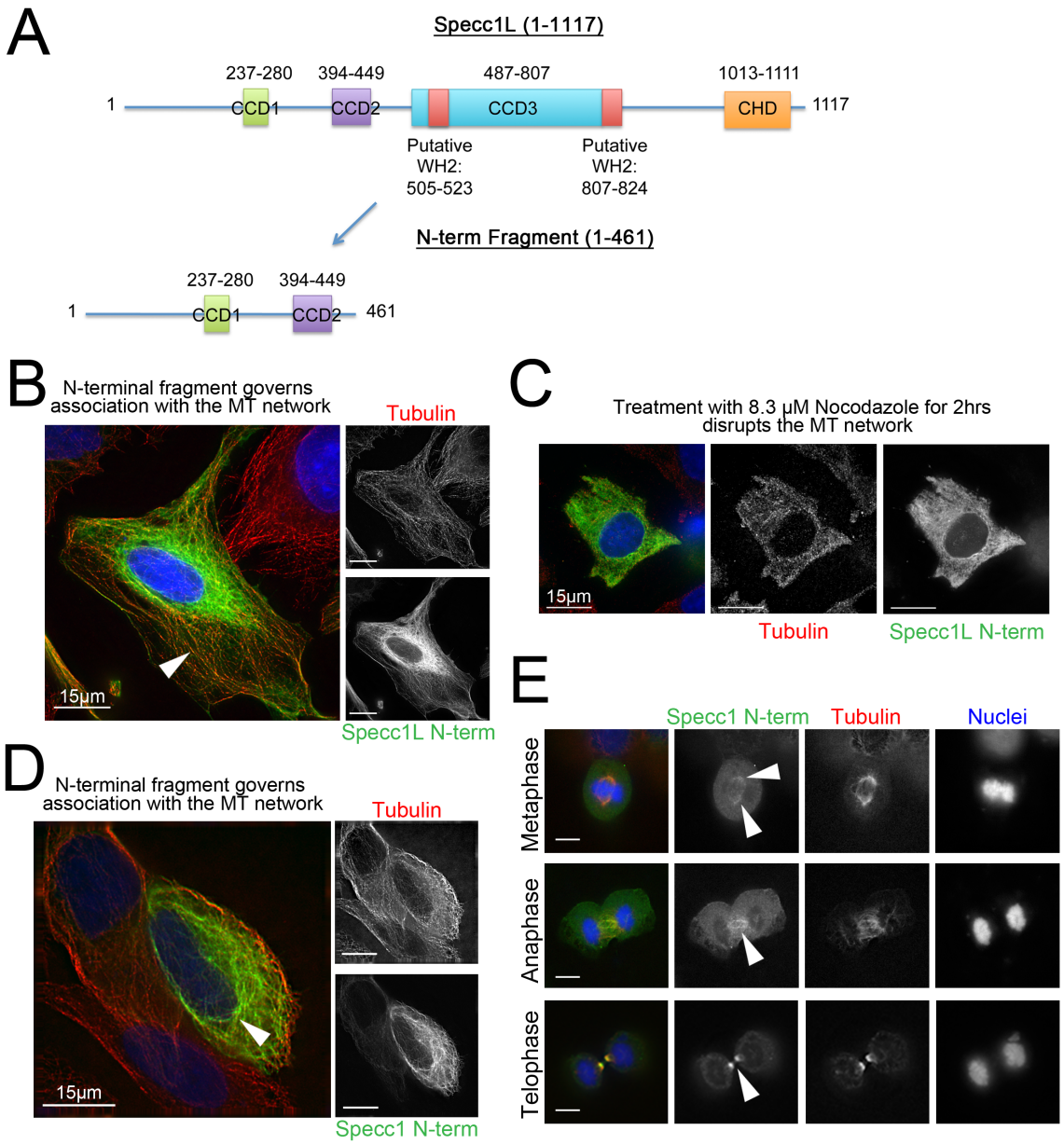

Figure 4.10. The N-terminal half (1-461) of Specc1/1L colocalizes with the MT network. A. Schematic illustrating the domains that are included in the 1-461 Specc1L Fragment. **B.** GFP- tagged Specc1L N-term shows a MT-like pattern that colocalizes with tubulin (red). **C.** Disruption of microtubules with 8.3 uM Nocodozole for two hours, confirmed by tubulin staining (red), disrupted the localization pattern of the N-term half of Specc1L, as seen by the diffuse cytoplasmic distribution. **D.** GFP-tagged Specc1 N-term shows a MT-like pattern that colocalizes with tubulin (red). **E.** GFP-tagged Specc1 N-term localizes to the mitotic spindle and cleavage furrow during mitosis. Cells were fixed with ice-cold methanol and DNA stained with DAPI (blue). Arrowheads indicate the MT network (B-D) and the mitotic spindle (E). Scale bars are 15 μm.

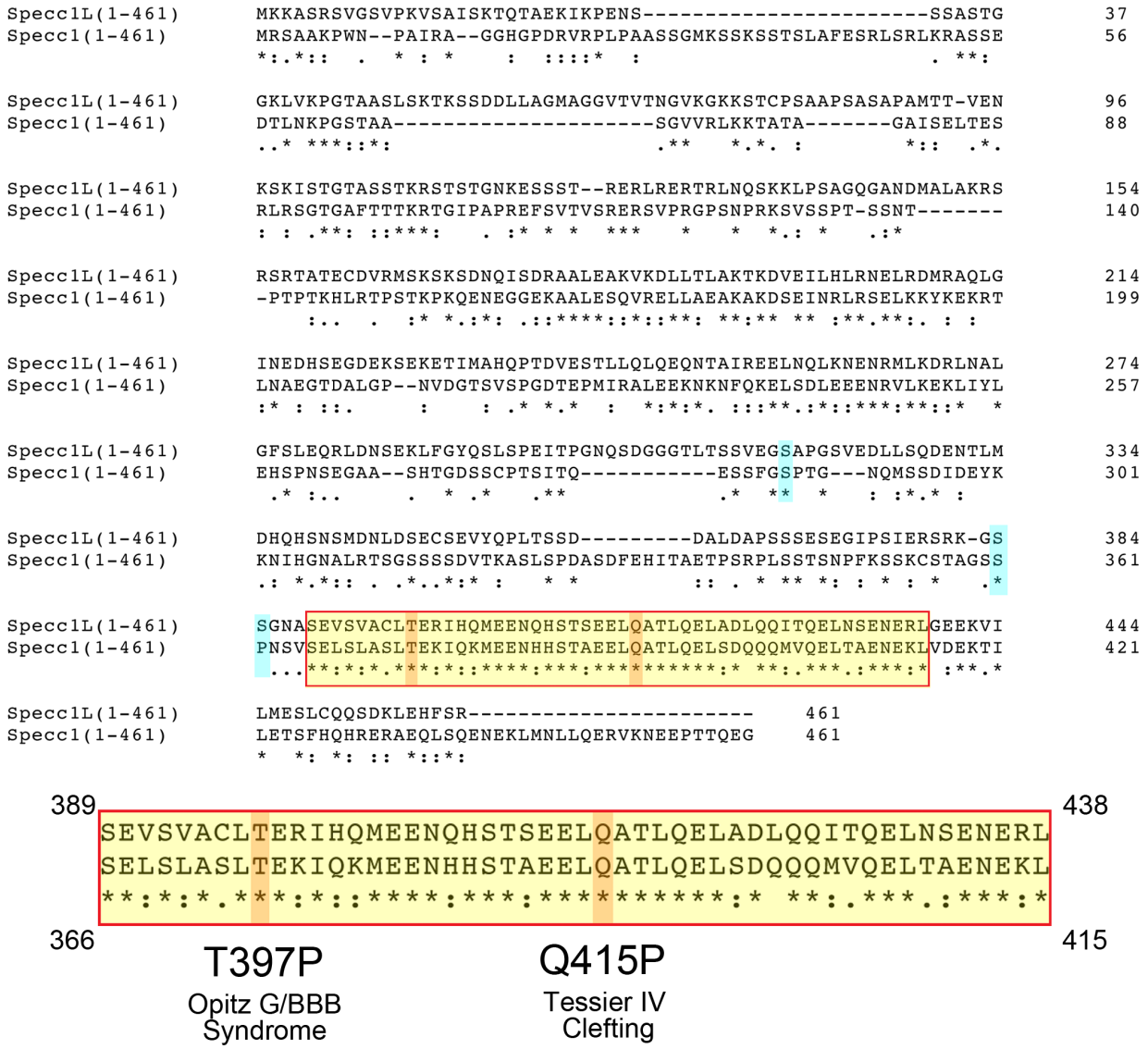

Figure 4.11. Clustal Omega Alignment of amino acids 1-461 of human Specc1L vs Specc1 (Isoform 1). The region highlighted in yellow shows a 70% identity between Specc1L and Specc1. Amino acids T397 and Q415 are found to be mutated in Specc1L in patients with Opitz G/BBB Syndrome and Tessier IV Clefting, respectively. The amino acids highlighted in blue, S355, S384 and S385, were identified as phosphorylated in Specc1L.

In order to test whether the association of Specc1L with MTs is direct or indirect, we performed a microtubule binding protein spin-down assay (Cytoskeleton). Purified recombinant His-tagged Specc1L N-term was mixed with freshly prepared MTs and the reaction mix centrifuged at 100,000 x g. At this speed, the MTs pellet through a glycerol cushion buffer, along with any protein that directly associates with them. The Specc1L fragment was observed to specifically pellet in the presence of MTs, but remained soluble in their absence (Figure 4.12). BSA was included as a negative control, as it does not bind MTs and thus remains in the soluble fraction, while the known MT binding protein MAP4 was included as a positive control. This assay confirms for the first time that Specc1L is a bona fide MT binding protein, and that the N-terminal half of the protein mediates this direct interaction.

4.7 Removal of the CH domain from Specc1L shifts the steady state localization away from filamentous actin and toward MTs

Given the strong association of the CH domain-containing region (Specc1L/890-1117) with actin, and the fact that the N-terminal half (1-462) of Specc1L mediates association with MTs, we hypothesized that the removal of the CH domain from the full-length protein would shift the actin/MT localization balance. Figure 4.13 demonstrates that removal of the CH domain from full-length Specc1L (Specc1LΔCHD mutant; Figure 4.13A) results in an increased association with the MT network (Figure 4.13B). The MT localization was retained following short-term treatment with LAT to disrupt filamentous actin, while short-term treatment with NOC to disrupt the MT network revealed an underlying actin CSK association, in a whorled internal filament pattern similar to that observed for Specc1L/462-890. These results indicate that the Specc1LΔCHD mutant is

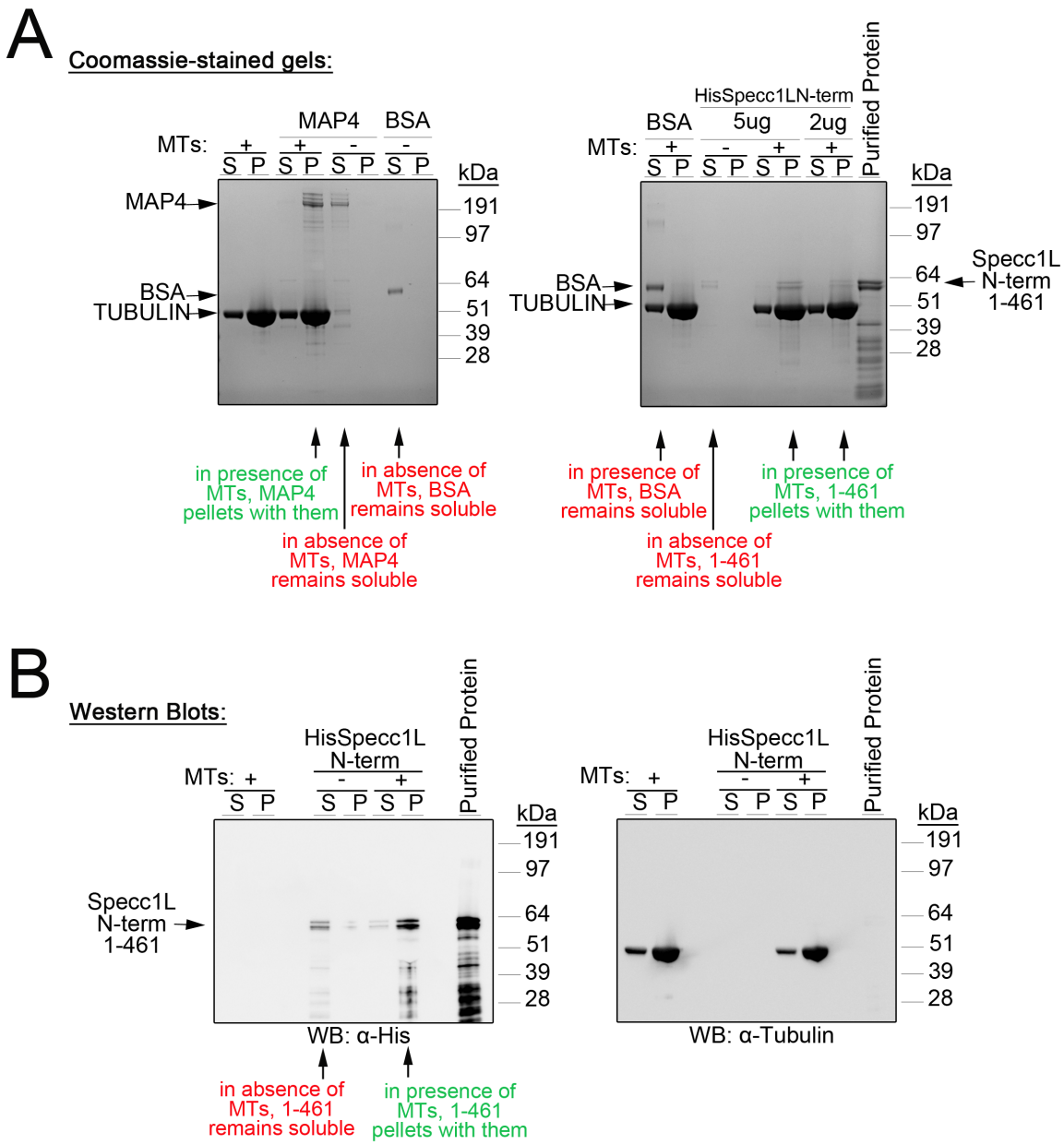

Figure 4.12. MT spin down assay confirms direct binding of the N-terminal half of Specc1L to MTs. Bacterially purified recombinant His-tagged Specc1L/1-461, purified BSA (- control) or purified MAP4 (+ control) was mixed with MTs freshly prepared from purified tubulin, and the reaction mix centrifuged at 100,000 x g. Soluble (S) fraction was separated from the pelleted (P) fraction and resolved by 1D SDS-PAGE. **A.** Coomassie stained gels illustrate that, like MAP4, Specc1L/1-461 is found with the MTs in the pelleted (P) fraction, while (BSA) remains in the soluble (S) fraction. **B.** Western Blots with an anti-His antibody confirmed that Specc1L/1-461 is found with the MTs in the pelleted (P) fraction, and in the soluble (S) fraction in the absence of MTs. Purified protein (His-Specc1L/1-461) is shown as a loading control.

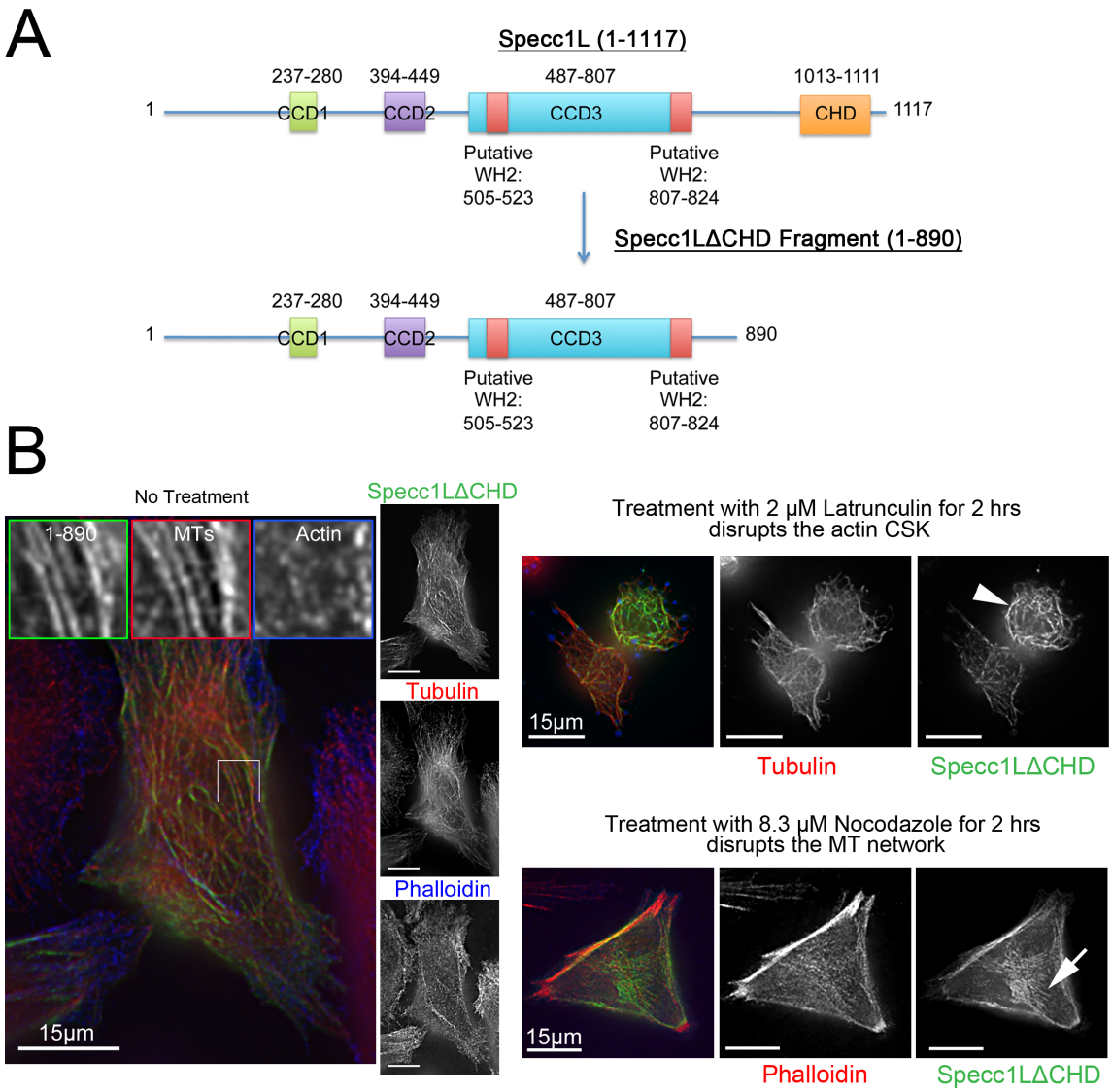

Figure 4.13. Removal of the CH domain disrupts the steady state localization of Specc1L. **A.** Schematic illustrating the domains that are included in the 1-890 Specc1L Fragment. **B.** GFP-tagged Specc1L/1-890 (green) shows a MT-like pattern that colocalizes primarily with tubulin (red). The white box highlights the region that is expanded in the inset. Following treatment with 2 µm Latrunculin for two hours to disrupt actin filaments, a MT localization pattern is still observed for Specc1L/1-890 (arrowhead), as confirmed by counter-staining with anti-α-tubulin (red). Treatment with 8.3 uM Nocodozole for two hours, to disrupt the MT network, revealed an underlying actin filament association (arrow), as confirmed by counter-staining with Phalloidin (red). Cells were fixed with PFA at 37°C for 10 min and DNA stained with DAPI (blue). Scale bars are 15 µm.

capable of associating with both the actin CSK and the MT network, which further confirms the presence of an additional actin binding region. Interestingly, this truncation mutant is not as efficient at promoting MT bundling/stabilization as full-length Specc1L when overexpressed at high levels, suggesting that the CH domain contributes to this phenotype.

4.8 Mypt1 directly interacts with Specc1L, and their association is mediated by their respective C-termini

Given that transiently overexpressed GFP-tagged Mypt1 was found in complex with only two proteins, PP1β and Specc1L, we speculated that Mypt1 interacts directly with both in a trimeric complex. Such complexes have been observed previously for PP1, and are believe to provide added specificity/regulation of the phosphatase holoenzyme complex (H. Wang & Brautigan 2002; Jin et al. 2003; Lee et al. 2010).

Initial attempts to demonstrate a direct interaction between Mypt1 and Specc1L were complicated by the fact that neither express well in bacteria and both are heavily degraded during purification. Using GlobPlot 2.3 to predict regions of disorder and globularity, we designed a truncation mutant strategy to probe for the association of specific regions of both proteins. Before testing direct association in vitro, we first assessed association of the truncation mutants in vivo.

We expressed the GFP-tagged N-terminal (aa 1-461) and C-terminal (aa 462-1117) halves of Specc1L in U2OS cells and affinity purified them from lysates using the GFP-Trap™. Our results indicate that the C-terminal half of Specc1L mediates association with endogenous Mypt1 (Figure 4.14A). Similarly, only the C-terminal half (aa 462-1068) of Specc1/Iso1 co-purified MYPT1 (Figure 4.14B). Testing the rest of our

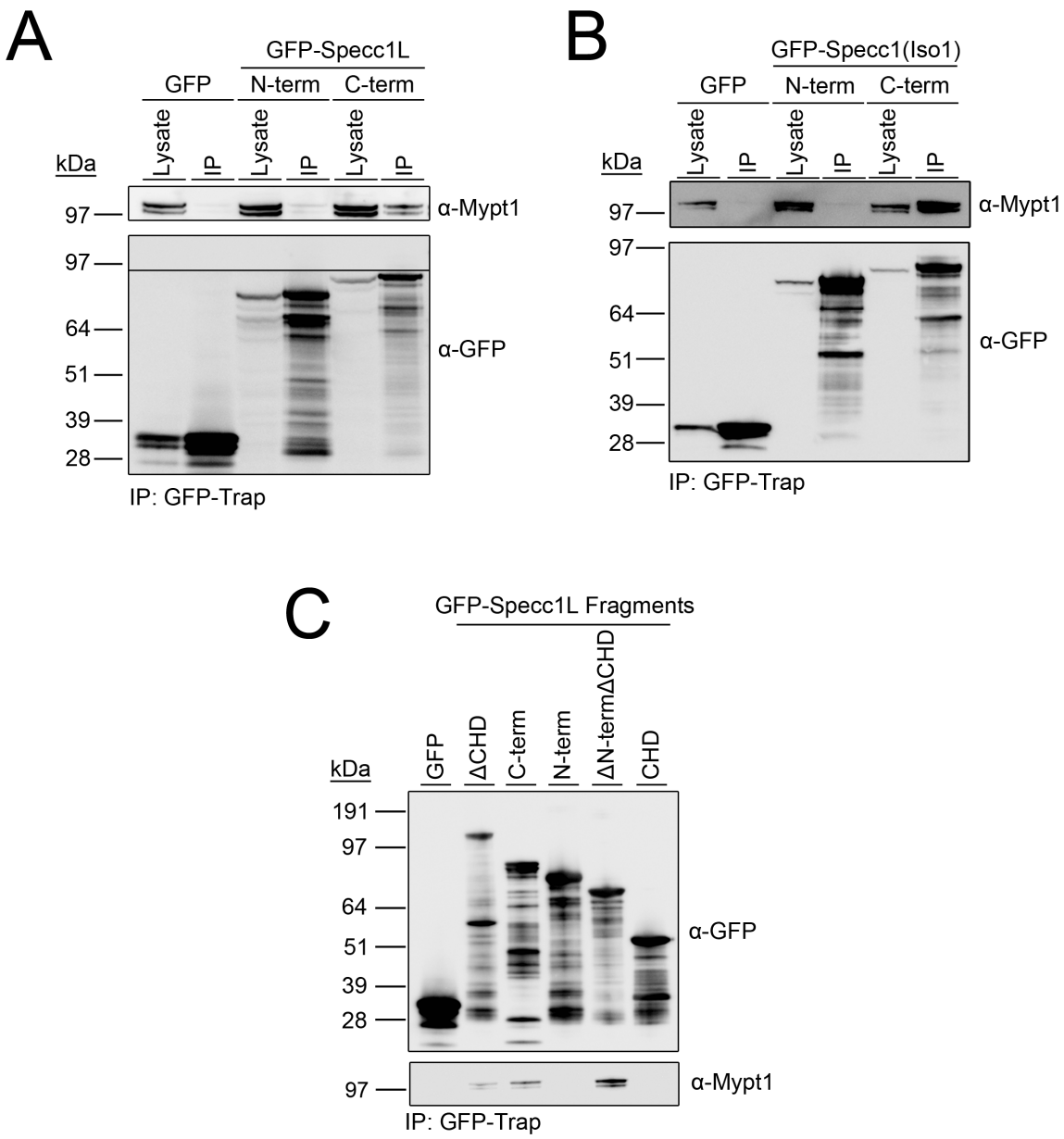

Figure 4.14. The C-terminal half of Specc1/1L mediates association with Mypt1. **A.** Endogenous Mypt1 co-purifies with the C-terminal (462-1117) but not N-terminal (1-462) half of Specc1L when transiently overexpressed in U2OS cells and pulled down on GFP-Trap beads. **B.** Similarly, only the C-terminal (462-1068) half of Specc1/Iso1 co-precipitates Mypt1. **C.** Pulldowns of all the Specc1L fragments reveal that the minimal region required for Mypt1 association is aa 462-890 (Δ N-termΔCHD).

Specc1L truncation mutants, we discovered that all of the C-terminal fragments are capable of interacting with endogenous Mypt1 (Figure 4.14C). The minimal region of Specc1L that we showed could mediate their association was the fragment containing aa 462-890 (ΔN-termΔCHD). This region is distinct from the MT binding domain (1-461) and the actin-binding CH domain (891-1117).

In order to determine which region(s) of Mypt1 associate with Specc1L, we divided Mypt1 into three regions: an N-terminal region containing the ankyrin repeats (ANK; aa 1-344), a middle region (MID; aa 345-653) and the C-terminal domain that contains a coiled coil region and a leucine zipper (LZ) domain (CD; aa 654-1030) (Figure 4.15A). The localization of the fragments, illustrated in Figure 4.15B, is consistent with results in the literature that have previously shown GFP-Mypt1(ANK) to be nuclear, (MID)Mypt1-GFP to be both nuclear and cytoplasmic and GFP-Mypt1(CD) to be predominantly cytoplasmic and associated with the cytoskeleton(Y. Wu et al. 2005). The GFP-tagged fragments were transiently overexpressed and affinity purified using the GFP-Trap^{TM}. As shown in Figure 4.15C, only the CD fragment of Mypt1 co-precipitates endogenous Specc1L. This is the same fragment that has been shown to mediate association with myosin(Grassie et al. 2011). As expected, both GFP-Mypt1(ANK) and GFP-Mypt1(CD) co-precipitated PP1β, which is consistent with literature showing PP1 association domains in both of these regions (Terrak et al. 2004; Khromov et al. 2009). Similarly, when co-expressed in cells, the mCherry-tagged C-terminal half of Specc1L co-precipitates with the GFP-tagged CD fragment of Mypt1 (Figure 4.15D).

We next set out to determine whether the interaction of Specc1L with Mypt1 is direct. To do this, we expressed and purified recombinant GST-Mypt1(CD), as the full-

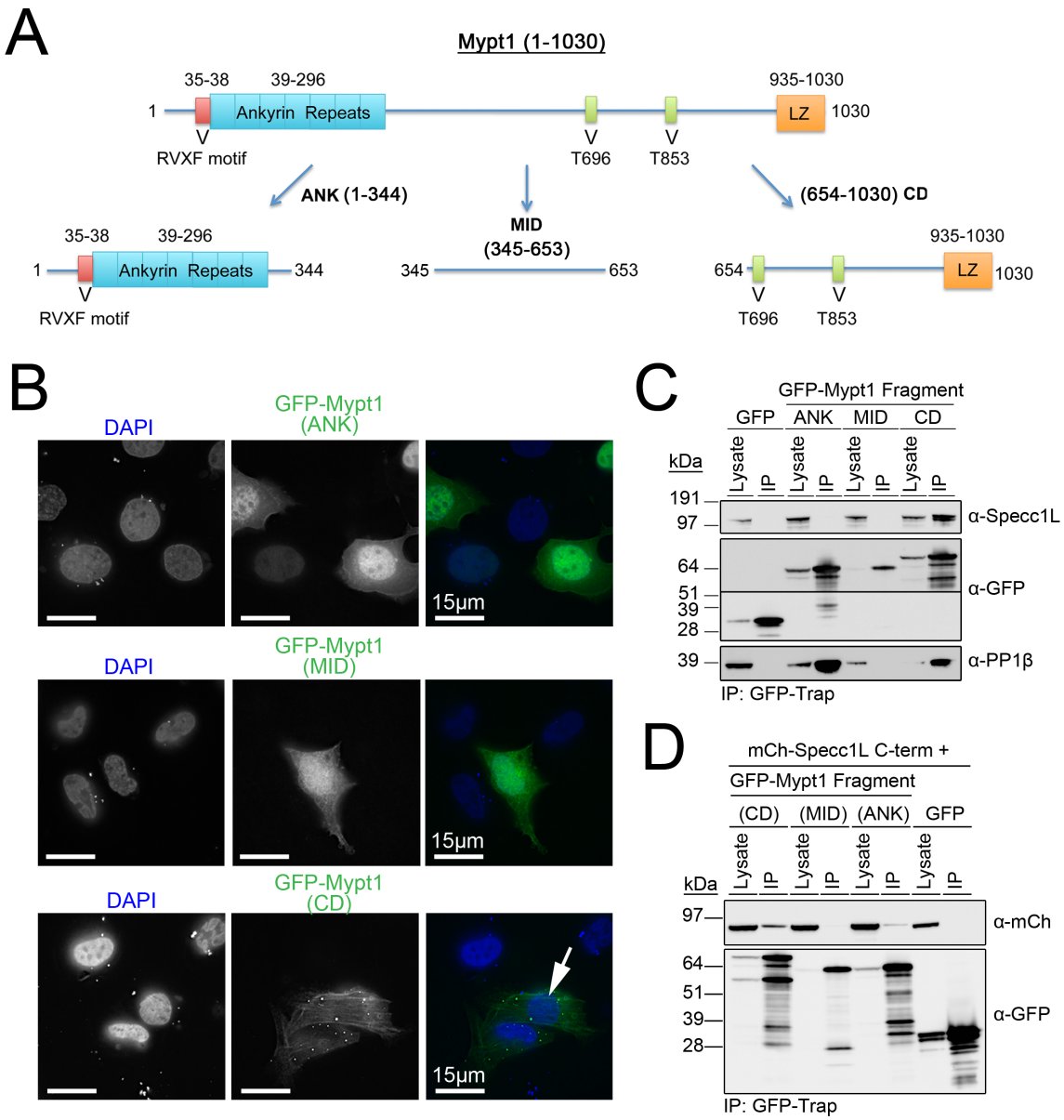

Figure 4.15. The C-terminal region (CD) of Mypt1 mediates association with Specc1L. A. Schematic showing key domains within Mypt1, including the N-terminal ankyrin repeat region, the phosphoresidues (T696 and T853) linked to regulation of Mypt1/PP1β activity and the C-terminal leucine zipper (LZ) motif. Our mutation strategy divided the protein into ANK (aa 1-344), MID (aa 345-653) and CD (654-1030) fragments for analysis. **B.** Localization of GFP-tagged Mypt1 fragments (green) transiently overexpressed in U2OS cells. Only the CD shows a filamentous pattern (arrow). Cells were PFA-fixed and stained with DAPI (blue). Scale bars are 15 μm. **C.** Co-precipitation of endogenous Specc1L with the GFP-tagged CD fragment of Mypt1. **D.** Co-precipitation of mCherry-tagged Specc1L/Cterm (aa 462-1117) when co-expressed with the GFP-tagged CD fragment of Mypt1. IP of free GFP is included as a negative control in C-D.

length protein is heavily degraded during expression/purification. Similarly, full-length Specc1L was heavily degraded. Therefore, we chose to work with Specc1LΔCHD (1-890), which is a close representation of the full-length protein but easier to express and purify, and retains the Mypt1 association region (Figure 4.14C). We also expressed and purified the C-terminal half of Specc1L (aa 462-1117), but like the full-length protein, it also showed substantial degradation.

To test direct interaction, we utilized a far Western blot approach in which purified His-Specc1LΔCHD was resolved on a 1D SDS-PAGE gel, transferred to a nitrocellulose membrane and overlaid with either purified GST-Mypt1(CD) or GST alone for 4 hrs. Figure 4.16A shows the specific and direct binding of GST-Mypt1(CD) to His-Specc1LΔCHD (aa 1-890). Although we did not observe binding to the His-Specc1L/462-1117 fragment, probing the stripped WB with anti-His revealed that it was much more heavily degraded. Interestingly, the single degradation/cleavage product that was observed, running between the 39 and 51 kDa MW markers, did bind to GST-Mypt1(CD). Given that the His tag is N-terminal to the protein, we can conclude that the observed fragments are produced by degradation/cleavage from the C-terminal end and estimate which regions may be conserved. The predicted molecular weight for the minimal Mypt1 binding region of aa 462-890 in Specc1L is 49 kDa (ExPASY), which falls within the size range (39-51 kDa) observed for the degradation/cleavage product of Specc1L/462-1117 that we observe binding to GST-Mypt1(CD). Taken together, these results support our observation that the Mypt1 binding region is located in the 462-890 region of Specc1L. Future work will attempt to map the region with higher specificity.

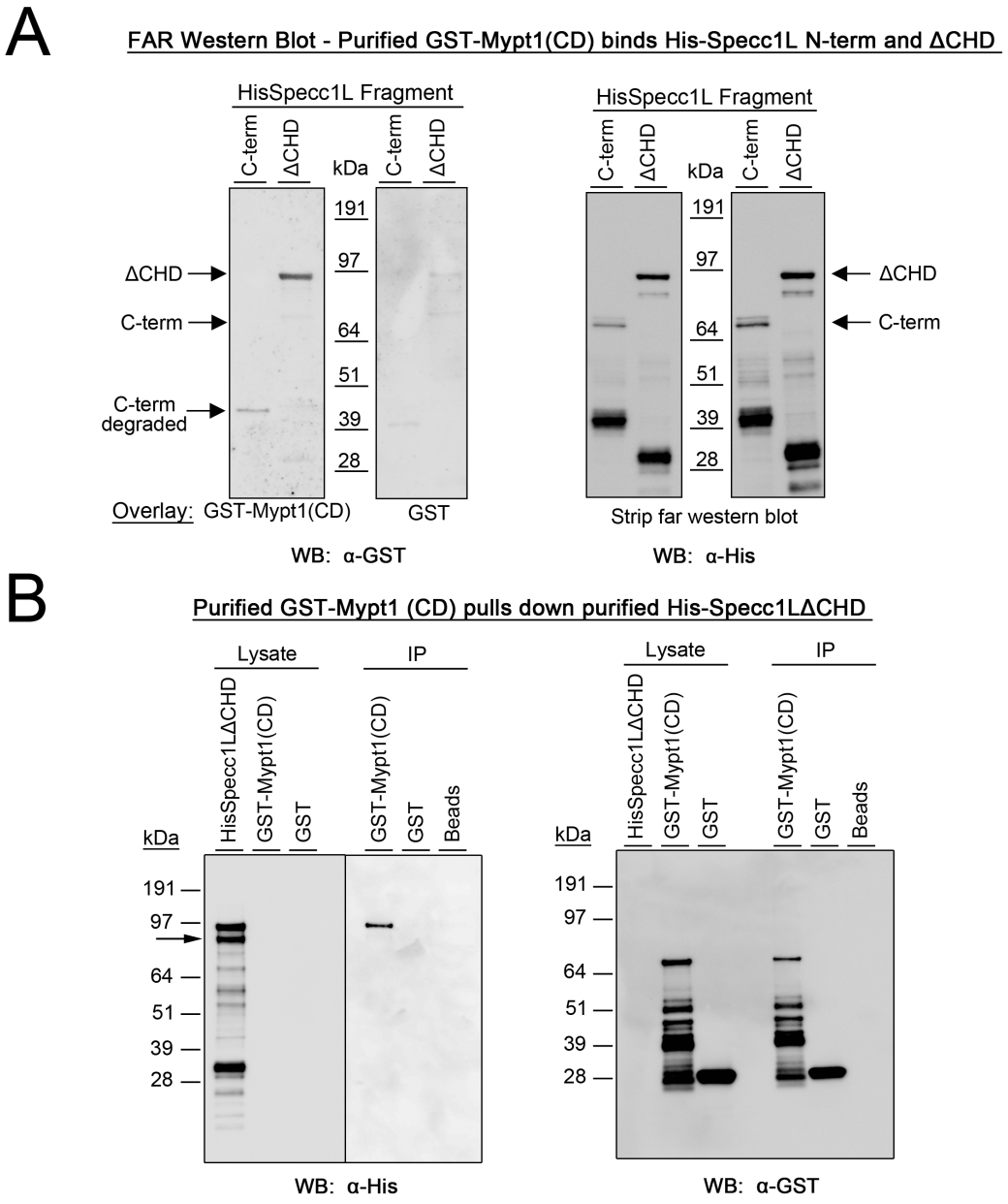

Figure 4.16. Specc1L directly interacts with Mypt1. **A.** Far Western blot approach in which purified recombinant His-tagged Specc1L fragments were separated on an SDS-PAGE gel, transferred to a nitrocellulose membrane and overlaid with purified GST-Mypt1(CD) or purified GST. **B.** Western blot demonstrating that HisSpecc1L1-890 co-IPs with GST-Mypt1(CD) but not with GST alone. In this experiment, purified recombinant HisSpecc1L1-890 was combined with GST-Mypt1(CD) in vitro, GST-Mypt1(CD) or GST alone immobilized on Glutathione Agarose beads and eluted proteins separated on an SDS-PAGE gel for transfer to nitrocellulose membrane and detection of the Specc1L fragment with anti-His antibodies. The WB was stripped and re-probed with anti-GST antibodies to detect GST-Mypt1(CD) and GST.

As a complementary approach, we combined the purified His-Specc1LΔCHD fragment with either purified GST-Mypt1(CD) or GST alone, immobilized the latter two proteins on Glutathione Agarose beads, and detected co-purified HisSpecc1LΔCHD by WB analysis using anti-His antibodies. Figure 4.16B shows the results of the pulldown assay demonstrating that HisSpecc1LΔCHD co-precipitates with GST-Mypt1(CD) but not with GST or beads alone. Interestingly, we observed that degraded/cleaved forms of HisSpecc1LΔCHD (even those relatively close to the size of the 1-890 fragment) do not associate with Mypt1, which caused us to take a closer look at the region of the protein upstream of aa 890.

We previously showed that the C-terminal halves of both Specc1L (aa 462-1117) and Specc1 (aa 462-1068) mediate association with Mypt1 (Figure 4.14A/B). As shown in Figure 4.17A, these regions contain either a single coiled coil domain (CCD3 in Specc1L; aa 487-707) or two coiled coil domains (CCDs 3-4 in Specc1; aa 480-532 and aa 579-777). Alignment of the CCD3 domain of Specc1L with these CCDs of Specc1 revealed the highest conservation (66.7% identity in yellow highlighted region) with the CCD4 domain (Figure 4.17B). The region of Specc1L that corresponds to the conserved domain is aa 685-792. If this conserved domain mediates Mypt1 binding, then we would predict that a Specc1L/1-890 fragment that degrades past this region would not associate with Mypt1. Specc1L/1-792 has a predicted molecular weight of ~89 kDa (EXPASY). If the region of aa 685-792 is the minimal binding region required, then a degraded form of Specc1LΔCHD deleted from the C-terminus and smaller than 89 kDa would not associate with Mypt1. It is thus tempting to speculate that the HisSpecc1LΔCHD degraded/cleaved band that runs just below the full-length protein (Figure 4.16B; arrow) and does not

A

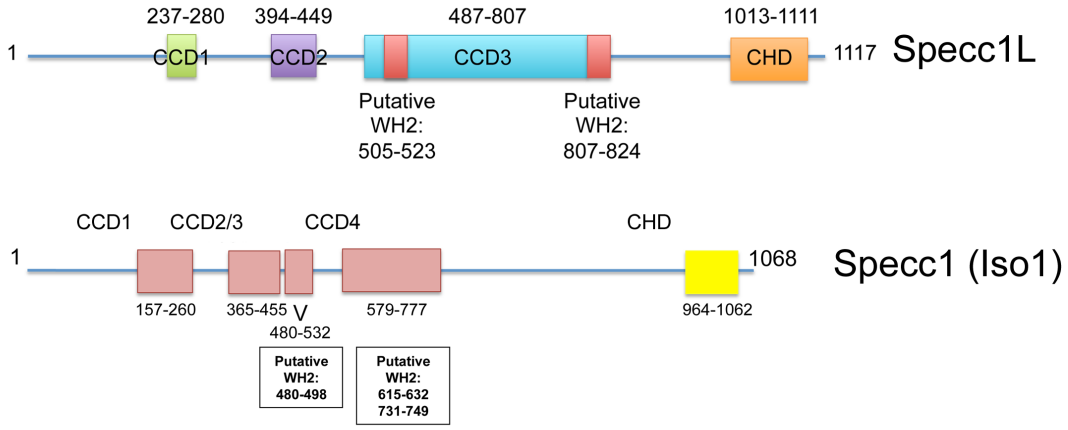

B

```
Specc1LCCD3(487-807)      RYMELEQRYMDLAENARFEREQLLGVQQHLSNTLKMAEQDNKEAQEMIGALKERSHHMER  60
Specc1CCD4(579-777)       ------------------------------------------------------------  0

Specc1LCCD3(487-807)      IIESEQKGKAALAATLEEYKATVASDQIEMNRLKAQLENEKQKVAELYSIHNSGDKSDIQ  120
Specc1CCD4(579-777)       ------------------------------------------------------------EVQ  3
                                                                                         ::*

Specc1LCCD3(487-807)      DLLESVRLDKEKAETLASSLQEDLAHTRNDANRLQDAIAKVEDEYRAFQEEAKKQIEDLN  180
Specc1CCD4(579-777)       EMLKVARAEKDLLELSCNELRQELLKANGEIKHVSSLLAKVEKDYSYLKEICDHQAEQLS  63
                          ::*: .* :*:  *  ...*:::* ::..: ::::. :****.:*  ::* ..:* *:*.

Specc1LCCD3(487-807)      MTLEKLRSDLDEKETERSDMKETIFELEDEVEQHRAVKLHDNLIISDLENTVKKLQDQKH  240
Specc1CCD4(579-777)       RTSLKLQEKASESDAEIKDMKETIFELEDQVEQHRAVKLHNNQLISELESSVIKLEEQKS  123
                           *  **:.. .*.::* .********** :********** :* :**:**.:* **::**

Specc1LCCD3(487-807)      DMEREIKTLHRRLREESAEWRQFQADLQTAVVIANDIKSEAQEEIGDLKRRLHEAQEKNE  300
Specc1CCD4(579-777)       DLERQLKTLTKQMKEETEEWRRFQADLQTAVVVANDIKCEAQQELRTVKRKLLEEEEKNA  183
                          *:**::*** :::::**: ***:********** :*****.***:*:  :**:* * :***

Specc1LCCD3(487-807)      KLTKELEEIKSRKQEEERGRV 321
Specc1CCD4(579-777)       RLQKELGDVQGHGRVV----- 199
                          :* *** :::.: :
```

72/108=66.7% identity

Figure 4.17. Clustal Omega Alignment of CCD3 (aa 487-807) in Specc1L with CCD4 (aa 579-777) in Specc1 reveals a highly conserved region. **A.** Schematic showing the location of the coiled coil domains (CCDs) within the C-terminal halves of Specc1L and Specc1. **B.** Alignment of Specc1L/CCD3 with Specc1/CCD4 identified a region (highlighted in yellow) that shows a 66.7% identity. This region corresponds to aa 685-792 in Specc1L and aa 660-767 in Specc1/Iso1.

associate with Mypt1 may be missing part of this conserved 685-792 region. Future experiments will address this directly, by testing additional truncation mutants.

Our results thus far demonstrate that the interaction of Specc1L with Mypt1 is direct, and that the minimal regions required for their association are aa 462-890 of Specc1L (contains the two CCDs) and aa 654-1030 of Mypt1 (contains a coiled coil domain and leucine zipper motif). Importantly, this illustrates that Mypt1 is capable of binding both PP1β and Specc1L at the same time in a trimeric complex, as the N-terminus of Mypt1 primarily mediates PP1β binding while the C-terminus mediates Specc1L binding. Furthermore, Specc1L binds Mypt1 via a region distinct from its MT binding domain and the CH actin association domain, which would allow it to access both the MT and actin networks while in complex with Mypt1/PP1β.

4.9 Mypt1/PP1β regulates a phosphosite in the N-terminal half of Specc1

Large-scale phosphoproteomic screens have identified phosphoresidues in both Specc1 and Specc1L, and given their association with a phosphatase complex, we wanted to determine whether these proteins are also substrates for Mypt1/PP1β complex. Many PP1 regulatory subunits have been shown to be substrates for the phosphatase under specific conditions, and in some cases their regulated phosphorylation mediates association with the phosphatase itself. Given that we do not have antibodies that reliably/specifically immunoprecipitate Specc1 or Specc1L, we utilized our U2OS$^{Specc1L\text{-}GFP}$ stable cell line in a Specc1L-GFP phosphopeptide mapping experiment to compare its phosphorylation status in control cells vs. cells transiently overexpressing Mypt1.

With transient overexpression of Mypt1 proving to be technically challenging (<10% transfection efficiency for most cell lines tested), we subcloned untagged Mypt1

into a lentiviral vector and generated/purified lentiviruses for infection of cells. U2OS$^{Specc1L\text{-}GFP}$ cells were cultured in Light (R0K0) or Heavy (R6K4) media for 7 days and then infected with lentivirus containing the empty plasmid (pLVX) or lentivirus containing pLVX-Mypt1 for 36 hours. The cells were harvested and whole cell extracts prepared, Specc1L-GFP captured on the GFP-Trap_A™ affinity matrix and the beads combined for elution and separation of bound proteins by 1D SDS-PAGE. The band representing Specc1L-GFP was excised and an in-gel tryptic digestion performed. Aliquots of the tryptic peptides were analyzed on a Thermo Orbitrap mass spectrometer and the raw data analyzed using MaxQuant v1.2.7.4. While several phosphosites were identified, including S220, S874, S868, S384, and S385, only the phosphosite S384/385 was found to decrease in response to overexpression of Mypt1 (reduced by 40%). The motifs suggests putative PKA or GSK3 kinase sites. Although both sites are found just upstream of the N-terminal region conserved between Specc1 and Specc1L (Figure 4.11), initial analysis of phosphomutants generated in both full-length Specc1L and the N-terminal half (Specc1L/1-461) suggests no obvious effect on MT association. Further work will be needed to assess the behavior of the phosphomutants throughout the cell cycle, and the response of Specc1L to inhibition or overexpression of PKA or GSK3 kinase.

We carried out a similar phosphopeptide mapping experiment to compare Specc1L-GFP in asynchronous vs. STLC-arrested cells. U2OS^{Specc1LGFP} cells were labeled in Light (R0K0) or Heavy (R6K4) media for 7 days, at which point the Heavy-labeled cells were treated with STLC for 18 hours to arrest them in metaphase with intact, monopolar spindles. The arrested cells were harvested by mitotic shake-off, while the untreated cells were harvested as per protocol. Specc1L-GFP was captured on GFP-

Trap_A™ affinity matrix and processed as described above. Phospho-S384/385 peptides were mapped, but we did not see a significant change in their levels between the 2 conditions. We did, however, see an enrichment of phosho-S1003 in the arrested cells, suggesting that regulation at this site may be important during mitosis. Interestingly, Specc1L (referred to as Mip1) was previously shown to be a phosphoprotein that associates with the mono-polar spindle kinase 1 (MPS1) to ensure proper spindle positioning at the onset of anaphase (Mattison et al. 2011). In this experiment, in vitro kinase assays showed MPS1 phosphorylating different fragments of Specc1L, including aa 1-351 and aa 851-1117, with aa 351-851 showing the highest level. Although inconclusive, this does suggest that the potential regulation of Specc1L by MPS1 and Mypt1/PP1β during mitosis is worth further analysis.

4.10 Specc1L regulates the subcellular localization and turnover dynamics of Mypt1/PP1β

As previously illustrated, increasing levels of Specc1L-GFP overexpression shifts the balance of its localization from the actin CSK to the MT network. Here, excess Specc1L-GFP accumulates on thick, bundled MT structures that show high levels of tubulin acetylation (a marker for stabilized MTs). Using a FRAP (Fluorescence Recovery After Photobleaching) approach in live cells, we observed that this change in localization is accompanied by a dramatic change in the mobility of Specc1L-GFP. In FRAP, GFP-tagged proteins within a region of interest (ROI) are irreversibly photobleached by brief exposure to high intensity 488 nm light. The recovery of the fluorescent signal within the region of interest is then monitored over time, as the bleached GFP-tagged protein exchanges with unbleached GFP-tagged protein that has diffused in from the area

outside the ROI (Figure 4.18A). If the GFP-tagged protein does not associate with any underlying structures/complex, it is fully mobile (shows 100% recovery) and has a rapid half-time of recovery that is determined solely by free diffusion into the ROI and thus governed by Brownian motion (< 0.02 sec). We use GFP as an indicator of free diffusion. Any difference in the mobile fraction (MF) and/or half-time of recovery (turnover rate) for a GFP-tagged protein compared to free GFP reflects the presence of underlying binding events. It should be noted that, for proteins with slow turnover dynamics, full recovery may occur on the scale of minutes to hours. For these experiments we focused on recovery within the first 90 sec after the bleach event.

FRAP analysis of Specc1L-GFP in the U2OS^{Specc1LGFP} stable cell line confirmed that the fusion protein does associate with subcellular structures/complexes, as judged by the slower turnover dynamics observed for the cytoplasmic pool (Figure 4.18B, green curve) compared to GFP alone (Figure 18B, purple curve). For the cytoplasmic pool the mobile fraction is the same as free GFP, but the initial recovery rate is slower. In cells in which Specc1L-GFP was observed to accumulate at bundled MTs, this pool of the fusion protein showed an even more dramatic drop in its recovery pool and a very slow turnover rate (Figure 18B, blue curve), suggesting near immobilization at these structures. We also observe a “halfway” phenotype in which Specc1L-GFP has just started to accumulate on MTs, in a pattern that looks like dots and dashes (similar to the MEDIUM expressing panel in Figure 3B). The recovery curve for Specc1L-GFP in this phenotype (Figure 18B, red curve) falls midway between that of the cytoplasmic pool and the pool at MT bundles, suggesting partial immobilization.

As previously noted, the N-terminal half of Specc1L (aa 1-461), when

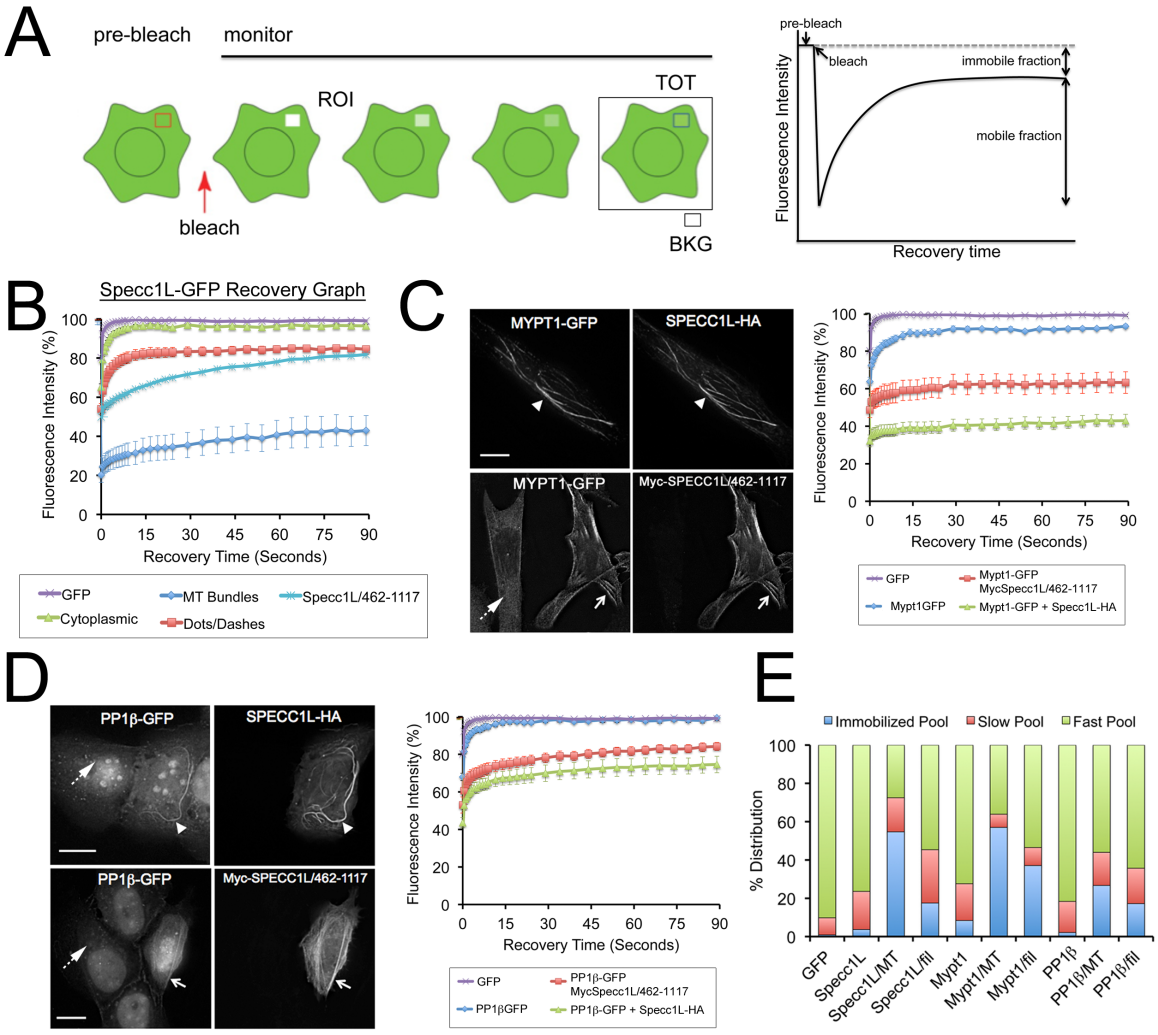

Figure 4.18. FRAP analysis reveals reduced mobility of Mypt1 and PP1β recruited to either MTs or the actin CSK by transiently overexpressed Specc1L. A. Schematic showing the design of a FRAP experiment, with the fluorescence intensity within a ROI monitored before and after the bleach event and recovery normalized for background (BKG) and total fluorescence (TOT). The resulting recovery curve, plotting fluorescence intensity vs. recovery time, reveals the mobile fraction of the protein (recovers fully within the time course) and the half-time of recovery for this mobile fraction. **B.** FRAP analysis of the turnover dynamics of different pools of Specc1L-GFP in the U2OS$^{Specc1L\text{-}GFP}$ stable cell line, and transiently overexpressed Specc1L/462-1117 on actin filaments. Values are plotted as mean ± SE for n >10 (three biological replicates). **C.** Overexpression of Specc1L in the HeLa BAC cell line relocalizes Mypt1-GFP to MT bundles (arrowhead), while overexpression of the C-terminal half recruits it to actin filaments (arrows). Recovery curves were plotted for Mypt1-GFP under these various conditions. **D.** Similarly, overexpression of full-length Specc1L and the 462-1117 C-terminal half in the U2OS$^{PP1\beta\text{-}GFP}$ cell line recruits PP1β–GFP to MT bundles (arrowhead) and actin filaments (arrow), respectively, with changes in its recovery curve observed. Scale bars are 15 μm and hashed arrows indicate localization patterns in untransfected cells. **E.** All of the recovery curves were best fit by a double exponential analysis, confirming the presence of two distinct pools of protein (slow and fast) in addition to the pool (immobilized) that did recovery during the 90 sec time course. This graph shows the change in distribution between these pools.

overexpressed as a GFP fusion in cells, accumulates on the MT network but does not induce bundling/stabilization. Assessment of its turnover dynamics by FRAP revealed full recovery within 90 sec post-bleach, and a slower recovery rate than free GFP, suggesting a normal on/off association with MTs. This suggests that the bundling/stabilization phenotype requires a specific region or regions within the C-terminal half of the protein. A similar analysis of the C-terminal Specc1L fragment (aa 462-1117), which we have shown to mediate association with both the actin CSK and Mypt1/PP1β, revealed a distinct actin CSK-associated pool that has a reduced mobile fraction and a very slow turnover rate (Figure 4.18B, turquoise curve). This is indicative of slow turnover of the fragment at this structure, and suggests that both the MT and actin binding domains of Specc1L are required for its homeostatic and dynamic steady-state distribution between these two cytoplasmic networks in interphase cells.

In order to determine whether overexpression of full-length Specc1L can also shift the balance of localization of Mypt1, we stained Specc1L-GFP overexpressing cells with anti-Mypt1 antibodies and confirmed that a pool of endogenous Mypt1 is indeed recruited to the Specc1L-containing MT bundles (Appendix III, Figure A.4). We next assessed the localization and turnover dynamics of Mypt1 in a HeLa BAC cell line that drives expression of GFP-tagged mouse Mypt1 (91.7% identical to the human protein) under the control of its endogenous promoter. For these experiments, we expressed non-fluorescent Specc1L fusion proteins, specifically BirA-tagged constructs that drive expression of the protein fused to a biotin ligase. These constructs are primarily used for BioID near neighbor labeling experiments, however in this case they allowed us to assess

effects on the localization and turnover dynamics of GFP-tagged Mypt1 without the presence of an additional fluorophore to complicate the measurements.

We first confirmed that overexpression of high levels of full-length Specc1L-BirA recruited Mypt1-GFP to bundled MT structures (Figure 4.18C), while overexpression of the C-terminal half (aa 462-1117) recruited Mypt1-GFP to actin filaments (Figure 4.18C). Expression and localization of the Specc1L fusion proteins were monitored by fixing and staining cells with Alexa568-conjugated Streptavidin, which visualized their biotinylation patterns. Overexpression of the N-terminal half of Specc1L (aa 1-461), which contains the MT binding domain but not the Mypt1 binding domain, fused to BirA had no effect on the MT network nor on Mypt1 localization. By carefully controlling for fluorophore bleedthrough and carrying out blind imaging experiments, we confirmed that the relocalization of Mypt1 is sufficiently dramatic to allow us to unambiguously identify Specc1L-BirA and BirA-Specc1L/462-1117 expressing cells based solely on the altered Mypt1-GFP localization pattern. This allowed us to assess turnover dynamics of the fusion protein by FRAP analysis in live cells expressing the non-fluorophore tagged Specc1L constructs.

In untransfected cells, cytoplasmic Mypt1-GFP (Figure 4.18C, blue curve), as a reduced mobile fraction and slower turnover rate compared to free GFP (Figure 18C, purple curve), which confirms the presence of underlying binding events. Overexpression of Specc1L-BirA induced both accumulation of a pool of Mypt1-GFP at bundled MTs and a dramatic reduction in its turnover dynamics at these structures (Figure 4.18C, green curve), suggestive of relative immobilization. Similarly, overexpression of the C-terminal half of Specc1L (aa 462-1117) induced accumulation of a pool of Mypt1-GFP on actin filaments and a concurrent reduced mobile fraction and slower turnover rate at this

structure (Figure 4.18C, red curve). These results confirm that Specc1L can directly mediate the homeostatic distribution of Mypt1 between the MT and actin CSK network in interphase cells.

Having observed that Specc1L/Mypt1/PP1β co-purifies as a complex, we expect that relocalization of Mypt1 by Specc1L would be accompanied by a change in the localization and turnover dynamics of PP1β. Bearing in mind that PP1β is also found in other holoenzyme complexes in interphase cells, the changes might not be as dramatic with only one pool of the phosphatase affected. That said, we have shown that a large proportion of PP1β is found in complex with Mypt1 (refer to Figure 3.19A in ch. 3.1 that shows distribution of PP1β between regulatory subunits in U2OS cells), and thus we should see detectable differences if this pool is affected. For these experiments we utilized our U2OS cell line that stably expresses GFP-tagged PP1β. We first confirmed that overexpression of full-length Specc1L recruits a visible pool of PP1β-GFP to bundled MTs, while overexpression of the C-terminal half recruits excess PP1β-GFP to actin filaments (Figure 18D). As with Mypt1-GFP, the localization changes can be unambiguously detected, permitting FRAP experiments in live cells.

In untransfected cells the cytoplasmic pool of the fusion protein, which includes Mypt1-PP1β complexes and other PP1β complexes (Figure 4.18D, blue curve) shows slower turnover dynamics than free GFP (Figure 4.18D, purple curve), confirming the presence of underlying binding events. Overexpression of Specc1L-BirA induced accumulation of a pool of PP1β-GFP at bundled MTs (Figure 4.18D, green curve), similar to the relocalization observed for Mypt1-GFP. Although its turnover dynamics decreased significantly, it did not show the same degree of immobilization as MYPT1 (Figure 4.18C,

green curve). This is not unexpected, as it may be that Specc1L and Mypt1 are both relatively immobile at these structures while PP1β can still turn over on Mypt1 as it exchanges with other PP1 holoenzyme complexes. Overexpression of the C-terminal fragment (aa 462-1117) of Specc1L led to accumulation of a pool of PP1β-GFP on actin filaments, with reduced (but not immobile) turnover dynamics (Figure 4.18 D, red curve).

The recovery curves shown in Figure 18B-D show the changes in turnover dynamics qualitatively (i.e. curves can be directly compared), however we wanted to quantitatively assess these changes and calculate mobile fractions and recovery half-times. Using GraphPad Prism, we first tried to fit single exponential recovery curves to the data, but the fits were poor, indicating the presence of more than one recovery pool. Double exponential curves provided a much better fit in each case (R^2 values > 0.95). For each condition, we determined the fraction that does not recover within 90 sec post-bleach, the fraction that recovers with fast kinetics and the fraction that recovers with slow kinetics. The half-times of recovery for the fast and slow pools were also determined. These values are summarized in Table 4.1, and the distribution of the GFP fusion proteins between immobile/slow/fast pools graphically represented in Figure 4.18E, which clearly shows that Specc1L has a profound effect on both the localization and turnover dynamics of Mypt1 and PP1β. Taken together, these data confirm that Specc1L can disrupt the MT-CSK homeostatic balance of Mypt1/PP1β by mediating its steady-state recruitment to these structures as part of a trimeric complex.

Given that Specc1L can recruit excess Mypt1/PP1β to MTs, and that overexpression of the MT binding region of Specc1L (which can't recruit the phosphatase

CONDITION	% that does not recover within 90 sec	SLOW POOL		FAST POOL	
		% recovered	Half-time (sec)	% recovered	Half-time (sec)
free GFP	0.9	8.9	1.14	90.2	0.0006303
Specc1L-GFP					
FRAP CP pool	3.7	19.9	1.67	76.4	0.00072
FRAP dots/dashes	16.1	20.9	3.13	63	0.00072
FRAP MT bundles	54.7	17.8	21.78	27.5	0.00092
462/1117 FRAP filaments	17.5	27.9	20.69	54.6	0.00056
Mypt1-GFP					
FRAP CP pool	8.4	19.2	4.23	72.4	0.00065
Tf Specc1L-BirA FRAP MT bundles	57	6.9	25.32	36.1	0.16
Tf 462-1117 FRAP filaments	37.1	9.4	9.96	53.5	0.00058
PP1β-GFP					
FRAP CP pool	2.1	16.3	2.80	81.6	7.752E-05
Tf Specc1L-BirA FRAP MT bundles	26.7	17.3	9.42	56	0.00092
Tf 462-1117 FRAP filaments	17.2	18.5	12.6	64.3	0.00080

Table 4.1. Values obtained for the respective recovery curves using double exponential curve fitting in GraphPad Prism. The R2 value for all curve fits was > 0.95. For the 90 sec post-bleach time course, the immobile fraction was determined (% that does not recover within 90 sec), and the distribution and recovery rates for two mobile fractions (slow and fast) characterized.

complex) does not induce the bundling phenotype, our hypothesis is that recruitment of Mypt1/PP1β is required for this functional effect. The key experiment to test this would be to overexpress Specc1L in cells in which Mypt1 levels have been transiently knocked down. Although we attempted this, using an siRNA approach, the knockdown efficiency fluctuated significantly (from 10-60%) and we could not assess the knockdown on a single cell basis because none of the available Mypt1 antibodies work reliably for IF. Future experiments will focus on full and partial knockout of Mypt1 using CRISPR/Cas9 and establishment of an inducible shRNA-mediated knockdown cell line.

4.11 Identification of potential Specc1L/ Mypt1/PP1β substrates on the MT network.

We hypothesized that the dramatic MT bundling/stabilization phenotype observed in response to forcible loading of excess Specc1L/Mypt1/PP1β on the MT network during interphase is due to disruption of the normal balance of net phosphorylation of MT-associated substrates. In order to identify protein-protein interactions under conditions in which the balance of localization has shifted less dramatically to MTs (i.e. steady-state localization is predominantly MT but phenotype is much less dramatic), we decided to map the interactome of the Specc1LΔCHD mutant (aa 1-890). This truncation mutant retains the MT and Mypt1 binding regions and the putative WH2 actin association domains, and localizes to both the MT network and actin filaments (Figure 4.13). To facilitate capture of putative substrates and other transient interactors, and to optimize detection of bona fide interactors above the background of bead contaminants and proteins that bind biotin directly, we combined the BioID near neighbor labeling approach with our quantitative SILAC AP/MS workstream (Figure 4.19A).

As detailed in Figure 4.19A, cells were differentially labeled for 7 days and then transiently transfected overnight for expression of GFP-Specc1LΔCHD (Light; R0K0) or BirA-Specc1LΔCHD (Heavy; R10K8) in the presence of excess biotin. Cells were harvested in high salt RIPA buffer for preparation of whole cell extracts, and biotinylated proteins were captured on Streptavidin-agarose beads. Proteins were eluted for 1D SDS-PAGE separation, in gel digestion and MS analysis as previously described. MaxQuant was used for protein identification and quantitation of H:L ratios, and the results summarized in the graph in Figure 4.19A, which plots log2 H:L ratios for each identified protein versus their relative abundance in the AP (full dataset shown in Appendix II). As expected, we observed H:L ratios of ~1:1 (i.e. log2 H:L ratios ~0) for several abundant mitochondrial proteins that are known to bind biotin directly (Figure 19A, green diamonds). This confirmed that the affinity purifications were carried out using equivalent total protein amounts of each extract. We also saw a cluster of proteins around a median log H:L ratio of 0.78, which most likely represents those that bind non-specifically to the beads. Specc1L itself had the highest H:L ratio and a very high abundance, which is consistent with the fusion protein biotinylating itself (and possibly endogenous Specc1L in multiprotein complexes). We also observed a significant increase in biotinylation for several actin CSK- (e.g. CORO1B/C, RAI14, LASP1), plasma membrane- (e.g. SDC1/2/4, AGRN) and MT- (e.g. MAP4, CKAP5) associated proteins. This fits with the observed localization of Specc1LΔCHD, which can be found on both actin and MT networks in distinct accumulations that are resistant to either nocodazole or latrunculin treatment, respectively (Figure 4.13). Most of the identified interactors have been implicated in adhesion and the tethering of the actin- and MT- networks to the

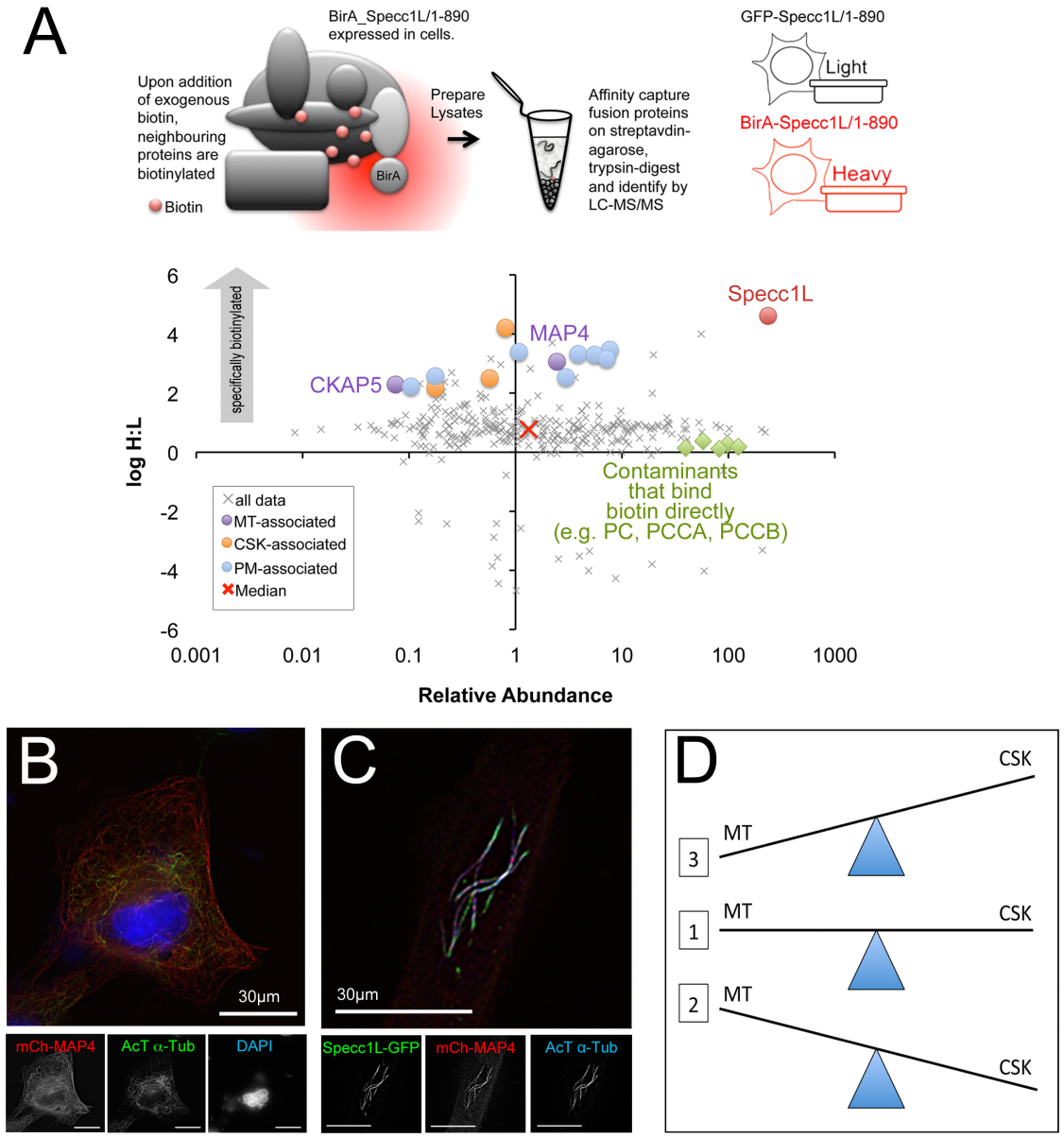

Figure 4.19. Quantitative BioID near neighbour labeling identifies proteins that associate with Specc1L/1-890. A. Schematic illustrating the design of the BioID experiment. Identified proteins were plotted as log(2) H:L ratio vs. relative abundance (normalized intensity). BirA-Specc1L/1-890 biotinylates itself (red circle), and several plasma membrane- (PM; blue circles), actin cytoskeletal- (CSK; orange circles) and microtubule- (MT; purple circles) associated proteins. The known MT phosphoproteins MAP4 and CKAP5 are indicated on the graph. Mitochondrial proteins known to bind biotin directly (green diamonds) act as an internal control to verify AP from equal total protein amounts of Light and Heavy cell extracts. **B.** mCherry-MAP4 (red) localizes to MTs when transiently expressed in U2OS cells. Acetylated MTs are shown in green and DAPI in blue. **C.** In U2OS$^{Specc1L\text{-}GFP}$ cells with the bundled MT phenotype, mCh-MAP4 was observed to accumulate at the bundles with Specc1L-GFP (green), which also stain with anti-acetylated-α-tubulin (blue). Cells were PFA-fixed at 37C for 10 min. Scale bars are 30 µm. **D.** The three MT/CSK localization.balance options.

plasma membrane. Interestingly, the association of MAP4 with MTs and its effect on their structure has been shown to be regulated by phosphorylation, with decreased phosphorylation correlating with MT stabilization (Ebneth et al. 1999; Chang et al. 2001). Future experiments in the lab will be aimed at evaluating the potential of MAP4 and CKAP5 as Mypt1/PP1β substrates that mediate MT stabilization, via regulated recruitment of the phosphatase complex by Specc1L. As shown in Figure 4.19D, we can test their phosphorylation status under 3 distinct MT/CSK balance conditions for the phosphatase complex: 1. Normal distribution, 2. Increased association with actin filaments/decreased association with the MT network and 3. Increased association with the MT network/decreased association with actin filaments. It is important to note that both MAP4 and CKAP5 have also been implicated in mitotic roles, and so it will be important to assess their potential regulation by Mypt1/PP1β throughout the cell cycle.

The association of Specc1L with the actin-CSK, MT network, and the PM, in addition to regulating the subcellular localization of the MP complex via its association with Mypt1, provides the potential to be a key regulator of cell migration, adhesion and division. In fact, Specc1L has been implicated in control of cell migration and adhesion, and as an important regulator to ensure proper spindle positioning during the onset of anaphase. We therefore wanted to investigate the effects that knockdown of SPECC1L would have on both Mypt1-PP1β localization and regulation, and on migration and adhesion. We attempted to knock down Specc1L but obtained outcomes similar to our Mypt1 knockdown (poor and variable efficiency, and lack of a reliable antibody to monitor expression levels by IF). We decided to try generating Specc1L knockout lines using a CRISPR/Cas9 approach, but unfortunately our strategy (guide RNAs directed in the

region surrounding Exon 1) resulted in an alternatively spliced variant, which is detectable by Western blot using our commercially available Specc1L antibody. Analysis of the genomic DNA in the region surrounding Exon 1 confirmed the presence of a frame shift that would preclude Exon 1 translation, indicating that the mRNA was alternately spliced to produce a shorter variant. Future strategies will be targeted at other regions of the gene, and inducible shRNA knockdown lines generated.

CHAPTER 5: DISCUSSION

Our study investigates the three PP1 isoforms in human cells, demonstrating that they share some overlapping associations but also exhibit distinct preferences for particular regulatory subunits. The relative affinities for particular regulatory subunits likely contribute to the distinct functions observed for the PP1c isoforms. Given that the isoforms differ primarily at their N- and C-termini, these regions have been implicated in their differential associations with regulatory subunits. Although the hydrophobic "RVxF"-type binding motif has been implicated in association of most regulatory subunits with PP1c, the presence of additional PP1 binding motifs (SILK, MyPHONE) in some suggests that they may mediate preferential binding to the variable N- or C-termini of the catalytic subunit. These other motifs may also have a functional readout, as demonstrated by the finding that the SILK motif in the ancient regulatory subunit, Inh2, is essential for its inhibitory function (H. B. Huang et al. 1999; Wakula et al. 2003; Hendrickx et al. 2009).

Moving forward, one way to assess compensation would be to knock down (or knock out) a particular isoform (e.g. endogenous PP1β in our HeLa/BAC GFP cell line) and assess changes in the PP1α interactome, such as increased association with regulatory subunits that normally show a preference for PP1β. These types of experiments would be a useful complement to loss-of-function phenotypic assessment of single isoform knockdowns/knockouts.

In our study, we assembled comprehensive maps of PP1 isoform targeting in different cell types, highlighting association with known/predicted regulatory subunits and assessing the enrichment of specific multiprotein complexes linked to known regulatory pathways (Table 5.1). Our HeLa/BAC and MCF7/cDNA screens are the first direct

comparisons of the interactomes of the three isoforms relative to each other, expressed stably under the control of their own endogenous promoters (BAC) or under the control of a CMV driven promoter (cDNA). Interestingly, whether the promoter was endogenous or exogenous, the amount of GFP-PP1α expressed was always higher than that of the other isoforms. This supports previous suggestions that the α isoform is the most abundant (Okada et al. 2004).

Directly comparing relative enrichment of each known/predicted regulatory subunit with the three isoforms enabled us to extrapolate information such as isoform preference and the estimated abundance of a particular holoenzyme complex in the pool of PP1 complexes recovered. Some of the preferences that we observed are in agreement with previously published results, such as the preferential association of TPRN (Ferrar et al. 2012) and Phostensin (Kao et al. 2007) with the alpha isoform, and the MYPT family members (Terrak et al. 2004; Scotto-Lavino et al. 2010; Grassie et al. 2011) with the beta isoform. Interactome data deposited in the BioGrid database has listed LMTK2 as both a PP1α and PP1γ interactor, so it likely has the capacity to associate with both. Despite representing less than 1% of the pool of PP1γ complexes identified, the fact that LMTK2 was not detected with PP1α in our HeLa/BAC screen, despite capturing nearly 3x more of that isoform on the beads, tells us that it likely does show a preference for the γ isoform in vivo. For this and most other regulatory subunits, the significance of preferential association with a particular isoform remains to be determined. Based on our results, and taken together with results deposited in databases such as BioGrid and the published literature, we think it is important to avoid the term “isoform-specific”, and only refer to isoform “preferences”.

Name	PPP1	Description	Localization	Cytoplasm						Nucleus						Nucleolus					
				HeLa/BAC	MCF7/cDNA	PP1α		PP1β	PP1γ	HeLa/BAC	MCF7/cDNA	PP1α		PP1β	PP1γ	PP1α		PP1β	PP1γ		
				α vs β vs γ	α vs β vs γ	H	U	U	H	U	α vs β vs γ	α vs β vs γ	H	U	U	H	U	U	H	U	H	U
ASPP1	R13B	p53BP2-like	PM, CP, NP	α								α										
ASPP2/TP53BP2	R13A	Tumor protein p53 binding protein 2	TJ, PM, NP	α > β/γ	α > β/γ						α	α										
AURKA	R47	Aurora kinase A	CP, NP, No																			
AURKB	R48	Aurora kinase B	CP, NP																			
c20orf27		Chromosome 20 open reading frame 27	CP, NP	α	α/γ																	
CASC5/KNL1	R55	Cancer susceptibility candidate 5	NP																			
CDCA2/Repo-man	R81	Cell division cycle associated 2	NP																			
CHCHD3	R22	Coiled-coil-helix-coiled-coil-helix domain	MIT																			
CNST	R64	Consortin	CP, NP																			
CREP	R15B	PP1 regulatory subunit 15B	CP, MIT, NP																			
CSRNP2	R72	Cysteine-serine-rich nuclear protein	CP																			
DDX21		DEAD box helicase 21	NP, No		β																	
DDX31	R25	DEAD box helicase 31																				
ENDOFIN/ZFYVE16	R69	Endosome-associated FYVE domain protein	CP, VES																			
HCFC1	R89	Host cell factor 1	NP, MIT																			
HDAC6	R14A	Histone deacetylase 6																				
iASPP	R13L	Inhibitor of apoptosis-stimulating protein of p53	CP, NP	α/β	α/β > γ						α											
Inh3	R11	Protein phosphatase inhibitor 3	CP, MIT, NP, No																			
Inhibitor 2	R2	PP1 inhibitor 2	CP, NP	α/γ > β								α/γ										
KIF18A	R99	Kinesin family member 18A	CP, NP																			
LENG3	R12C	PP1 myosin-binding subunit p85	PM, CP, NP	β	β																	
LMTK2/KPI-2	R100	Lemur tyrosine kinase 2	NP, CP, MTOC	γ	γ							γ										
LRRC68	R37	Leucine rich repeat-containing protein			α > β,γ																	
MAP1B	R102	Microtubule-associated protein 1B	CP																			
MCM7	R104	Minichromosome maintenance complex component 7	NP																			
MKI67	R105	Monoclonal antibody Ki-67	No, NP		β						γ > α,β	γ > α/β										
MPHOSPH10	R106	M-phase phosphoprotein 10	No																			
MYPT1	R12A	Myosin phosphatase-targeting subunit 1	CP, CSK, NP, No	β	β						β	β										
MYPT2	R12B	Myosin phosphatase-targeting subunit 2	CP, CSK	β																		
MYPT3	R16A	Myosin phosphatase-targeting subunit 3	PM, CP, NP		β																	
Neurabin	R9A	Neural tissue-specific F-actin binding protein	PM, CP, NP	α/γ							α/γ											
NIPP1	R8	Nuclear inhibitor of PP1	NP		α/γ > β																	
NOC2L	R112	Nucleolar complex associated 2 homolog	No																			
NOM1	R113	Nucleolar protein with MIF4G domain 1	No																			
NONO	R114	Non-POU domain containing, octamer binding	PM, NP, No																			
ORC5	R117	Origin recognition complex subunit 5	CP, NP																			
PARD3	R118	Partitioning defective 3 homolog	TJ																			
PFKM	R122	Phosphofructokinase muscle	ER																			
PHACTR4	R124	Phosphatase and actin regulator 4	TJ, PM, CSK, CP																			
Phostensin	R18	PP1 F-actin cytoskeleton targeting subunit	CP	α							α											
PNUTS	R10	PP1 nuclear targeting subunit	NP																			
PPP1R3B	R3B	Protein targeting to glycogen			α																	
PPP1R3D	R3D	Protein targeting to glycogen			α																	
RIF1		Rap1 interacting factor homolog																				
RPL5	R135	Ribosomal protein L5	CP, NP, No																			
RRP1B	R136	Ribosomal RNA processing protein 1 homolog B	No									γ										
SARA/ZFYVE9	R173	Smad anchor for receptor activation	CP, END																			
SDS22	R7	PP1 regulatory subunit 7	CP, MIT, NP									α/γ										
SFPQ/PSF	R140	PTB-associated splicing factor	NP																			
SH2D4A	R38	SH2 domain-containing protein 4A	CP	β	β						β											
SMARCB1/SNF5	R144	SWI/SNF-related, actin-dependent regulator of chromatin	NP, NO																			
Spinophilin	R9B	Neurabin II	CP, CSK, NP	α,γ > β	α/γ						α/γ > β	α/γ > β										
SRSF10/FUSIP1	R149	FUS-interacting protein 2	CP, NP																			
TPRN		Taperin	PM, CP, NP	α							α	α										
TRA2B	R156	Transformer 2 protein homolog B	NP																			
URI1	R19	Prefoldin-like chaperone	CP, MIT, NP																			
WBP11/SIPP1	R165	Splicing factor that interacts with PQBP-1 nad PP1	CP, CSK																			
YLPM1/ZAP3	R169	YLP motif containing 1	NP	α																		
YWHAG	R170	14-3-3 gamma	CP, NP																			
ZCCHC9	R41	Zinc finger CCHC domain-containing protein	NP, No																			

Detected Significantly enriched Enriched >2-fold

Table 5.1. Annotation of 59 known/predicted PP1 regulatory subunits identified in PP1 isoform interactome screens, and addition of the novel subunit c20orf27.

An important caveat to assigning isoform preference, and another reason that it is essential to know the method used to determine it, is that overexpression of a particular regulatory subunit can override preferences. Our lab previously demonstrated this for the chromatin-associated regulatory subunit RepoMan, which we originally identified via its selective association with GFP-PP1γ over GFP-PP1α in nuclear extracts from HeLa/cDNA stable cell lines. When overexpressed, RepoMan was shown to recruit excess PP1α to chromatin, disrupting its normal subcellular distribution in interphase and mitotic cells (Trinkle-Mulcahy et al. 2006). At the same time, overexpressed RepoMan also recruited excess PP1γ (and likely PP1β) from other complexes, disrupting the normal balance of their distribution. This highlights the strong potential for off-target effects when assessing the functional role of a particular regulatory subunit by overexpression, as it is difficult to separate the direct effect of excess PP1 recruitment to a particular site from the indirect effect of recruiting it away from other important substrates.

The most interesting result from our screens was the consistent finding that a significant fraction of PP1c associates with regulatory subunits that have been evolutionarily conserved, such as SDS22, NIPP1, Inhibitor 2 and Inhibitor 3. In the HeLa/BAC screen, these 4 subunits represent, by normalized relative abundance in the AP, approximately 45% of the pool of known regulatory proteins captured on the beads in sufficient amounts to be detectable by MS (Figure A5.A). Similarly, in the MCF7/cDNA screen they represent ~54% of the pool of identified regulatory subunits (Figure A5.B). We believe that these regulatory subunits may function as PP1 “sinks”, binding and inhibiting the activity of any free catalytic subunit in the cell. As PP1 is required at specific times and in specific places, it can then be recruited from these complexes. With

respect to subcellular localization, most have been shown to distribute between the CP and NUC although NIPP1 is predominantly nuclear (Table 5.1).

It is important to note that although all four of these proteins were initially identified as PP1 “inhibitors”, that distinction cannot readily be made for phosphatases because it depends on the substrate that is used to assess inhibition. For example, the glycogen regulatory subunit activates the activity of PP1 against glycogen phosphorylase, but inhibits its activity against myosin. Conversely, the myosin regulatory subunit activates the activity of PP1 against myosin while inhibiting its activity against glycogen phosphorylase. These evolutionarily conserved subunits have been shown to positively regulate PP1 in specific pathways (Van Dessel et al. 2010; J. Wu et al. 2016) as well as inhibiting its activity against unrelated substrates. Support for their potential as PP1 “sinks” is provided by a study showing that two of these ancient regulatory subunits, SDS22 and Inh3 form an inhibitory heterotrimeric complex with PP1 in vivo (Lesage et al. 2007).

Also consistent with this hypothesis is the fact that the regulatory subunits are expressed in excess over the catalytic subunit (Heroes et al. 2013; Nagaraj et al. 2011; Lundberg et al. 2010), which would explain how cells could adapt to fluctuations in PP1 levels, including its stable overexpression. The fact that we map more than just these four regulatory subunits in our GFP-PP1 interactome screens reassures us that, although they may be buffering some of the excess PP1, a significant amount is also being incorporated into other holoenzyme complexes. Similarly, interactome screens based on transient overexpression of PP1, which is toxic to cells in the long-term, have also identified some of the lower abundance complexes, as shown by BioGrid depositions of high-throughput datasets.

The only ancient regulatory subunit that has been studied in detail via mouse KO studies is NIPP1, and the KO was shown to be embryonic lethal with severe developmental defects (Van Eynde et al. 2004). This would be consistent with these evolutionarily conserved proteins playing an essential (and more general role) in regulating PP1 activity, in addition to their more specialized roles in human cells.

Another interesting result of our large-scale screens was the observation that PP1α is the only isoform that accumulates at centrosomes in interphase cells in the three cell lines tested, and that this localization appears to be predominantly regulated in these cells by the ASPP family member ASPP2. This was surprising because the centrosomal kinase NEK2 had been proposed as a key centrosomal regulatory subunit for PP1, binding it directly and regulating centrosome splitting (Helps et al. 2000; Mi et al. 2007). More recently, two other proteins, LRRC67/PPP1R42 and CEP192, were also identified as centrosomal-associated PP1 regulatory subunits (DeVaul et al. 2013; Nasa et al. 2017). We did not, however, identify any of these proteins in our PP1 interactome screens. This is likely a detection issue, as these complexes could represent only a small fraction of the total pool in these particular cell lines. Of the large panel of regulatory subunits that we cloned and screened by imaging, only ASPP2 was observed to accumulate at centrosomes. Furthermore, although detected with the other isoforms, a significantly larger fraction of PP1α was found in complex with ASPP2. In addition, three RASS family proteins, RASSF7, F8 and F9, were identified in our PP1α screens, and all three were observed to accumulate at centrosomes. As they didn't have predicted RVxF motifs, we hypothesized that they associated with PP1 indirectly, via a regulatory subunit.

ASPP2 was the top candidate, and we confirmed the association of RASSF7, RASSF8 and RASSF9 with ASPP2 by co-immunoprecipitation.

These findings are consistent with studies in Drosophila that linked dASPP, the single homolog of human ASPP1 and ASPP2, to the RASSF8 homolog dRASSF8, and showed that the complex regulates cell-cell adhesion during retinal morphogenesis (Langton et al. 2009). With respect to centrosomes, work was published in 2015 that suggested the ASPP family proteins can recruit PP1α to centrosomes and regulate centrosome splitting via dephosphorylaton of the linker protein C-Nap1 (Langton et al. 2009). The dephosphorylated state of C-Nap1 enables the protein to tether the interphase parental chromosomes together. Although we saw no obvious centrosomal defects when RASSF7/8/9 were transiently overexpressed in cells, we did observe that ASPP2 overexpression was toxic, and it was difficult to find healthy cells expressing it. Future experiments will further assess the role of this PP1 complex, and its RASS family binding partners, in centrosomal regulation.

Interestingly, Hauri et al. have demonstrated that the ASPP2-PP1α complex may be important in the regulation of the HIPPO pathway (Figure 5.1) (Hauri et al. 2013), which regulates tissue homeostasis. Briefly, when the HIPPO pathway is active, the downstream transcription co-activators, YAP1 and TAZ, are phosphorylated through 14-3-3 mediated cytoplasm sequestration. The phosphorylation leads to the inactivation of YAP1 and TAZ. When the HIPPO pathway is inactive, YAP1 and TAZ can bind to the TEAD family of transcription factors and transcribe pro-growth and anti-apoptotic genes. The authors demonstrate that overexpression of PP1α and ASPP2 can enhance expression of TEAD luciferase reporter construct, confirming a role for the ASPP2-PP1

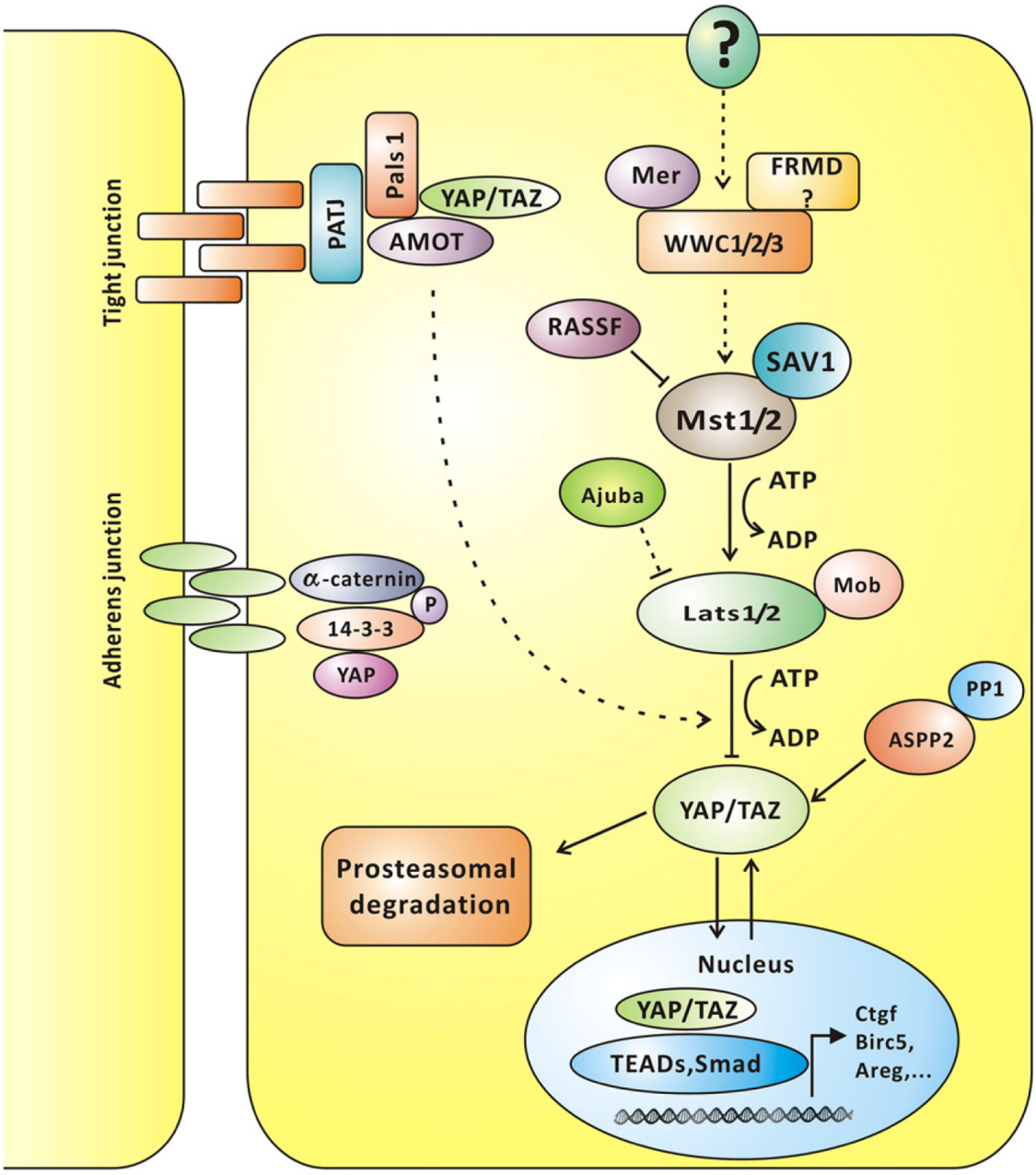

Figure 5.1. Illustration of the Hippo Signaling pathway. *Reproduced by permission from Elseivier: [Cellular Signaling].*(Hao et al. 2014)*, copyright (2014).*

complex in regulating the HIPPO pathway (Hauri et al. 2013). Although overexpression of PP1γ was also shown to enhance expression of the TEAD luciferase reporter construct, PP1β and the ASPP2 family member, ASPP1 had no significant effect (Hauri et al. 2013). This is consistent with our results, which indicate that although ASPP2 shows preferential binding to PP1, the other isoforms are also capable of associating with ASPP1/2. Taken together, this suggests that compensation could occur for PP1-ASPP2 signaling in the absence of the alpha isoform.

Interestingly, we also identified two other PP1 partners that have been linked to regulation of the HIPPO pathway, suggesting the phosphatase may feed into this signalling cascade at more than one level, or at more than one time/place. These include the regulatory subunit PARD3, which is involved in cell polarity regulation and has been shown to induce TAZ activation by promoting the interaction of PP1 with the LATS1 kinase (Lv et al. 2015), and PEAK1, a protein tyrosine kinase that associated with the actin cytoskeleton and has been linked to HIPPO pathway regulation via eIF5A-PEAK1 signaling-mediated control of YAP1/TAZ expression levels (Strnadel et al. 2017). PEAK1 was one of the commonly enriched interactors that caught our attention in the isoform interactome screens, and it also contains a putative RVXF motif at aa 922-929 (PKRWISFK). Although we validated the association of endogenous PEAK1 with PP1 both by co-immunoprecipitation/Western blot analysis and BioID near neighbour labeling, we have not yet tested whether it binds PP1 directly via this motif, which would confirm it as a bona fide regulatory subunit rather than an indirect associate. Future work will test association of wild type and RAXA mutant PEAK1 with PP1 in the same F2H and BiFC screens used to validate c20orf27 as a novel PP1 regulatory subunit. It will also be

interesting to dissect the respective contributions of these PP1 complexes to HIPPO pathway regulation, similar to our ongoing dissection of the contributions of the nuclear regulatory subunits Repo-man, PNUTS and TPRN to DNA damage response(Prevost et al. 2013; Ferrar et al. 2012; Landsverk et al. 2005; Peng et al. 2010).

In addition to its broad range of regulatory roles in interphase cells, mitotic-specific roles have also been described for PP1 (Andreassen et al. 1998; Trinkle-Mulcahy et al. 2003; Trinkle-Mulcahy et al. 2006; Trinkle-Mulcahy & Lamond 2006; De Wever et al. 2012; De Wever et al. 2014), and our data confirm that a subset of regulatory complexes is upregulated at G2/M, at least for the PP1β and PP1γ isoforms. Some, such as Repo-man and MKI67, are associated with PP1 throughout the cell cycle, but their levels increase prior to mitosis due to their essential roles in this process (Trinkle-Mulcahy et al. 2006; Booth et al. 2014). When cells arrested at G2/M by nocodazole treatment were compared to asynchronous cells, we observed a 2-fold increase in the amount of these proteins associated with PP1γ, and a 5-7-fold increase in the amount associated with PP1β. KIF18A was only detected in our mitotic screens, and showed a 3-4-fold increase in G/M-arrested cells, consistent with its role as a mitotic kinesin (De Wever et al. 2014). We did not detect any PP1α complexes that were upregulated at G2/M, and in fact there was a general decrease in its association with several regulatory subunits. PP1 has been shown to be regulated in mitosis, at least in part, via inhibitory phosphorylation of a threonine residue (Thr320 in PP1α) by the mitotic kinase CDK1 (Kwon, Lee, et al. 1997; J. Q. Wu et al. 2009). This may indicate that the primary regulatory roles for this isoform are carried out in interphase, and that it remains predominantly inactive throughout

mitosis. Alternatively, it may already exist in the complexes that regulate its mitotic role(s), with no need for increased levels of these complexes.

This mitotic screen is our first comparison of the dynamic interactomes of the PP1 isoforms, although we do have preliminary data suggesting changes in their distribution between regulatory complexes in response to hypoxia. Moving forward, our unperturbed interactome "snapshots" will be useful comparisons for the changes that occur during different cellular conditions (e.g. proliferation vs. differentiation or the epithelial-to-mesenchymal transition) and in response to various cellular perturbations. It will also help us to identify changes that have occurred in various disease states.

Of particular interest is recent work confirming that the first small inhibitor targeted at a PP1 complex, Sephin1, can prolong the benefits of an adaptive phosphorylation-mediated signalling event that protects cells from otherwise lethal ER protein misfolding stress. It does this by specifically disrupting the GADD34/PP1 complex that mediates dephosphorylation of the relevant substrate (Figure 5.2) (Das et al. 2015). In this study, published in 2015, Sephin1 treatment prevented defects associated with Charcot-Marie-Tooth 1B and amyotrophic lateral sclerosis, two unrelated protein misfolding diseases, in mouse model systems.

Our work has now uncovered another protein degradation-related PP1 complex, although much work remains to be done to characterize it functionally. Having noted c20orf27, which possesses a putative RVxF motif, as one of our "commonly enriched interactors" in more than one PP1 interactome screen, we cloned the gene, confirmed their direct binding and demonstrated that it is mediated via the RVXF motif in c20orf27. Our work was hindered by the lack of an antibody that recognizes endogenous c20orf27, and we thus decided to focus first on mapping the interactome of GFP-tagged c20orf27 to

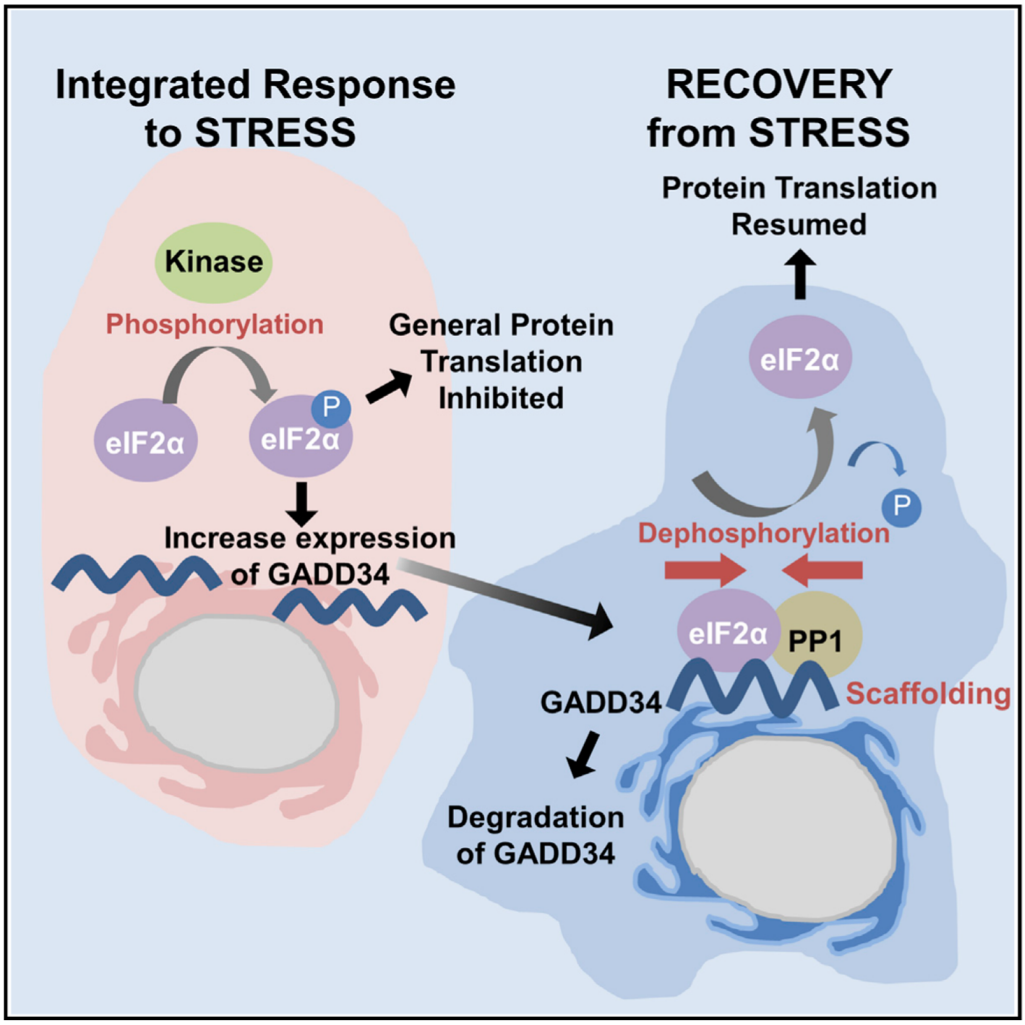

Figure 5.2. Activation of Unfolded Protein Response. *Reproduced from* (Choy et al. 2015)

gain functional clues to its cellular role(s). A series of quantitative AP/MS experiments confirmed co-precipitation of PP1 and also revealed a consistent interaction with APPBP2 (amyloid beta precursor protein binding protein 2), the human homolog of Drosophila PAT1. PAT1 is known for its upregulation in certain cancers (Monni et al. 2001; Hirasawa et al. 2003), possible link to microtubule trafficking (Zheng et al. 1998) and androgen receptor transactivation (Zhang et al. 2004).

The c20orf27 interactome also identified associations with ElonginB/C proteins TCEB2/1, and the Cullin protein CUL2. A previous study identified APPBP2 as a novel VHL-type Elongin BC-box CUL2 binding E3 ubiquitin ligase substrate specifier (Mahrour et al. 2008) (Figure 5.3). No substrates have yet been identified for the APPBP2/ElonginBC/CUL2 complex, but our identification of the intact complex in a non-biased screen supports a physiological role. Interestingly, we did not identify the complex members that are recruited by CUL2 for the actual ubiquitin ligation steps, namely Rbx and a ubiquitin ligase. That could indicate that these modules are recruited as needed. It is possible that association of APPBP2 with c20orf27/PP1 may mediate this recruitment, or perhaps substrate specificity. Future experiments will assess which region of APPBP2 mediates association with c20orf27/PP1, and whether altered levels of this particular phosphatase complex affect global ubiquitination and protein degradation. One other ubiquitination-related protein that was enriched in the c20orf27 interactome was UBR2 (Recognin), which plays a role in a unique branch of the ubiquitin-proteasome system called the “N-end rule pathway”. In this pathway the N-terminal residue of a protein serves as an N-degron, which is marked by various post-translational mechanisms and targeted for degradation (Liu et al. 2016). Failures in this pathway have been implicated

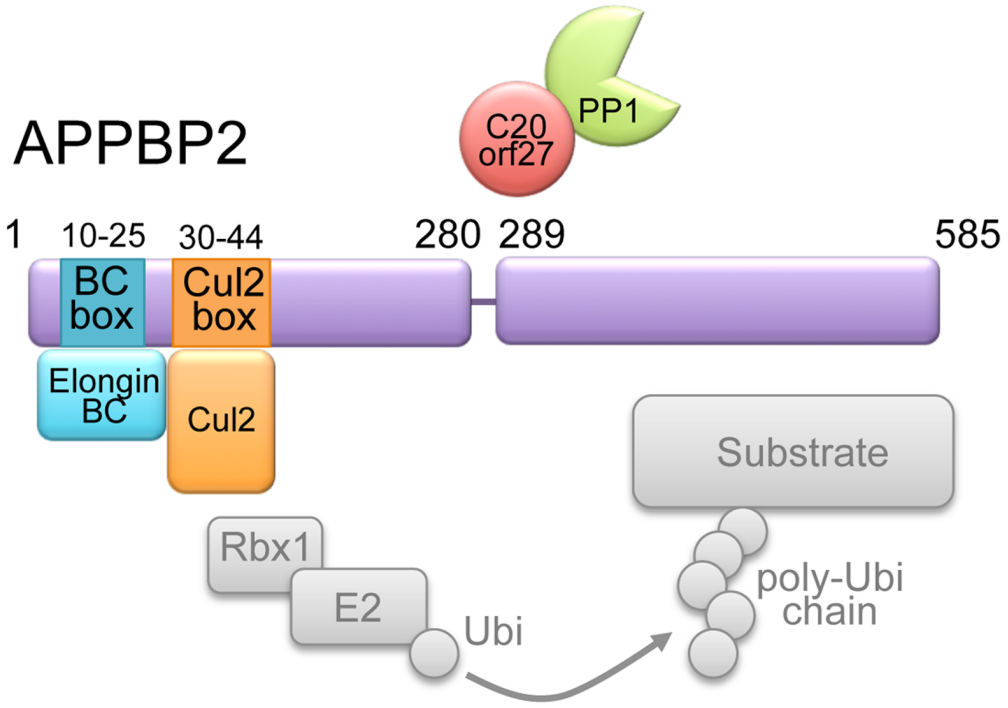

Figure 5.3. Schematic illustrating the regions in APPBP2 that mediate association with Elongin BC (TCEB2/1) and CUL2. Complex members not detected are shown in gray. The region that mediates association with c20orf27/PP1 is not yet known.

in the development of human diseases such as Johanson–Blizzard syndrome and neurodegenerative disorders, and the Alzheimer's Disease-associated fragment of APP has been identified as an N-end rule pathway substrate (Brower et al. 2013). This suggests that the pathway counteracts neurodegeneration, and thus our novel complex that links a regulatory protein (c20orf27/PP1) to a key N-end pathway factor and an E3 ubiquitin ligase substrate specifier (APPBP2) that also binds APP is of significant therapeutic interest.

Also of considerable therapeutic interest is the regulation of the MYPT1/PP1β phosphatase complex, which was one of the first PP1 complexes identified (as the myosin phosphatase) but has since been linked to several key regulatory roles in both muscle and non-muscle cells. Having identified Mypt1 as a PP1β binding partner in our interactome screens was not a novel revelation. Of interest was that a large percentage of PP1β complexed with Mypt1 during interphase (30%), and that PP1β showed an increased association with Mypt1 in Nocodazole treated (G2/M) cells. Mypt1 is found to interact with several proteins, and the identification of Mypt1 in both CP and NUC fractions supported its proposed regulatory roles in both cellular compartments. One odd observation was that endogenous Mypt1 co-precipitated its known actomyosin associates from nuclear rather than cytoplasmic extracts. We first thought this might be due to inefficient cell disruption, however the majority of myosins and actins are found in the cytoplasmic extracts, as expected. Another possibility is that filamentous actomyosin remains tethered to and co-purifies with nuclei. We also cannot rule out the possibility that Mypt1 interacts with myosin and actin in the nucleus (as has been suggested), and that fractionation selectively dissociates cytoplasmic complexes while retaining nuclear complexes. It is thought that myosins may act as a type of motor to drive both the

chromatin remodelling required for transcription and the chromosome migration observed following cell division, although the mechanism remains unclear. NM I (MYO1C), a member of the uncoventional myosin I subfamily, is present in nucleoli, for example, where it associates with RNA polymerase I and transcribing ribosomal genes (Fomproix & Percipalle 2004; Kysela et al. 2005). MYO1C and nuclear myosin VI also associate with RNA polymerase II and have been proposed to contribute to regulation of gene transcription (Hofmann et al. 2006; Kysela et al. 2005; Pestic-Dragovich et al. 2000; Vreugde et al. 2006). Furthermore, actin has been found in the nucleus, with evidence suggesting functions in chromatin remodelling and RNA polymerase complexes (de Lanerolle et al. 2005; Grummt 2006; Percipalle & Visa 2006). The role of Mypt1 in regulating nuclear myosins remains to be investigated in detail, however recent work suggests it may regulate an arginine methyltransferase that controls RNA processing, splicing and gene expression (Sipos et al. 2017).

Given that only a handful of identified binding partners in our interactome screens were PP1β specific, and that the Specc1/1L family proteins have been linked to cytoskeletal roles, we speculated that the association of Specc1/1L (which do not contain predicted PP1 binding motifs) with the catalytic subunit may be mediated by the regulatory subunit Mypt1. Having identified Specc1L and PP1β as the top two proteins enriched in our GFP-tagged Mypt1 interactome screen suggested that the transient overexpression of Mypt1 precludes its proper localization (and association with known substrates such as myosin), and that the association with both Specc1L and PP1β under these conditions indicates the preservation of a core trimeric complex. Other multimeric PP1 complexes have been identified. Some trimeric complexes involve the direct binding

of PP1c to one targeting or substrate-specifying regulatory subunit and one inhibitory subunit (Heroes et al. 2013). Others, such as the complex composed of PNUTS, TOX4, WDR82 and PP1 (Lee et al. 2010), which we also identified in our screens, have PP1 associate with one or more complex members indirectly. In this complex, PP1 associates with TOX4 and WDR82 indirectly via PNUTS. This multimeric complex was shown to be important in the establishment of chromatin structure during the transition from mitosis into interphase (Lee et al. 2010). Other trimeric complexes, such as Mypt1/PP1/CPI1-17 (CPI-17, an inhibitor of the myosin phosphatase complex expressed predominantly in mature smooth muscle) (Kitazawa et al. 1991; Eto et al. 2007), have both Mypt1 and CPI-17 binding non-overlapping sites on PP1, while they also have binding sites for each other (Eto et al. 2007). Furthermore, there are cases where regulatory subunits compete for common binding sites on PP1, such as the RVxF binding channel (i.e. GADD34/inhibitor-1, spinophilin/inhibitor-2) (Heroes et al. 2013). We believe that Specc1/L, which have no obvious PP1 binding motifs, associates with PP1β indirectly via their direct interaction with Mypt1.

As mentioned earlier, Mypt1 is found to associate with a large number of proteins. In addition to its key role in the regulation of actomyosin in non-muscle cells, several non-myosin Mypt1/PP1β substrates have been identified recently, including polo-like kinase 1 (PLK1) and histone deacetylase 6 (HDAC6). PLK1 is involved in a variety of mitotic events including centrosome maturation and separation, kinetochore-microtubule attachment and cleavage furrow ingression (Petronczki et al. 2008; Bruinsma et al. 2012; Zitouni et al. 2014). Yamashiro et al. demonstrated that Mypt1 contributes to mitotic regulation via its interaction with PLK1, colocalizing with PLK1 on centrosomes (Yamashiro et al. 2008). Joo et al. have shown that HDAC6, which plays an important

role in microtubule deacetylation, is a substrate for the Mypt1/PP1β complex (Joo & Yamada 2014). They suggest that the complex balances contractility and microtubule acetylation by associating either with myosin light chain or HDAC6 (Joo & Yamada 2014), although it is not clear how the distribution of MYPT1/PP1β between these two subcellular structures would be regulated (Figure 5.4).

Our identification of a novel complex comprising Mypt1/PP1β and proteins capable of associating dynamically with both the MT and actin CSK networks makes the Specc1/L family proteins attractive candidates for this "missing link" that regulates the distribution of phosphatase activity between these two structures. We demonstrate that Specc1/L associates with MTs and with the actin CSK, and directly binds Mypt1. Furthermore, we demonstrate that Specc1/L can regulate the subcellular localization and turnover dynamics of the MYPT1/PP1β complex in cells, pushing the balance more toward MTs (which show a stabilized/bundled phenotype) or the actin CSK (which show differences in actin organization) (Figure 4.19D).

We also show that this complex is maintained throughout the cell cycle, and that Specc1/L and MYPT1 localize to mitotic spindles at metaphase, and the cleavage furrow during cytokinesis, consistent with proposed roles in these events. Although specific substrates remain to be identified, our interactome screens identified potential associations with phosphoproteins such as MAP4 (which regulates MT stability) and beta-tubulin (which is regulated by phosphorylation in mitosis).

Taken together, our data identify the Specc1/1L protein family members as key regulators of the MYPT1/PP1β complex, regulating its distribution between the actin CSK and the microtubule network throughout the cell cycle. Further work will be necessary to

characterize the functional significance of this regulation, and to harness its therapeutic potential in diseases such as cancer and hypertension.

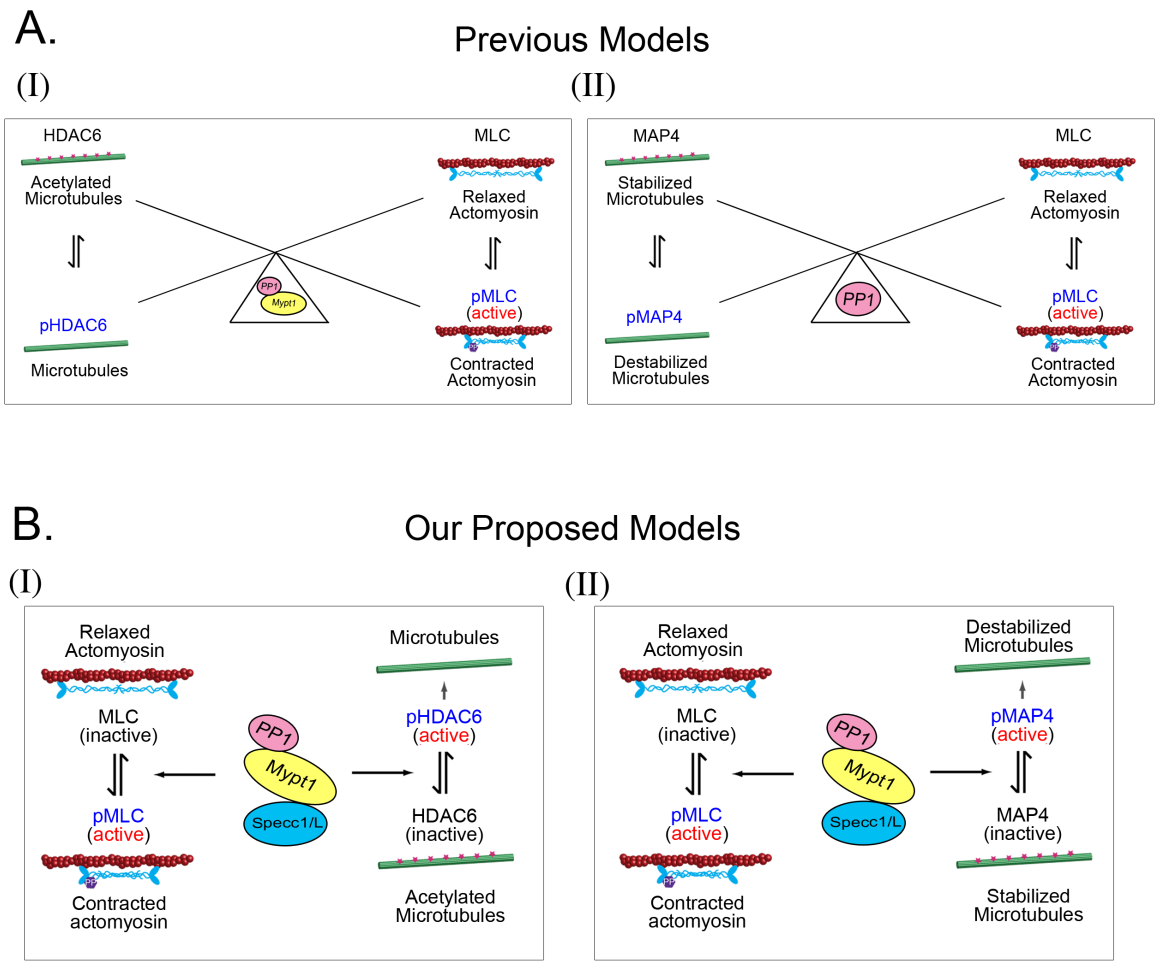

Figure 5.4 Balancing the actomyosin and MT phosphatase activity of Mypt1/PP1β. Schematic summary of **A.** previously proposed models in the literature for the role of PP1 in balancing contractility with microtubule stability for adhesion disassembly. A shift in the balance can effect migration, proliferation and contractility leading to a wide range of diseases. Although changing Mypt1 levels were shown to affect HDAC6 phosphorylation levels, it remains unclear how the phosphatase is recruited to the acetylase (I). Similarly, use of catalytic site inhibitors suggested that PP1 can dephosphorylate MAP4, but the relevant complex was not identified. **B.** Our proposed models in which Specc1L associates with the phosphatase complex by binding Mypt1, directing it to key substrates such as HDAC6 and MAP4 to achieve a balance between cellular contractility and microtubule stability throughout the cell cycle.

APPENDICES

APPENDIX I

Construct	Forward (FWD) Primer/ Reverse (REV) Primer (Restriction Site in red)	Restriction site on FWD/REV primer
pFGFP-Mypt1	FWD: GATC***GAATTC***TATGAAGATGGCGGACGCGAAGCAG REV: GATC***GGTACC***TTTGGAAAGTTTGCTTATAACTCTGATC AAGGCCCC	EcoRI/ASP718
PGEX-4-T3 MyptN98	FWD Same as above REV: GATC***GTCGAC***ATATTTGCTCCATTTTCTACCAGAAACT TCACCATATCAACATTGTCATCAATGC	EcoRI/SalI
PGEX-4-T3 Mypt1(CD)	FWD: GATC***GAATTC***CATGGGCACTGTCTCCTCCACAACAGA GGTC REV: GATC***GTCGAC***TTTGGAAAGTTTGCTTATAACTCTGATC	EcoRI/SalI
pEGFP-Mypt1 (ANK)	FWD: GATC***GAATTC***TATGAAGATGGCGGACGCGAAGCAGAA GCGG REV: GATC***GGTACC***TTCATCAACCTTTTCTTGTTC	EcoRI/ASP718
(MID)Mypt1-pEGFP (N3)	FWD: GATC***GAATTC***TATGGAAGAAGAAGGAAAGAAGGATGA G REV: GATC***GGTACC***AGCAGTAGTTGTAGTCAGGGTTGTGGT AG	EcoRI/ASP718
pEGFP-Mypt1 (CD)	FWD: GATC***GAATTC***TATGGGCACTGTCTCCTCCACAACAGA GGTC REV: GATC***GGTACC***TTTGGAAAGTTTGCTTATAACTCTGATC	EcoRI/ASP718

Table A1. Cloning of Mypt1 full-length and fragments into pEGFP-C1 (the table indicates if the cDNA was cloned into pEGFP-N3) and PGEX-4-T3

Construct	Forward (FWD) Primer/ Reverse (REV) Primer (Restriction Site in red)	Restriction site on FWD/REV primer
Specc1L-pEGFP (N3)	FWD: GATC***GAATTC***TATGAAGAAAGCAAGCAGGAGTGTTGGC REV: GATC***GGATCC***GGTCTCAAAGTACTTGTAGATCGCCG	EcoRI/BamHI
pEGFP-Specc1L (N-term)	FWD: GATC***GAATTC***TATGAAGAAAGCAAGCAGGAGTGTTGGC REV: GATC***GGATCC***TCGACTAAAGTGTTCCAACTTATCGCT	EcoRI/BamHI
pEGFP-Specc1L (C-term)	FWD: GATC***GAATTC***TCAGATTGAATACTTCCGCTCTCTTCTA REV: GATC***GGATCC***GGTCTCAAAGTACTTGTAGATCGCCG	EcoRI/BamHI
pEGFP-Specc1L (CHD)	FWD: GATC***GAATTC***TCCAATCTCAACATCCAAACCCCTG REV: GATC***GGATCC***GGTCTCAAAGTACTTGTAGATCGCCG	EcoRI/BamHI
pEGFP-Specc1L (ΔN-term/ ΔCHD)	FWD: GATC***GAATTC***TCAGATTGAATACTTCCGCTCTCTTCTA REV: GATC***GGATCC***TCCACTTATGGAATGTCTCTGCATAG	EcoRI/BamHI
pEGFP-Specc1L (ΔCHD)	FWD: GATC***GAATTC***TATGAAGAAAGCAAGCAGGAGTGTTGGC REV: GATC***GGATCC***TCCACTTATGGAATGTCTCTGCATAG	EcoRI/BamHI

Table A2: Cloning of Specc1L fragments into pEGFP-C1, where full length Specc1L was cloned into pEGFP-N3.

Construct	Forward (FWD) Primer/ Reverse (REV) Primer (Restriction Site in red)	Restriction site on FWD/REV primer
Specc1L-BirA-HA	Digest of Specc1L-pEGFP and pcDNA3.1 MCS-BirA(R118G)-HA with EcoRI/BamH1 and ligated.	EcoRI/BamHI
Myc-BirA-Specc1L N-term	Digest of pEGFP-Specc1L (N-term) and pcDNA3.1 MycBirA(R118G)-MCS with EcoRI/BamH1 and ligated	EcoRI/BamHI
Myc-BirA-Specc1L C-term	Digest of pEGFP-Specc1L (C-term) and pcDNA3.1 MycBirA(R118G)-MCS with EcoRI/BamH1 and ligated	EcoRI/BamHI
His-Specc1LΔCHD (pET-47B (+))	FWD: GATC***GGATCC***GATGAAGAAAGCAAGCAGGAGTGTTGG REV GATC***GAATTC***GGTCCACTTATGGAATGTCTCTGCATAG	BamH1/EcoRI
His-Specc1L N-term (pET-47B (+))	FWD: GATC***GGATCC***GATGAAGAAAGCAAGCAGGAGTGTTGG REV GATC***GAATTC***GGTCGACTAAAGTGTTCCAACTTATCGCT	BamH1/EcoRI
His-Specc1L C-term (pET-47B (+))	FWD: GATC***GGATCC***GATGCAGATTGAATACTTCCGCTCTCTTCTA REV: GATC***GAATTC***GGGGTCTCAAAGTACTTGTAGATCGCCG	BamH1/EcoRI

Table A3. Cloning of Specc1L full-length and fragments into pCDNA3.1 BioID-HA or Myc-BioID and pET-47B (+).

Construct	Forward (FWD) Primer/ Reverse (REV) Primer (Restriction Site in red)	Restriction site on FWD/REV primer
Specc1(Iso1)-pEGFP (N3)	FWD: GACT***GAATTC***TATGCGGAGTGCAGCCAAGCCCTGGAAC REV: GATC***GGTACC***CGTCTCAAAGTACTTGTAGATTTGGGCCACG	EcoR1/ASP718
Specc1(Iso4)-pEGFP (N3)	FWD: GATC***GAATTC***TATGGGCAACCACTCAGGACGGCCCGAGG REV: GATC***GGTACC***CGTCTCAAAGTACTTGTAGATTTGGGCCACG	EcoR1/ASP718
pEGFP-Specc1 (Iso1) (N-term)	FWD: GACT***GAATTC***TATGCGGAGTGCAGCCAAGCCCTGGAAC	EcoR1/ASP718
pEGFP-Specc1 (Iso1/4) (C-term)	REV: GATC***GGTACC***CGTCTCAAAGTACTTGTAGATTTGGGCCACG	EcoR1/ASP718

Table A4. Cloning of Specc1 (Iso1 and 4) full-length and fragments into pEGFP-C1/N3 (pEGFP-N3 cloning is indicated)

Construct	Forward (FWD) Primer/ Reverse (REV) Primer (Restriction Site in red)	Restriction site on FWD/REV primer
mCH-MAP4	FWD: GATC***AAGCTT***CGATGGCTGACCTCAGTCTTGCAGATGC REV GATC***GGTACC***GATGCTTGTCTCCTGGATCTGGCTGTCC	HindIII/Asp718
PEAK1	FWD: GATC***GAATTC***ATGTCTGCTTGTAACACCTTTACTG REV: GATC***GGTACC***TTAACGGTGCTGCAGAAT	EcoRI/Kpn1
Leng3-pEGFP (N3)	FWD: GATC***GAATTC***TATGTCTGGTGAGGATGGACCAGCTGC REV: GATC***GGATCC***CTTGGAGAGTTTGCTGATGACGCGGATC	EcoR1/BamHI
pEGFP-C20orf27	FWD: GATC***CTCGAG***CTATGGCTGCAGCCAACAAGGG REV: GATC***GAATTC***GAGTCAAAGCCGTGCCAGTCGC	Xho1/EcoR1
pEGFP-ASPP2	FWD: GATC***CTCGAG***ATGATGCCGATGATATTAACTGTTTTCTT GAG REV: GATC***GGTACC***ACCGGCGAGTGTTCGCTGTCGGGG	Xho1/Asp718

Table A5: Cloning of MAP4, PEAK1, Leng3, C20orf27 and ASPP2 into mCH-C1 or pEGFP-C1/N3. Cloning done in pEGFP-N3 is indicated.

Construct	Forward (FWD) Primer/ Reverse (REV) Primer (Restriction Site in red)
GFP-C20orf27KAGA	FWD: CAGCAGCTTTCTGGTCAAGGCTGGCGCCCTGAAGATCC TGCAC REV: GTGCAGGATCTTCAGGGCGCCAGCCTTGACCAGAAAGC TGCTG

Table A6: Primers used for Site-Directed Mutagenesis

Primary Antibody Target	Species	Assay	Dilution	Company	Catalogue#
SDS22 (PPP1R7)	Goat	WB	1:500	Santa Cruz	sc162164
CYTSA (SPECC1L)	Rabbit	WB IF	1:300 1:25	Protein Tech	25390-1-AP
MYH9	Rabbit	WB	1:1000	Sigma Aldrich	SAB2101542
MYL12B	Rabbit	WB	1:1000	Abcam	AB137063
MYPT1	Rabbit	WB IP	1:1000	Bethyl Laboratories	A300-889A A300-888A
MYPT1	Rabbit	WB	1:1000	In-house	LTM Lab
Pericentrin	Rabbit	WB	1:1000	Abcam	ab4448
PP1α	Rabbit	WB	1 mg/mL	In-house	Greg Moorhead
PP1γ	Rabbit	WB	1 mg/mL	In-house	Greg Moorhead
PP1β	Rabbit	WB	1 mg/mL	Homemade	Greg Moorhead
Pan-PP1	Rabbit	WB	1:200	Millipore	07-1217
RIF1	Rabbit	WB	1:1000	Bethyl Laboratories	A300-567A-1
mCherry	Rat	WB	1:350	In-house	Greg Moorhead
Acetylated-αTubulin	Mouse	WB/IF	1:1000	Sigma Aldrich	T6793
ASPP2	Mouse	WB	1:1000	BD Biosciences	611354
GFP	Mouse	WB	1:500	Roche	11-814-460-001
Inhibitor 2 (PPP1R2)	Mouse	WB	1:500	Abnova	H00005504-A01
Lamin A/C	Mouse	WB	1:250	Santa Cruz	Sc-7292
αTubulin	Mouse	WB IF	1:1000 1:1000	Sigma Aldrich	T6199
PNUTS	Sheep	WB	1:500	In-house	Greg Moorhead
NIPP1	Sheep	WB	1:200	In-house	Greg Moorhead

Table A7. List of Primary antibodies used for Western blot analysis and immunofluorescence.

Secondary Antibody	Assay	Dilution	Company	Catalogue#
Goat Anti-Mouse IgG HRP	WB	1:5000	Thermo Scientific	31430
Goat Anti-Rabbit IgG HRP	WB	1:5000	Thermo Scientific	31460
Goat Anti-Rat IgG HRP	WB	1:5000	Thermo Scientific	31470

Table A8. List of Secondary antibodies used for Western blot analysis.

Dye	Assay	Dilution	Company	Catalogue#
Phalloidin-AlexaFluor647	IF	1:300	Life Technologies	A22287
Phalloidin-AlexaFluor488	IF	1:300	Life Technologies	A12379
Streptavidin 568	IF	1:1000	Life Technologies	S-11226
Hoechst	IF	1:15000	Invitrogen	H1399
DAPI	IF	1:15000	SIGMA	D9542

Table A9. List of Dyes used for cell staining.

Culture Format	DNA (μg)	PEI (μl)	Volume of medium to add to complexes (μl)	Volume of medium to add to cells (μl)
12-well plate	1	2.5	150	800
6-well plate	3	7.5	300	1600
100 mm dish	10	25	600	9000
150 mm dish	15	37.5	600	14000

Table A10. Amount of DNA and PEI used for cell transfection.

APPENDIX II

HeLa^GFP Cytoplasmic (CP)/ Stable cell line
Light: HeLa Heavy: HeLa^GFP
MaxQuant Version: 1.2.7.4
Median log Ratio H/L = 0.50
Threshold (> 1 log median) =1.50

Uniprot ID	Gene Name	Peptides	Unique Peptides	Mol. weight [kDa]	Ratio H/L	Log Ratio H/L	Intensity	NINT	Intensity L	Intensity H	Ratio H/L Significance B
P08670	VIM	43	40	53.651	14.02	3.80962	1.23E+10	228.7	7.12E+08	1.16E+10	2.06E-04
Q9U6Y5	GFP	19	19	28.106	11.82	3.56328	1.11E+11	3939	7.18E+08	1.10E+11	5.87E-04
Q16527	CSRP2	4	4	20.954	8.993	3.16877	1.14E+08	5.442	6.61E+06	1.07E+08	2.70E-03
E7EPA7	TKT	7	7	68.813	8.928	3.158256	1.56E+08	2.273	1.63E+07	1.40E+08	2.81E-03
P10809	HSPD1	18	18	61.054	7.5	2.906852	4.56E+08	7.477	4.41E+07	4.12E+08	6.75E-03
A8MV58	DBN1	5	5	76.299	6.811	2.767803	1.26E+08	1.654	1.18E+07	1.14E+08	1.06E-02
P10599	TXN	3	3	11.737	6.632	2.729444	1.04E+10	884.2	2.37E+08	1.01E+10	1.20E-02
P50454	SERPINH1	8	8	46.44	6.05	2.597007	2.13E+08	4.576	2.86E+07	1.84E+08	1.80E-02
H0YGP4	CPS1	4	4	165.93	5.558	2.474514	6.25E+07	0.377	2.53E+07	3.72E+07	2.58E-02
Q9H0C2	SLC25A31	1	1	35.021	5.068	2.341303	3.35E+07	0.957	4.52E+06	2.90E+07	3.75E-02
P25705	ATP5A1	3	3	59.75	4.893	2.290601	2.55E+07	0.426	4.32E+06	2.11E+07	4.29E-02
Q9BUQ0	PTBP1	10	10	59.632	4.384	2.132314	2.39E+08	4.008	4.53E+07	1.94E+08	6.45E-02
P11021	HSPA5	10	9	72.332	4.288	2.10017	1.94E+08	2.677	3.74E+07	1.56E+08	6.98E-02
O43707	ACTN4	8	8	104.85	4.115	2.040822	1.18E+08	1.127	2.07E+07	9.74E+07	8.06E-02
A6NG51	SPTAN1	23	23	284.94	4.104	2.036925	2.17E+08	0.761	4.14E+07	1.75E+08	8.14E-02
P21333	FLNA	52	49	280.74	3.974	1.990737	1.27E+09	4.507	2.36E+08	1.03E+09	9.08E-02
P13010	XRCC5	3	3	82.704	3.966	1.98783	3.79E+07	0.458	6.55E+06	3.13E+07	9.14E-02
Q00839	HNRNPU	9	9	90.583	3.844	1.942683	1.89E+08	2.081	3.97E+07	1.49E+08	1.01E-01
Q15149	PLEC	219	5	531.78	3.777	1.917279	1.12E+10	21.01	2.18E+09	8.99E+09	1.07E-01
Q05682	CALD1	3	3	93.23	3.749	1.906313	2.33E+07	0.25	3.53E+06	1.98E+07	1.10E-01
Q15149		215	1	516.19	3.702	1.888227	4.94E+07	0.096	9.75E+06	3.97E+07	1.15E-01
G8JLB6	HNRNPH1	6	4	51.229	3.664	1.873538	1.83E+08	3.582	4.11E+07	1.42E+08	1.18E-01
P38646	HSPA9	7	7	73.68	3.623	1.857145	9.23E+07	1.253	1.89E+07	7.35E+07	1.23E-01
P68431	HIST1H3A	4	4	15.404	3.538	1.823056	4.79E+08	31.12	1.25E+08	3.55E+08	1.32E-01
P49411	TUFM	3	3	49.541	3.394	1.763029	3.87E+07	0.781	7.56E+06	3.11E+07	1.50E-01
Q01082	SPTBN1	10	10	274.61	3.368	1.751806	5.04E+07	0.184	9.79E+06	4.06E+07	1.54E-01
G5E9M5	ILF3	2	2	95.807	3.248	1.699685	2.34E+07	0.245	4.77E+06	1.87E+07	1.71E-01
P12956	XRCC6	3	3	69.842	3.149	1.654665	3.06E+07	0.439	6.38E+06	2.43E+07	1.87E-01
P17844	DDX5	2	2	69.147	3.124	1.643487	6.04E+07	0.874	1.48E+07	4.56E+07	1.92E-01
P35520	CBS	2	2	61.862	3.059	1.61306	7.72E+06	0.125	1.03E+06	6.68E+06	2.03E-01
P58107	EPPK1	41	19	555.61	2.874	1.52311	7.44E+08	1.339	1.87E+08	5.57E+08	2.41E-01

Table A11. Hela^{GFP} Cytoplasmic Interactome data set. Data above threshold >log median Ratio H:L 1.50 shown.

HeLa^GFP Nucleoplasmic (NP)/ Stable cell line

Light: HeLa Heavy: HeLa^GFP

MaxQuant Version: 1.2.7.4

Median log Ratio H/L = -0.31

Threshold (> 1 log median) =0.69

Uniprot ID	Gene Name	Peptides	Unique Peptides	Mol. weight [kDa]	Ratio H/L	Log Ratio H/L	Intensity	NINT	Intensity L	Intensity H	Ratio H/L Significance B
Q9U6Y5	GFP	15	15	28.106	10.3	3.36387	8.77E+09	312	1.01E+08	8.67E+09	2.72E-11
P09211	GSTP1	3	3	23.356	4.857	2.28015	8.79E+07	3.765	1.21E+07	7.58E+07	2.59E-06
P31040	SDHA	1	1	72.691	3.379	1.7566	2.11E+07	0.29	4.43E+06	1.66E+07	1.74E-04
O43175	PHGDH	2	2	56.65	2.486	1.31388	8.83E+06	0.156	3.14E+06	5.70E+06	3.15E-03
P31689	DNAJA1	3	3	44.868	2.345	1.22934	1.38E+08	3.073	4.61E+07	9.18E+07	5.11E-03
Q12800	TFCP2	2	2	57.255	2.282	1.19043	2.67E+07	0.467	8.47E+06	1.83E+07	6.34E-03
P68371	TUBB4B	15	3	49.83	2.183	1.12618	7.66E+07	1.537	2.40E+07	5.26E+07	8.96E-03
Q14151	SAFB2	2	2	107.47	2.03	1.02148	4.93E+07	0.458	1.85E+07	3.07E+07	1.53E-02
P78406	RAE1	4	4	40.968	1.981	0.98586	7.58E+07	1.85	2.29E+07	5.29E+07	1.83E-02
Q16527	CSRP2	5	5	20.954	1.757	0.81344	4.67E+08	22.3	1.59E+08	3.08E+08	4.06E-02
Q32Q12	NME1-NME2	2	2	32.642	1.665	0.73587	1.59E+08	4.871	4.83E+07	1.11E+08	5.64E-02
F8VQ10	DDX39B	4	4	50.745	1.664	0.73483	5.95E+07	1.172	2.23E+07	3.72E+07	5.67E-02
B5MC40	GATAD2A	2	2	70.349	1.641	0.71484	1.84E+07	0.262	7.15E+06	1.13E+07	6.15E-02

Table A12. Hela^{GFP} Nucleoplasmic Interactome data set. Data above threshold >log median Ratio H:L 0.69 shown.

HeLa^PP1alpha Cytoplasmic (CP)/ Stable cell line

Light: HeLa Heavy: HeLa^GFP-PP1α

MaxQuant Version: 1.2.7.4

Median log Ratio H/L = 0.257

Threshold (> 1 log median) =1.257

Uniprot ID	Gene Name	Peptides	Unique Peptides	Mol. weight [kDa]	Ratio H/L	Log Ratio H/L	Intensity	NINT	Intensity L	Intensity H	Ratio H/L Significance B
Q8NHQ8	RASSF8	20	20	48.326	36.88	5.20477	7.57E+07	1.57	1.06E+06	7.46E+07	1.27E-04
Q6UXN9	WDR82	6	6	35.079	26.69	4.73801	9.67E+06	0.28	1.91E+05	9.48E+06	5.14E-04
G8JLJ4	PPP1R18	24	24	68.041	26.05	4.70305	1.66E+08	2.44	2.06E+06	1.64E+08	5.68E-04
Q02833-2	RASSF7	12	12	36.343	25.99	4.69983	2.03E+07	0.56	5.10E+05	1.98E+07	5.73E-04
Q9U6Y5	GFP	17	17	28.106	21.19	4.40504	1.17E+09	41.8	8.23E+06	1.17E+09	1.29E-03
P41236	PPP1R2	12	2	23.015	20.5	4.35769	3.06E+07	1.33	3.10E+05	3.03E+07	1.47E-03
Q13625	TP53BP2	38	37	125.61	20.43	4.35233	2.48E+08	1.98	5.12E+06	2.43E+08	1.49E-03
Q8WUF5	PPP1R13L	33	33	89.09	19.37	4.27598	4.44E+08	4.98	4.63E+06	4.39E+08	1.82E-03
Q96KQ4	PPP1R13B	29	28	119.56	18.91	4.24123	5.52E+07	0.46	1.85E+06	5.34E+07	1.99E-03
P62136	PPP1CA	34	12	37.512	18.16	4.18293	2.75E+09	73.3	3.11E+07	2.72E+09	2.32E-03
Q9GZN8	C20orf27	6	6	21.645	17.53	4.13134	5.01E+06	0.23	1.03E+05	4.90E+06	2.64E-03
Q15435	PPP1R7	25	25	41.564	17.24	4.10769	4.69E+08	11.3	3.67E+07	4.32E+08	2.80E-03
Q15834	CCDC85B	5	5	22.091	16.06	4.00531	8.06E+05	0.04	2.91E+04	7.77E+05	3.62E-03
Q12972	PPP1R8	17	17	38.478	16.02	4.00216	5.09E+07	1.32	9.55E+05	5.00E+07	3.65E-03
Q96QC0	PPP1R10	15	15	99.057	15.34	3.93894	2.78E+07	0.28	9.85E+05	2.68E+07	4.25E-03
Q9UBK9	UXT	3	3	18.246	15.23	3.92894	1.20E+06	0.07	3.48E+04	1.17E+06	4.36E-03
Q96MX6	WDR92	8	8	39.74	14.94	3.90092	4.58E+06	0.12	1.64E+05	4.42E+06	4.66E-03
Q96SB3	PPP1R9B	39	37	89.191	14.91	3.89811	1.91E+08	2.14	8.36E+06	1.82E+08	4.70E-03
O94842	TOX4	6	6	66.194	14.23	3.83076	9.05E+06	0.14	2.99E+05	8.76E+06	5.51E-03
P00966	ASS1	15	15	46.53	13.73	3.77926	8.41E+07	1.81	5.33E+06	7.87E+07	6.22E-03
Q4KMQ1	TPRN	27	27	75.555	13.31	3.73455	1.28E+08	1.69	5.55E+06	1.22E+08	6.90E-03
P19388	POLR2E	3	3	24.551	11.72	3.55053	7.71E+05	0.03	5.67E+04	7.14E+05	1.05E-02
P49750	YLPM1	59	59	241.64	11.47	3.51979	7.25E+07	0.3	5.30E+06	6.72E+07	1.12E-02
P38646	HSPA9	17	17	73.68	11.18	3.48336	2.93E+07	0.4	2.08E+06	2.73E+07	1.21E-02
E9PDX1	PPP1R9A	25	23	154.05	10.49	3.39094	2.10E+07	0.14	1.03E+06	2.00E+07	1.48E-02
F5H5T0	PARD3	31	0	149.69	10.42	3.3817	2.98E+07	0.2	1.22E+06	2.86E+07	1.51E-02
P49411	TUFM	11	11	49.541	9.164	3.19598	9.49E+06	0.19	8.72E+05	8.62E+06	2.22E-02
Q96AB3	ISOC2	3	3	24.097	9.047	3.1775	1.03E+06	0.04	9.50E+04	9.39E+05	2.30E-02
Q8N1F0	PPP3CB	1	1	59.123	9.004	3.17053	1.87E+06	0.03	9.89E+04	1.77E+06	2.34E-02
O95229	ZWINT	3	3	31.293	8.844	3.14473	3.17E+05	0.01	2.79E+04	2.89E+05	2.46E-02
F5GWA6	MYPN	13	13	145.32	8.42	3.07373	4.88E+06	0.03	2.85E+05	4.60E+06	2.83E-02
O75901	RASSF9	8	8	50.02	8.302	3.05344	1.46E+07	0.29	7.24E+05	1.39E+07	2.94E-02
E9PCR8	ERBB2IP	36	1	159.02	7.897	2.98136	3.63E+07	0.23	2.19E+06	3.41E+07	3.38E-02
Q14160	SCRIB	13	11	177.69	7.502	2.90735	1.25E+07	0.07	1.43E+06	1.11E+07	3.89E-02
Q9BTT6	LRRC1	5	3	59.241	7.377	2.88311	1.47E+06	0.02	1.32E+05	1.34E+06	4.07E-02
Q9H792	PEAK1	34	34	193.1	7.023	2.81203	2.36E+07	0.12	1.38E+06	2.22E+07	4.64E-02
O75864	PPP1R37	12	12	74.766	6.736	2.75196	7.57E+06	0.1	4.78E+05	7.09E+06	5.17E-02
Q8NG31	CASC5	9	9	265.39	6.682	2.74028	6.31E+05	0	3.53E+04	5.96E+05	5.28E-02
Q96IY1	NSL1	2	2	32.162	6.286	2.65205	3.88E+05	0.01	3.66E+04	3.51E+05	6.16E-02
Q9H6T3	RPAP3	10	10	75.718	6.282	2.65125	5.33E+06	0.07	5.84E+05	4.74E+06	6.17E-02
Q9NWS0	PIH1D1	5	5	32.363	6.15	2.62056	1.76E+06	0.05	1.20E+05	1.64E+06	6.51E-02
Q6PJW8	CNST	7	7	79.596	6.019	2.58962	3.37E+06	0.04	1.73E+05	3.20E+06	6.86E-02
P10809	HSPD1	31	31	61.054	6.012	2.58773	1.12E+08	1.83	1.70E+07	9.48E+07	6.89E-02
A6NKD9	CCDC85C	8	8	45.209	5.954	2.57391	4.62E+06	0.1	5.72E+05	4.05E+06	7.05E-02
P05141	SLC25A5	6	3	32.852	5.918	2.56516	7.11E+06	0.22	9.49E+05	6.16E+06	7.15E-02
O15212	PFDN6	2	2	14.582	5.672	2.50373	4.32E+05	0.03	6.98E+04	3.62E+05	7.93E-02
P32119	PRDX2	9	8	21.892	5.4	2.43285	1.17E+07	0.53	1.83E+06	9.82E+06	8.91E-02
P36542	ATP5C1	2	2	32.996	5.317	2.41059	3.53E+05	0.01	6.67E+04	2.86E+05	9.24E-02
Q9NRW3	APOBEC3C	2	2	22.826	5.299	2.40561	2.90E+05	0.01	3.94E+04	2.50E+05	9.31E-02
Q5SWA1	PPP1R15B	8	8	79.151	5.205	2.37998	3.09E+06	0.04	1.80E+05	2.91E+06	9.70E-02
P45880	VDAC2	2	2	33.371	5.01	2.3249	8.25E+05	0.02	1.32E+05	6.93E+05	1.06E-01
Q9Y230	RUVBL2	7	7	51.156	4.978	2.31557	4.29E+06	0.08	9.00E+05	3.39E+06	1.07E-01
P22695	UQCRC2	2	2	48.442	4.936	2.3034	1.11E+06	0.02	2.19E+05	8.90E+05	1.09E-01
Q9P2K8	EIF2AK4	13	13	186.91	4.71	2.2357	2.88E+06	0.02	4.03E+05	2.47E+06	1.21E-01
P61981	YWHAG	4	2	28.302	4.577	2.19437	1.12E+06	0.04	1.60E+05	9.62E+05	1.29E-01
P14625	HSP90B1	6	4	92.468	4.525	2.17805	1.92E+06	0.02	2.82E+05	1.64E+06	1.33E-01

Continuation …

Uniprot ID	Gene Name	Peptides	Unique Peptides	Mol. weight [kDa]	Ratio H/L	Log Ratio H/L	Intensity	NINT	Intensity L	Intensity H	Ratio H/L Significance B
P30048	PRDX3	4	4	27.692	4.434	2.14854	2.45E+06	0.09	4.33E+05	2.01E+06	1.38E-01
O94763	URI1	8	8	59.832	4.427	2.14639	6.04E+06	0.1	9.25E+05	5.11E+06	1.39E-01
F8WAR4	CHCHD3	3	3	27.735	4.418	2.14346	1.12E+05	0	2.19E+04	9.04E+04	1.40E-01
H0YGP4	CPS1	9	9	165.93	4.318	2.11036	4.11E+06	0.02	6.00E+05	3.51E+06	1.46E-01
Q6P1K2	PMF1	2	2	22.946	4.306	2.10638	1.46E+05	0.01	2.24E+04	1.23E+05	1.47E-01
Q9UHV9	PFDN2	4	4	16.648	4.218	2.07666	2.13E+06	0.13	4.29E+05	1.70E+06	1.54E-01
P25705	ATP5A1	9	9	59.75	4.203	2.07149	7.28E+06	0.12	1.45E+06	5.83E+06	1.55E-01
P06748	NPM1	5	5	32.575	4.174	2.06157	2.37E+06	0.07	4.31E+05	1.93E+06	1.57E-01
Q00839	HNRNPU	21	21	90.583	3.981	1.99324	3.02E+07	0.33	5.79E+06	2.44E+07	1.73E-01
P31930	UQCRC1	7	7	52.645	3.943	1.97918	1.01E+07	0.19	2.10E+06	7.97E+06	1.77E-01
E7EX29	YWHAZ	8	5	28.036	3.729	1.89863	2.25E+06	0.08	4.53E+05	1.80E+06	1.97E-01
Q9NS69	TOMM22	1	1	15.521	3.702	1.8883	2.07E+05	0.01	3.59E+04	1.71E+05	2.00E-01
Q96S65	CSRNP1	2	2	63.508	3.629	1.85969	6.58E+05	0.01	7.81E+04	5.80E+05	2.08E-01
O00148	DDX39A	2	2	49.129	3.616	1.85455	1.02E+06	0.02	2.06E+05	8.13E+05	2.09E-01
Q9Y265	RUVBL1	6	6	50.227	3.549	1.82745	1.06E+07	0.21	5.25E+06	5.34E+06	2.17E-01
Q16763	UBE2S	3	3	23.845	3.429	1.77775	2.49E+05	0.01	5.44E+04	1.94E+05	2.32E-01
Q9Y2T3	GDA	12	12	52.837	3.387	1.76001	1.84E+07	0.35	3.82E+06	1.46E+07	2.37E-01
Q07021	C1QBP	2	2	31.362	3.331	1.73604	3.67E+05	0.01	6.53E+04	3.02E+05	2.44E-01
P35232	PHB	4	4	29.804	3.327	1.73414	1.80E+05	0.01	3.08E+04	1.50E+05	2.45E-01
P62258	YWHAE	9	7	29.174	3.308	1.72578	3.34E+06	0.11	6.91E+05	2.65E+06	2.48E-01
P60468	SEC61B	2	2	9.9743	3.25	1.70026	2.37E+05	0.02	5.31E+04	1.83E+05	2.56E-01
Q99714	HSD17B10	8	8	26.923	3.226	1.68988	1.90E+06	0.07	4.27E+05	1.47E+06	2.59E-01
Q9BUQ0	PTBP1	10	10	59.632	3.04	1.60407	1.34E+07	0.23	3.01E+06	1.04E+07	2.88E-01
E7EWS7	UBE2L3	3	3	24.003	3.014	1.59163	3.24E+05	0.01	8.29E+04	2.41E+05	2.92E-01
Q00534	CDK6	2	2	36.938	3.013	1.59125	4.50E+05	0.01	1.05E+05	3.44E+05	2.92E-01
P61081	UBE2M	3	3	20.9	2.989	1.57976	4.13E+05	0.02	7.69E+04	3.36E+05	2.96E-01
Q92769	HDAC2	2	2	55.364	2.989	1.57947	1.13E+06	0.02	2.33E+05	8.93E+05	2.97E-01
Q13501	SQSTM1	5	5	47.687	2.956	1.5636	5.67E+06	0.12	1.42E+06	4.25E+06	3.02E-01
P43246	MSH2	2	2	104.74	2.86	1.51602	3.82E+05	0	9.39E+04	2.88E+05	3.20E-01
P41091	EIF2S3	4	4	51.109	2.844	1.50802	3.67E+06	0.07	9.79E+05	2.69E+06	3.23E-01
Q16527	CSRP2	9	9	20.954	2.791	1.48063	8.88E+06	0.42	2.25E+06	6.63E+06	3.33E-01
P35579	MYH9	73	66	226.53	2.713	1.44	4.35E+07	0.19	1.37E+07	2.98E+07	3.49E-01
Q5T440	IBA57	2	2	38.155	2.698	1.43173	1.49E+05	0	3.83E+04	1.10E+05	3.52E-01
P19338	NCL	8	8	76.613	2.67	1.41679	8.64E+06	0.11	2.20E+06	6.44E+06	3.58E-01
O95340	PAPSS2	4	4	69.97	2.66	1.41159	1.40E+06	0.02	3.40E+05	1.06E+06	3.60E-01
Q06830	PRDX1	21	18	22.11	2.626	1.39265	1.50E+08	6.8	4.06E+07	1.10E+08	3.68E-01
P68032	ACTC1	14	1	42.019	2.548	1.3492	1.38E+07	0.33	3.30E+06	1.05E+07	3.86E-01
P53611	RABGGTB	3	3	36.924	2.543	1.34625	8.24E+05	0.02	2.34E+05	5.90E+05	3.87E-01
P09211	GSTP1	4	4	23.356	2.512	1.32866	1.74E+06	0.07	4.90E+05	1.25E+06	3.95E-01
P11142	HSPA8	35	29	70.897	2.509	1.32723	1.74E+08	2.45	4.76E+07	1.26E+08	3.95E-01
Q9Y6C9	MTCH2	5	5	33.331	2.488	1.31504	1.63E+06	0.05	4.45E+05	1.19E+06	4.01E-01
P23396	RPS3	3	3	26.688	2.436	1.28469	6.95E+05	0.03	1.98E+05	4.97E+05	4.14E-01
Q9NVI7	ATAD3A	3	3	71.368	2.411	1.26951	2.60E+06	0.04	1.75E+06	8.56E+05	4.21E-01

Table A13. Hela$^{GFP\text{-}PP1}\alpha$ Cytoplasmic Interactome data set. Data above threshold >log median Ratio H:L 1.257 shown.

HeLa^PP1alpha Nucleoplasmic (NP)/ Stable cell line

Light: HeLa Heavy: HeLa^GFP-PP1α

MaxQuant Version: 1.2.7.4

Median log Ratio H/L = -0.28

Threshold (> 1 log median) =0.72

Uniprot ID	Gene Name	Peptides	Unique Peptides	Mol. weight [kDa]	Ratio H/L	Log Ratio H/L	Intensity	NINT	Intensity L	Intensity H	Ratio H/L Significance B
Q6UXN9	WDR82	13	13	35.079	19.55	4.28902	4.22E+07	1.203	1.58E+06	4.06E+07	2.93E-05
G8JLJ4	PPP1R18	16	16	68.041	18.88	4.23871	4.93E+07	0.725	2.51E+06	4.68E+07	3.57E-05
Q9U6Y5	GFP	9	9	28.106	16.63	4.05589	2.67E+08	9.488	3.88E+06	2.63E+08	7.15E-05
Q12972	PPP1R8	16	16	38.478	16.2	4.01828	3.67E+07	0.953	9.56E+05	3.57E+07	8.22E-05
P49750-4	YLPM1	72	72	241.64	15.32	3.93716	1.53E+08	0.633	9.27E+06	1.44E+08	1.11E-04
Q96QC0	PPP1R10	29	29	99.057	13.95	3.80219	9.11E+07	0.92	2.38E+06	8.87E+07	1.80E-04
P41236	PPP1R2	5	5	23.015	13.84	3.79025	2.33E+06	0.101	5.15E+04	2.28E+06	1.33E-06
O94842	TOX4	8	8	66.194	10.04	3.3274	8.65E+06	0.131	6.13E+05	8.03E+06	8.91E-04
Q96SB3	PPP1R9B	24	22	89.191	9.693	3.277	5.67E+07	0.636	4.96E+06	5.17E+07	1.04E-03
Q4KMQ1	TPRN	16	16	75.555	8.163	3.02901	2.82E+07	0.373	4.31E+06	2.39E+07	2.23E-03
P62136	PPP1CA	24	7	37.512	8.138	3.02471	4.51E+08	12.03	2.78E+07	4.23E+08	2.26E-03
Q8WUF5	PPP1R13L	6	6	89.09	7.902	2.98222	2.38E+06	0.027	3.84E+05	1.99E+06	1.12E-04
E9PDX1	PPP1R9A	4	2	154.05	7.561	2.91858	1.16E+06	0.008	1.60E+05	1.00E+06	1.53E-04
Q05639	EEF1A2	11	2	50.47	7.219	2.8517	6.85E+06	0.136	1.15E+06	5.71E+06	3.74E-03
Q13625	TP53BP2	8	8	125.61	6.839	2.77374	5.22E+06	0.042	5.82E+05	4.64E+06	4.65E-03
P00966	ASS1	2	2	46.53	6.441	2.68724	3.57E+06	0.077	3.46E+05	3.22E+06	4.51E-04
Q5UIP0	RIF1	24	24	274.46	4.318	2.11046	9.99E+06	0.036	1.59E+06	8.40E+06	2.51E-02
P48643	CCT5	10	10	59.67	4.193	2.06802	1.84E+07	0.309	3.12E+06	1.53E+07	2.76E-02
Q69YH5	CDCA2	3	3	112.68	3.755	1.90889	2.07E+06	0.018	3.49E+05	1.72E+06	1.01E-02
Q12800	TFCP2	4	4	57.255	3.438	1.78165	8.51E+06	0.149	1.61E+06	6.90E+06	5.15E-02
P42166	TMPO	24	14	75.491	3.121	1.64205	1.03E+08	1.37	3.38E+07	6.96E+07	6.83E-02
Q96T88	UHRF1	14	14	89.813	2.802	1.48651	1.63E+07	0.182	4.26E+06	1.21E+07	9.20E-02
P09211	GSTP1	10	10	23.356	2.698	1.43168	5.32E+07	2.279	1.42E+07	3.90E+07	1.02E-01
Q99832	CCT7	2	2	59.366	2.581	1.36771	1.68E+06	0.028	4.99E+05	1.18E+06	5.46E-02
E7ENU4	ADAR	37	37	140.83	2.545	1.34778	8.40E+07	0.597	2.41E+07	6.00E+07	1.18E-01
P30740	SERPINB1	7	7	42.741	2.482	1.31168	3.25E+06	0.076	8.55E+05	2.39E+06	6.37E-02
O14965	AURKA	5	5	45.809	2.342	1.22743	7.78E+06	0.17	3.39E+06	4.39E+06	1.46E-01
Q15181	PPA1	3	3	32.66	2.325	1.21698	1.95E+06	0.06	9.46E+05	1.01E+06	8.18E-02
Q13242	SRSF9	3	2	25.542	2.318	1.21288	1.14E+06	0.045	2.80E+05	8.62E+05	8.27E-02
Q3ZCM7	TUBB8	9	1	49.775	2.271	1.18358	1.37E+07	0.276	2.52E+06	1.12E+07	1.57E-01
O43175	PHGDH	5	5	56.65	2.27	1.18288	4.65E+06	0.082	1.41E+06	3.24E+06	8.92E-02
G5E9Q6	PFN2	5	1	20.787	2.234	1.15963	1.68E+07	0.806	5.20E+06	1.16E+07	1.63E-01
P52298	NCBP2	2	2	18.001	2.226	1.15465	1.56E+06	0.087	4.24E+05	1.14E+06	9.58E-02
P04080	CSTB	5	5	11.139	2.214	1.14679	2.41E+07	2.166	7.09E+06	1.70E+07	1.67E-01
O75607	NPM3	2	2	19.343	2.198	1.13626	1.50E+07	0.777	4.50E+06	1.05E+07	1.70E-01
Q9BQ75	C3orf26	4	4	31.884	2.162	1.11243	7.84E+05	0.025	2.46E+05	5.37E+05	1.06E-01
P23921	RRM1	5	5	90.069	2.155	1.10749	4.72E+06	0.052	1.42E+06	3.30E+06	1.08E-01
P10599	TXN	6	6	11.737	2.149	1.10387	8.52E+07	7.256	2.65E+07	5.86E+07	1.79E-01
Q9BTC0	DIDO1	6	6	243.87	2.138	1.09613	5.19E+05	0.002	1.60E+05	3.59E+05	1.11E-01
H0YGP4	CPS1	27	27	165.93	2.131	1.09173	3.67E+07	0.221	1.06E+07	2.62E+07	1.82E-01
P50991	CCT4	2	2	57.924	2.127	1.08875	3.39E+06	0.059	1.04E+06	2.35E+06	1.13E-01
Q99590	SCAF11	2	2	164.65	2.099	1.06998	1.21E+06	0.007	4.40E+05	7.72E+05	1.18E-01
P68371	TUBB4B	23	1	49.83	2.082	1.05804	2.46E+08	4.942	7.52E+07	1.71E+08	1.92E-01
P84103	SRSF3	10	9	19.329	2.074	1.05221	1.49E+08	7.69	4.49E+07	1.04E+08	1.94E-01
P78371	CCT2	2	2	57.488	2.035	1.02503	2.35E+06	0.041	7.99E+05	1.55E+06	1.31E-01
F5H2F4	MTHFD1	15	14	110.61	2.034	1.02439	2.04E+07	0.185	6.48E+06	1.39E+07	2.03E-01
P23246	SFPQ	8	7	76.149	2.033	1.02347	9.31E+06	0.122	2.99E+06	6.31E+06	2.03E-01
P35659	DEK	9	9	42.674	2.027	1.01956	1.01E+07	0.237	3.23E+06	6.86E+06	2.04E-01
P14866	HNRNPL	13	13	64.132	2.021	1.01521	7.82E+07	1.219	2.57E+07	5.25E+07	2.06E-01
Q99661	KIF2C	4	4	81.312	2.016	1.0115	3.34E+06	0.041	1.07E+06	2.27E+06	1.35E-01
P52597	HNRNPF	12	10	45.671	2.015	1.01071	6.51E+07	1.425	1.96E+07	4.54E+07	2.07E-01
Q96J01	THOC3	2	2	38.771	2.007	1.00468	1.36E+06	0.035	4.41E+05	9.20E+05	1.38E-01
Q8IYL3	C1orf174	2	2	25.977	2	1.00014	5.52E+05	0.021	1.80E+05	3.72E+05	1.39E-01
P26358	DNMT1	4	4	184.82	1.996	0.99711	1.93E+06	0.01	7.54E+05	1.17E+06	1.40E-01
Q9NRG9	AAAS	7	7	59.573	1.969	0.97768	1.47E+07	0.247	4.77E+06	9.94E+06	2.18E-01
O00148	DDX39A	14	14	49.129	1.954	0.96614	9.55E+07	1.943	3.13E+07	6.41E+07	2.22E-01

Continuation …

Uniprot ID	Gene Name	Peptides	Unique Peptides	Mol. weight [kDa]	Ratio H/L	Log Ratio H/L	Intensity	NINT	Intensity L	Intensity H	Ratio H/L Significance B
Q16763	UBE2S	2	2	23.845	1.945	0.96007	3.61E+06	0.151	2.75E+06	8.54E+05	1.52E-01
Q96EP5	DAZAP1	3	3	43.383	1.934	0.95129	1.25E+07	0.287	4.12E+06	8.33E+06	2.27E-01
Q01664	TFAP4	3	3	38.725	1.923	0.94313	6.85E+05	0.018	2.06E+05	4.79E+05	1.58E-01
Q16576	RBBP7	9	4	47.82	1.919	0.93998	1.25E+07	0.262	3.97E+06	8.56E+06	2.31E-01
P36873	PPP1CC	19	2	38.518	1.91	0.93365	2.26E+06	0.059	8.09E+05	1.45E+06	1.62E-01
O94906	PRPF6	4	4	106.92	1.904	0.92873	2.60E+06	0.024	1.27E+06	1.33E+06	1.63E-01
A8MXP9	MATR3	17	17	99.966	1.9	0.92608	4.26E+07	0.426	1.46E+07	2.79E+07	2.36E-01
Q96RR5	HCA90	9	9	89.392	1.89	0.91808	5.79E+06	0.065	1.97E+06	3.83E+06	2.38E-01
P52789	HK2	5	5	102.38	1.869	0.90219	2.73E+06	0.027	1.06E+06	1.66E+06	1.73E-01
Q6P2Q9	PRPF8	11	11	273.6	1.863	0.89794	7.50E+05	0.003	2.60E+05	4.90E+05	1.75E-01
P17844	DDX5	41	32	69.147	1.857	0.89297	3.74E+08	5.406	1.31E+08	2.43E+08	2.47E-01
Q14151	SAFB2	10	6	107.47	1.856	0.89196	1.39E+07	0.13	4.55E+06	9.37E+06	2.48E-01
Q14807	KIF22	4	4	73.261	1.852	0.88877	3.38E+06	0.046	1.23E+06	2.14E+06	1.78E-01
Q9BV86	METTL11A	2	2	25.387	1.851	0.88838	1.62E+06	0.064	4.95E+05	1.12E+06	1.79E-01
P06748	NPM1	16	16	32.575	1.851	0.88792	4.55E+07	1.396	1.53E+07	3.02E+07	2.49E-01
Q15424	SAFB	6	2	102.64	1.849	0.88667	1.56E+06	0.015	5.27E+05	1.04E+06	1.79E-01
P60891	PRPS1	3	3	34.834	1.847	0.88487	1.77E+06	0.051	6.79E+05	1.09E+06	1.80E-01
Q7RTV0	PHF5A	2	2	12.405	1.826	0.86884	2.32E+06	0.187	8.13E+05	1.51E+06	1.86E-01
Q59F66	DDX17	33	24	81.067	1.823	0.86663	1.12E+08	1.378	3.84E+07	7.33E+07	2.57E-01
Q15365	PCBP1	13	10	37.497	1.823	0.86624	1.15E+08	3.062	3.87E+07	7.61E+07	2.57E-01
Q15029	EFTUD2	10	9	109.43	1.82	0.8641	6.74E+06	0.062	2.27E+06	4.47E+06	2.58E-01
Q5JVF3	PCID2	2	2	52.099	1.816	0.86037	1.34E+05	0.003	4.32E+04	9.09E+04	1.90E-01
P78549	NTHL1	2	2	34.389	1.814	0.85878	1.07E+06	0.031	3.85E+05	6.84E+05	1.90E-01
Q9HAV4	XPO5	2	2	136.31	1.804	0.85112	3.38E+05	0.002	1.21E+05	2.17E+05	1.93E-01
P78406	RAE1	10	10	40.968	1.798	0.84655	6.79E+06	0.166	2.32E+06	4.48E+06	2.65E-01
Q14192	FHL2	4	4	32.193	1.786	0.83689	1.97E+06	0.061	7.06E+05	1.26E+06	1.99E-01
O43809	NUDT21	2	2	26.227	1.785	0.83617	1.66E+06	0.063	5.43E+05	1.12E+06	2.00E-01
P18846	ATF1	2	2	29.232	1.774	0.8266	9.31E+05	0.032	2.85E+05	6.46E+05	2.04E-01
Q96AB3	ISOC2	8	8	24.097	1.773	0.82611	7.44E+07	3.09	2.51E+07	4.93E+07	2.73E-01
P62316	SNRPD2	4	4	13.527	1.749	0.80628	3.28E+06	0.243	1.21E+06	2.07E+06	2.13E-01
P14635	CCNB1	2	2	48.337	1.748	0.80546	2.29E+06	0.047	7.18E+05	1.57E+06	2.13E-01
Q15717	ELAVL1	16	16	36.091	1.747	0.80513	4.02E+07	1.114	1.45E+07	2.57E+07	2.81E-01
Q9BW27	NUP85	2	2	75.019	1.746	0.8043	1.02E+06	0.014	3.82E+05	6.43E+05	2.13E-01
Q9H3K6	BOLA2	5	5	10.116	1.743	0.80124	1.88E+07	1.862	6.50E+06	1.23E+07	2.82E-01
Q9NQG5	RPRD1B	3	2	36.899	1.729	0.79002	9.56E+05	0.026	2.89E+05	6.67E+05	2.20E-01
P62304	SNRPE	5	5	10.803	1.711	0.77442	1.69E+07	1.561	5.69E+06	1.12E+07	2.93E-01
P07437	TUBB	23	5	49.67	1.707	0.77146	7.18E+07	1.447	2.51E+07	4.68E+07	2.94E-01
P00492	HPRT1	3	3	24.579	1.706	0.7707	7.47E+06	0.304	2.76E+06	4.72E+06	2.95E-01
E7EPP6	CHEK1	2	2	55.517	1.703	0.76799	9.60E+05	0.017	3.65E+05	5.95E+05	2.30E-01
O95983	MBD3	2	2	32.844	1.703	0.76774	4.60E+05	0.014	1.85E+05	2.75E+05	2.30E-01
P62306	SNRPF	3	3	9.7251	1.701	0.76613	6.64E+06	0.683	2.50E+06	4.15E+06	2.97E-01
Q12834	CDC20	3	3	54.722	1.681	0.74966	1.69E+06	0.031	5.77E+05	1.11E+06	2.39E-01
Q92945	KHSRP	23	20	73.114	1.681	0.74949	7.16E+07	0.98	2.68E+07	4.48E+07	3.03E-01
P62314	SNRPD1	2	2	13.281	1.667	0.73699	1.14E+07	0.856	4.07E+06	7.30E+06	3.09E-01
Q5VT52	RPRD2	3	3	156.02	1.666	0.73639	1.30E+06	0.008	4.63E+05	8.41E+05	2.45E-01
P29372	MPG	7	7	32.868	1.663	0.73361	5.34E+06	0.162	2.12E+06	3.22E+06	3.10E-01
P48507	GCLM	2	2	30.727	1.66	0.73118	1.08E+06	0.035	3.91E+05	6.91E+05	2.48E-01
P52272	HNRNPM	34	34	77.515	1.656	0.7277	5.97E+07	0.77	2.16E+07	3.81E+07	3.13E-01
P51948	MNAT1	2	2	35.823	1.655	0.72683	4.81E+05	0.013	1.56E+05	3.25E+05	2.50E-01
Q9UBD5	ORC3	2	2	82.324	1.654	0.72561	9.69E+05	0.012	4.06E+05	5.62E+05	2.50E-01
Q01081	U2AF2	6	6	53.5	1.653	0.72509	1.74E+07	0.325	6.28E+06	1.11E+07	2.51E-01
P26368	U2AF1	6	6	27.872	1.653	0.72509	4.79E+06	0.172	1.67E+06	3.12E+06	3.14E-01
O75643	SNRNP200	9	9	244.5	1.651	0.72351	9.76E+05	0.004	3.54E+05	6.22E+05	2.51E-01

Table A14. Hela$^{GFP\text{-}PP1}\alpha$ Nucleoplasmic Interactome data set. Data above threshold >log median Ratio H:L 0.72 shown.

HeLa^PP1alpha Concatenated/ Stable cell line

Light: HeLa Heavy: HeLa^GFP-PP1α

MaxQuant Version: 1.2.7.4

Median log Ratio H/L = -0.164

Threshold (> 1 log median) = 0.836

Uniprot ID	Gene Name	Peptides	Unique Peptides	Mol. weight [kDa]	Ratio H/L	Log Ratio H/L	Intensity	NINT	Intensity L	Intensity H
Q8NHQ8	RASSF8	21	21	48.326	37.96	5.24652	8.06E+07	1.667	1.10E+06	7.95E+07
Q02833	RASSF7	12	12	36.343	25.99	4.69983	2.39E+07	0.658	5.46E+05	2.34E+07
Q6UXN9	WDR82	13	13	35.079	23.23	4.53798	5.90E+07	1.681	2.27E+06	5.67E+07
G8JLJ4	PPP1R18	28	28	68.041	23.14	4.53207	3.53E+08	5.188	4.99E+06	3.48E+08
Q96KQ4	PPP1R13B	32	31	119.56	22.73	4.50672	8.22E+07	0.688	2.16E+06	8.01E+07
Q13625	TP53BP2	45	44	125.61	21.49	4.42546	4.50E+08	3.584	6.69E+06	4.44E+08
Q9U6Y5	GFP	19	19	28.106	20.73	4.37365	1.77E+09	63.13	1.57E+07	1.76E+09
Q9UBK9	UXT	2	2	18.246	20.03	4.32373	1.09E+06	0.06	2.64E+04	1.07E+06
P41236	PPP1R2	15	3	23.015	19.7	4.30005	4.29E+07	1.863	4.66E+05	4.24E+07
Q9GZN8	C20orf27	6	6	21.645	17.53	4.13134	5.01E+06	0.231	1.03E+05	4.90E+06
Q8WUF5	PPP1R13L	37	37	89.09	17.1	4.09601	5.77E+08	6.473	6.50E+06	5.70E+08
Q15435	PPP1R7	24	24	41.564	16.77	4.06815	5.02E+08	12.08	3.68E+07	4.65E+08
Q12972	PPP1R8	19	19	38.478	16.6	4.05311	1.33E+08	3.446	2.52E+06	1.30E+08
Q15834	CCDC85B	6	6	22.091	16.06	4.00531	8.87E+05	0.04	2.91E+04	8.58E+05
Q96QC0	PPP1R10	34	34	99.057	15.34	3.93894	1.69E+08	1.703	4.80E+06	1.64E+08
Q96MX6	WDR92	8	8	39.74	14.7	3.87794	4.80E+06	0.121	1.83E+05	4.62E+06
P49750	YLPM1	82	82	241.64	14.42	3.8498	2.52E+08	1.044	1.49E+07	2.38E+08
O94842	TOX4	9	9	66.194	14.08	3.81547	2.50E+07	0.378	1.01E+06	2.40E+07
P62136	PPP1CA	34	12	37.512	13.64	3.76956	3.92E+09	104.4	6.67E+07	3.85E+09
P00966	ASS1	17	17	46.53	11.82	3.5634	9.16E+07	1.969	5.72E+06	8.59E+07
Q4KMQ1	TPRN	32	32	75.555	11.33	3.5022	2.03E+08	2.692	1.03E+07	1.93E+08
Q96SB3	PPP1R9B	41	39	89.191	11.32	3.50055	2.95E+08	3.311	1.36E+07	2.82E+08
F5H5T0	PARD3	31	0	149.69	10.42	3.3817	2.98E+07	0.199	1.22E+06	2.86E+07
E9PDX1	PPP1R9A	26	24	154.05	10.16	3.34469	2.36E+07	0.153	1.23E+06	2.23E+07
Q8N1F0	PPP3CB	1	1	59.123	9.004	3.17053	1.87E+06	0.032	9.89E+04	1.77E+06
O95229	ZWINT	3	3	31.293	8.844	3.14473	3.17E+05	0.01	2.79E+04	2.89E+05
Q05639	EEF1A2	14	2	50.47	8.552	3.09626	1.14E+07	0.225	1.40E+06	9.98E+06
F5GWA6	MYPN	15	14	145.32	8.455	3.07987	6.76E+06	0.047	3.91E+05	6.37E+06
O75901	RASSF9	8	8	50.02	8.302	3.05344	1.46E+07	0.292	7.24E+05	1.39E+07
E9PCR8	ERBB2IP	35	1	159.02	7.784	2.96053	3.72E+07	0.234	2.39E+06	3.48E+07
Q9BTT6	LRRC1	5	3	59.241	7.377	2.88311	1.47E+06	0.025	1.32E+05	1.34E+06
Q9NWS0	PIH1D1	6	6	32.363	6.862	2.77855	2.36E+06	0.073	1.73E+05	2.19E+06
Q9H792	PEAK1	40	40	193.1	6.655	2.73448	2.60E+07	0.135	1.52E+06	2.45E+07
O75864	PPP1R37	12	12	74.766	6.442	2.68744	8.23E+06	0.11	5.22E+05	7.71E+06
Q8NG31	CASC5	10	10	265.39	6.32	2.65983	7.61E+05	0.003	1.03E+05	6.58E+05
Q96IY1	NSL1	2	2	32.162	6.286	2.65205	3.88E+05	0.012	3.66E+04	3.51E+05
Q6PJW8	CNST	6	6	79.596	6.019	2.58962	3.33E+06	0.042	1.73E+05	3.16E+06
Q9H6T3	RPAP3	11	11	75.718	5.742	2.52145	6.05E+06	0.08	9.28E+05	5.12E+06
Q5SWA1	PPP1R15B	7	7	79.151	5.205	2.37998	3.09E+06	0.039	1.80E+05	2.91E+06
Q9NRW3	APOBEC3C	3	3	22.826	5.01	2.32493	1.06E+06	0.046	1.32E+05	9.27E+05
Q14160	SCRIB	16	14	177.69	4.841	2.27516	1.39E+07	0.078	2.35E+06	1.15E+07
Q9P2K8	EIF2AK4	13	13	186.91	4.71	2.2357	2.88E+06	0.015	4.03E+05	2.47E+06
O94763	URI1	8	8	59.832	4.6	2.20176	5.34E+06	0.089	7.82E+05	4.56E+06
Q5UIP0	RIF1	22	22	274.46	4.347	2.12005	1.01E+07	0.037	1.64E+06	8.51E+06
Q6P1K2	PMF1	2	2	22.946	4.306	2.10638	1.46E+05	0.006	2.24E+04	1.23E+05
A6NKD9	CCDC85C	9	9	45.209	4.26	2.09099	5.04E+06	0.111	5.94E+05	4.45E+06
Q9UHV9	PFDN2	5	5	16.648	4.199	2.06991	3.18E+06	0.191	8.89E+05	2.29E+06
Q69YH5	CDCA2	3	3	112.68	3.755	1.90889	2.07E+06	0.018	3.49E+05	1.72E+06
Q96S65	CSRNP1	2	2	63.508	3.629	1.85969	6.58E+05	0.01	7.81E+04	5.80E+05

Continuation …

Uniprot ID	Gene Name	Peptides	Unique Peptides	Mol. weight [kDa]	Ratio H/L	Log Ratio H/L	Intensity	NINT	Intensity L	Intensity H
E7EX29	YWHAZ	9	5	28.036	3.444	1.78421	3.05E+06	0.109	9.98E+05	2.05E+06
Q12800	TFCP2	4	4	57.255	3.365	1.75074	9.14E+06	0.16	1.95E+06	7.19E+06
P61981	YWHAG	6	2	28.302	3.27	1.70907	1.63E+06	0.058	4.58E+05	1.17E+06
O95340	PAPSS2	3	3	69.97	3.268	1.70858	1.17E+06	0.017	2.77E+05	8.89E+05
Q9Y2T3	GDA	12	12	52.837	3.245	1.69804	1.95E+07	0.369	4.09E+06	1.54E+07
Q9NS69	TOMM22	1	1	15.521	3.226	1.68975	1.27E+06	0.082	7.93E+05	4.76E+05
P42166	TMPO	24	14	75.491	3.112	1.6377	1.02E+08	1.351	3.35E+07	6.85E+07
Q96D46	NMD3	9	9	57.603	3.101	1.63273	1.13E+06	0.02	2.35E+05	8.95E+05
P62258	YWHAE	10	7	29.174	3.092	1.62859	8.49E+06	0.291	3.13E+06	5.37E+06
Q9Y265	RUVBL1	7	7	50.227	3.032	1.60003	1.56E+07	0.311	7.83E+06	7.78E+06
Q13501	SQSTM1	5	5	47.687	2.956	1.5636	5.67E+06	0.119	1.42E+06	4.25E+06
Q96T88	UHRF1	14	14	89.813	2.802	1.48651	1.63E+07	0.182	4.26E+06	1.21E+07
O60927	PPP1R11	5	5	13.952	2.799	1.48491	1.92E+07	1.376	3.05E+06	1.62E+07
P23381	WARS	4	4	53.165	2.701	1.43339	3.77E+06	0.071	9.20E+05	2.85E+06
P09211	GSTP1	10	10	23.356	2.652	1.40697	5.59E+07	2.395	1.49E+07	4.10E+07
O00233	PSMD9	1	1	24.682	2.635	1.39758	2.99E+05	0.012	9.78E+04	2.02E+05
P53611	RABGGTB	2	2	36.924	2.628	1.39408	7.33E+05	0.02	2.06E+05	5.27E+05
E7EWS7	UBE2L3	4	4	24.003	2.568	1.36036	5.12E+06	0.213	1.92E+06	3.20E+06
Q16763	UBE2S	4	4	23.845	2.523	1.33531	3.86E+06	0.162	2.81E+06	1.05E+06
Q13242	SRSF9	3	2	25.542	2.318	1.21288	1.14E+06	0.045	2.80E+05	8.62E+05
Q00534	CDK6	4	3	36.938	2.297	1.19988	5.49E+05	0.015	1.73E+05	3.77E+05
Q13200	PSMD2	3	3	100.2	2.257	1.17447	1.07E+06	0.011	4.12E+05	6.59E+05
Q96EN8	MOCOS	8	8	98.119	2.237	1.16176	5.25E+06	0.054	1.47E+06	3.78E+06
P52298	NCBP2	2	2	18.001	2.226	1.15465	1.56E+06	0.087	4.24E+05	1.14E+06
P11142	HSPA8	36	30	70.897	2.196	1.13481	3.44E+08	4.857	1.26E+08	2.18E+08
O14965	AURKA	6	6	45.809	2.191	1.13139	9.38E+06	0.205	3.98E+06	5.40E+06
Q9H7B2	RPF2	9	9	35.582	2.174	1.12035	2.68E+06	0.075	8.63E+05	1.82E+06
P62191	PSMC1	3	3	49.184	2.172	1.11876	3.06E+06	0.062	8.99E+05	2.16E+06
Q9BQ75	C3orf26	4	4	31.884	2.162	1.11243	7.84E+05	0.025	2.46E+05	5.37E+05
Q9BTC0	DIDO1	6	6	243.87	2.16	1.11116	5.59E+05	0.002	1.67E+05	3.91E+05
P48643	CCT5	26	26	59.67	2.15	1.1044	6.87E+07	1.151	2.11E+07	4.76E+07
Q16831	UPP1	3	3	33.934	2.123	1.08604	5.00E+05	0.015	1.44E+05	3.56E+05
Q99590	SCAF11	2	2	164.65	2.099	1.06998	1.21E+06	0.007	4.40E+05	7.72E+05
O94906	PRPF6	3	3	106.92	2.078	1.05506	2.15E+06	0.02	1.08E+06	1.08E+06
P84103	SRSF3	10	9	19.329	2.061	1.04327	1.49E+08	7.702	4.50E+07	1.04E+08
Q9UMS4	PRPF19	3	3	55.18	2.045	1.03224	1.38E+06	0.025	5.14E+05	8.64E+05
P35659	DEK	9	9	42.674	2.027	1.01956	1.01E+07	0.237	3.23E+06	6.86E+06
O95433	AHSA1	4	4	38.274	2.017	1.01235	8.88E+05	0.023	3.11E+05	5.77E+05
Q96J01	THOC3	2	2	38.771	2.007	1.00468	1.36E+06	0.035	4.41E+05	9.20E+05
Q8IYL3	C1orf174	2	2	25.977	2	1.00014	5.52E+05	0.021	1.80E+05	3.72E+05
P10599	TXN	8	8	11.737	1.999	0.99906	1.11E+08	9.481	4.37E+07	6.76E+07
Q9NRG9	AAAS	7	7	59.573	1.969	0.97768	1.47E+07	0.247	4.77E+06	9.94E+06
O43809	NUDT21	3	3	26.227	1.965	0.97438	2.19E+06	0.084	7.09E+05	1.48E+06
Q99832	CCT7	17	17	59.366	1.961	0.97159	2.66E+07	0.448	8.84E+06	1.78E+07
Q5JXB2	UBE2NL	1	1	17.377	1.945	0.95999	5.92E+05	0.034	2.75E+05	3.17E+05
Q96EP5	DAZAP1	3	3	43.383	1.929	0.94785	1.25E+07	0.288	4.15E+06	8.35E+06
O00148	DDX39A	14	5	49.129	1.928	0.94711	1.01E+08	2.062	3.28E+07	6.85E+07
Q9HAV4	XPO5	2	2	136.31	1.926	0.94576	4.87E+05	0.004	1.64E+05	3.24E+05
Q01664	TFAP4	3	3	38.725	1.923	0.94313	6.85E+05	0.018	2.06E+05	4.79E+05
Q9NVX2	NLE1	21	21	53.32	1.912	0.93531	3.07E+07	0.577	1.02E+07	2.06E+07
P36873	PPP1CC	23	2	38.518	1.91	0.93365	8.39E+06	0.218	1.38E+06	7.01E+06
P50991	CCT4	12	12	57.924	1.905	0.92994	2.02E+07	0.348	7.06E+06	1.31E+07
A8MXP9	MATR3	17	17	99.966	1.9	0.92608	4.10E+07	0.411	1.41E+07	2.70E+07
P52597	HNRNPF	12	10	45.671	1.894	0.92151	7.27E+07	1.593	2.39E+07	4.89E+07
Q96RR5	HCA90	9	9	89.392	1.89	0.91808	5.79E+06	0.065	1.97E+06	3.83E+06
Q9NZL9	MAT2B	7	7	37.551	1.89	0.918	5.56E+06	0.148	2.11E+06	3.45E+06

Continuation…

Uniprot ID	Gene Name	Peptides	Unique Peptides	Mol. weight [kDa]	Ratio H/L	Log Ratio H/L	Intensity	NINT	Intensity L	Intensity H
Q9UHD1	CHORDC1	8	8	37.489	1.874	0.90574	4.39E+06	0.117	1.60E+06	2.79E+06
Q16186	ADRM1	5	5	42.153	1.86	0.89499	3.89E+06	0.092	1.49E+06	2.41E+06
Q14807	KIF22	4	4	73.261	1.852	0.88877	3.38E+06	0.046	1.23E+06	2.14E+06
Q15424	SAFB	6	2	102.64	1.849	0.88667	1.56E+06	0.015	5.27E+05	1.04E+06
Q14151	SAFB2	9	5	107.47	1.848	0.8862	1.36E+07	0.127	4.44E+06	9.19E+06
Q9NTK5	OLA1	1	1	44.743	1.841	0.88057	6.93E+05	0.015	3.18E+05	3.75E+05
Q0VDF9	HSPA14	3	3	54.794	1.833	0.87381	1.07E+07	0.195	4.70E+06	6.00E+06
Q96AB3	ISOC2	8	8	24.097	1.832	0.87358	7.56E+07	3.139	2.53E+07	5.04E+07
Q06587	RING1	2	2	42.429	1.828	0.87042	8.75E+05	0.021	3.20E+05	5.55E+05
Q15029	EFTUD2	11	10	109.43	1.824	0.86711	6.86E+06	0.063	2.31E+06	4.56E+06
P49321	NASP	2	2	86.267	1.817	0.86164	7.75E+05	0.009	2.81E+05	4.94E+05
Q5JVF3	PCID2	2	2	52.099	1.816	0.86037	1.34E+05	0.003	4.32E+04	9.09E+04
P78549	NTHL1	2	2	34.389	1.814	0.85878	1.07E+06	0.031	3.85E+05	6.84E+05
P14866	HNRNPL	15	14	64.132	1.797	0.84575	8.20E+07	1.278	2.76E+07	5.43E+07

Table A15. Hela$^{GFP\text{-}PP1}\alpha$ Concatenated Interactome data set. Data above threshold >log median Ratio H:L 0.836 shown.

HeLa^PP1gammaCytoplasmic (CP)/ Stable cell line

Light: HeLa Heavy: HeLa^GFP-PP1γ

MaxQuant Version: 1.2.7.4

Median log Ratio H/L = 0.72

Threshold (> 1 log median) =1.72

Uniprot ID	Gene Name	Peptides	Unique Peptides	Mol. weight [kDa]	Ratio H/L	Log Ratio H/L	Intensity	NINT	Intensity L	Intensity H	Ratio H/L Significance B
O60927	PPP1R11	5	5	13.952	30.15	4.91418	3.70E+08	26.52	4.58E+07	3.24E+08	7.75E-05
P19388	POLR2E	3	3	24.551	18.7	4.22458	6.11E+07	2.487	3.66E+06	5.74E+07	9.39E-04
P36873	PPP1CC	14	4	38.518	15.92	3.99268	8.18E+09	212.4	1.22E+08	8.06E+09	1.99E-03
Q9GZN8	C20orf27	2	2	21.645	15.31	3.93603	9.09E+07	4.197	3.19E+06	8.77E+07	2.38E-03
Q96MX6	WDR92	5	5	39.74	15.06	3.91303	5.49E+07	1.382	1.71E+06	5.32E+07	2.55E-03
_Q9U6Y5	GFP	11	11	28.106	13.17	3.71951	8.46E+09	301.1	1.33E+08	8.33E+09	4.56E-03
Q8IWU2	LMTK2	5	5	164.9	10.63	3.41048	3.81E+07	0.231	3.82E+06	3.43E+07	1.08E-02
Q15435	PPP1R7	16	16	41.564	10.25	3.35811	1.09E+09	26.17	1.78E+08	9.09E+08	1.24E-02
Q12972	PPP1R8	12	12	38.478	9.773	3.28883	3.35E+08	8.694	1.01E+07	3.24E+08	1.49E-02
Q9UBK9	UXT	5	5	18.246	9.291	3.21579	5.67E+07	3.108	3.92E+06	5.28E+07	1.80E-02
P08670	VIM	28	26	53.651	8.57	3.09936	2.63E+09	48.96	2.31E+08	2.40E+09	2.40E-02
P41236	PPP1R2	9	9	23.015	8.195	3.03478	3.15E+08	13.67	8.01E+06	3.07E+08	2.80E-02
Q96KQ4	PPP1R13B	4	3	119.56	7.939	2.98899	1.29E+07	0.108	9.70E+05	1.20E+07	3.12E-02
Q6UXN9	WDR82	3	3	35.079	7.81	2.96523	2.45E+07	0.698	1.14E+06	2.33E+07	3.30E-02
Q96SB3	PPP1R9B	7	7	89.191	6.805	2.76653	2.40E+08	2.694	6.01E+07	1.80E+08	5.16E-02
Q9NWS0	PIH1D1	2	2	32.363	6.623	2.72746	1.89E+07	0.585	2.22E+06	1.67E+07	5.61E-02
E7EPA7	TKT	6	6	68.813	6.43	2.68491	1.17E+08	1.695	1.28E+07	1.04E+08	6.14E-02
P10809	HSPD1	12	12	61.054	6.338	2.66396	4.09E+08	6.704	7.22E+07	3.37E+08	6.42E-02
F8VW96	CSRP2	2	2	26.736	6.201	2.63245	1.87E+07	0.699	2.13E+06	1.66E+07	6.85E-02
P49750	YLPM1	24	24	241.64	6.128	2.61539	3.32E+08	1.374	3.00E+07	3.02E+08	7.10E-02
P58107	EPPK1	17	11	555.61	5.896	2.55974	5.24E+07	0.094	7.74E+06	4.47E+07	7.95E-02
Q9P2K8	EIF2AK4	9	9	186.91	5.818	2.54042	3.81E+07	0.204	4.51E+06	3.36E+07	8.26E-02
Q9H792	PEAK1	11	11	193.1	5.581	2.48063	6.18E+07	0.32	3.68E+06	5.81E+07	9.30E-02
Q9H6T3	RPAP3	8	8	75.718	5.566	2.47672	1.06E+08	1.394	1.49E+07	9.06E+07	9.37E-02
P38646	HSPA9	11	11	73.68	5.455	2.44755	1.85E+08	2.505	1.98E+07	1.65E+08	9.91E-02
F5GWA6	MYPN	4	4	145.32	4.825	2.27041	1.67E+07	0.115	2.39E+06	1.43E+07	1.38E-01
Q14160	SCRIB	11	11	177.69	4.8	2.26303	6.96E+07	0.392	1.54E+07	5.42E+07	1.40E-01
Q96QC0	PPP1R10	7	7	99.057	4.693	2.23036	6.71E+07	0.677	7.39E+06	5.97E+07	1.48E-01
Q9UHV9	PFDN2	4	4	16.648	4.56	2.18897	4.21E+07	2.529	7.89E+06	3.42E+07	1.59E-01
Q13625	TP53BP2	7	6	125.61	4.379	2.1305	4.91E+07	0.391	6.06E+06	4.31E+07	1.76E-01
Q69YH5	CDCA2	2	2	112.68	4.182	2.06409	1.29E+07	0.114	1.23E+06	1.17E+07	1.97E-01
P21333	FLNA	55	52	280.74	4.087	2.03097	7.52E+08	2.68	1.33E+08	6.19E+08	2.08E-01
O94763	URI1	3	3	59.832	3.934	1.97607	1.81E+07	0.302	1.89E+06	1.62E+07	2.27E-01
P38919	EIF4A3	2	1	46.871	3.918	1.97015	1.29E+07	0.274	2.07E+06	1.08E+07	2.29E-01
P68366	TUBA4A	10	2	49.924	3.828	1.93648	9.71E+07	1.946	1.73E+07	7.98E+07	2.41E-01
P11021	HSPA5	9	8	72.332	3.785	1.92045	1.67E+08	2.311	3.44E+07	1.33E+08	2.47E-01
P05141	SLC25A5	4	3	32.852	3.586	1.84246	2.28E+07	0.695	4.55E+06	1.83E+07	2.78E-01
O43813	LANCL1	2	2	45.283	3.514	1.81311	8.53E+06	0.188	1.79E+06	6.75E+06	2.91E-01
P49411	TUFM	2	2	49.541	3.505	1.80941	1.41E+07	0.284	3.32E+06	1.08E+07	2.92E-01
Q99714	HSD17B10	6	6	26.923	3.443	1.7835	7.53E+07	2.797	1.66E+07	5.87E+07	3.03E-01
Q15149	PLEC	106	100	516.19	3.369	1.75241	9.83E+08	1.904	2.38E+08	7.44E+08	3.17E-01
Q9Y265	RUVBL1	2	2	50.227	3.36	1.74855	1.58E+07	0.315	3.22E+06	1.26E+07	3.19E-01

Table A16. Hela$^{GFP\text{-}PP1}\gamma$ Cytoplasmic Interactome data set. Data above threshold >log median Ratio H:L 1.72 shown.

HeLa^PP1gamma Nucleoplasmic (NP)/ Stable cell line

Light: HeLa Heavy: HeLa^GFP-PP1γ

MaxQuant Version: 1.2.7.4

Median log Ratio H/L = -0.233

Threshold (> 1 log median) =0.767

Uniprot ID	Gene Name	Peptides	Unique Peptides	Mol. weight [kDa]	Ratio H/L	Log Ratio H/L	Intensity	NINT	Intensity L	Intensity H	Ratio H/L Significance B
Q9U6Y5	GFP	7	7	28.106	10.89	3.4444	5.70E+09	202.8	2.10E+08	5.49E+09	5.21E-11
Q12972	PPP1CC	12	3	38.518	6.524	2.70578	6.28E+09	163.01	1.57E+08	6.12E+09	1.42E-10
Q96QC0	PPP1R8	4	4	38.478	10.26	3.35882	2.40E+08	6.2493	1.76E+07	2.23E+08	4.00E-10
P49750	PPP1R10	20	20	99.057	9.632	3.2679	5.87E+08	5.9282	3.85E+07	5.49E+08	1.74E-09
Q6UXN9	YLPM1	48	48	241.64	8.787	3.13535	2.57E+09	10.645	1.32E+08	2.44E+09	6.50E-09
Q69YH5	WDR82	4	4	35.079	8.067	3.01198	4.28E+08	12.192	3.64E+07	3.91E+08	9.47E-08
P36873-2	CDCA2	9	9	112.68	6.713	2.74691	2.29E+08	2.0322	1.62E+07	2.13E+08	1.41E-07
Q96SB3	PPP1R9B	12	12	89.191	6.445	2.6882	4.98E+08	5.586	5.25E+07	4.46E+08	1.67E-07
P09211	GSTP1	2	2	23.356	5.805	2.5372	8.29E+07	3.5482	1.13E+07	7.16E+07	6.79E-07
P31040	SDHA	4	4	72.691	3.915	1.96901	2.23E+08	3.0708	4.72E+07	1.76E+08	7.28E-05
Q12800	TFCP2	2	2	57.255	2.634	1.39704	8.54E+07	1.4909	2.14E+07	6.40E+07	3.08E-03
E7ETI0	ARPC4-TTLL3	2	2	71.718	2.322	1.21518	3.08E+07	0.4288	8.23E+06	2.25E+07	8.30E-03
Q5UIP0	RIF1	8	8	274.46	2.224	1.15335	4.77E+07	0.174	1.50E+07	3.27E+07	1.14E-02
Q16527	CSRP2	7	7	20.954	2.157	1.10923	4.70E+08	22.442	1.40E+08	3.30E+08	1.42E-02
P11413	G6PD	3	3	63.826	2.133	1.09268	6.18E+07	0.9678	2.02E+07	4.16E+07	1.54E-02
P31689	DNAJA1	3	3	44.868	2.106	1.07464	5.72E+07	1.2741	1.84E+07	3.88E+07	1.68E-02
F8VQ10	DDX39B	8	8	50.745	1.989	0.99168	5.75E+08	11.324	1.82E+08	3.93E+08	2.47E-02
P00966	ASS1	2	2	46.53	1.917	0.9387	8.24E+07	1.7716	2.62E+07	5.63E+07	3.14E-02
Q8NF37	LPCAT1	2	2	59.151	1.912	0.93523	1.50E+07	0.2541	5.41E+06	9.62E+06	3.18E-02
P61158	ACTR3	1	1	47.371	1.791	0.84044	9.68E+06	0.2043	3.22E+06	6.46E+06	4.78E-02
P78406	RAE1	5	5	40.968	1.774	0.82725	2.07E+08	5.0434	7.71E+07	1.30E+08	5.04E-02

Table A17. Hela$^{GFP\text{-}PP1}\gamma$ Nucleoplasmic Interactome data set. Data above threshold >log median Ratio H:L 0.767 shown.

HeLa^PP1gamma Concatenated/ Stable cell line

Light: HeLa Heavy: HeLa^GFP-PP1γ

MaxQuant Version: 1.2.7.4

Median log Ratio H/L = 0.180

Threshold (> 1 log median) = 1.180

Uniprot ID	Gene Name	Peptides	Unique Peptides	Mol. weight [kDa]	Ratio H/L	Log Ratio H/L	Intensity	NINT	Intensity L	Intensity H
O60927	PPP1R11	4	4	13.952	45.64	5.5122	3.47E+08	24.85	4.52E+07	3.02E+08
Q9GZN8	C20orf27	3	3	21.645	19.78	4.3059	1.17E+08	5.428	4.70E+06	1.13E+08
P19388	POLR2E	3	3	24.551	18.7	4.22458	6.11E+07	2.487	3.66E+06	5.74E+07
Q9U6Y5	GFP	14	14	28.106	12.94	3.69321	1.54E+10	549	3.65E+08	1.51E+10
P36873	PPP1CC	16	5	38.518	12.45	3.63807	1.64E+10	425.1	4.96E+08	1.59E+10
Q9UBK9	UXT	4	4	18.246	10.73	3.42344	4.18E+07	2.291	2.71E+06	3.91E+07
Q8IWU2	LMTK2	5	5	164.9	10.63	3.41048	3.81E+07	0.231	3.82E+06	3.43E+07
P16401	HIST1H1B	11	10	22.58	10.34	3.36947	9.04E+09	400.3	9.42E+08	8.10E+09
Q15435	PPP1R7	16	16	41.564	10.25	3.35811	1.09E+09	26.17	1.78E+08	9.09E+08
Q96MX6	WDR92	4	4	39.74	10.22	3.35389	2.51E+07	0.631	1.17E+06	2.39E+07
Q12972	PPP1R8	14	14	38.478	10.03	3.32654	7.27E+08	18.89	3.55E+07	6.91E+08
Q96QC0	PPP1R10	21	21	99.057	8.569	3.09916	8.28E+08	8.355	5.60E+07	7.72E+08
P41236	PPP1R2	9	9	23.015	8.323	3.05717	3.41E+08	14.82	8.40E+06	3.33E+08
Q6UXN9	WDR82	6	6	35.079	7.986	2.99744	5.00E+08	14.26	4.09E+07	4.59E+08
Q96KQ4	PPP1R13B	4	3	119.56	7.939	2.98899	1.29E+07	0.108	9.70E+05	1.20E+07
P49750	YLPM1	53	53	241.64	7.934	2.98807	3.00E+09	12.4	1.68E+08	2.83E+09
Q8N726	CDKN2A	3	3	18.006	7.742	2.95261	3.82E+08	21.19	4.03E+07	3.41E+08
Q96SB3	PPP1R9B	15	15	89.191	6.946	2.79616	8.21E+08	9.209	1.16E+08	7.05E+08
Q9NWS0	PIH1D1	2	2	32.363	6.623	2.72746	1.89E+07	0.585	2.22E+06	1.67E+07
P05186	ALPL	2	2	57.304	6.584	2.71888	2.94E+07	0.513	1.79E+06	2.76E+07
O94763	URI1	4	4	59.832	6.34	2.66451	3.81E+07	0.637	5.80E+06	3.23E+07
Q69YH5	CDCA2	9	9	112.68	6.099	2.60867	2.42E+08	2.147	1.75E+07	2.24E+08
E7EPA7	TKT	7	7	68.813	5.847	2.54777	1.26E+08	1.837	1.44E+07	1.12E+08
Q9H792	PEAK1	11	11	193.1	5.581	2.48063	6.18E+07	0.32	3.68E+06	5.81E+07
Q9H6T3	RPAP3	8	8	75.718	5.566	2.47672	1.06E+08	1.394	1.49E+07	9.06E+07
P09211	GSTP1	2	2	23.356	5.465	2.45022	9.78E+07	4.187	1.31E+07	8.47E+07
Q9P2K8	EIF2AK4	10	10	186.91	5.236	2.38855	4.84E+07	0.259	6.45E+06	4.19E+07
F5GWA6	MYPN	4	4	145.32	4.825	2.27041	1.67E+07	0.115	2.39E+06	1.43E+07
Q9UHV9	PFDN2	4	4	16.648	4.56	2.18897	4.21E+07	2.529	7.89E+06	3.42E+07
Q13625	TP53BP2	7	6	125.61	4.379	2.1305	4.91E+07	0.391	6.06E+06	4.31E+07
P68366	TUBA4A	10	2	49.924	3.828	1.93648	9.71E+07	1.946	1.73E+07	7.98E+07
P31040	SDHA	4	4	72.691	3.738	1.90231	2.88E+08	3.968	6.49E+07	2.24E+08
O43813	LANCL1	2	2	45.283	3.514	1.81311	8.53E+06	0.188	1.79E+06	6.75E+06
P11413	G6PD	10	10	63.826	3.094	1.62947	2.71E+08	4.244	6.38E+07	2.07E+08
E9PF41	ACTR2	2	2	45.376	3.056	1.61174	2.36E+07	0.519	6.35E+06	1.72E+07
P17066	HSPA6	4	1	71.027	2.915	1.54369	4.25E+08	5.978	1.84E+08	2.41E+08
Q9UL15	BAG5	2	2	56.026	2.901	1.53675	7.42E+06	0.132	1.53E+06	5.89E+06
Q07161	PPP1CA	13	2	38.631	2.887	1.52952	4.04E+07	1.047	1.39E+07	2.66E+07
Q32Q12	NME1-NME2	9	4	32.642	2.876	1.52391	9.43E+08	28.89	2.27E+08	7.16E+08
E7ETB3	DNPEP	4	4	54.53	2.81	1.49031	7.74E+07	1.42	1.69E+07	6.06E+07
Q14160	SCRIB	16	16	177.69	2.789	1.47949	1.67E+08	0.942	5.27E+07	1.15E+08
P15531	NME1	6	1	19.653	2.759	1.4642	9.60E+07	4.884	2.49E+07	7.10E+07
P23381	WARS	2	2	53.165	2.694	1.4297	2.10E+07	0.395	6.73E+06	1.43E+07
E7ETI0	ARPC4-TTLL3	2	2	71.718	2.642	1.40185	1.61E+07	0.225	4.52E+06	1.16E+07
O43175	PHGDH	4	4	56.65	2.637	1.39901	7.74E+07	1.366	2.16E+07	5.58E+07
Q12800	TFCP2	2	2	57.255	2.634	1.39704	8.54E+07	1.491	2.14E+07	6.40E+07
Q13535	ATR	4	4	301.36	2.562	1.3571	3.80E+07	0.126	1.00E+07	2.80E+07
Q12792	TWF1	2	2	40.282	2.541	1.34511	6.94E+06	0.172	1.76E+06	5.19E+06
E7ENH9	ACLY	23	23	126.22	2.474	1.30696	4.80E+08	3.802	1.80E+08	2.99E+08
Q32MZ4	LRRFIP1	3	3	89.252	2.463	1.30048	9.66E+06	0.108	2.42E+06	7.24E+06
Q16527	CSRP2	6	6	20.954	2.45	1.29278	4.75E+08	22.66	1.27E+08	3.48E+08
Q9NZM5	GLTSCR2	10	10	54.389	2.444	1.2893	3.07E+09	56.38	8.74E+08	2.19E+09
P22234	PAICS	3	3	47.958	2.434	1.28327	7.30E+07	1.523	2.36E+07	4.95E+07
Q9H7B2	RPF2	14	14	35.582	2.422	1.2762	3.77E+09	106.1	1.07E+09	2.71E+09

Continuation …

Uniprot ID	Gene Name	Peptides	Unique Peptides	Mol. weight [kDa]	Ratio H/L	Log Ratio H/L	Intensity	NINT	Intensity L	Intensity H
Q9NZM5	GLTSCR2	10	10	54.389	2.444	1.2893	3.07E+09	56.38	8.74E+08	2.19E+09
P22234	PAICS	3	3	47.958	2.434	1.28327	7.30E+07	1.523	2.36E+07	4.95E+07
Q9H7B2	RPF2	14	14	35.582	2.422	1.2762	3.77E+09	106.1	1.07E+09	2.71E+09
P50991	CCT4	6	6	57.924	2.348	1.23137	2.08E+08	3.593	6.24E+07	1.46E+08
Q9NU22	MDN1	12	12	632.81	2.308	1.20677	2.30E+08	0.363	7.11E+07	1.58E+08
P11142	HSPA8	22	19	70.897	2.296	1.19881	4.22E+09	59.47	1.63E+09	2.59E+09
P38919	EIF4A3	3	2	46.871	2.294	1.19805	2.18E+08	4.651	7.30E+07	1.45E+08
Q8N1G4	LRRC47	2	2	63.472	2.284	1.19182	6.06E+07	0.955	2.00E+07	4.06E+07

Table A18. Hela$^{GFP\text{-}PP1\gamma}$ Concatenated Interactome data set. Data above threshold >log median Ratio H:L 1.180 shown.

U2OS^GFP Cytoplasmic (CP)/ Stable cell line
Light: U2OS Heavy: U2OS^GFP
MaxQuant Version: 1.2.7.4
Median log Ratio H/L = 0.0081
Threshold (> 1 log median) =1.0081

Uniprot ID	Gene Name	Peptides	Unique Peptides	Mol. weight [kDa]	Ratio H/L	Log Ratio H/L	Intensity	NINT	Intensity L	Intensity H	Ratio H/L Significance B
Q9U6Y5	GFP	23	23	28.106	13.578	3.7632	6.45E+09	229.6	4.30E+07	6.41E+09	3.75E-29
P08670	VIM	9	9	53.651	3.5722	1.83681	1.71E+06	0.032	3.52E+05	1.36E+06	4.41E-08
P0CG48	UBC	4	4	77.028	2.872	1.52206	6.72E+06	0.087	1.81E+06	4.91E+06	5.72E-06
B4DR52	HIST2H2BF	2	2	18.041	2.0204	1.01464	8.55E+05	0.047	2.89E+05	5.65E+05	2.48E-03
P16104	H2AFX	3	3	15.144	1.9425	0.95791	1.53E+06	0.101	4.46E+05	1.09E+06	4.27E-03
P62805	HIST1H4A	4	4	11.367	1.8212	0.86489	1.02E+06	0.089	3.51E+05	6.64E+05	9.86E-03
Q9BVA1	TUBB2B	22	3	49.953	1.8103	0.85623	1.44E+06	0.029	5.13E+05	9.30E+05	1.06E-02
Q9NRW3	APOBEC3C	4	4	22.826	1.7898	0.8398	3.44E+06	0.151	1.14E+06	2.29E+06	1.22E-02
Q13268	DHRS2	4	4	29.007	1.7873	0.83778	9.22E+05	0.032	3.14E+05	6.08E+05	1.24E-02
P04080	CSTB	5	5	11.139	1.7585	0.81435	7.09E+06	0.637	2.55E+06	4.54E+06	1.51E-02
Q9UBV8	PEF1	3	3	30.381	1.7454	0.80356	1.05E+06	0.035	3.98E+05	6.54E+05	1.65E-02
P11021	HSPA5	27	26	72.332	1.743	0.80157	1.41E+07	0.195	5.12E+06	9.02E+06	1.68E-02
P68431	HIST1H3A	2	2	15.404	1.7099	0.77391	7.31E+05	0.047	2.69E+05	4.62E+05	2.09E-02
P33992	MCM5	7	7	82.285	1.6123	0.68912	1.10E+06	0.013	4.40E+05	6.61E+05	3.96E-02

Table A19. U2OS^{GFP} Cytoplasmic Interactome data set. Data above threshold >log median Ratio H:L 1.01 shown.

U2OS^GFP Nucleoplasmic (NP)/ Stable cell line
Light: U2OS Heavy: U2OS^GFP
MaxQuant Version: 1.2.7.4
Median log Ratio H/L = -0.34
Threshold (> 1 log median) =0.66

Uniprot ID	Gene Name	Peptides	Unique Peptides	Mol. weight [kDa]	Ratio H/L	Log Ratio H/L	Intensity	NINT	Intensity L	Intensity H	Ratio H/L Significance B
Q9U6Y5	GFP	10	10	28.106	12.99	3.69933	5.99E+07	2.131	4.24E+06	5.56E+07	3.88E-78
P82932	MRPS6	2	2	14.226	2.2292	1.156526	1.01E+06	0.071	2.77E+05	7.36E+05	4.03E-12
Q13268	DHRS2	13	13	27.438	1.8475	0.885574	9.51E+07	3.466	3.40E+07	6.11E+07	1.34E-08
Q16658	FSCN1	3	3	54.529	1.6489	0.721504	1.15E+06	0.021	4.20E+05	7.31E+05	8.60E-07
P48681	NES	42	42	177.44	1.6063	0.683741	3.13E+07	0.176	1.21E+07	1.92E+07	2.07E-06
F8W8J4	MYOF	10	10	234.65	1.4455	0.531569	4.11E+06	0.018	1.73E+06	2.38E+06	5.31E-05
P29590	PML	2	2	97.55	1.2567	0.32964	1.04E+06	0.011	4.56E+05	5.86E+05	1.89E-03
Q9NRW3	APOBEC3C	4	4	22.826	1.2473	0.318809	6.92E+06	0.303	2.96E+06	3.96E+06	2.24E-03
Q9Y3D9	MRPS23	2	2	21.77	1.2198	0.286645	8.90E+05	0.041	4.69E+05	4.21E+05	3.65E-03
P40939	HADHA	2	2	82.999	1.2049	0.268913	2.27E+06	0.027	1.18E+06	1.09E+06	4.73E-03
Q14151	SAFB2	3	2	107.47	1.1993	0.262193	1.50E+06	0.014	6.48E+05	8.55E+05	5.21E-03
P09382	LGALS1	12	12	14.716	1.187	0.24732	5.84E+08	39.68	2.56E+08	3.28E+08	6.43E-03
E7ENZ6	HLA-B	4	1	47.954	1.1869	0.247198	2.57E+06	0.054	1.21E+06	1.36E+06	6.44E-03
Q12874	SF3A3	1	1	58.848	1.1779	0.236217	3.16E+05	0.005	1.46E+05	1.70E+05	7.50E-03
Q8N3V7	SYNPO	11	11	96.395	1.1631	0.217975	2.41E+07	0.25	1.11E+07	1.30E+07	9.62E-03
P0C0S5	H2AFZ	4	2	13.553	1.1595	0.213503	1.75E+06	0.129	7.35E+05	1.01E+06	1.02E-02
Q6UVK1	CSPG4	4	4	250.53	1.1545	0.207268	2.68E+06	0.011	1.25E+06	1.43E+06	1.11E-02
Q96PK6	RBM14	2	2	69.491	1.1537	0.206268	1.83E+06	0.026	9.54E+05	8.75E+05	1.12E-02
Q96JY6	PDLIM2	2	2	37.458	1.1506	0.202386	3.27E+06	0.087	1.54E+06	1.73E+06	1.18E-02
P18754	RCC1	5	5	48.145	1.1348	0.182438	1.25E+07	0.26	5.79E+06	6.72E+06	1.53E-02
P83111	LACTB	4	4	60.693	1.1232	0.167615	4.40E+06	0.073	2.32E+06	2.09E+06	1.85E-02
P09038	FGF2	2	2	30.77	1.1115	0.152508	8.56E+05	0.028	3.73E+05	4.82E+05	2.23E-02
A6NCZ6	SFXN3	4	4	35.978	1.1072	0.146916	3.52E+06	0.098	1.67E+06	1.85E+06	2.38E-02
B4DR52	HIST2H2BF	5	2	18.041	1.0992	0.136454	1.31E+08	7.24	6.24E+07	6.83E+07	2.70E-02
O75616	ERAL1	2	2	48.349	1.0982	0.135141	2.89E+06	0.06	1.49E+06	1.41E+06	2.74E-02
A8MYQ9	RAB34	13	13	29.2	1.0901	0.124461	2.24E+07	0.766	1.05E+07	1.19E+07	3.11E-02
P11166	SLC2A1	3	3	54.083	1.0893	0.123401	1.73E+06	0.032	7.72E+05	9.56E+05	3.15E-02
P62805	HIST1H4A	9	9	11.367	1.0664	0.092749	1.37E+08	12.03	6.45E+07	7.23E+07	4.45E-02
P12270	TPR	2	2	267.29	1.062	0.086784	3.24E+05	0.001	1.53E+05	1.71E+05	4.75E-02
B7Z596	TPM1	12	5	31.753	1.061	0.085425	2.61E+06	0.082	1.29E+06	1.32E+06	4.82E-02
G5E9Q6	PFN2	5	2	20.787	1.0586	0.082157	6.89E+06	0.331	3.43E+06	3.46E+06	5.00E-02

Table A20. U2OS^{GFP} Nucleoplasmic Interactome data set. Data above threshold >log median Ratio H:L 0.66 shown.

U2OS^PP1alpha Cytoplasmic (CP)/ Stable cell line

Light: U2OS Heavy: U2OS^GFP-PP1α

MaxQuant Version: 1.2.7.4

Median log Ratio H/L = -0.80

Threshold (> 1 log median) = 0.20

Uniprot ID	Gene Name	Peptides	Unique Peptides	Mol. weight [kDa]	Ratio H/L	Log Ratio H/L	Intensity	NINT	Intensity L	Intensity H	Ratio H/L Significance B
Q15435	PPP1R7	27	4	41.564	27.84	4.79929	2.26E+10	544.1	8.17E+08	2.18E+10	7.29E-06
O60927	PPP1R11	4	4	13.952	18.13	4.18039	1.41E+09	101.2	7.82E+07	1.33E+09	6.56E-05
Q9U6Y5	GFP	14	14	28.106	17.32	4.11412	4.32E+10	1539	8.28E+08	4.24E+10	8.18E-05
P62136	PPP1CA	25	11	37.512	17.31	4.11353	2.83E+10	754.3	7.85E+08	2.75E+10	8.20E-05
Q8WUF5	PPP1R13L	27	27	89.09	14.82	3.88967	8.50E+09	95.38	2.05E+08	8.29E+09	1.70E-04
Q13625	TP53BP2	14	13	125.61	14.01	3.80839	1.16E+09	9.217	4.06E+07	1.12E+09	2.20E-04
P50991	CCT4	15	15	57.924	13.25	3.72759	2.05E+09	35.31	1.28E+08	1.92E+09	2.82E-04
Q9UBK9	UXT	2	2	18.246	11.74	3.55324	3.03E+07	1.661	2.05E+06	2.83E+07	4.79E-04
P49368	CCT3	17	17	60.533	11.61	3.53717	3.16E+09	52.2	2.00E+08	2.96E+09	5.03E-04
P48643	CCT5	19	19	59.67	11.46	3.51841	2.27E+09	37.96	1.64E+08	2.10E+09	5.32E-04
P0CG48	UBC	6	6	77.028	11.18	3.48272	4.37E+09	56.69	1.71E+08	4.20E+09	5.91E-04
P40227	CCT6A	15	15	58.024	11.06	3.46676	2.39E+09	41.27	2.06E+08	2.19E+09	6.19E-04
P50990	CCT8	25	25	59.62	10.83	3.43683	3.39E+09	56.89	2.46E+08	3.15E+09	6.76E-04
Q6PJW8	CNST	3	3	79.596	10.17	3.34682	4.21E+07	0.529	3.05E+06	3.91E+07	8.76E-04
Q99832	CCT7	15	15	59.366	10.09	3.33528	1.18E+09	19.9	7.48E+07	1.11E+09	9.05E-04
P78371	CCT2	25	25	57.488	10.01	3.32323	3.44E+09	59.91	2.33E+08	3.21E+09	9.37E-04
P51784	USP11	14	14	109.82	9.763	3.28731	3.47E+08	3.155	2.99E+07	3.17E+08	1.04E-03
P41236	PPP1R2	9	9	23.015	9.701	3.27807	5.57E+08	24.22	1.99E+07	5.37E+08	1.06E-03
P17987	TCP1	24	24	60.343	9.586	3.26093	3.30E+09	54.7	2.27E+08	3.07E+09	1.12E-03
Q13268	DHRS2	5	5	29.007	9.031	3.17492	2.14E+08	7.376	2.31E+07	1.91E+08	1.42E-03
Q96SB3	PPP1R9B	4	4	89.191	8.891	3.15239	5.43E+07	0.609	5.34E+06	4.90E+07	1.51E-03
O75864	PPP1R37	10	10	74.766	7.926	2.98659	2.76E+08	3.689	2.65E+07	2.49E+08	2.36E-03
P19388	POLR2E	4	4	24.551	7.522	2.9111	5.20E+07	2.119	5.79E+06	4.62E+07	2.88E-03
Q96MX6	WDR92	4	4	39.74	6.447	2.68867	8.63E+07	2.172	9.16E+06	7.72E+07	5.06E-03
Q02833	RASSF7	8	8	36.343	6.078	2.60362	2.91E+08	8.008	3.32E+07	2.58E+08	6.23E-03
Q12972	PPP1R8	5	5	38.478	5.52	2.46467	2.76E+08	7.185	2.64E+07	2.50E+08	8.67E-03
Q8TEW0	PARD3	12	12	151.42	5.305	2.40727	2.09E+08	1.38	2.61E+07	1.83E+08	9.91E-03
P49750	YLPM1	7	7	241.64	5.238	2.3891	2.68E+07	0.111	1.69E+06	2.51E+07	1.03E-02
Q9H6T3	RPAP3	6	6	75.718	5.022	2.32838	9.31E+07	1.229	1.18E+07	8.13E+07	1.19E-02
Q96KQ4	PPP1R13B	8	7	119.56	4.793	2.26087	1.91E+08	1.596	1.26E+07	1.78E+08	1.38E-02
G8JLJ4	PPP1R18	3	3	68.041	4.759	2.25066	3.90E+07	0.573	6.53E+06	3.25E+07	1.41E-02
E7EVU8	HUWE1	42	42	482.14	4.751	2.24811	3.77E+08	0.782	6.77E+07	3.10E+08	1.42E-02
O95816	BAG2	3	3	23.772	4.736	2.24358	9.10E+07	3.829	1.35E+07	7.75E+07	1.43E-02
O94763	URI1	2	2	59.832	4.585	2.19692	3.24E+07	0.541	4.35E+06	2.80E+07	1.59E-02
Q86W26	NLRP10	4	4	75.031	4.432	2.14783	3.71E+07	0.494	3.38E+06	3.37E+07	1.77E-02
H0YG33	HSPA1B	17	11	77.405	4.243	2.08519	1.01E+09	13.02	1.84E+08	8.23E+08	2.02E-02
P11142	HSPA8	29	25	70.897	3.29	1.71787	6.17E+09	87.05	1.27E+09	4.90E+09	4.24E-02
Q9BTA0	FAM167B	2	2	18.414	3.088	1.62663	6.11E+07	3.317	1.39E+07	4.72E+07	5.04E-02
P27708	CAD	32	32	242.98	2.993	1.58179	3.88E+08	1.598	1.04E+08	2.85E+08	5.47E-02
P55884	EIF3B	3	3	99.028	2.779	1.47446	4.53E+07	0.458	1.28E+07	3.25E+07	6.64E-02
Q9UHV9	PFDN2	3	3	16.648	2.129	1.09018	6.23E+07	3.74	1.79E+07	4.44E+07	1.26E-01
Q8IXB1	DNAJC10	4	4	91.079	1.811	0.85639	5.10E+07	0.56	1.83E+07	3.27E+07	1.79E-01
O95817	BAG3	2	2	61.594	1.754	0.81081	2.00E+07	0.325	6.57E+06	1.34E+07	1.91E-01
P10809	HSPD1	3	3	61.054	1.742	0.80091	4.57E+07	0.748	1.73E+07	2.84E+07	1.94E-01
P04792	HSPB1	9	9	22.782	1.594	0.67247	3.34E+08	14.68	1.22E+08	2.12E+08	2.32E-01
Q13057	COASY	2	2	65.339	1.531	0.61485	5.07E+07	0.776	2.10E+07	2.97E+07	2.50E-01
Q9NYU2	UGGT1	2	2	177.19	1.531	0.61466	3.67E+06	0.021	1.45E+06	2.22E+06	2.50E-01
Q13885	TUBB2A	21	2	49.906	1.45	0.53605	1.07E+08	2.143	4.50E+07	6.20E+07	2.77E-01
Q9UL25	RAB21	1	1	24.347	1.449	0.53506	8.48E+06	0.348	4.03E+06	4.45E+06	2.77E-01
Q92616	GCN1L1	3	3	292.75	1.439	0.52517	7.15E+06	0.024	3.13E+06	4.02E+06	2.81E-01
Q86VP6	CAND1	3	3	136.37	1.437	0.52286	1.89E+07	0.138	7.00E+06	1.19E+07	2.81E-01
Q04917	YWHAH	4	2	28.218	1.344	0.426	4.62E+07	1.638	1.78E+07	2.85E+07	3.17E-01
P31946	YWHAB	5	3	28.082	1.313	0.39265	8.22E+07	2.927	3.29E+07	4.93E+07	3.30E-01
P61981	YWHAG	4	2	28.302	1.285	0.36188	3.85E+07	1.36	1.63E+07	2.22E+07	3.43E-01
Q71U36	TUBA1A	19	0	50.135	1.269	0.34369	6.33E+07	1.262	2.69E+07	3.64E+07	3.50E-01
Q9UNF1	MAGED2	13	13	64.953	1.243	0.31406	4.23E+08	6.509	1.73E+08	2.50E+08	3.62E-01
P23921	RRM1	2	2	90.069	1.154	0.20639	2.88E+07	0.319	1.14E+07	1.74E+07	4.09E-01

Table A21. U2OS$^{GFP\text{-}PP1}\alpha$ Cytoplasmic Interactome data set. Data above threshold >log median Ratio H:L 0.20 shown.

U2OS^PP1alpha Nucleoplasmic (NP)/ Stable cell line

Light: U2OS Heavy: U2OS^GFP-PP1α

MaxQuant Version: 1.2.7.4

Median log Ratio H/L = -0.67

Threshold (> 1 log median) = 0.33

Uniprot ID	Gene Name	Peptides	Unique Peptides	Mol. weight [kDa]	Ratio H/L	Log Ratio H/L	Intensity	NINT	Intensity L	Intensity H	Ratio H/L Significance B
G8JLJ4	PPP1R18	14	14	68.041	14.7	3.87784239	3.06E+09	44.93	1.74E+08	2.88E+09	1.59E-26
Q9U6Y5	GFP	10	10	28.106	11.94	3.5776101	9.98E+09	355.1	2.50E+08	9.73E+09	2.38E-23
Q96SB3	PPP1R9B	20	18	89.191	9.525	3.25176453	3.31E+09	37.12	1.94E+08	3.12E+09	3.82E-20
P49750	YLPM1	55	55	241.64	9.181	3.1986513	4.79E+09	19.81	3.13E+08	4.47E+09	1.20E-19
Q13625	TP53BP2	7	7	125.61	6.259	2.64600132	2.54E+08	2.024	3.33E+07	2.21E+08	7.55E-15
Q13268	DHRS2	6	6	27.438	6.179	2.62727998	9.56E+08	34.84	1.24E+08	8.32E+08	1.07E-14
Q96QC0	PPP1R10	8	8	99.057	6.171	2.62541078	2.21E+08	2.236	1.74E+07	2.04E+08	1.10E-14
P62136	PPP1CA	22	7	37.512	5.658	2.50016468	1.33E+10	355	7.34E+08	1.26E+10	1.06E-13
Q9H792	PEAK1	3	3	193.1	5.639	2.49536259	6.35E+07	0.329	9.03E+06	5.45E+07	1.15E-13
Q15435	PPP1R7	2	2	41.564	5.101	2.35075182	4.89E+07	1.177	1.03E+07	3.86E+07	1.40E-12
Q8WUF5	PPP1R13L	5	5	89.09	5.067	2.34118877	1.25E+08	1.403	2.06E+07	1.04E+08	1.65E-12
Q4KMQ1	TPRN	2	2	75.555	4.745	2.2465297	4.03E+07	0.533	6.39E+06	3.39E+07	7.93E-12
Q6UXN9	WDR82	4	4	35.079	4.496	2.16848158	2.01E+08	5.724	2.93E+07	1.71E+08	2.79E-11
E9PCR8	ERBB2IP	2	2	159.02	3.729	1.89875011	1.58E+07	0.099	3.27E+06	1.25E+07	1.68E-09
P36873	PPP1CC	17	2	38.518	3.41	1.7696025	1.92E+08	4.985	3.98E+07	1.52E+08	1.04E-08
Q5UIP0	RIF1	5	5	274.46	3.36	1.74859004	4.47E+07	0.163	7.89E+06	3.68E+07	1.39E-08
P33947	KDELR2	2	2	24.422	1.985	0.98935703	2.06E+07	0.842	6.83E+06	1.37E+07	9.74E-05
E9PDX1	PPP1R9A	7	5	154.05	1.967	0.97592361	8.60E+07	0.558	2.08E+07	6.51E+07	1.11E-04
Q8TEW0	PARD3	3	3	151.42	1.951	0.96436166	5.36E+07	0.354	1.68E+07	3.68E+07	1.24E-04
Q8IY33	MICALL2	2	2	97.501	1.645	0.71826298	1.34E+07	0.137	4.57E+06	8.80E+06	1.11E-03
P31689	DNAJA1	2	2	44.868	1.632	0.70628741	8.23E+07	1.833	3.06E+07	5.17E+07	1.22E-03
A7MAP0	CORO1C	3	3	54.066	1.463	0.54932416	6.03E+08	11.16	2.40E+08	3.64E+08	4.15E-03
E7EVA0	MAP4	19	19	245.44	1.437	0.52265842	1.40E+09	5.723	5.75E+08	8.30E+08	5.04E-03
C9JWM7	ARPC4	2	2	21.588	1.31	0.38967694	6.62E+07	3.064	3.05E+07	3.56E+07	1.27E-02

Table A22. U2OS$^{GFP\text{-}PP1}\alpha$ Nucleoplasmic Interactome data set. Data above threshold >log median Ratio H:L 0.33 shown.

U2OS^PP1alpha Concatenated/ Stable cell line

Light: U2OS Heavy: U2OS^GFP-PP1α

MaxQuant Version: 1.2.7.4

Median log Ratio H/L = -1.120

Threshold (> 1 log median) = -0.120

Uniprot ID	Gene Name	Peptides	Unique Peptides	Mol. weight [kDa]	Ratio H/L	Log Ratio H/L	Intensity	NINT	Intensity L	Intensity H
O60927	PPP1R11	4	4	13.952	34.02	5.08844	1.62E+09	116.2	8.10E+07	1.54E+09
Q15435	PPP1R7	28	4	41.564	28.62	4.83895	2.38E+10	572.9	8.62E+08	2.30E+10
Q9U6Y5	GFP	16	16	28.106	14.77	3.88489	5.27E+10	1875	1.02E+09	5.17E+10
G8JLJ4	PPP1R18	14	14	68.041	14.06	3.81352	2.99E+09	44	1.46E+08	2.85E+09
Q8WUF5	PPP1R13L	30	30	89.09	13.69	3.77473	9.59E+09	107.6	2.42E+08	9.35E+09
Q13625	TP53BP2	17	16	125.61	11.76	3.55594	1.45E+09	11.53	7.56E+07	1.37E+09
Q9UBK9	UXT	2	2	18.246	11.74	3.55324	3.03E+07	1.661	2.05E+06	2.83E+07
P49368	CCT3	18	18	60.533	11.52	3.52569	3.25E+09	53.62	2.42E+08	3.00E+09
P50990	CCT8	23	23	59.62	11.34	3.50348	3.33E+09	55.81	2.39E+08	3.09E+09
P78371	CCT2	25	25	57.488	11.03	3.46336	3.99E+09	69.41	3.42E+08	3.65E+09
P62136	PPP1CA	27	8	37.512	11.02	3.46231	5.01E+10	1336	2.40E+09	4.77E+10
P40227	CCT6A	16	16	58.024	10.97	3.45602	2.40E+09	41.38	2.07E+08	2.19E+09
P48643	CCT5	18	18	59.67	10.74	3.42492	2.31E+09	38.75	1.87E+08	2.13E+09
Q99832	CCT7	15	15	59.366	10.06	3.32984	1.39E+09	23.43	1.02E+08	1.29E+09
P41236	PPP1R2	9	9	23.015	9.701	3.27807	5.57E+08	24.22	1.99E+07	5.37E+08
P50991	CCT4	16	16	57.924	9.25	3.20945	2.32E+09	40.1	2.37E+08	2.09E+09
P17987	TCP1	25	25	60.343	9.225	3.20547	3.65E+09	60.43	3.28E+08	3.32E+09
P49750	YLPM1	52	52	241.64	8.974	3.16567	4.94E+09	20.44	3.22E+08	4.62E+09
Q96SB3	PPP1R9B	22	20	89.191	8.891	3.15239	3.47E+09	38.91	2.07E+08	3.26E+09
Q12972	PPP1R8	5	5	38.478	8.036	3.00651	2.89E+08	7.512	2.70E+07	2.62E+08
P51784	USP11	16	16	109.82	7.907	2.98319	3.81E+08	3.474	3.88E+07	3.43E+08
Q8NHQ8	RASSF8	3	3	48.326	7.591	2.92421	1.04E+08	2.162	5.77E+06	9.87E+07
O75864	PPP1R37	11	11	74.766	7.555	2.91737	3.04E+08	4.07	2.96E+07	2.75E+08
Q96MX6	WDR92	5	5	39.74	6.886	2.78369	1.02E+08	2.571	1.04E+07	9.18E+07
Q13268	DHRS2	10	10	27.438	6.872	2.78077	6.22E+09	226.6	6.47E+08	5.57E+09
Q02833	RASSF7	8	8	36.343	6.168	2.62483	4.56E+08	12.55	3.82E+07	4.18E+08
P19388	POLR2E	4	4	24.551	6.114	2.61221	9.95E+07	4.054	2.79E+07	7.16E+07
Q9NWS0	PIH1D1	3	3	32.363	5.936	2.56937	5.45E+07	1.683	5.26E+06	4.92E+07
Q96QC0	PPP1R10	7	7	99.057	5.892	2.55873	2.30E+08	2.32	2.34E+07	2.06E+08
Q9H792	PEAK1	4	4	193.1	5.386	2.42916	9.48E+07	0.491	1.40E+07	8.08E+07
Q86W26	NLRP10	5	5	75.031	5.036	2.33216	5.41E+07	0.721	4.76E+06	4.94E+07
Q9H6T3	RPAP3	6	6	75.718	5.022	2.32838	9.31E+07	1.229	1.18E+07	8.13E+07
Q96KQ4	PPP1R13B	8	7	119.56	4.793	2.26087	1.91E+08	1.596	1.26E+07	1.78E+08
Q4KMQ1	TPRN	2	2	75.555	4.745	2.24653	4.03E+07	0.533	6.39E+06	3.39E+07
Q8TEW0	PARD3	14	14	151.42	4.633	2.21204	2.63E+08	1.734	4.29E+07	2.20E+08
E7EVU8	HUWE1	39	39	482.14	4.624	2.20927	3.64E+08	0.754	7.00E+07	2.94E+08
O94763	URI1	2	2	59.832	4.585	2.19692	3.24E+07	0.541	4.35E+06	2.80E+07
Q6UXN9	WDR82	4	4	35.079	4.496	2.16848	2.01E+08	5.724	2.93E+07	1.71E+08
Q6PJW8	CNST	3	3	79.596	4.348	2.12025	4.36E+07	0.548	3.39E+06	4.03E+07
H0YG33	HSPA1B	18	11	77.405	3.881	1.95639	1.63E+09	21.05	4.56E+08	1.17E+09
Q5UIP0	RIF1	5	5	274.46	3.36	1.74859	4.47E+07	0.163	7.89E+06	3.68E+07
P54132	BLM	2	2	159	3.033	1.60094	4.64E+08	2.921	9.33E+07	3.71E+08
P27708	CAD	31	31	242.98	3.002	1.58602	3.70E+08	1.522	9.12E+07	2.79E+08
P11142	HSPA8	32	28	70.897	2.991	1.58039	1.14E+10	160.7	4.12E+09	7.27E+09
P36873	PPP1CC	21	3	38.518	2.877	1.52446	8.91E+08	23.14	6.18E+08	2.74E+08
P55884	EIF3B	3	3	99.028	2.779	1.47446	4.53E+07	0.458	1.28E+07	3.25E+07
E9PDX1	PPP1R9A	6	4	154.05	2.661	1.41186	6.26E+07	0.406	1.28E+07	4.98E+07
E9PCR8	ERBB2IP	3	3	159.02	2.65	1.40577	2.65E+07	0.167	6.60E+06	1.99E+07
Q9UHV9	PFDN2	3	3	16.648	2.129	1.09018	6.23E+07	3.74	1.79E+07	4.44E+07

Continuation …

Uniprot ID	Gene Name	Peptides	Unique Peptides	Mol. weight [kDa]	Ratio H/L	Log Ratio H/L	Intensity	NINT	Intensity L	Intensity H
Q8N1G4	LRRC47	2	2	63.472	1.686	0.75369	6.85E+07	1.079	3.10E+07	3.75E+07
P31689	DNAJA1	2	2	44.868	1.667	0.73734	8.91E+07	1.986	3.20E+07	5.71E+07
Q8IY33	MICALL2	2	2	97.501	1.645	0.71826	1.34E+07	0.137	4.57E+06	8.80E+06
O95817	BAG3	3	3	61.594	1.643	0.71598	5.69E+07	0.924	3.36E+07	2.33E+07
Q13057	COASY	2	2	65.339	1.531	0.61485	5.07E+07	0.776	2.10E+07	2.97E+07
P04792	HSPB1	8	8	22.782	1.495	0.57976	4.68E+08	20.55	2.04E+08	2.64E+08
A7MAP0	CORO1C	3	3	54.066	1.463	0.54932	6.03E+08	11.16	2.40E+08	3.64E+08
Q13885	TUBB2A	22	2	49.906	1.45	0.53605	1.07E+08	2.143	4.50E+07	6.20E+07
C9JWM7	ARPC4	3	3	21.588	1.31	0.38968	6.62E+07	3.064	3.05E+07	3.56E+07
P61981	YWHAG	4	2	28.302	1.285	0.36188	3.85E+07	1.36	1.63E+07	2.22E+07
Q9UL25	RAB21	6	6	24.347	1.285	0.36121	4.89E+08	20.09	2.03E+08	2.86E+08
Q71U36	TUBA1A	18	0	50.135	1.266	0.34016	1.22E+08	2.443	5.52E+07	6.72E+07
Q9UNF1	MAGED2	13	13	64.953	1.227	0.29478	4.83E+08	7.43	2.26E+08	2.57E+08
P30876	POLR2B	2	2	133.9	1.224	0.29149	1.85E+08	1.384	9.88E+07	8.65E+07
E7EVA0	MAP4	19	19	245.44	1.219	0.2857	1.60E+09	6.531	7.18E+08	8.85E+08
Q14966	ZNF638	2	2	220.62	1.206	0.26975	1.42E+07	0.065	4.96E+06	9.27E+06
Q13315	ATM	2	2	350.71	1.191	0.25205	8.98E+06	0.026	4.06E+06	4.92E+06
Q14444	CAPRIN1	2	2	78.365	1.188	0.24793	5.69E+07	0.726	2.52E+07	3.17E+07
P31946	YWHAB	5	3	28.082	1.153	0.20527	1.08E+08	3.832	4.72E+07	6.04E+07
A5YKK6	CNOT1	4	4	266.94	1.148	0.199	1.98E+07	0.074	9.85E+06	9.98E+06
Q14160	SCRIB	22	22	177.69	1.139	0.18827	8.02E+08	4.514	3.68E+08	4.34E+08
P62258	YWHAE	6	4	29.174	1.105	0.14405	1.04E+08	3.56	4.91E+07	5.48E+07
C9JGC4	SPC24	1	1	22.478	1.096	0.13238	1.57E+07	0.697	6.51E+06	9.16E+06
E7ENH9	ACLY	5	5	126.22	1.085	0.11823	1.20E+08	0.949	6.38E+07	5.59E+07
P51452	DUSP3	2	2	20.478	1.082	0.11423	1.19E+07	0.582	5.50E+06	6.41E+06
Q04917	YWHAH	4	2	28.218	1.075	0.10434	1.04E+08	3.685	5.04E+07	5.36E+07
E9PI68	SPCS2	1	1	28.503	1.058	0.08079	4.39E+07	1.542	1.93E+07	2.46E+07
O00192	ARVCF	4	4	104.64	1.053	0.07478	8.48E+07	0.81	4.06E+07	4.42E+07
P12236	SLC25A6	13	5	32.866	1.051	0.07149	1.09E+09	33.21	5.82E+08	5.09E+08
P05141	SLC25A5	16	8	32.852	1.042	0.05922	7.72E+09	235	5.73E+09	1.99E+09
O95782	AP2A1	2	2	107.54	1.038	0.05311	3.04E+07	0.283	1.55E+07	1.49E+07
O95816	BAG2	6	6	23.772	1.032	0.04572	4.05E+08	17.04	1.70E+08	2.35E+08
P54136	RARS	2	2	75.378	1.025	0.03492	3.91E+07	0.519	1.48E+07	2.44E+07
Q96N67	DOCK7	3	3	242.56	1.024	0.03365	1.06E+07	0.044	4.94E+06	5.67E+06
Q93008	USP9X	2	2	292.28	1.022	0.03182	6.07E+06	0.021	2.73E+06	3.34E+06
Q9Y315	DERA	2	2	35.23	1.022	0.03125	1.09E+07	0.309	4.98E+06	5.90E+06
Q96ME1	FBXL18	2	2	88.34	1.015	0.02162	2.72E+07	0.308	1.55E+07	1.17E+07
F8W1H5	RAB5C	3	3	27.035	1.014	0.01963	2.31E+08	8.54	1.13E+08	1.18E+08
P52630	STAT2	2	2	97.915	1.012	0.01664	9.06E+06	0.092	4.30E+06	4.75E+06
Q9NQW6	ANLN	4	4	124.2	0.998	-0.0026	1.04E+08	0.841	5.45E+07	4.99E+07
P11021	HSPA5	17	16	72.332	0.996	-0.0062	1.62E+09	22.33	8.78E+08	7.37E+08
O00139	KIF2A	2	2	84.088	0.992	-0.0116	3.21E+07	0.382	1.75E+07	1.46E+07
Q8WX93	PALLD	13	13	150.56	0.984	-0.0227	7.72E+08	5.125	3.73E+08	3.98E+08
B4DYH1	HSPH1	7	7	97.459	0.974	-0.0384	1.36E+08	1.394	6.64E+07	6.95E+07
Q8WWM7	ATXN2L	3	3	115.58	0.933	-0.0995	7.92E+07	0.685	3.86E+07	4.07E+07
P40763	STAT3	5	5	88.067	0.93	-0.1043	1.24E+08	1.407	5.86E+07	6.53E+07
B4E1T7	PPP2R2A	5	5	52.999	0.93	-0.1049	1.50E+08	2.833	8.84E+07	6.17E+07
O96007	MOCS2	3	3	20.944	0.927	-0.1086	6.33E+07	3.025	3.27E+07	3.06E+07
O15145	ARPC3	3	3	20.546	0.923	-0.116	9.40E+07	4.575	4.84E+07	4.56E+07

Table A23. U2OS$^{GFP\text{-}PP1}\alpha$ Concatenated Interactome data set. Data above threshold >log median Ratio H:L -0.120 shown.

U2OS^PP1beta Cytoplasmic (CP)/ Stable cell line

Light: U2OS Heavy: U2OS^PP1β-GFP

MaxQuant Version: 1.2.7.4

Median log Ratio H/L = 0.61

Threshold (> 1 log median) = 1.61

Uniprot ID	Gene Name	Peptides	Unique Peptides	Mol. weight [kDa]	Ratio H/L	Log Ratio H/L	Intensity	NINT	Intensity L	Intensity H	Ratio H/L Significance B
Q12972	PPP1R8	19	19	38.478	24.77	4.63064	8.11E+07	2.11	2.08E+06	7.90E+07	2.63E-09
P41236	PPP1R2	9	9	23.015	23.6	4.56078	2.32E+07	1.01	4.46E+05	2.28E+07	4.91E-09
O60927	PPP1R11	3	3	13.952	17.98	4.16816	2.27E+07	1.63	2.66E+05	2.24E+07	1.35E-07
P62140	PPP1CB	24	24	37.186	15.99	3.9991	2.38E+09	64	3.52E+07	2.34E+09	5.09E-07
Q9BZL4	PPP1R12C	18	2	84.88	12.79	3.67706	4.30E+07	0.51	3.33E+06	3.97E+07	5.40E-06
Q9U6Y5	GFP	13	13	28.106	12.39	3.63099	1.31E+09	46.7	2.45E+07	1.29E+09	7.43E-06
O14974	PPP1R12A	62	62	115.28	11.4	3.51122	5.37E+08	4.66	2.74E+07	5.10E+08	1.67E-05
Q15435	PPP1R7	19	4	41.564	11.33	3.5022	4.40E+08	10.6	1.03E+08	3.37E+08	1.78E-05
Q96I34	PPP1R16A	4	4	57.811	10.22	3.35361	7.34E+06	0.13	6.27E+05	6.71E+06	4.65E-05
Q8WUF5	PPP1R13L	29	29	89.09	9.379	3.22937	2.33E+08	2.62	9.15E+06	2.24E+08	1.01E-04
Q96KQ4	PPP1R13B	11	10	119.56	8.784	3.13483	8.35E+06	0.07	8.55E+05	7.50E+06	1.77E-04
Q13625	TP53BP2	12	11	125.61	8.601	3.10455	1.31E+07	0.1	1.16E+06	1.19E+07	2.11E-04
Q9BZL4		17	1	84.681	7.477	2.9024	3.05E+06	0.04	3.68E+05	2.68E+06	6.55E-04
Q9P2K8	EIF2AK4	2	2	186.91	6.967	2.80058	9.10E+05	0	1.59E+05	7.50E+05	1.12E-03
O95405	ZFYVE9	3	3	156.4	5.713	2.51422	2.27E+06	0.01	3.33E+05	1.93E+06	4.57E-03
Q8IZ21	PHACTR4	21	21	79.128	5.277	2.39961	7.95E+07	1	1.82E+07	6.13E+07	7.65E-03
Q9H175	CSRNP2	7	7	59.591	5	2.32201	7.14E+06	0.12	8.47E+05	6.29E+06	1.07E-02
H0YG33	HSPA1B	16	8	77.405	4.864	2.28211	6.29E+07	0.81	9.05E+06	5.39E+07	1.26E-02
O75864	PPP1R37	9	9	74.766	4.375	2.12922	5.59E+06	0.07	1.02E+06	4.57E+06	2.33E-02
P0C0S5	H2AFZ	3	2	13.553	4.299	2.10407	1.02E+08	7.55	2.10E+07	8.14E+07	2.56E-02
P36969	GPX4	3	3	22.192	3.975	1.99099	1.18E+06	0.05	2.55E+05	9.26E+05	3.89E-02
P04406	GAPDH	11	11	36.053	3.95	1.98196	1.62E+07	0.45	3.29E+06	1.29E+07	4.02E-02
P11142	HSPA8	31	27	70.897	3.764	1.91238	5.12E+08	7.23	1.04E+08	4.09E+08	5.12E-02
Q7Z3T8	ZFYVE16	7	7	168.9	3.747	1.90574	3.28E+06	0.02	6.83E+05	2.60E+06	5.24E-02
P06733	ENO1	2	2	47.168	3.547	1.82664	3.73E+06	0.08	9.11E+05	2.82E+06	6.83E-02
Q16658	FSCN1	6	6	54.529	3.113	1.63835	8.59E+06	0.16	2.17E+06	6.42E+06	1.22E-01
Q8TEW0	PARD3	2	2	151.42	3.092	1.62835	7.62E+05	0.01	1.28E+05	6.34E+05	1.26E-01

Table A24. U2OS$^{PP1\beta\text{-}GFP}$ Cytoplasmic Interactome data set. Data above threshold >log median Ratio H:L 1.61 shown.

U2OS^PP1beta Nucleoplasmic (NP)/ Stable cell line

Light: U2OS Heavy: U2OS^PP1β-GFP

MaxQuant Version: 1.2.7.4

Median log Ratio H/L = 0.55

Threshold (> 1 log median) = 1.55

Uniprot ID	Gene Name	Peptides	Unique Peptides	Mol. weight [kDa]	Ratio H/L	Log Ratio H/L	Intensity	NINT	Intensity L	Intensity H	Ratio H/L Significance B
Q02539	HIST1H1A	16	7	21.842	13.33	3.7365	4.20E+08	19.25	2.90E+07	3.91E+08	5.43E-05
P34741	SDC2	4	4	22.16	11.63	3.54028	6.20E+06	0.28	3.65E+05	5.83E+06	1.51E-04
Q6UXN9	WDR82	6	6	35.079	11.08	3.46963	6.26E+07	1.784	5.49E+06	5.71E+07	2.16E-04
O14974	PPP1R12A	26	26	115.28	10.13	3.34028	4.12E+08	3.577	2.93E+07	3.83E+08	4.05E-04
GFP	GFP	9	9	28.106	10.09	3.33443	9.87E+08	35.13	3.24E+07	9.55E+08	4.17E-04
P16403	HIST1H1C	22	7	21.364	8.546	3.09518	9.39E+09	439.3	1.08E+09	8.31E+09	1.25E-03
P62140	PPP1CB	20	8	37.186	8.399	3.07023	1.52E+09	40.89	1.15E+08	1.41E+09	1.39E-03
P10412	HIST1H1E	17	2	21.865	7.049	2.81732	5.55E+07	2.536	5.74E+06	4.97E+07	4.01E-03
Q96QC0	PPP1R10	11	11	99.057	6.928	2.79252	1.09E+08	1.104	1.43E+07	9.51E+07	4.43E-03
Q12972	YLPM1	21	21	241.64	6.514	2.70357	1.04E+08	0.43	1.39E+07	9.00E+07	6.26E-03
P49750	PPP1R8	7	7	38.478	6.514	2.70357	3.22E+07	0.836	2.52E+06	2.96E+07	6.26E-03
Q96I34	PPP1R16A	5	5	57.811	5.645	2.49692	3.64E+07	0.629	5.35E+06	3.10E+07	1.34E-02
P04908	HIST1H2AB	11	2	14.135	5.297	2.40528	2.37E+08	16.76	3.41E+07	2.03E+08	1.84E-02
Q9Y625	GPC6	3	2	62.735	5.204	2.37957	1.07E+07	0.171	1.21E+06	9.50E+06	2.01E-02
P35052	GPC1	8	8	61.68	4.62	2.20799	6.16E+07	0.999	1.14E+07	5.03E+07	3.49E-02
P0CG48	UBC	5	5	77.028	4.43	2.1474	1.92E+09	24.87	3.49E+08	1.57E+09	4.21E-02
O75531	BANF1	5	5	10.058	4.378	2.13037	2.85E+08	28.33	5.16E+07	2.33E+08	4.43E-02
O75487	GPC4	4	3	62.411	4.33	2.1144	2.30E+07	0.368	3.19E+06	1.98E+07	4.65E-02
P07305	H1F0	5	5	20.863	4.315	2.10939	5.91E+08	28.32	9.91E+07	4.92E+08	4.72E-02
Q04837	SSBP1	3	3	17.259	4.229	2.08015	2.90E+07	1.679	6.99E+06	2.20E+07	5.14E-02
B4DLA9	HIST2H2BF	21	0	14.841	4.147	2.05196	2.70E+10	1821	5.39E+09	2.16E+10	5.58E-02
P05204	HMGN2	3	3	9.3926	4.095	2.03369	2.90E+06	0.309	5.92E+05	2.31E+06	5.89E-02
P23527	HIST1H2BO	17	0	13.906	4.057	2.02045	1.34E+09	96.02	2.53E+08	1.08E+09	6.11E-02
P12004	PCNA	6	6	28.768	4.029	2.01042	5.00E+07	1.737	1.08E+07	3.92E+07	6.29E-02
P18827	SDC1	2	2	32.461	3.981	1.99309	3.29E+06	0.101	5.98E+05	2.69E+06	6.60E-02
Q6FI13	HIST2H2AA3	13	1	14.095	3.943	1.9794	1.43E+10	1015	2.78E+09	1.15E+10	6.86E-02
E9PCS5	CBX1	4	3	21.915	3.729	1.89863	3.43E+07	1.566	5.68E+06	2.86E+07	8.56E-02
P23284	PPIB	3	3	23.742	3.637	1.86263	3.16E+07	1.333	5.70E+06	2.59E+07	9.42E-02
Q9BS16	CENPK	3	3	31.655	3.53	1.81955	1.82E+07	0.575	3.50E+06	1.47E+07	1.05E-01
P45973	CBX5	4	3	22.225	3.512	1.81209	1.49E+07	0.67	3.24E+06	1.17E+07	1.07E-01
P11215	ITGAM	1	1	127.18	3.497	1.80604	3.60E+08	2.827	8.27E+07	2.77E+08	1.09E-01
P12956	XRCC6	7	7	69.842	3.49	1.80327	3.50E+07	0.501	7.92E+06	2.71E+07	1.10E-01
Q92945	KHSRP	8	8	73.114	3.434	1.77985	7.32E+07	1.001	1.75E+07	5.58E+07	1.17E-01
P13010	XRCC5	8	8	82.704	3.421	1.77421	5.03E+07	0.609	1.22E+07	3.81E+07	1.18E-01
P62937	PPIA	3	3	18.012	3.391	1.76171	2.59E+07	1.436	6.31E+06	1.96E+07	1.22E-01
Q9BZL4	PPP1R12C	5	5	84.88	3.371	1.75326	6.64E+06	0.078	1.58E+06	5.06E+06	1.25E-01
P16104	H2AFX	9	0	15.144	3.355	1.74618	1.06E+09	70.09	2.24E+08	8.37E+08	1.27E-01
Q969G3	SMARCE1	2	2	46.649	3.303	1.72391	1.31E+07	0.282	2.80E+06	1.03E+07	1.34E-01
P0C0S5	H2AFZ	6	4	13.553	3.25	1.70062	1.95E+09	144	3.96E+08	1.56E+09	1.42E-01
Q8WXX5	DNAJC9	2	2	29.909	3.207	1.68104	6.27E+06	0.209	1.52E+06	4.74E+06	1.49E-01
Q6PL18	ATAD2	10	7	158.55	3.153	1.65659	1.01E+08	0.639	2.06E+07	8.07E+07	1.57E-01
Q13185	CBX3	6	4	20.811	3.131	1.64644	3.72E+08	17.9	8.21E+07	2.90E+08	1.61E-01
Q08945	SSRP1	13	13	81.074	3.111	1.63742	1.81E+08	2.231	4.45E+07	1.36E+08	1.65E-01
Q9H6F5	CCDC86	2	2	40.235	3.088	1.62658	1.65E+07	0.411	3.56E+06	1.30E+07	1.69E-01
P62805	HIST1H4A	14	14	11.367	3.06	1.61344	2.71E+10	2386	6.71E+09	2.04E+10	1.74E-01
Q5UIP0	RIF1	3	3	274.46	3.055	1.61136	4.88E+06	0.018	1.17E+06	3.70E+06	1.75E-01
Q96T88	UHRF1	3	3	89.813	3.008	1.58866	1.11E+07	0.124	2.54E+06	8.56E+06	1.84E-01
O75475	PSIP1	5	5	60.103	3.003	1.58655	6.36E+07	1.058	1.58E+07	4.77E+07	1.85E-01
Q03252	LMNB2	20	17	67.688	3.003	1.5864	1.74E+08	2.566	4.96E+07	1.24E+08	1.85E-01

Table A25. U2OS$^{PP1\beta\text{-}GFP}$ Nucleoplasmic Interactome data set. Data above threshold >log median Ratio H:L 1.55 shown.

U2OS^PP1beta Concatenated/ Stable cell line

Light: U2OS Heavy: U2OS^PP1β-GFP

MaxQuant Version: 1.2.7.4

Median log Ratio H/L = 0.434

Threshold (> 1 log median) = 1.434

Uniprot ID	Gene Name	Peptides	Unique Peptides	Mol. weight [kDa]	Ratio H/L	Log Ratio H/L	Intensity	NINT	Intensity L	Intensity H
P41236	PPP1R2	9	9	23.015	24.71	4.62702	2.26E+07	0.982	4.33E+05	2.22E+07
O60927	PPP1R11	2	2	13.952	22.51	4.49249	2.24E+07	1.605	2.69E+05	2.21E+07
Q12972	PPP1R8	22	22	38.478	19.742	4.3032	1.42E+08	3.685	5.20E+06	1.37E+08
Q8WUF5	PPP1R13L	37	37	89.09	18.32	4.19535	8.85E+08	9.932	1.98E+07	8.65E+08
Q9U6Y5	GFP	13	13	28.106	14.689	3.87666	4.12E+09	146.5	7.54E+07	4.04E+09
Q15435	PPP1R7	20	4	41.564	13.393	3.74341	6.63E+08	15.95	1.09E+08	5.54E+08
O14974	PPP1R12A	67	67	115.28	12.695	3.66619	1.68E+09	14.57	7.91E+07	1.60E+09
P62140	PPP1CB	27	11	37.186	11.579	3.53344	4.77E+09	128.2	2.01E+08	4.57E+09
Q9BZL4	PPP1R12C	19	2	84.88	9.5521	3.25582	5.05E+07	0.595	4.96E+06	4.55E+07
P34741	SDC2	3	3	22.16	8.9757	3.16602	4.83E+06	0.218	2.50E+05	4.58E+06
Q6UXN9	WDR82	6	6	35.079	8.9229	3.15751	6.29E+07	1.792	5.51E+06	5.74E+07
Q96KQ4	PPP1R13B	11	10	119.56	8.7837	3.13483	8.35E+06	0.07	8.55E+05	7.50E+06
Q96I34	PPP1R16A	6	6	57.811	8.7809	3.13437	3.99E+07	0.69	5.20E+06	3.47E+07
Q9BZL4		18	1	84.681	7.4767	2.9024	3.05E+06	0.036	3.68E+05	2.68E+06
Q13625	TP53BP2	11	10	125.61	7.3452	2.8768	1.02E+07	0.081	9.02E+05	9.26E+06
Q5DJT8	CT45A2	3	3	21.302	7.333	2.8744	2.41E+07	1.132	2.90E+06	2.12E+07
Q02539	HIST1H1A	16	7	21.842	7.2502	2.85802	6.48E+08	29.69	7.35E+07	5.75E+08
Q96QC0	PPP1R10	9	9	99.057	7.1043	2.82869	8.94E+07	0.902	9.42E+06	7.99E+07
Q9P2K8	EIF2AK4	2	2	186.91	6.9672	2.80058	9.10E+05	0.005	1.59E+05	7.50E+05
P49750	YLPM1	20	20	241.64	6.6216	2.72718	8.64E+07	0.357	1.15E+07	7.49E+07
P16403	HIST1H1C	22	7	21.364	5.8978	2.56018	1.25E+10	584.2	2.03E+09	1.05E+10
O95405	ZFYVE9	3	3	156.4	5.7129	2.51422	2.27E+06	0.014	3.33E+05	1.93E+06
Q8IZ21-2	PHACTR4	23	23	79.128	5.4884	2.45639	9.32E+07	1.178	1.81E+07	7.51E+07
Q9Y625	GPC6	3	2	62.735	5.2038	2.37957	1.07E+07	0.171	1.21E+06	9.50E+06
Q9H175	CSRNP2	7	7	59.591	5.0003	2.32201	7.14E+06	0.12	8.47E+05	6.29E+06
P04908	HIST1H2AB	10	2	14.135	4.8176	2.26831	2.92E+08	20.68	4.95E+07	2.43E+08
O75864	PPP1R37	10	10	74.766	4.624	2.20914	6.26E+06	0.084	1.11E+06	5.16E+06
O75487	GPC4	4	3	62.411	4.3301	2.1144	2.30E+07	0.368	3.19E+06	1.98E+07
P15498	VAV1	1	1	98.313	4.3215	2.11153	5.44E+07	0.553	9.95E+06	4.44E+07
Q04837	SSBP1	3	3	17.259	4.2285	2.08015	2.90E+07	1.679	6.99E+06	2.20E+07
P07305	H1F0	6	6	20.863	4.1944	2.06846	8.12E+08	38.91	2.00E+08	6.12E+08
P12004	PCNA	6	6	28.768	4.029	2.01042	5.00E+07	1.737	1.08E+07	3.92E+07
P18827	SDC1	3	3	32.461	3.9809	1.99309	3.29E+06	0.101	5.98E+05	2.69E+06
P36969	GPX4	3	3	22.192	3.9751	1.99099	1.18E+06	0.053	2.55E+05	9.26E+05
O75531	BANF1	4	4	10.058	3.9192	1.97056	2.76E+08	27.45	5.05E+07	2.26E+08
H0YG33	HSPA1B	17	10	77.405	3.8638	1.95002	9.08E+07	1.173	1.86E+07	7.22E+07
B4DLA9	HIST2H2BF	20	0	14.841	3.7879	1.9214	3.18E+10	2145	7.07E+09	2.48E+10
P35052	GPC1	8	8	61.68	3.7805	1.91858	5.11E+07	0.829	9.52E+06	4.16E+07
Q7Z3T8	ZFYVE16	7	7	168.9	3.747	1.90574	3.28E+06	0.019	6.83E+05	2.60E+06
E9PCS5	CBX1	4	3	21.915	3.7156	1.8936	3.49E+07	1.591	5.75E+06	2.91E+07
P0C0S5	H2AFZ	6	4	13.553	3.7013	1.88803	2.14E+09	157.8	4.39E+08	1.70E+09
P23527	HIST1H2BO	17	0	13.906	3.6747	1.87763	1.52E+09	109.5	3.11E+08	1.21E+09
P12956	XRCC6	7	7	69.842	3.5505	1.82802	4.40E+07	0.63	9.84E+06	3.41E+07
P06733	ENO1	2	2	47.168	3.5471	1.82664	3.73E+06	0.079	9.11E+05	2.82E+06
Q9BS16	CENPK	3	3	31.655	3.5297	1.81955	1.82E+07	0.575	3.50E+06	1.47E+07
P11215	ITGAM	1	1	127.18	3.4968	1.80604	3.60E+08	2.827	8.27E+07	2.77E+08
P13010	XRCC5	9	9	82.704	3.4353	1.78044	5.50E+07	0.665	1.29E+07	4.21E+07
Q92945	KHSRP	9	9	73.114	3.4289	1.77775	7.44E+07	1.017	1.79E+07	5.65E+07
P04406	GAPDH	10	10	36.053	3.3069	1.72548	6.14E+07	1.703	1.91E+07	4.23E+07
Q969G3	SMARCE1	2	2	46.649	3.3033	1.72391	1.31E+07	0.282	2.80E+06	1.03E+07

Continuation …

Uniprot ID	Gene Name	Peptides	Unique Peptides	Mol. weight [kDa]	Ratio H/L	Log Ratio H/L	Intensity	NINT	Intensity L	Intensity H
Q9P0M6	H2AFY2	11	9	40.058	3.2455	1.69844	1.09E+08	2.718	2.66E+07	8.23E+07
Q6FI13	HIST2H2AA3	12	1	14.095	3.2246	1.68912	1.56E+10	1110	3.52E+09	1.21E+10
Q5UIP0	RIF1	2	2	274.46	3.2246	1.68912	4.34E+06	0.016	1.05E+06	3.29E+06
Q8WXX5	DNAJC9	2	2	29.909	3.2066	1.68104	6.27E+06	0.209	1.52E+06	4.74E+06
Q6PL18	ATAD2	8	8	158.55	3.1509	1.65576	9.59E+07	0.605	1.92E+07	7.67E+07
Q03135	CAV1	3	3	20.471	3.1474	1.65416	3.22E+06	0.157	8.32E+05	2.38E+06
Q8TEW0	PARD3	2	2	151.42	3.0916	1.62835	7.62E+05	0.005	1.28E+05	6.34E+05
P0CG48	UBC	5	5	77.028	3.0782	1.62209	2.12E+09	27.5	4.08E+08	1.71E+09
Q13185	CBX3	7	5	20.811	3.0314	1.59998	3.96E+08	19.03	9.06E+07	3.06E+08
Q96T88	UHRF1	3	3	89.813	3.0077	1.58866	1.11E+07	0.124	2.54E+06	8.56E+06
Q03252	LMNB2	20	17	67.688	3.003	1.5864	1.74E+08	2.566	4.96E+07	1.24E+08
O75475	PSIP1	7	6	60.103	2.9481	1.55979	1.05E+08	1.749	3.20E+07	7.32E+07
P11021	HSPA5	23	22	72.332	2.9093	1.54067	1.39E+08	1.926	3.88E+07	1.01E+08
P18754	RCC1	8	8	48.145	2.9027	1.5374	7.84E+07	1.628	2.11E+07	5.73E+07
Q16658	FSCN1	5	5	54.529	2.8915	1.53182	1.08E+07	0.197	2.85E+06	7.90E+06
Q08945	SSRP1	13	13	81.074	2.8875	1.52982	2.34E+08	2.881	6.52E+07	1.68E+08
P62805	HIST1H4A	15	15	11.367	2.8566	1.5143	3.11E+10	2740	8.07E+09	2.31E+10
P11142	HSPA8	32	28	70.897	2.8329	1.50228	9.69E+08	13.67	2.64E+08	7.05E+08
P68431	HIST1H3A	7	1	15.404	2.8233	1.49738	1.13E+10	734.4	3.03E+09	8.28E+09
P16104	H2AFX	8	0	15.144	2.8012	1.48604	1.25E+09	82.34	2.92E+08	9.55E+08
O75367	H2AFY	14	12	39.617	2.7432	1.45586	1.22E+09	30.73	3.23E+08	8.94E+08
P35520	CBS	7	7	61.862	2.7181	1.4426	1.87E+07	0.302	5.14E+06	1.35E+07
P04792	HSPB1	4	4	22.782	2.7088	1.43765	9.44E+06	0.415	2.57E+06	6.87E+06

Table A26. U2OS$^{PP1\beta\text{-}GFP}$ Concatenated Interactome data set. Data above threshold >log median Ratio H:L 1.61 shown.

U2OS^PP1gamma Cytoplasmic (CP)/ Stable cell line

Light: U2OS Heavy: U2OS^GFP-PP1γ

MaxQuant Version: 1.2.7.4

Median log Ratio H/L = -0.877

Threshold (> 1 log median) = 0.123

Uniprot ID	Gene Name	Peptides	Unique Peptides	Mol. weight [kDa]	Ratio H/L	Log Ratio H/L	Intensity	NINT	Intensity L	Intensity H	Ratio H/L Significance B
Q15435	PPP1R7	21	21	41.564	12.28	3.61836	2.3E+09	54.7	3.02E+08	1.97E+09	3.54728E-26
Q6PJW8	CNST	2	2	79.596	9.7	3.27796	2.2E+07	0.28	1.53E+06	2.07E+07	1.30912E-22
Q12972	PPP1R8	18	18	38.478	9.666	3.27293	2.2E+09	58.2	6.97E+07	2.17E+09	1.47075E-22
Q9U6Y5	GFP	11	11	28.106	9.65	3.27059	9.3E+09	331	2.04E+08	9.09E+09	1.55286E-22
Q13268	DHRS2	3	3	27.438	8.047	3.00852	5.6E+07	2.04	5.82E+06	5.02E+07	5.56866E-20
Q96SB3	PPP1R9B	3	3	89.191	7.847	2.9721	1.2E+08	1.37	4.88E+07	7.38E+07	1.22432E-19
P36873	PPP1CC	16	6	38.518	7.61	2.92788	8.3E+09	215	2.05E+08	8.08E+09	3.15631E-19
P41236	PPP1R2	7	7	23.015	6.894	2.78534	3.1E+08	13.4	2.16E+07	2.88E+08	6.21182E-18
Q8IZ21	PHACTR4	4	4	79.128	6.816	2.76882	8.9E+07	1.13	6.60E+06	8.25E+07	8.71182E-18
Q13625	TP53BP2	2	2	125.61	6.685	2.74099	2.4E+07	0.19	2.36E+06	2.14E+07	1.53482E-17
P49750	YLPM1	3	3	241.64	5.82	2.54102	2.9E+07	0.12	3.10E+06	2.56E+07	7.93807E-16
Q8WUF5	PPP1R13L	2	2	89.09	3.287	1.71664	1.5E+07	0.16	3.01E+06	1.15E+07	9.33909E-10
Q9H792	PEAK1	2	2	193.1	3.252	1.70111	1.2E+07	0.06	8.86E+05	1.10E+07	1.17327E-09
P14621	ACYP2	2	2	11.139	1.808	0.85431	1.5E+07	1.35	4.92E+06	1.01E+07	4.1959E-05
Q92945	KHSRP	2	2	73.114	1.589	0.66839	3E+07	0.41	1.17E+07	1.81E+07	0.000252163
P33992	MCM5	12	12	82.285	1.48	0.5655	3.9E+08	4.69	1.62E+08	2.24E+08	0.000629526
P06703	S100A6	3	3	10.18	1.389	0.47425	6.8E+07	6.72	2.91E+07	3.93E+07	0.001353402
P25205	MCM3	22	22	90.98	1.348	0.43125	8.8E+08	9.64	3.66E+08	5.12E+08	0.001912635
P62269	RPS18	2	2	17.718	1.201	0.26472	5.5E+07	3.12	1.77E+07	3.76E+07	0.006675376

Table A27. U2OS$^{GFP\text{-}PP1}\gamma$ Cytoplasmic Interactome data set. Data above threshold >log median Ratio H:L 0.123 shown.

U2OS^PP1gamma Nucleoplasmic (NP)/ Stable cell line

Light: U2OS Heavy: U2OS^GFP-PP1γ

MaxQuant Version: 1.2.7.4

Median log Ratio H/L = -0.683

Threshold (> 1 log median) = 0.317

Uniprot ID	Gene Name	Peptides	Unique Peptides	Mol. weight [kDa]	Ratio H/L	Log Ratio H/L	Intensity	NINT	Intensity L	Intensity H	Ratio H/L Significance B
Q96QC0	PPP1R10	9	9	99.057	10.09	3.33414	7.2E+08	7.23	4.68E+07	6.70E+08	5.86E-22
P49750	YLPM1	46	46	241.64	9.774	3.28899	4.4E+09	18.2	2.86E+08	4.12E+09	1.67E-21
P36873	PPP1CC	13	2	38.518	8.527	3.09199	1.5E+09	39.6	6.20E+07	1.46E+09	1.40E-19
Q9U6Y5	GFP	9	9	28.106	7.547	2.91598	4.6E+09	164	1.29E+08	4.49E+09	6.10E-18
Q96SB3	PPP1R9B	15	15	89.191	7.016	2.81061	2.6E+09	28.9	2.33E+08	2.35E+09	5.37E-17
Q12972	PPP1R8	3	3	38.478	5.796	2.53513	1E+08	2.67	9.55E+06	9.31E+07	1.18E-14
Q13268	DHRS2	5	5	27.438	5.073	2.3429	5.9E+08	21.4	9.02E+07	4.97E+08	3.92E-13
Q6UXN9	WDR82	4	4	35.079	4.318	2.11033	5.3E+08	15.2	1.00E+08	4.33E+08	2.06E-11
P62136	PPP1CA	14	3	37.512	3.615	1.8538	4.9E+09	130	5.47E+08	4.35E+09	1.15E-09
P33947	KDELR2	2	2	24.422	1.561	0.64284	3.8E+07	1.55	1.32E+07	2.47E+07	1.44E-03
P62857	RPS28	2	2	7.8409	1.321	0.40141	1.4E+08	17.8	6.00E+07	8.00E+07	9.08E-03
P08865	RPSA	5	5	32.854	1.272	0.34653	1.6E+09	47.2	6.73E+08	8.79E+08	1.32E-02
Q14444	CAPRIN1	5	5	78.365	1.252	0.32423	2.1E+08	2.65	8.39E+07	1.23E+08	1.53E-02

Table A28. U2OS$^{GFP\text{-}PP1}\gamma$ Nucleoplasmic Interactome data set. Data above threshold >log median Ratio H:L 0.317 shown.

U2OS^PP1gamma Concatenated/ Stable cell line

Light: U2OS Heavy: U2OS^GFP-PP1γ

MaxQuant Version: 1.2.7.4

Median log Ratio H/L = -1.014

Threshold (> 1 log median) = -0.014

Uniprot ID	Gene Name	Peptides	Unique Peptides	Mol. weight [kDa]	Ratio H/L	Log Ratio H/L	Intensity	NINT	Intensity L	Intensity H
Q15435	PPP1R7	19	19	41.564	12.4	3.63227	2.50E+09	60.04	2.94E+08	2.20E+09
Q96QC0	PPP1R10	9	9	99.057	10.09	3.33414	7.65E+08	7.724	5.04E+07	7.15E+08
Q12972	PPP1R8	16	16	38.478	9.666	3.27293	2.23E+09	57.83	7.25E+07	2.15E+09
P49750	YLPM1	47	47	241.64	9.49	3.24641	4.72E+09	19.53	3.06E+08	4.41E+09
Q9U6Y5	GFP	11	11	28.106	8.719	3.1242	1.40E+10	499.3	3.51E+08	1.37E+10
Q96SB3	PPP1R9B	15	15	89.191	7.263	2.86059	2.70E+09	30.28	2.82E+08	2.42E+09
P36873	PPP1CC	18	3	38.518	6.894	2.7854	1.75E+10	453.9	1.36E+09	1.61E+10
Q8IZ21	PHACTR4	4	4	79.128	6.816	2.76882	8.91E+07	1.126	6.60E+06	8.25E+07
Q13625	TP53BP2	2	2	125.61	6.685	2.74099	2.38E+07	0.19	2.36E+06	2.14E+07
P41236	PPP1R2	6	6	23.015	5.969	2.57742	2.03E+08	8.811	1.42E+07	1.89E+08
Q13268	DHRS2	11	11	27.438	5.947	2.57214	4.16E+09	151.5	5.33E+08	3.62E+09
Q9H792	PEAK1	2	2	193.1	4.326	2.113	4.36E+07	0.226	4.51E+06	3.90E+07
Q6UXN9	WDR82	4	4	35.079	4.318	2.11033	5.33E+08	15.18	1.00E+08	4.33E+08
Q8WUF5	PPP1R13L	2	2	89.09	3.287	1.71664	1.45E+07	0.163	3.01E+06	1.15E+07
P14621	ACYP2	2	2	11.139	1.808	0.85431	1.51E+07	1.352	4.92E+06	1.01E+07
P33947	KDELR2	2	2	24.422	1.503	0.58823	1.26E+08	5.172	5.26E+07	7.38E+07
Q5RHS7	S100A2	1	1	15.695	1.393	0.4784	1.52E+07	0.971	6.10E+06	9.14E+06
P62136	PPP1CA	18	3	37.512	1.372	0.45607	2.73E+08	7.268	1.10E+08	1.62E+08
P62857	RPS28	2	2	7.8409	1.319	0.39955	5.02E+08	64.02	2.99E+08	2.03E+08
Q14444	CAPRIN1	5	5	78.365	1.252	0.32423	2.07E+08	2.646	8.39E+07	1.23E+08
P06703	S100A6	2	2	10.18	1.249	0.32124	6.24E+07	6.13	2.66E+07	3.58E+07
A7MAP0	CORO1C	3	3	54.066	1.223	0.29054	5.31E+08	9.821	2.41E+08	2.90E+08
Q15717	ELAVL1	7	7	36.091	1.165	0.21971	1.44E+09	39.8	7.01E+08	7.35E+08
D6REE5	GNB2L1	1	1	34.95	1.162	0.21624	3.14E+08	8.993	1.32E+08	1.82E+08
P61158	ACTR3	1	1	47.371	1.152	0.20364	5.37E+07	1.133	2.47E+07	2.90E+07
P61011	SRP54	2	2	55.704	1.109	0.149	9.32E+07	1.674	4.36E+07	4.97E+07
P31350	RRM2	2	2	44.877	1.064	0.08923	3.57E+07	0.797	1.71E+07	1.87E+07
O15145	ARPC3	2	2	20.546	1.044	0.06267	6.74E+07	3.281	3.17E+07	3.57E+07
P11166	SLC2A1	2	2	54.083	1.038	0.05408	8.14E+07	1.505	3.78E+07	4.36E+07
Q56VL3	OCIAD2	5	5	16.953	1.036	0.05116	9.64E+08	56.88	4.88E+08	4.76E+08
P21359	NF1	2	2	319.37	1.015	0.02134	6.70E+06	0.021	3.23E+06	3.47E+06
P08865	RPSA	6	6	32.854	1.012	0.01778	2.65E+09	80.66	1.44E+09	1.21E+09
P49674	CSNK1E	3	3	47.315	1.009	0.01221	1.87E+08	3.96	8.92E+07	9.82E+07
Q14152	EIF3A	3	3	166.57	1.003	0.00432	1.22E+08	0.734	6.51E+07	5.72E+07
B4DW28	RPS20	3	3	16.005	1	-0.00055	1.16E+09	72.71	6.40E+08	5.24E+08
Q99961	SH3GL1	2	2	41.489	0.994	-0.00806	8.01E+07	1.93	3.49E+07	4.51E+07

Table A29. U2OS$^{GFP\text{-}PP1}\gamma$ Concatenated Interactome data set. Data above threshold >log median Ratio H:L -0.014 shown.

GFP-MYPT1 Concatenated/ U2OS cell transiently transfected

Light: GFP Heavy: GFP-Mypt1

MaxQuant Version: 1.2.7.4

Median log Ratio H/L = -0.202

Threshold (> 1 log median) = 0.798

Uniprot ID	Gene Name	Peptides	Unique Peptides	Mol. weight [kDa]	Ratio H/L	Log Ratio H/L	Intensity	NINT	Intensity L	Intensity H
O14974	PPP1R12A	39	39	115.28	17.07	4.09	9.35E+09	81.11	1.38E+08	9.21E+09
P62140	PPP1CB	15	5	37.186	10.716	3.42	3.75E+09	100.83	1.95E+08	**3.55E+09**
Q69YQ0	SPECC1L	3	3	124.6	5.0524	2.34	4.86E+07	0.39	1.20E+07	3.66E+07
P55201	BRPF1	1	1	138.18	4.7806	2.26	7.02E+06	0.05	6.75E+05	6.34E+06
P11021	HSPA5	16	15	72.332	2.1423	1.10	3.21E+08	4.43	1.06E+08	2.15E+08

Table A30. U2OS transiently transfected with GFP/GFP-Mypt1 Concatenated Interactome data set. Data above threshold >log median Ratio H:L 0.798 shown.

Endogenous-MYPT1 Concatenated/ U2OS cells

Light: Rabbit IgG IP Heavy: Mypt1 IP

Exp#1 MaxQuant Version: 1.2.7.4

Median log Ratio H/L = 2.542

Threshold (> 1 log median) = 3.542

Uniprot ID	Gene Name	Peptides	Unique Peptides	Mol. weight [kDa]	Ratio H/L	Log Ratio H/L	Intensity	NINT	Intensity L	Intensity H
P08590	MYL3	1	1	21.932	34.23	5.09732	1.62E+08	7.387	5.48E+06	1.57E+08
Q9BPX5	ARPC5L	3	3	16.941	33.03	5.04566	5.34E+07	3.155	1.52E+06	5.19E+07
C9JWM7	ARPC4	5	5	21.588	32.87	5.03852	1.34E+08	6.195	4.07E+06	1.30E+08
Q9BTE1	DCTN5	7	7	20.126	32.56	5.02481	7.47E+08	37.1	8.09E+06	7.39E+08
E9PR17	CD59	3	3	14.529	31.88	4.99458	1.62E+08	11.16	4.57E+06	1.58E+08
P27449	ATP6V0C	1	1	15.736	28.88	4.8522	1.44E+08	9.138	4.76E+06	1.39E+08
P61163	ACTR1A	27	17	42.613	28.29	4.82217	8.64E+09	202.7	9.45E+07	8.54E+09
Q13561	DCTN2	27	27	44.23	27.89	4.80147	6.41E+09	144.9	1.99E+08	6.21E+09
O00161	SNAP23	10	10	23.354	27.49	4.78068	4.07E+08	17.45	1.21E+07	3.95E+08
P04908	HIST1H2AB	7	2	14.135	27.46	4.77921	4.72E+08	33.4	1.73E+07	4.55E+08
P67936	TPM4	14	6	28.521	25.82	4.69036	8.81E+07	3.087	2.80E+06	8.53E+07
G3V1S3	DENND5B	1	1	149.34	25.77	4.68773	3.90E+07	0.261	1.47E+06	3.75E+07
P06753	TPM3	22	2	29.032	25.42	4.66812	1.48E+09	51.11	7.66E+07	1.41E+09
E7EP37	MICA	3	3	43.026	24.73	4.62802	2.58E+07	0.599	3.86E+05	2.54E+07
Q14203	DCTN1	80	80	141.69	22.12	4.46695	8.81E+09	62.17	9.03E+07	8.72E+09
D9YZV3	TPM1	23	0	32.736	21.67	4.43769	9.35E+08	28.57	3.99E+07	8.95E+08
H0YDI9	THY1	4	4	18.585	21.31	4.41359	8.83E+08	47.5	3.22E+07	8.51E+08
P06899	HIST1H2BJ	8	2	13.904	21.28	4.41136	7.03E+08	50.59	2.54E+07	6.78E+08
G8JLA2	MYL6	12	10	17.089	21.23	4.40803	1.40E+09	81.72	5.29E+07	1.34E+09
O14950	MYL12B	13	7	19.779	21.18	4.40449	1.84E+09	92.81	7.27E+07	1.76E+09
Q8ND76	CCNY	4	3	39.336	21.07	4.39732	1.42E+07	0.362	7.09E+05	1.35E+07
Q9NYL9	TMOD3	13	13	39.594	21.05	4.39575	4.77E+08	12.05	1.87E+07	4.58E+08
P16070	CD44	5	5	81.537	20.82	4.37969	7.84E+08	9.618	2.72E+07	7.57E+08
H0YK48	TPM1	19	2	28.579	20.77	4.37664	8.45E+07	2.956	3.10E+06	8.14E+07
P62805	HIST1H4A	14	14	11.367	20.28	4.34199	8.76E+09	770.9	3.83E+08	8.38E+09
P63261	ACTG1	29	2	41.792	20.13	4.3312	1.81E+10	432.2	7.00E+08	1.74E+10
P58107	EPPK1	8	1	555.61	20.08	4.32776	9.71E+07	0.175	4.61E+06	9.25E+07
P07951	TPM2	16	5	32.989	19.76	4.30415	4.19E+07	1.27	1.76E+06	4.01E+07
P62140	PPP1CB	14	7	37.186	19.13	4.25799	8.19E+08	22.03	1.71E+07	8.02E+08
A7MAP0	CORO1C	10	10	54.066	19.11	4.25603	6.24E+08	11.55	2.50E+07	5.99E+08
H0Y7A7	CALM2	7	7	20.762	19.03	4.2499	2.39E+08	11.52	1.00E+07	2.29E+08
Q9NZ32	ACTR10	16	16	46.306	19.02	4.24975	8.06E+08	17.41	6.41E+07	7.42E+08
P0C0S5	H2AFZ	5	3	13.553	18.78	4.23128	7.76E+08	57.23	3.41E+07	7.42E+08
P04156	PRNP	3	3	27.661	18.77	4.23036	9.09E+07	3.285	2.91E+06	8.80E+07
Q15149	PLEC	319	4	531.78	18.72	4.22628	4.41E+10	82.93	2.20E+09	4.19E+10
Q9UNN8	PROCR	2	2	26.671	18.7	4.22489	2.81E+07	1.054	1.10E+06	2.70E+07
P16104	H2AFX	5	0	15.144	18.57	4.21506	4.29E+07	2.831	2.14E+06	4.07E+07
P05783	KRT18	25	24	48.057	18.56	4.21389	5.34E+09	111	2.75E+08	5.06E+09
Q5TEC6	HIST2H3PS2	3	1	15.43	18.54	4.21265	1.95E+08	12.62	6.52E+06	1.88E+08
Q9UJW0	DCTN4	29	29	52.337	18.45	4.20578	2.39E+09	45.71	4.28E+07	2.35E+09
P0C0S8	HIST1H2AG	8	3	14.091	18.27	4.19172	5.41E+09	383.6	2.55E+08	5.15E+09
Q0ZGT2	NEXN	13	1	79.361	18.03	4.17265	1.78E+08	2.243	8.88E+06	1.69E+08
P08670	VIM	62	58	53.651	17.86	4.15866	4.49E+10	836	2.31E+09	4.25E+10
Q16643	DBN1	14	14	71.428	17.84	4.15737	1.36E+09	19.09	4.07E+07	1.32E+09
O14974	PPP1R12A	46	46	115.28	17.82	4.15502	8.50E+09	73.77	1.28E+08	8.38E+09
O00159	MYO1C	57	1	117.91	17.51	4.13044	6.98E+09	59.22	3.91E+08	6.59E+09
P52907	CAPZA1	15	13	32.922	17.48	4.12739	6.87E+08	20.86	1.92E+07	6.68E+08
Q8N3V7	SYNPO	16	16	96.395	17.06	4.09238	2.25E+08	2.329	1.28E+07	2.12E+08
P35579	MYH9	127	109	226.53	16.77	4.06807	1.28E+10	56.59	6.12E+08	1.22E+10

Continuation …

Uniprot ID	Gene Name	Peptides	Unique Peptides	Mol. weight [kDa]	Ratio H/L	Log Ratio H/L	Intensity	NINT	Intensity L	Intensity H
P48681	NES	41	41	177.44	16.77	4.06738	6.30E+08	3.55	3.97E+07	5.90E+08
B7Z1Z5	NTM	6	6	39.209	16.5	4.04422	3.47E+08	8.84	1.48E+07	3.32E+08
Q96IZ0	PAWR	1	1	36.567	16.5	4.04422	9.01E+06	0.246	2.93E+05	8.72E+06
F5H4U5	GNAI2	13	7	41.13	16.39	4.03448	4.03E+08	9.797	1.92E+07	3.84E+08
O95816	BAG2	3	3	23.772	16.38	4.03351	3.11E+07	1.307	2.07E+06	2.90E+07
P15328	FOLR1	3	3	29.819	16.35	4.03078	1.44E+07	0.484	8.75E+05	1.36E+07
F5GXF7	ZNF185	9	9	76.856	16.23	4.02086	1.05E+08	1.368	6.98E+06	9.82E+07
Q03135	CAV1	4	1	17.023	16.05	4.00468	8.46E+07	4.97	4.99E+06	7.96E+07
E9PK25	CFL1	2	2	22.728	15.85	3.9865	6.65E+07	2.925	4.17E+06	6.23E+07
Q69YQ0	SPECC1L	37	37	124.6	15.7	3.97242	9.06E+08	7.274	3.86E+07	8.68E+08
Q01082	SPTBN1	67	67	274.61	15.15	3.92125	7.76E+08	2.827	4.45E+07	7.32E+08
Q8N5C8	TAB3	1	1	78.682	15.06	3.91294	8.09E+07	1.028	4.91E+06	7.60E+07
P50479	PDLIM4	3	3	35.398	14.73	3.8802	2.04E+07	0.577	1.55E+06	1.89E+07
B4DR52	HIST2H2BF	9	3	18.041	14.66	3.87332	7.49E+09	415.4	3.64E+08	7.13E+09
O75326	SEMA7A	9	9	74.823	14.56	3.86404	1.13E+08	1.511	5.42E+06	1.08E+08
P61225	RAP2B	6	5	20.504	14.31	3.83885	4.18E+07	2.038	3.05E+06	3.87E+07
P35580	MYH10	93	72	229	14.28	3.83603	2.04E+09	8.901	1.17E+08	1.92E+09
E7EMK3	FLOT2	13	13	53.137	14.18	3.82558	2.28E+08	4.299	1.29E+07	2.16E+08
P09382	LGALS1	6	6	14.716	14.15	3.82222	6.43E+07	4.37	3.75E+06	6.06E+07
E9PGC8	MAP1A	23	22	331.25	14.09	3.8167	2.65E+08	0.799	5.11E+06	2.60E+08
O43707	ACTN4	37	25	104.85	13.98	3.80498	1.25E+09	11.94	7.48E+07	1.18E+09
P42025	ACTR1B	20	10	42.293	13.88	3.79535	2.16E+09	50.96	3.23E+08	1.83E+09
F8VXB4	KRT8	40	33	56.608	13.82	3.78889	1.15E+10	203.2	6.18E+08	1.09E+10
Q13242	SRSF9	3	2	25.542	13.55	3.76065	5.86E+06	0.229	3.81E+05	5.48E+06
Q562R1	ACTBL2	5	1	42.003	13.54	3.75916	3.47E+07	0.825	1.99E+06	3.27E+07
P08754	GNAI3	13	7	40.532	13.54	3.75862	9.83E+07	2.425	4.30E+06	9.40E+07
Q13813	SPTAN1	95	95	284.54	13.4	3.74427	1.42E+09	4.978	1.18E+08	1.30E+09
Q03135	CAV1	6	3	20.471	13.4	3.74395	2.51E+08	12.24	1.68E+07	2.34E+08
P11142	HSPA8	24	20	70.897	13.37	3.74082	6.31E+08	8.897	4.46E+07	5.86E+08
P02786	TFRC	4	4	84.87	13.18	3.72039	8.54E+06	0.101	8.08E+05	7.74E+06
E7EW20	MYO6	31	31	148.83	12.9	3.6893	3.78E+08	2.538	3.31E+07	3.45E+08
Q9H0B6	KLC2	26	18	68.934	12.9	3.68919	2.53E+08	3.671	1.17E+07	2.41E+08
F5GWP8	JUP	22	0	66.35	12.76	3.67356	1.81E+09	27.33	1.88E+08	1.63E+09
O75367	H2AFY	9	7	39.617	12.56	3.65042	8.58E+07	2.166	4.75E+06	8.11E+07
P22626	HNRNPA2B1	4	4	37.429	12.55	3.6495	2.58E+07	0.689	2.20E+06	2.36E+07
G5E9E7	TJP1	29	1	189.67	12.48	3.64097	2.83E+08	1.492	2.64E+07	2.57E+08
Q9Y277	VDAC3	6	6	30.658	12.33	3.62433	7.79E+07	2.54	5.13E+06	7.27E+07
O94832	MYO1D	33	33	116.2	12.29	3.61894	3.98E+08	3.421	2.87E+07	3.69E+08
P61160	ACTR2	8	8	44.76	12.14	3.60193	6.15E+07	1.375	3.79E+06	5.78E+07
Q14126	DSG2	14	14	122.29	11.94	3.57785	2.20E+08	1.801	2.06E+07	2.00E+08
O75935	DCTN3	14	14	21.119	11.88	3.57058	4.76E+09	225.2	5.17E+07	4.70E+09
P33176	KIF5B	29	29	109.68	11.84	3.56584	1.69E+08	1.538	2.19E+07	1.47E+08
Q8IVF2	AHNAK2	9	9	616.62	11.8	3.56035	2.44E+07	0.04	2.39E+06	2.20E+07
E7EQ40	CAPZB	19	19	37.455	11.76	3.55545	1.30E+09	34.67	4.18E+07	1.26E+09
P11021	HSPA5	25	24	72.332	11.72	3.55078	5.00E+08	6.906	3.87E+07	4.61E+08
P11182	DBT	3	3	53.486	11.72	3.55065	9.44E+06	0.177	4.03E+05	9.04E+06
Q13595	TRA2A	3	3	32.688	11.68	3.54535	1.15E+07	0.351	9.81E+05	1.05E+07
Q1HE25	ACTN1	36	24	105.57	11.66	3.54325	1.00E+09	9.508	5.75E+07	9.46E+08

Table A31. Endogenous Mypt1 Concatenated Interactome data set. Data above threshold >log median Ratio H:L 3.542 shown.

U2OS^Specc1L-GFP Concatenated/ Stable cell line

Light: U2OS^GFP Heavy: U2OS^Specc1L-GFP

Exp#2 MaxQuant Version: 1.2.7.4

Median log Ratio H/L = 0.135

Threshold (> 1 log median) = 1.135

Uniprot ID	Gene Name	Peptides	Unique Peptides	Mol. weight [kDa]	Ratio H/L	Log Ratio H/L	Intensity	NINT	Intensity L	Intensity H
P08590	MYL3	1	1	21.932	30.99	4.95364	4.05E+09	184.78	1.19E+08	3.93E+09
G8JLL9	MYH14	6	1	232.04	25.08	4.64824	1.60E+09	6.9001	5.80E+07	1.54E+09
B7Z6Z4	MYL6	8	6	26.707	24.41	4.60928	2.49E+10	931.7	9.59E+08	2.39E+10
O14950	MYL12B	13	1	19.779	22.96	4.5213	1.60E+10	810	4.82E+08	1.55E+10
Q69YQ0	SPECC1L	67	67	124.6	20.26	4.34035	5.88E+10	471.95	1.16E+09	5.76E+10
P35579	MYH9	138	120	226.53	19.2	4.26318	2.78E+11	1228.9	1.10E+10	2.67E+11
E9PR17	CD59	3	3	14.529	15.51	3.95541	1.86E+09	127.85	1.22E+08	1.74E+09
P07951	TPM2	19	8	32.989	13.23	3.72552	4.81E+09	145.83	1.90E+08	4.62E+09
P19105	MYL12A	13	1	19.794	12.52	3.64605	1.60E+08	8.0585	7.57E+06	1.52E+08
H0YDI9	THY1	4	4	18.585	12.07	3.59323	2.42E+09	130.47	1.86E+08	2.24E+09
F5H1B6	PPP1R12A	12	12	115.26	11.45	3.51665	1.50E+09	12.986	1.28E+08	1.37E+09
P16070	CD44	1	1	81.537	11.28	3.49557	3.02E+08	3.7089	3.08E+07	2.72E+08
Q9NYL9	TMOD3	12	12	39.594	10.58	3.40272	2.51E+09	63.51	1.60E+08	2.35E+09
O00159	MYO1C	53	52	121.68	10.56	3.4004	2.66E+10	218.66	2.03E+09	2.46E+10
D9YZV3	TPM1	16	2	32.736	8.937	3.15976	1.49E+09	45.629	1.71E+08	1.32E+09
F8W6L6	MYH10	69	51	230.77	8.903	3.15424	1.23E+10	53.196	1.01E+09	1.13E+10
O94832	MYO1D	16	16	116.2	8.831	3.14258	1.76E+09	15.168	2.24E+08	1.54E+09
O43795	MYO1B	25	23	131.98	6.99	2.80527	2.74E+09	20.795	2.79E+08	2.47E+09
Q9UPQ0	LIMCH1	6	6	121.87	5.702	2.51139	4.74E+08	3.8932	1.17E+08	3.58E+08
Q6WCQ1	MPRIP	13	8	118.1	5.508	2.46163	1.06E+09	9.0093	1.56E+08	9.08E+08
E7EW20	MYO6	10	10	148.83	5.474	2.4527	1.06E+09	7.1189	1.94E+08	8.65E+08
Q71DI3	HIST2H3A	4	2	15.388	5.166	2.36916	8.50E+09	552.26	3.11E+09	5.39E+09
Q15149		266	1	516.19	4.94	2.30439	2.03E+11	392.84	3.54E+10	1.67E+11
P08670	VIM	47	44	53.651	4.602	2.20236	1.45E+11	2695.6	2.50E+10	1.20E+11
P14923	JUP	2	2	81.744	3.89	1.95962	1.51E+08	1.8455	5.23E+07	9.86E+07
P05783	KRT18	19	17	48.057	3.869	1.952	5.58E+09	116.16	1.23E+09	4.36E+09
B7Z596	TPM1	12	2	31.753	3.806	1.92839	4.80E+08	15.131	9.00E+07	3.90E+08
O43707	ACTN4	23	11	104.85	3.702	1.88815	1.62E+09	15.472	8.27E+08	7.95E+08
G3V1L9	TJP1	8	8	197.46	3.64	1.86386	3.88E+08	1.9627	8.84E+07	2.99E+08
F8VXB4	KRT8	20	14	56.608	3.54	1.82375	4.83E+09	85.292	1.04E+09	3.79E+09
Q13045	FLII	2	2	144.75	3.407	1.76854	5.64E+07	0.3898	1.15E+07	4.50E+07
P51911	CNN1	10	10	33.17	3.398	1.76469	1.90E+09	57.275	4.44E+08	1.46E+09
Q01082	SPTBN1	47	47	274.61	3.347	1.74287	6.81E+09	24.805	1.64E+09	5.17E+09
P62879	GNB2	4	2	37.331	3.314	1.72836	8.73E+08	23.38	1.94E+08	6.79E+08
E9PEB9	DST	2	2	880.55	3.209	1.68208	3.69E+07	0.0419	1.01E+07	2.68E+07
P67936	TPM4	13	5	28.521	3.181	1.66925	1.53E+09	53.55	3.79E+08	1.15E+09
A6NG51	SPTAN1	75	75	284.94	3.107	1.63552	1.20E+10	42.198	2.98E+09	9.05E+09
Q1HE25	ACTN1	34	22	105.57	3.072	1.61904	6.55E+09	62.085	1.57E+09	4.99E+09
Q15149		265	1	518.03	3.058	1.61259	3.68E+08	0.7097	7.49E+07	2.93E+08
P62873	GNB1	4	2	37.377	3.05	1.60881	3.44E+08	9.1992	8.53E+07	2.59E+08
O15511	ARPC5	2	1	16.631	2.979	1.57473	1.58E+08	9.522	4.26E+07	1.16E+08
P23284	PPIB	2	2	23.742	2.969	1.57003	1.38E+08	5.8272	5.00E+07	8.83E+07
F5H4U5	GNAI2	8	5	41.13	2.847	1.50934	1.42E+09	34.537	3.56E+08	1.06E+09
Q9NS25	SPANXB1	2	2	11.826	2.799	1.48471	2.60E+07	2.1955	6.70E+06	1.93E+07
P37802	TAGLN2	10	10	22.391	2.78	1.47493	4.33E+09	193.19	1.17E+09	3.16E+09
H0Y7A7	CALM2	2	2	20.762	2.755	1.46216	3.65E+08	17.561	6.60E+07	2.99E+08
Q96SB3	PPP1R9B	2	2	89.191	2.669	1.41652	2.00E+08	2.2388	6.02E+07	1.39E+08
Q92621	NUP205	4	4	227.92	2.646	1.40387	1.54E+08	0.6758	8.01E+07	7.39E+07
O95425	SVIL	2	2	200.84	2.624	1.39188	1.10E+08	0.5456	2.84E+07	8.12E+07
Q9BUJ2	HNRNPUL1	4	4	95.737	2.581	1.36787	3.45E+08	3.5989	9.54E+07	2.49E+08
O75381	PEX14	3	3	41.236	2.557	1.3544	2.57E+08	6.2319	6.42E+07	1.93E+08
P09651	HNRNPA1	4	4	38.746	2.531	1.33965	1.18E+09	30.488	3.24E+08	8.57E+08

Continuation …

Uniprot ID	Gene Name	Peptides	Unique Peptides	Mol. weight [kDa]	Ratio H/L	Log Ratio H/L	Intensity	NINT	Intensity L	Intensity H
C9JWM7	ARPC4	4	1	21.588	2.504	1.32406	8.40E+08	38.898	2.54E+08	5.86E+08
Q8IVF2	AHNAK2	2	2	616.62	2.503	1.32337	1.00E+08	0.1626	2.49E+07	7.54E+07
Q9H583	HEATR1	4	4	242.37	2.484	1.31284	8.75E+07	0.3612	2.44E+07	6.31E+07
P31942	HNRNPH3	3	3	36.926	2.445	1.28995	3.16E+08	8.5441	1.00E+08	2.16E+08
P17096	HMGA1	2	2	10.679	2.371	1.24531	1.54E+08	14.39	3.87E+07	1.15E+08
P06753	TPM3	23	12	29.032	2.364	1.24092	1.83E+10	630.65	5.22E+09	1.31E+10
P61158	ACTR3	5	5	47.371	2.361	1.23934	5.68E+08	11.994	1.77E+08	3.91E+08
O15145	ARPC3	3	3	20.546	2.336	1.22416	3.71E+08	18.064	1.12E+08	2.59E+08
P22626	HNRNPA2B1	11	11	37.429	2.286	1.19283	1.61E+09	43.017	5.02E+08	1.11E+09
B2ZZ83	FLNB	95	87	281.63	2.271	1.1832	2.17E+10	76.881	6.73E+09	1.49E+10
P38646	HSPA9	12	12	73.68	2.264	1.17894	8.52E+08	11.562	4.38E+08	4.14E+08
Q14315	FLNC	56	49	291.02	2.246	1.16729	7.27E+09	24.984	2.31E+09	4.96E+09
P62140	PPP1CB	9	4	37.186	2.225	1.15355	1.14E+09	30.74	3.55E+08	7.88E+08
P07195	LDHB	2	2	36.638	2.217	1.14841	1.73E+07	0.4729	5.23E+06	1.21E+07
E7EQ40	CAPZB	12	12	37.455	2.205	1.14071	3.49E+09	93.096	1.07E+09	2.41E+09

Table A32. U2OS$^{Specc1L\text{-}GFP}$ Concatenated Interactome data set. Data above threshold >log median Ratio H:L 1.135 shown.

MycBirA-Specc1L/1-890 / U2OS cell transiently transfected
Light: GFP-Specc1L/1-890 Heavy: MycBirA-Specc1L/1-890
MaxQuant Version: 1.2.7.4
Median log Ratio H/L =0.778
Threshold (> 1 log median) =1.778

Uniprot ID	Gene Name	Peptides	Unique Peptides	Mol. weight [kDa]	Ratio H/L	Log Ratio H/L	Intensity	NINT	Intensity L	Intensity H	In Gringras BG
Q69YQ0	SPECC1L	63	63	124.6	24.37	4.60715	2.94E+10	236	4.12E+08	2.90E+10	NO
Q9BR76	CORO1B	3	3	54.234	18.56	4.21405	4.36E+07	0.805	2.97E+06	4.07E+07	some tagged
P21333	FLNA	109	17	280.74	15.97	3.99693	1.56E+10	55.57	8.76E+08	1.47E+10	lots tagged
Q8WUH6	C12orf23	2	2	11.748	13	3.70011	2.60E+07	2.215	1.41E+06	2.46E+07	a few BirA
P31431	SDC4	4	4	21.641	11.04	3.4648	1.66E+08	7.692	1.15E+07	1.55E+08	NO
P18827	SDC1	3	3	32.461	10.51	3.39383	3.49E+07	1.075	2.11E+06	3.28E+07	NO
O00468	AGRN	35	35	214.84	10.01	3.32265	8.32E+08	3.874	6.90E+07	7.63E+08	NO
P35052	GPC1	12	12	61.68	9.858	3.30125	3.42E+08	5.541	4.70E+07	2.95E+08	NO
Q14978	NOLC1	16	16	73.744	9.81	3.2943	1.46E+09	19.74	1.29E+08	1.33E+09	lots
P34741	SDC2	7	7	22.16	8.947	3.16139	1.59E+08	7.189	9.20E+06	1.50E+08	NO
G5E9Q2	CSDE1	2	2	93.741	8.935	3.15944	5.50E+07	0.587	4.89E+06	5.02E+07	a few tagged
E7EVA0	MAP4	11	11	245.44	8.338	3.05968	6.02E+08	2.454	3.81E+08	2.21E+08	2-3 peps BirA alone
A8MZ22	NAP1L4	5	4	44.162	7.808	2.96503	3.20E+07	0.724	3.30E+06	2.87E+07	a few tagged
P38432	COIL	6	6	62.608	7.081	2.82403	8.62E+07	1.377	1.03E+07	7.59E+07	some tagged
E7EX17	EIF4B	3	3	69.697	6.465	2.69272	1.75E+07	0.251	1.38E+06	1.61E+07	some tagged
P98160	HSPG2	12	12	468.83	5.951	2.57306	8.28E+07	0.177	9.92E+06	7.29E+07	NO
Q09666	AHNAK	82	82	629.09	5.795	2.53481	1.87E+09	2.971	2.18E+08	1.65E+09	a few tagged
P37802	TAGLN2	5	5	22.391	5.733	2.51919	8.17E+07	3.651	1.16E+07	7.02E+07	several
A7MAP0	CORO1C	4	4	54.066	5.674	2.50444	3.09E+07	0.571	2.73E+06	2.82E+07	several tagged
A8MV58	DBN1	2	2	76.299	5.179	2.37273	1.64E+07	0.216	1.98E+06	1.45E+07	lots tagged
Q86V48	LUZP1	7	7	120.27	5.056	2.33808	3.26E+07	0.271	4.77E+06	2.78E+07	NO
Q8NC51	SERBP1	2	2	44.965	4.981	2.31635	5.68E+06	0.126	8.02E+05	4.88E+06	lots
Q14008	CKAP5	3	3	226.25	4.882	2.28747	1.69E+07	0.075	1.95E+06	1.49E+07	NO
Q14847	LASP1	2	2	36.014	4.678	2.22602	3.76E+06	0.104	6.03E+05	3.16E+06	NO
Q9P0K7	RAI14	5	5	110.42	4.53	2.17954	1.95E+07	0.177	2.50E+06	1.70E+07	a few NLS
Q13283	G3BP1	2	2	52.164	4.102	2.03629	1.09E+07	0.208	2.14E+06	8.71E+06	NO
P09382	LGALS1	6	6	14.716	3.972	1.98968	2.84E+08	19.31	5.17E+07	2.32E+08	NO
E7EUU4	EIF4G1	11	11	171.64	3.937	1.97699	8.02E+07	0.467	2.11E+07	5.91E+07	several tagged
P50990	CCT8	10	10	59.62	3.754	1.90847	9.67E+07	1.622	2.07E+07	7.60E+07	lots
P55209	NAP1L1	3	2	45.374	3.641	1.86437	2.38E+07	0.526	4.47E+06	1.94E+07	several
O75526	RBMXL2	2	2	42.814	3.633	1.86096	8.85E+06	0.207	2.28E+06	6.57E+06	NO
E9PRY8	EEF1D	2	2	76.569	3.534	1.82147	3.65E+07	0.476	7.70E+06	2.88E+07	a few
P19338	NCL	2	2	76.613	3.469	1.7946	1.37E+07	0.179	3.22E+06	1.05E+07	lots

Table A33. U2OS transiently transfected with GFP-Specc1L1-890/ MycBirA-Specc1L1-890 Concatenated Interactome data set. Data above threshold >log median Ratio H:L 1.778 shown.

APPENDIX III

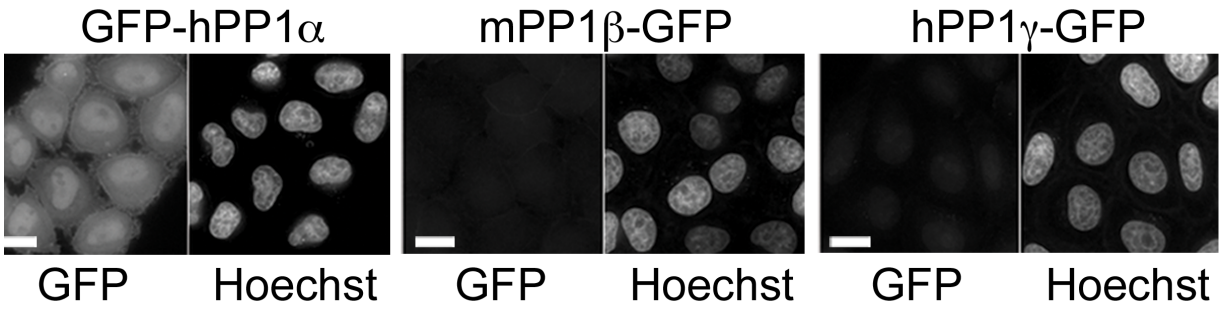

Figure A.1. PP1α is the most highly expressed isoform in the BAC cell lines. Live images acquired of the GFP-tagged PP1 isoforms expressed in their respective BAC cell lines, which were stained with the permeable DNA dye Hoechst. The same acquisition parameters were utilized (40x/1.35NA objective, bin 1x1, 1 sec exposure Ex490/20 and Em 525/36 for GFP and 0.2 sec exposure Ex402/15 and Em455/50 for Hoechst) and the images were deconvolved and displayed using the same intensity scales.

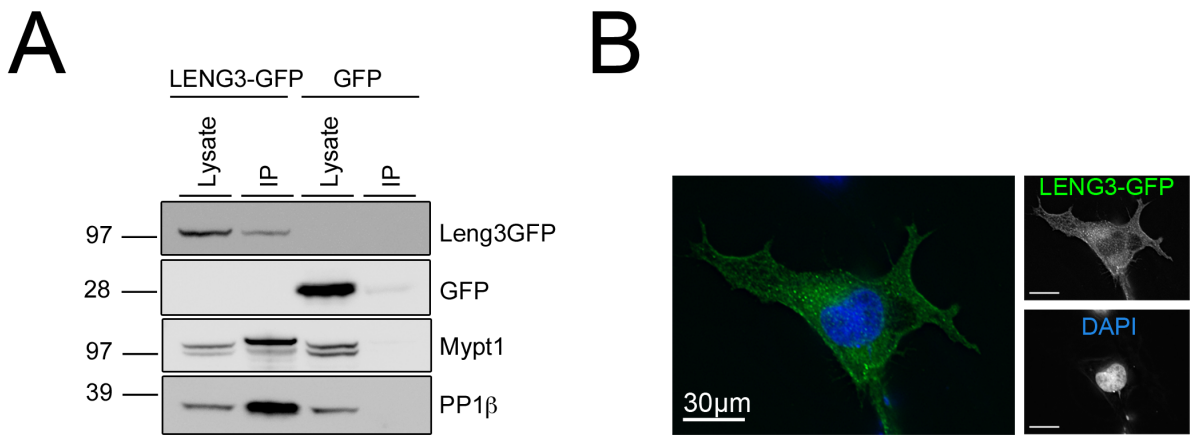

Figure A.2. In vivo association of the MYPT family members Mypt1 and Leng3. A. Western blot analysis demonstrating the co-purification of endogenous Mypt1 (anti-Mypt1, Bethyl Lab.) with GFP-tagged LENG3 (anti-GFP) confirmed the in vivo association highlighted in the Mypt1 interactome datasets. **B.** HeLa cells transiently expressing LENG3-GFP (green) were PFA-fixed and stained with DAPI (blue).

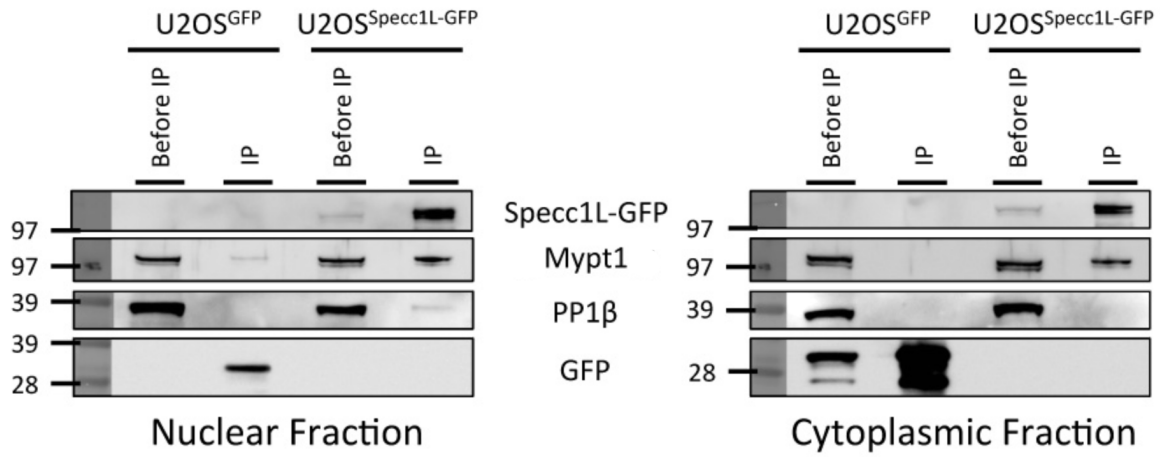

Figure A.3. Specc1L co-precipitates PP1. Western blot analysis demonstrating co-purification of endogenous Mypt1 (anti-Mypt1; Bethyl Labs) with Specc1L-GFP (anti-GFP; Roche) from nuclear and cytoplasmic extracts prepared from the U2OSSpecc1L-GFP stable cell line. In addition, a PP1 band was detected in the pulldown from the nuclear extract.

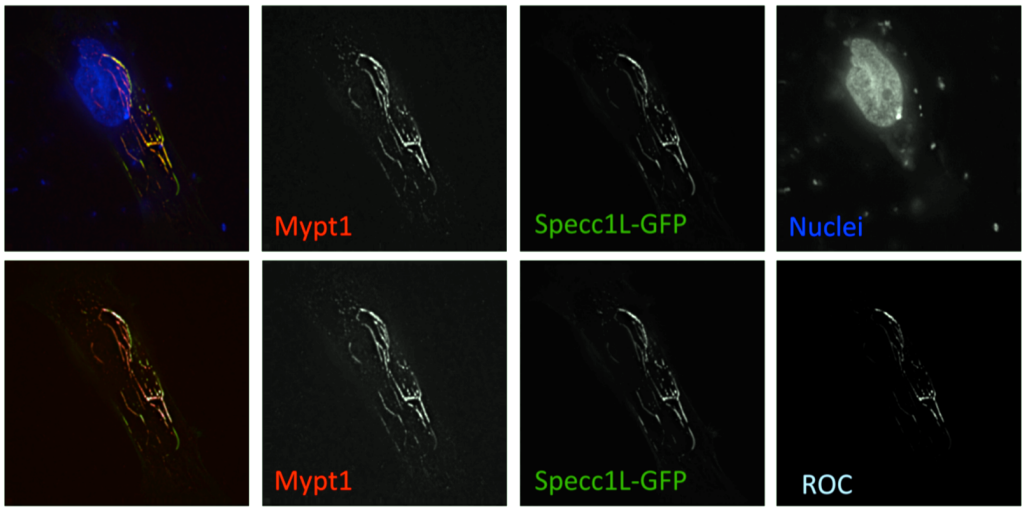

Figure A.4. Mypt1 is recruited to the microtubule (MT) bundles. Endogenous Mypt1 (red) is recruited to the MT bundles induced by transient overexpression of Specc1L-GFP (green) in U2OS cells that were PFA-fixed and stained with DAPI (blue). The region of colocalization (ROC) between Mypt1 and Specc1L is shown in the bottom right panel.

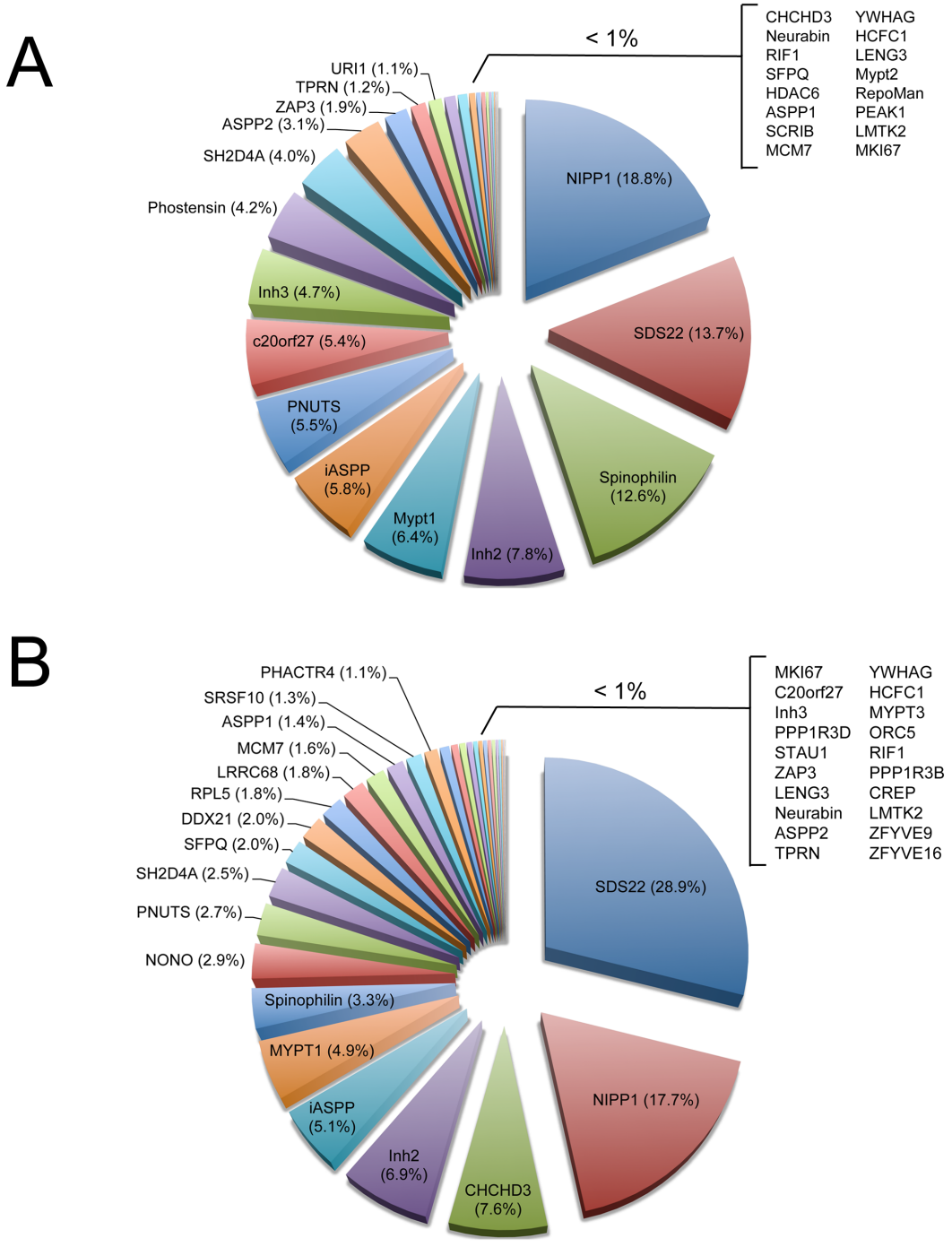

Figure A.5. Distribution of PP1c between all identified regulatory subunits in the direct isoform interacome comparison screens. The pie charts shows the relative distribution of all known/predicted regulatory subunits identified in the concatenated analysis of the CP and NUC datasets for GFP-PP1α vs. PP1β-GFP vs. GFP-PP1γ pulled down from stably expressing HeLa/BAC (A) and MCF7/cDNA (B) cell lines. Values are the % of the total pool of regulatory subunits (based on normalized intensity values) that each represents. For the lists to the right, these values were less that 1%.

REFERENCES

Aggen, J.B., Nairn, A.C. & Chamberlin, R., 2000. Regulation of protein phosphatase-1. *Chemistry & biology*, 7(1), pp.R13–23.

Akhmanova, A. & Steinmetz, M.O., 2008. Tracking the ends: a dynamic protein network controls the fate of microtubule tips. *Nature reviews. Molecular cell biology*, 9(4), pp.309–322.

Alessi, D. et al., 1992. The control of protein phosphatase-1 by targetting subunits. The major myosin phosphatase in avian smooth muscle is a novel form of protein phosphatase-1. *European journal of biochemistry / FEBS*, 210(3), pp.1023–1035.

Allen, P.B. et al., 1998. Isolation and characterization of PNUTS, a putative protein phosphatase 1 nuclear targeting subunit. *The Journal of biological chemistry*, 273(7), pp.4089–4095.

Alonso, A. et al., 2004. Protein tyrosine phosphatases in the human genome. *Cell*, 117(6), pp.699–711.

Amano, M. et al., 2003. Identification of Tau and MAP2 as novel substrates of Rho-kinase and myosin phosphatase. *Journal of neurochemistry*, 87(3), pp.780–790.

Amano, M., Fukata, Y. & Kaibuchi, K., 2000. Regulation and functions of Rho-associated kinase. *Experimental cell research*, 261(1), pp.44–51.

Andersen, J.N. et al., 2005. Computational analysis of protein tyrosine phosphatases: practical guide to bioinformatics and data resources. *Methods (San Diego, Calif.)*, 35(1), pp.90–114.

Anderson, T.W., Vaughan, A.N. & Cramer, L.P., 2008. Retrograde flow and myosin II activity within the leading cell edge deliver F-actin to the lamella to seed the formation of graded polarity actomyosin II filament bundles in migrating fibroblasts. *Molecular biology of the cell*, 19(11), pp.5006–5018.

Andreassen, P.R. et al., 1998. Differential subcellular localization of protein phosphatase-1 alpha, gamma1, and delta isoforms during both interphase and mitosis in mammalian cells. *The Journal of cell biology*, 141(5), pp.1207–1215.

Andresen, C.A. et al., 2014. Protein interaction screening for the ankyrin repeats and suppressor of cytokine signaling (SOCS) box (ASB) family identify Asb11 as a novel endoplasmic reticulum resident ubiquitin ligase. *The Journal of biological chemistry*, 289(4), pp.2043–2054.

Attwood, P.V. et al., 2007. Focus on phosphohistidine. *Amino acids*, 32(1), pp.145–156.

Azevedo, C., Livermore, T. & Saiardi, A., 2015. Protein polyphosphorylation of lysine residues by inorganic polyphosphate. *Molecular Cell*, 58(1), pp.71–82.

Barker, H.M. et al., 1993. Sequence of human protein serine/threonine phosphatase 1 gamma and localization of the gene (PPP1CC) encoding it to chromosome bands 12q24.1-q24.2. *Biochimica et biophysica acta*, 1178(2), pp.228–233.

Barker, H.M. et al., 1994. Three genes for protein phosphatase 1 map to different human chromosomes: sequence, expression and gene localisation of protein serine/threonine phosphatase 1 beta (PPP1CB). *Biochimica et biophysica acta*, 1220(2), pp.212–218.

Bennett, D. & Alphey, L., 2002. PP1 binds Sara and negatively regulates Dpp signaling in Drosophila melanogaster. *Nature genetics*, 31(4), pp.419–423.

Bennett, D. et al., 2006. Towards a comprehensive analysis of the protein phosphatase 1 interactome in Drosophila. *Journal of molecular biology*, 364(2), pp.196–212.

Berg, J.S., Powell, B.C. & Cheney, R.E., 2001. A millennial myosin census. *Molecular biology of the cell*, 12(4), pp.780–794.

Bhoj, E.J. et al., 2015. Expanding the SPECC1L mutation phenotypic spectrum to include Teebi hypertelorism syndrome. *American journal of medical genetics. Part A*, 167A(11), pp.2497–2502.

Bollen, M., 2001. Combinatorial control of protein phosphatase-1. *Trends in biochemical sciences*, 26(7), pp.426–431.

Bollen, M. et al., 2010. The extended PP1 toolkit: designed to create specificity. *Trends in biochemical sciences*, 35(8), pp.450–458.

Booth, D.G. et al., 2014. Ki-67 is a PP1-interacting protein that organises the mitotic chromosome periphery. *eLife*, 3, p.e01641.

Boudrez, A. et al., 1999. Identification of MYPT1 and NIPP1 as subunits of protein phosphatase 1 in rat liver cytosol. *FEBS letters*, 455(1-2), pp.175–178.

Boudrez, A. et al., 2000. NIPP1-mediated interaction of protein phosphatase-1 with CDC5L, a regulator of pre-mRNA splicing and mitotic entry. *The Journal of biological chemistry*, 275(33), pp.25411–25417.

Boyer, P.D. et al., 1962. Identification of phosphohistidine in digests from a probable intermediate of oxidative phosphorylation. *The Journal of biological chemistry*, 237, pp.PC3306–PC3308.

Brendel, C. et al., 2004. Characterization of Staufen 1 ribonucleoprotein complexes. *The Biochemical journal*, 384(Pt 2), pp.239–246.

Brower, C.S., Piatkov, K.I. & Varshavsky, A., 2013. Neurodegeneration-associated protein fragments as short-lived substrates of the N-end rule pathway. *Molecular Cell*, 50(2), pp.161–171.

Brozovich, F.V., 2002. Myosin light chain phosphatase: it gets around. *Circulation research*, 90(5), pp.500–502.

Bruinsma, W., Raaijmakers, J.A. & Medema, R.H., 2012. Switching Polo-like kinase-1 on and off in time and space. *Trends in biochemical sciences*, 37(12), pp.534–542.

Brush, M.H., Weiser, D.C. & Shenolikar, S., 2003. Growth arrest and DNA damage-inducible protein GADD34 targets protein phosphatase 1 alpha to the endoplasmic reticulum and promotes dephosphorylation of the alpha subunit of eukaryotic translation initiation factor 2. *Molecular and cellular biology*, 23(4), pp.1292–1303.

Caldwell, J.E. et al., 1989. Effects of CapZ, an actin capping protein of muscle, on the polymerization of actin. *Biochemistry*, 28(21), pp.8506–8514.

Carmody, L.C. et al., 2004. A protein phosphatase-1gamma1 isoform selectivity determinant in dendritic spine-associated neurabin. *The Journal of biological chemistry*, 279(21), pp.21714–21723.

Casella, J.F. et al., 1987. Cap Z(36/32), a barbed end actin-capping protein, is a component of the Z-line of skeletal muscle. *The Journal of cell biology*, 105(1), pp.371–379.

Ceulemans, H. & Bollen, M., 2004. Functional diversity of protein phosphatase-1, a cellular economizer and reset button. *Physiological reviews*, 84(1), pp.1–39.

Ceulemans, H., Stalmans, W. & Bollen, M., 2002. Regulator-driven functional diversification of protein phosphatase-1 in eukaryotic evolution. *BioEssays : news and reviews in molecular, cellular and developmental biology*, 24(4), pp.371–381.

Ceulemans, H., Vulsteke, V., et al., 2002. Binding of the concave surface of the Sds22 superhelix to the alpha 4/alpha 5/alpha 6-triangle of protein phosphatase-1. *The Journal of biological chemistry*, 277(49), pp.47331–47337.

Chamousset, D., De Wever, V., et al., 2010. RRP1B targets PP1 to mammalian cell nucleoli and is associated with Pre-60S ribosomal subunits. *Molecular biology of the cell*, 21(23), pp.4212–4226.

Chamousset, D., Mamane, S., et al., 2010. Efficient extraction of nucleolar proteins for interactome analyses. *Proteomics*, 10(16), pp.3045–3050.

Chang, W. et al., 2001. Phosphorylation of MAP4 affects microtubule properties and cell cycle progression. *Journal of cell science*, 114(Pt 15), pp.2879–2887.

Cheney, R.E. & Mooseker, M.S., 1992. Unconventional myosins. *Current opinion in cell biology*, 4(1), pp.27–35.

Cheney, R.E., Riley, M.A. & Mooseker, M.S., 1993. Phylogenetic analysis of the myosin superfamily. *Cell motility and the cytoskeleton*, 24(4), pp.215–223.

Choy, M.S. et al., 2015. Structural and Functional Analysis of the GADD34:PP1 eIF2α Phosphatase. *Cell reports*, 11(12), pp.1885–1891.

Ciurciu, A. et al., 2013. PNUTS/PP1 regulates RNAPII-mediated gene expression and is necessary for developmental growth. *PLoS genetics*, 9(10), p.e1003885.

Clark, K. et al., 2007. Myosin II and mechanotransduction: a balancing act. *Trends in cell biology*, 17(4), pp.178–186.

Conti, M.A. & Adelstein, R.S., 2008. Nonmuscle myosin II moves in new directions. *Journal of cell science*, 121(Pt 1), pp.11–18.

Cox, J. et al., 2009. A practical guide to the MaxQuant computational platform for SILAC-based quantitative proteomics. *Nature protocols*, 4(5), pp.698–705.

Cox, J. et al., 2011. Andromeda: a peptide search engine integrated into the MaxQuant environment. *Journal of proteome research*, 10(4), pp.1794–1805.

D'Agostino, L. & Giordano, A., 2011. A novel dual signaling axis for NSP 5a3a induced apoptosis in head and neck carcinoma. *Oncotarget*, 2(12), pp.1055–1074.

D'Agostino, L. & Giordano, A., 2008. Possible functional role of NSPs in cancer. *Cell cycle (Georgetown, Tex.)*, 7(12), pp.1810–1827.

D'Antonio, M. et al., 2013. Resetting translational homeostasis restores myelination in Charcot-Marie-Tooth disease type 1B mice. *The Journal of experimental medicine*, 210(4), pp.821–838.

Das, I. et al., 2015. Preventing proteostasis diseases by selective inhibition of a phosphatase regulatory subunit. *Science (New York, N.Y.)*, 348(6231), pp.239–242.

Davé, A. et al., 2014. Protein phosphatase 1 recruitment by Rif1 regulates DNA replication origin firing by counteracting DDK activity. *Cell reports*, 7(1), pp.53–61.

de Lanerolle, P., Johnson, T. & Hofmann, W.A., 2005. Actin and myosin I in the nucleus: what next? *Nature structural & molecular biology*, 12(9), pp.742–746.

De Wever, V. et al., 2012. Isolation of human mitotic protein phosphatase complexes: identification of a complex between protein phosphatase 1 and the RNA helicase Ddx21. *PloS one*, 7(6), p.e39510.

De Wever, V. et al., 2014. The human mitotic kinesin KIF18A binds protein phosphatase 1 (PP1) through a highly conserved docking motif. *Biochemical and biophysical research communications*, 453(3), pp.432–437.

Deisenroth, C. et al., 2010. Mitochondrial Hep27 is a c-Myb target gene that inhibits Mdm2 and stabilizes p53. *Molecular and cellular biology*, 30(16), pp.3981–3993.

del Rio, A. et al., 2009. Stretching single talin rod molecules activates vinculin binding.

Science (New York, N.Y.), 323(5914), pp.638–641.

Deleyiannis, F.W.-B., TeBockhorst, S. & Castro, D.A., 2013. The financial impact of multidisciplinary cleft care: an analysis of hospital revenue to advance program development. *Plastic and reconstructive surgery*, 131(3), pp.615–622.

DeVaul, N., Wang, R. & Sperry, A.O., 2013. PPP1R42, a PP1 binding protein, regulates centrosome dynamics in ARPE-19 cells. *Biology of the cell*, 105(8), pp.359–371.

Djouder, N. et al., 2007. S6K1-mediated disassembly of mitochondrial URI/PP1gamma complexes activates a negative feedback program that counters S6K1 survival signaling. *Molecular Cell*, 28(1), pp.28–40.

Doherty, M.J. et al., 1995. Amino acid sequence and expression of the hepatic glycogen-binding (GL)-subunit of protein phosphatase-1. *FEBS letters*, 375(3), pp.294–298.

Ebneth, A. et al., 1999. Phosphorylation of MAP2c and MAP4 by MARK kinases leads to the destabilization of microtubules in cells. *Cell motility and the cytoskeleton*, 44(3), pp.209–224.

Egloff, M.P. et al., 1997. Structural basis for the recognition of regulatory subunits by the catalytic subunit of protein phosphatase 1. *The EMBO journal*, 16(8), pp.1876–1887.

Emanuele, M.J. et al., 2008. Aurora B kinase and protein phosphatase 1 have opposing roles in modulating kinetochore assembly. *The Journal of cell biology*, 181(2), pp.241–254.

Endo, S. et al., 1996. Multiple structural elements define the specificity of recombinant human inhibitor-1 as a protein phosphatase-1 inhibitor. *Biochemistry*, 35(16), pp.5220–5228.

Engelhardt, W.A.A.L.M.N., 1939. Myosin and adenosine triphosphatase. *Nature (London)*, 144, pp.668–669.

Esteves, S.L.C. et al., 2013. Protein phosphatase 1γ isoforms linked interactions in the brain. *Journal of molecular neuroscience : MN*, 50(1), pp.179–197.

Etienne-Manneville, S., 2004. Actin and microtubules in cell motility: which one is in control? *Traffic (Copenhagen, Denmark)*, 5(7), pp.470–477.

Etienne-Manneville, S., 2010. From signaling pathways to microtubule dynamics: the key players. *Current opinion in cell biology*, 22(1), pp.104–111.

Etienne-Manneville, S., 2013. Microtubules in cell migration. *Annual review of cell and developmental biology*, 29, pp.471–499.

Eto, M. et al., 2002. Inhibitor-2 regulates protein phosphatase-1 complexed with NimA-related kinase to induce centrosome separation. *The Journal of biological chemistry*,

277(46), pp.44013–44020.

Eto, M. et al., 2007. Phosphorylation-induced conformational switching of CPI-17 produces a potent myosin phosphatase inhibitor. *Structure (London, England : 1993)*, 15(12), pp.1591–1602.

Eto, M., Kirkbride, J.A. & Brautigan, D.L., 2005. Assembly of MYPT1 with protein phosphatase-1 in fibroblasts redirects localization and reorganizes the actin cytoskeleton. *Cell motility and the cytoskeleton*, 62(2), pp.100–109.

Euteneuer, U. & Schliwa, M., 1984. Persistent, directional motility of cells and cytoplasmic fragments in the absence of microtubules. *Nature*, 310(5972), pp.58–61.

Fardilha, M. et al., 2011. Identification of the human testis protein phosphatase 1 interactome. *Biochemical pharmacology*, 82(10), pp.1403–1415.

Fedwick, J.P. et al., 2005. Helicobacter pylori activates myosin light-chain kinase to disrupt claudin-4 and claudin-5 and increase epithelial permeability. *Infection and immunity*, 73(12), pp.7844–7852.

Feng, J. et al., 1999. Inhibitory phosphorylation site for Rho-associated kinase on smooth muscle myosin phosphatase. *The Journal of biological chemistry*, 274(52), pp.37385–37390.

Ferrar, T. et al., 2012. Taperin (c9orf75), a mutated gene in nonsyndromic deafness, encodes a vertebrate specific, nuclear localized protein phosphatase one alpha (PP1α) docking protein. *Biology open*, 1(2), pp.128–139.

Fife, C.M., McCarroll, J.A. & Kavallaris, M., 2014. Movers and shakers: cell cytoskeleton in cancer metastasis. *British journal of pharmacology*, 171(24), pp.5507–5523.

Flores-Delgado, G. et al., 2007. A limited screen for protein interactions reveals new roles for protein phosphatase 1 in cell cycle control and apoptosis. *Journal of proteome research*, 6(3), pp.1165–1175.

Fomproix, N. & Percipalle, P., 2004. An actin-myosin complex on actively transcribing genes. *Experimental cell research*, 294(1), pp.140–148.

Fox, A. et al., 2015. Extracting, enriching, and identifying nuclear body sub-complexes using label-based quantitative mass spectrometry. *Methods in molecular biology (Clifton, N.J.)*, 1262, pp.215–238.

Friedland, J.C., Lee, M.H. & Boettiger, D., 2009. Mechanically activated integrin switch controls alpha5beta1 function. *Science (New York, N.Y.)*, 323(5914), pp.642–644.

Fuhs, S.R. & Hunter, T., 2017. pHisphorylation: the emergence of histidine phosphorylation as a reversible regulatory modification. *Current opinion in cell biology*, 45, pp.8–16.

Fuhs, S.R. et al., 2015. Monoclonal 1- and 3-Phosphohistidine Antibodies: New Tools to Study Histidine Phosphorylation. *Cell*, 162(1), pp.198–210.

Furusawa, T. et al., 2000. Isolation of a novel PDZ-containing myosin from hematopoietic supportive bone marrow stromal cell lines. *Biochemical and biophysical research communications*, 270(1), pp.67–75.

Galliher, A.J. & Schiemann, W.P., 2007. Src phosphorylates Tyr284 in TGF-beta type II receptor and regulates TGF-beta stimulation of p38 MAPK during breast cancer cell proliferation and invasion. *Cancer research*, 67(8), pp.3752–3758.

Galliher-Beckley, A.J. & Schiemann, W.P., 2008. Grb2 binding to Tyr284 in TbetaR-II is essential for mammary tumor growth and metastasis stimulated by TGF-beta. *Carcinogenesis*, 29(2), pp.244–251.

Gardner, M.K. et al., 2008. Microtubule assembly dynamics: new insights at the nanoscale. *Current opinion in cell biology*, 20(1), pp.64–70.

Geiger, B. et al., 1990. The molecular basis for the assembly and modulation of adherens-type junctions. *Cell differentiation and development : the official journal of the International Society of Developmental Biologists*, 32(3), pp.343–353.

Genisca, A.E. et al., 2009. Orofacial clefts in the National Birth Defects Prevention Study, 1997-2004. *American journal of medical genetics. Part A*, 149A(6), pp.1149–1158.

Gfrerer, L. et al., 2014. Functional analysis of SPECC1L in craniofacial development and oblique facial cleft pathogenesis. *Plastic and reconstructive surgery*, 134(4), pp.748–759.

Gimona, M. et al., 2002. Functional plasticity of CH domains. *FEBS letters*, 513(1), pp.98–106.

Goodson, H.V. & Spudich, J.A., 1993. Molecular evolution of the myosin family: relationships derived from comparisons of amino acid sequences. *Proceedings of the National Academy of Sciences of the United States of America*, 90(2), pp.659–663.

Grassie, M.E. et al., 2011. The myosin phosphatase targeting protein (MYPT) family: A regulated mechanism for achieving substrate specificity of the catalytic subunit of protein phosphatase type 1delta. *ARCHIVES OF BIOCHEMISTRY AND BIOPHYSICS*, 510(2), pp.147–159.

Grummt, I., 2006. Actin and myosin as transcription factors. *Current opinion in genetics & development*, 16(2), pp.191–196.

Gunawardena, S.R. et al., 2008. NOM1 targets protein phosphatase I to the nucleolus. *The Journal of biological chemistry*, 283(1), pp.398–404.

Gurney, M.E. et al., 1994. Motor neuron degeneration in mice that express a human

Cu,Zn superoxide dismutase mutation. *Science (New York, N.Y.)*, 264(5166), pp.1772–1775.

Hao, J. et al., 2014. Role of extracellular matrix and YAP/TAZ in cell fate determination. *Cellular signalling*, 26(2), pp.186–191.

Hardy, C.F., Sussel, L. & Shore, D., 1992. A RAP1-interacting protein involved in transcriptional silencing and telomere length regulation. *Genes & development*, 6(5), pp.801–814.

Hartshorne, D.J., Ito, M. & Erdodi, F., 1998. Myosin light chain phosphatase: subunit composition, interactions and regulation. *Journal of muscle research and cell motility*, 19(4), pp.325–341.

Hauri, S. et al., 2013. Interaction proteome of human Hippo signaling: modular control of the co-activator YAP1. *Molecular systems biology*, 9, p.713.

Heath, J.P. & Holifield, B.F., 1991. Cell locomotion: new research tests old ideas on membrane and cytoskeletal flow. *Cell motility and the cytoskeleton*, 18(4), pp.245–257.

Helps, N.R. et al., 2000. NIMA-related kinase 2 (Nek2), a cell-cycle-regulated protein kinase localized to centrosomes, is complexed to protein phosphatase 1. *The Biochemical journal*, 349(Pt 2), pp.509–518.

Hendrickx, A. et al., 2009. Docking motif-guided mapping of the interactome of protein phosphatase-1. *Chemistry & biology*, 16(4), pp.365–371.

Heroes, E. et al., 2013. The PP1 binding code: a molecular-lego strategy that governs specificity. *The FEBS journal*, 280(2), pp.584–595.

Herr, P. et al., 2015. A genome-wide IR-induced RAD51 foci RNAi screen identifies CDC73 involved in chromatin remodeling for DNA repair. *Cell discovery*, 1, p.15034.

Hiraga, S.-I. et al., 2017. Human RIF1 and protein phosphatase 1 stimulate DNA replication origin licensing but suppress origin activation. *EMBO reports*, 18(3), pp.403–419.

Hiraga, S.-I. et al., 2014. Rif1 controls DNA replication by directing Protein Phosphatase 1 to reverse Cdc7-mediated phosphorylation of the MCM complex. *Genes & development*, 28(4), pp.372–383.

Hirano, K., Phan, B.C. & Hartshorne, D.J., 1997. Interactions of the subunits of smooth muscle myosin phosphatase. *The Journal of biological chemistry*, 272(6), pp.3683–3688.

Hirasawa, A. et al., 2003. Association of 17q21-q24 gain in ovarian clear cell adenocarcinomas with poor prognosis and identification of PPM1D and APPBP2 as

likely amplification targets. *Clinical cancer research : an official journal of the American Association for Cancer Research*, 9(6), pp.1995–2004.

Hodge, T. & Cope, M.J., 2000. A myosin family tree. *Journal of cell science*, 113 Pt 19, pp.3353–3354.

Hofmann, W.A. et al., 2006. From transcription to transport: emerging roles for nuclear myosin I. *Biochemistry and cell biology = Biochimie et biologie cellulaire*, 84(4), pp.418–426.

Honjo, Y. et al., 2015. Increased GADD34 in oligodendrocytes in Alzheimer's disease. *Neuroscience letters*, 602, pp.50–55.

Hrabchak, C. & Varmuza, S., 2004. Identification of the spermatogenic zip protein Spz1 as a putative protein phosphatase-1 (PP1) regulatory protein that specifically binds the PP1cgamma2 splice variant in mouse testis. *The Journal of biological chemistry*, 279(35), pp.37079–37086.

Huang, H.-S. et al., 2005. Protein phosphatase-1 inhibitor-3 is co-localized to the nucleoli and centrosomes with PP1gamma1 and PP1alpha, respectively. *ARCHIVES OF BIOCHEMISTRY AND BIOPHYSICS*, 443(1-2), pp.33–44.

Huang, H.B. et al., 1999. Characterization of the inhibition of protein phosphatase-1 by DARPP-32 and inhibitor-2. *The Journal of biological chemistry*, 274(12), pp.7870–7878.

Huet, G. et al., 2013. Actin-regulated feedback loop based on Phactr4, PP1 and cofilin maintains the actin monomer pool. *Journal of cell science*, 126(Pt 2), pp.497–507.

Humphrey, S.J., James, D.E. & Mann, M., 2015. Protein Phosphorylation: A Major Switch Mechanism for Metabolic Regulation. *Trends in endocrinology and metabolism: TEM*, 26(12), pp.676–687.

Ichikawa, K. et al., 1996. Interactions and properties of smooth muscle myosin phosphatase. *Biochemistry*, 35(20), pp.6313–6320.

Ito, M. et al., 2004. Myosin phosphatase: structure, regulation and function. *Molecular and cellular biochemistry*, 259(1-2), pp.197–209.

Jayashankar, V. et al., 2013. Protein phosphatase 1 β paralogs encode the zebrafish myosin phosphatase catalytic subunit. *PloS one*, 8(9), p.e75766.

Jiménez, J. et al., 2017. Polyphosphate: popping up from oblivion. *Current genetics*, 63(1), pp.15–18.

Jin, Q. et al., 2003. The protein phosphatase-1 (PP1) regulator, nuclear inhibitor of PP1 (NIPP1), interacts with the polycomb group protein, embryonic ectoderm development (EED), and functions as a transcriptional repressor. *The Journal of biological*

chemistry, 278(33), pp.30677–30685.

Johnson, D. et al., 1997. Identification of the regions on the M110 subunit of protein phosphatase 1M that interact with the M21 subunit and with myosin. *European journal of biochemistry / FEBS*, 244(3), pp.931–939.

Johnson, D.F. et al., 1996. Identification of protein-phosphatase-1-binding domains on the glycogen and myofibrillar targetting subunits. *European journal of biochemistry / FEBS*, 239(2), pp.317–325.

Joo, E.E. & Yamada, K.M., 2014. MYPT1 regulates contractility and microtubule acetylation to modulate integrin adhesions and matrix assembly. *Nature communications*, 5, p.3510.

Kanaba, T. et al., 2013. Microtubule-binding sites of the CH domain of EB1 and its autoinhibition revealed by NMR. *Biochimica et biophysica acta*, 1834(2), pp.499–507.

Kaneko, K. et al., 2002. Myosin light chain kinase inhibitors can block invasion and adhesion of human pancreatic cancer cell lines. *Pancreas*, 24(1), pp.34–41.

Kao, S.-C. et al., 2007. Identification of phostensin, a PP1 F-actin cytoskeleton targeting subunit. *Biochemical and biophysical research communications*, 356(3), pp.594–598.

Kaverina, I., Rottner, K. & Small, J.V., 1998. Targeting, capture, and stabilization of microtubules at early focal adhesions. *The Journal of cell biology*, 142(1), pp.181–190.

Kelber, J.A. & Klemke, R.L., 2010. PEAK1, a novel kinase target in the fight against cancer. *Oncotarget*, 1(3), pp.219–223.

Keren, K. et al., 2008. Mechanism of shape determination in motile cells. *Nature*, 453(7194), pp.475–480.

Khromov, A. et al., 2009. Phosphorylation-dependent autoinhibition of myosin light chain phosphatase accounts for Ca2+ sensitization force of smooth muscle contraction. *The Journal of biological chemistry*, 284(32), pp.21569–21579.

Kiebler, M.A. et al., 1999. The mammalian staufen protein localizes to the somatodendritic domain of cultured hippocampal neurons: implications for its involvement in mRNA transport. *The Journal of neuroscience : the official journal of the Society for Neuroscience*, 19(1), pp.288–297.

Kill, I.R., 1996. Localisation of the Ki-67 antigen within the nucleolus. Evidence for a fibrillarin-deficient region of the dense fibrillar component. *Journal of cell science*, 109 (Pt 6), pp.1253–1263.

Kim, Y. et al., 2010. Aurora kinases and protein phosphatase 1 mediate chromosome congression through regulation of CENP-E. *Cell*, 142(3), pp.444–455.

Kimura, K. et al., 1996. Regulation of myosin phosphatase by Rho and Rho-associated kinase (Rho-kinase). *Science (New York, N.Y.)*, 273(5272), pp.245–248.

Kislauskis, E.H., Zhu, X. & Singer, R.H., 1997. beta-Actin messenger RNA localization and protein synthesis augment cell motility. *The Journal of cell biology*, 136(6), pp.1263–1270.

Kitazawa, T., Masuo, M. & Somlyo, A.P., 1991. G protein-mediated inhibition of myosin light-chain phosphatase in vascular smooth muscle. *Proceedings of the National Academy of Sciences of the United States of America*, 88(20), pp.9307–9310.

Korrodi-Gregório, L., Esteves, S.L.C. & Fardilha, M., 2014. Protein phosphatase 1 catalytic isoforms: specificity toward interacting proteins. *Translational research : the journal of laboratory and clinical medicine*, 164(5), pp.366–391.

Kozjak-Pavlovic, V., 2017. The MICOS complex of human mitochondria. *Cell and tissue research*, 367(1), pp.83–93.

Krebs, E.G. & Fischer, E.H., 1956. The phosphorylase b to a converting enzyme of rabbit skeletal muscle. *Biochimica et biophysica acta*, 20(1), pp.150–157.

Krebs, E.G., Kent, A.B. & Fischer, E.H., 1958. The muscle phosphorylase b kinase reaction. *The Journal of biological chemistry*, 231(1), pp.73–83.

Kreivi, J.P. et al., 1997. Purification and characterisation of p99, a nuclear modulator of protein phosphatase 1 activity. *FEBS letters*, 420(1), pp.57–62.

Krendel, M. & Mooseker, M.S., 2005. Myosins: tails (and heads) of functional diversity. *Physiology (Bethesda, Md.)*, 20, pp.239–251.

Kruszka, P. et al., 2015. Mutations in SPECC1L, encoding sperm antigen with calponin homology and coiled-coil domains 1-like, are found in some cases of autosomal dominant Opitz G/BBB syndrome. *Journal of medical genetics*, 52(2), pp.104–110.

Krylyshkina, O. et al., 2003. Nanometer targeting of microtubules to focal adhesions. *The Journal of cell biology*, 161(5), pp.853–859.

Kwon, Y.G., Huang, H.B., et al., 1997. Characterization of the interaction between DARPP-32 and protein phosphatase 1 (PP-1): DARPP-32 peptides antagonize the interaction of PP-1 with binding proteins. *Proceedings of the National Academy of Sciences of the United States of America*, 94(8), pp.3536–3541.

Kwon, Y.G., Lee, S.Y., et al., 1997. Cell cycle-dependent phosphorylation of mammalian protein phosphatase 1 by cdc2 kinase. *Proceedings of the National Academy of Sciences of the United States of America*, 94(6), pp.2168–2173.

Kysela, K. et al., 2005. Nuclear distribution of actin and myosin I depends on transcriptional activity of the cell. *Histochemistry and cell biology*, 124(5), pp.347–358.

Landsverk, H.B. et al., 2005. PNUTS enhances in vitro chromosome decondensation in a PP1-dependent manner. *The Biochemical journal*, 390(Pt 3), pp.709–717.

Langton, P.F. et al., 2009. The dASPP-dRASSF8 complex regulates cell-cell adhesion during Drosophila retinal morphogenesis. *Current biology : CB*, 19(23), pp.1969–1978.

Lee, J.-H. et al., 2010. Identification and characterization of a novel human PP1 phosphatase complex. *The Journal of biological chemistry*, 285(32), pp.24466–24476.

Lesage, B. et al., 2007. A complex of catalytically inactive protein phosphatase-1 sandwiched between Sds22 and inhibitor-3. *Biochemistry*, 46(31), pp.8909–8919.

Lesage, B. et al., 2005. Determinants of the nucleolar targeting of protein phosphatase-1. *FEBS letters*, 579(25), pp.5626–5630.

Lesage, B. et al., 2004. Interactor-mediated nuclear translocation and retention of protein phosphatase-1. *The Journal of biological chemistry*, 279(53), pp.55978–55984.

Liao, G., Nagasaki, T. & Gundersen, G.G., 1995. Low concentrations of nocodazole interfere with fibroblast locomotion without significantly affecting microtubule level: implications for the role of dynamic microtubules in cell locomotion. *Journal of cell science*, 108 (Pt 11), pp.3473–3483.

Liu, Y. et al., 2016. Physiological functions and clinical implications of the N-end rule pathway. *Frontiers of medicine*, 10(3), pp.258–270.

Llanos, S. et al., 2011. Inhibitory member of the apoptosis-stimulating proteins of the p53 family (iASPP) interacts with protein phosphatase 1 via a noncanonical binding motif. *The Journal of biological chemistry*, 286(50), pp.43039–43044.

Lundberg, E. et al., 2010. Defining the transcriptome and proteome in three functionally different human cell lines. *Molecular systems biology*, 6, p.450.

Lv, X.-B. et al., 2015. PARD3 induces TAZ activation and cell growth by promoting LATS1 and PP1 interaction. *EMBO reports*, 16(8), pp.975–985.

MacCallum, D.E. & Hall, P.A., 2000. The location of pKi67 in the outer dense fibrillary compartment of the nucleolus points to a role in ribosome biogenesis during the cell division cycle. *The Journal of pathology*, 190(5), pp.537–544.

Macdonald, J.A. et al., 2001. Identification of the endogenous smooth muscle myosin phosphatase-associated kinase. *Proceedings of the National Academy of Sciences of the United States of America*, 98(5), pp.2419–2424.

Mahrour, N. et al., 2008. Characterization of Cullin-box sequences that direct recruitment of Cul2-Rbx1 and Cul5-Rbx2 modules to Elongin BC-based ubiquitin ligases. *The*

Journal of biological chemistry, 283(12), pp.8005–8013.

Manning, G. et al., 2002. The protein kinase complement of the human genome. *Science (New York, N.Y.)*, 298(5600), pp.1912–1934.

Marión, R.M. et al., 1999. A human sequence homologue of Staufen is an RNA-binding protein that is associated with polysomes and localizes to the rough endoplasmic reticulum. *Molecular and cellular biology*, 19(3), pp.2212–2219.

Matsumura, F. & Hartshorne, D.J., 2008. Myosin phosphatase target subunit: Many roles in cell function. *Biochemical and biophysical research communications*, 369(1), pp.149–156.

Mattarocci, S. et al., 2014. Rif1 controls DNA replication timing in yeast through the PP1 phosphatase Glc7. *Cell reports*, 7(1), pp.62–69.

Mattison, C.P. et al., 2011. Mip1 associates with both the Mps1 kinase and actin, and is required for cell cortex stability and anaphase spindle positioning. *Cell cycle (Georgetown, Tex.)*, 10(5), pp.783–793.

Meraldi, P. & Nigg, E.A., 2001. Centrosome cohesion is regulated by a balance of kinase and phosphatase activities. *Journal of cell science*, 114(Pt 20), pp.3749–3757.

Mi, J. et al., 2007. Protein phosphatase-1alpha regulates centrosome splitting through Nek2. *Cancer research*, 67(3), pp.1082–1089.

Monni, O. et al., 2001. Comprehensive copy number and gene expression profiling of the 17q23 amplicon in human breast cancer. *Proceedings of the National Academy of Sciences of the United States of America*, 98(10), pp.5711–5716.

Moorhead, G.B. et al., 2008. Displacement affinity chromatography of protein phosphatase one (PP1) complexes. *BMC biochemistry*, 9, p.28.

Moorhead, G.B.G., Trinkle-Mulcahy, L. & Ulke-Lemée, A., 2007. Emerging roles of nuclear protein phosphatases. *Nature reviews. Molecular cell biology*, 8(3), pp.234–244.

Morrison, D.K., Murakami, M.S. & Cleghon, V., 2000. Protein kinases and phosphatases in the Drosophila genome. *The Journal of cell biology*, 150(2), pp.F57–62.

Muramatsu, M. & Onishi, T., 1978. Isolation and purification of nucleoli and nucleolar chromatin from mammalian cells. *Methods in cell biology*, 17, pp.141–161.

Muranyi, A. et al., 2005. Phosphorylation of Thr695 and Thr850 on the myosin phosphatase target subunit: inhibitory effects and occurrence in A7r5 cells. *FEBS letters*, 579(29), pp.6611–6615.

Nagaraj, N. et al., 2011. Deep proteome and transcriptome mapping of a human cancer

cell line. *Molecular systems biology*, 7, p.548.

Nasa, I. et al., 2017. Recruitment of PP1 to the centrosomal scaffold protein CEP192. *Biochemical and biophysical research communications*, 484(4), pp.864–870.

Nemethova, M., Auinger, S. & Small, J.V., 2008. Building the actin cytoskeleton: filopodia contribute to the construction of contractile bundles in the lamella. *The Journal of cell biology*, 180(6), pp.1233–1244.

Nordlund, A. & Oliveberg, M., 2008. SOD1-associated ALS: a promising system for elucidating the origin of protein-misfolding disease. *HFSP journal*, 2(6), pp.354–364.

Novoa, I. et al., 2001. Feedback inhibition of the unfolded protein response by GADD34-mediated dephosphorylation of eIF2alpha. *The Journal of cell biology*, 153(5), pp.1011–1022.

Nuytten, M. et al., 2008. The transcriptional repressor NIPP1 is an essential player in EZH2-mediated gene silencing. *Oncogene*, 27(10), pp.1449–1460.

Okada, T. et al., 2004. Analysis of isoform specific function of PP1 catalytic subunits in mammalian cells using siRNA. *International journal of oncology*, 25(5), pp.1383–1388.

Okamoto, R. et al., 2005. The targeted disruption of the MYPT1 gene results in embryonic lethality. *Transgenic research*, 14(3), pp.337–340.

Okumura, F. et al., 2012. The Role of Elongin BC-Containing Ubiquitin Ligases. *Frontiers in oncology*, 2, p.10.

Oliver, C.J. et al., 2002. Targeting protein phosphatase 1 (PP1) to the actin cytoskeleton: the neurabin I/PP1 complex regulates cell morphology. *Molecular and cellular biology*, 22(13), pp.4690–4701.

Olivier, N. et al., 2013. Simple buffers for 3D STORM microscopy. *Biomedical optics express*, 4(6), pp.885–899.

Olsen, J.V. et al., 2006. Global, in vivo, and site-specific phosphorylation dynamics in signaling networks. *Cell*, 127(3), pp.635–648.

Peng, A. et al., 2010. Repo-man controls a protein phosphatase 1-dependent threshold for DNA damage checkpoint activation. *Current biology : CB*, 20(5), pp.387–396.

Pennuto, M. et al., 2008. Ablation of the UPR-mediator CHOP restores motor function and reduces demyelination in Charcot-Marie-Tooth 1B mice. *Neuron*, 57(3), pp.393–405.

Percipalle, P. & Visa, N., 2006. Molecular functions of nuclear actin in transcription. *The Journal of cell biology*, 172(7), pp.967–971.

Pestic-Dragovich, L. et al., 2000. A myosin I isoform in the nucleus. *Science (New York, N.Y.)*, 290(5490), pp.337–341.

Peti, W., Nairn, A.C. & Page, R., 2013. Structural basis for protein phosphatase 1 regulation and specificity. *The FEBS journal*, 280(2), pp.596–611.

Petronczki, M., Lénárt, P. & Peters, J.-M., 2008. Polo on the Rise-from Mitotic Entry to Cytokinesis with Plk1. *Developmental cell*, 14(5), pp.646–659.

Pidgeon, T.E. et al., 2014. From birth to maturity: midline tessier 0-14 craniofacial cleft patients who have completed protocol management at a single craniofacial unit. *The Cleft palate-craniofacial journal : official publication of the American Cleft Palate-Craniofacial Association*, 51(4), pp.e70–9.

Piekny, A.J. et al., 2003. The Caenorhabditis elegans nonmuscle myosin genes nmy-1 and nmy-2 function as redundant components of the let-502/Rho-binding kinase and mel-11/myosin phosphatase pathway during embryonic morphogenesis. *Development (Cambridge, England)*, 130(23), pp.5695–5704.

Ponti, A. et al., 2004. Two distinct actin networks drive the protrusion of migrating cells. *Science (New York, N.Y.)*, 305(5691), pp.1782–1786.

Poser, I. et al., 2008. BAC TransgeneOmics: a high-throughput method for exploration of protein function in mammals. *Nature methods*, 5(5), pp.409–415.

Prevost, M. et al., 2013. Quantitative fragmentome mapping reveals novel, domain-specific partners for the modular protein RepoMan. *Molecular & cellular proteomics : MCP*.

Ren, X.D., Kiosses, W.B. & Schwartz, M.A., 1999. Regulation of the small GTP-binding protein Rho by cell adhesion and the cytoskeleton. *The EMBO journal*, 18(3), pp.578–585.

Roadcap, D.W., Brush, M.H. & Shenolikar, S., 2007. Identification of cellular protein phosphatase-1 regulators. *Methods in molecular biology (Clifton, N.J.)*, 365, pp.181–196.

Rodrigues, N.T.L. et al., 2015. Kinetochore-localized PP1-Sds22 couples chromosome segregation to polar relaxation. *Nature*, 524(7566), pp.489–492.

Rooney, C. et al., 2010. The Rac activator STEF (Tiam2) regulates cell migration by microtubule-mediated focal adhesion disassembly. *EMBO reports*, 11(4), pp.292–298.

Rosenberg, J.S., Cross, F.R. & Funabiki, H., 2011. KNL1/Spc105 recruits PP1 to silence the spindle assembly checkpoint. *Current biology : CB*, 21(11), pp.942–947.

Rothbauer, U. et al., 2008. A versatile nanotrap for biochemical and functional studies

with fluorescent fusion proteins. *Molecular & cellular proteomics : MCP*, 7(2), pp.282–289.

Saadi, I. et al., 2011. Deficiency of the cytoskeletal protein SPECC1L leads to oblique facial clefting. *American journal of human genetics*, 89(1), pp.44–55.

Sasaki, K. et al., 1990. Identification of members of the protein phosphatase 1 gene family in the rat and enhanced expression of protein phosphatase 1 alpha gene in rat hepatocellular carcinomas. *Jpn J Cancer Res*, 81(12), pp.1272–1280.

Sawada, Y. et al., 2006. Force sensing by mechanical extension of the Src family kinase substrate p130Cas. *Cell*, 127(5), pp.1015–1026.

Schmidt, A. & Hall, M.N., 1998. Signaling to the actin cytoskeleton. *Annual review of cell and developmental biology*, 14, pp.305–338.

Schröder, M. & Kaufman, R.J., 2005. The mammalian unfolded protein response. *Annual review of biochemistry*, 74, pp.739–789.

Scotto-Lavino, E. et al., 2010. Basis for the isoform-specific interaction of myosin phosphatase subunits protein phosphatase 1c beta and myosin phosphatase targeting subunit 1. *The Journal of biological chemistry*, 285(9), pp.6419–6424.

Sedgwick, S.G. & Smerdon, S.J., 1999. The ankyrin repeat: a diversity of interactions on a common structural framework. *Trends in biochemical sciences*, 24(8), pp.311–316.

Seet, L.F. & Hong, W., 2001. Endofin, an endosomal FYVE domain protein. *The Journal of biological chemistry*, 276(45), pp.42445–42454.

Sellers, J.R., 1999. Unphosphorylated crossbridges and latch: smooth muscle regulation revisited. *Journal of muscle research and cell motility*, 20(4), pp.347–349.

Sellers, J.R., Eisenberg, E. & Adelstein, R.S., 1982. The binding of smooth muscle heavy meromyosin to actin in the presence of ATP. Effect of phosphorylation. *The Journal of biological chemistry*, 257(23), pp.13880–13883.

Shenolikar, S., 1994. Protein serine/threonine phosphatases--new avenues for cell regulation. *Annual review of cell biology*, 10, pp.55–86.

Shi, W. et al., 2007. Endofin acts as a Smad anchor for receptor activation in BMP signaling. *Journal of cell science*, 120(Pt 7), pp.1216–1224.

Shimizu, H. et al., 1994. Characterization of the myosin-binding subunit of smooth muscle myosin phosphatase. *The Journal of biological chemistry*, 269(48), pp.30407–30411.

Shirazi, A. et al., 1994. Purification and characterization of the mammalian myosin light chain phosphatase holoenzyme. The differential effects of the holoenzyme and its subunits on smooth muscle. *The Journal of biological chemistry*, 269(50), pp.31598–

31606.

Sipos, A. et al., 2017. Myosin phosphatase and RhoA-activated kinase modulate arginine methylation by the regulation of protein arginine methyltransferase 5 in hepatocellular carcinoma cells. *Scientific reports*, 7, p.40590.

Somlyo, A.P. & Somlyo, A.V., 2003. Ca2+ sensitivity of smooth muscle and nonmuscle myosin II: modulated by G proteins, kinases, and myosin phosphatase. *Physiological reviews*, 83(4), pp.1325–1358.

Stossel, T.P., 1993. On the crawling of animal cells. *Science (New York, N.Y.)*, 260(5111), pp.1086–1094.

Strnadel, J. et al., 2017. eIF5A-PEAK1 Signaling Regulates YAP1/TAZ Protein Expression and Pancreatic Cancer Cell Growth. *Cancer research*, 77(8), pp.1997–2007.

Surks, H.K. et al., 1999. Regulation of myosin phosphatase by a specific interaction with cGMP- dependent protein kinase Ialpha. *Science (New York, N.Y.)*, 286(5444), pp.1583–1587.

Sutherland, E.W. & Wosilait, W.D., 1955. Inactivation and activation of liver phosphorylase. *Nature*, 175(4447), pp.169–170.

Szklarczyk, D. et al., 2015. STRING v10: protein-protein interaction networks, integrated over the tree of life. *Nucleic acids research*, 43(Database issue), pp.D447–52.

Tan, I. et al., 2001. Phosphorylation of a novel myosin binding subunit of protein phosphatase 1 reveals a conserved mechanism in the regulation of actin cytoskeleton. *The Journal of biological chemistry*, 276(24), pp.21209–21216.

Tanaka, J. et al., 1998. Interaction of myosin phosphatase target subunit 1 with the catalytic subunit of type 1 protein phosphatase. *Biochemistry*, 37(47), pp.16697–16703.

Taylor, M.P., Koyuncu, O.O. & Enquist, L.W., 2011. Subversion of the actin cytoskeleton during viral infection. *Nature reviews. Microbiology*, 9(6), pp.427–439.

Terrak, M. et al., 2004. Structural basis of protein phosphatase 1 regulation. *Nature*, 429(6993), pp.780–784.

Terry-Lorenzo, R.T. et al., 2002. Neurabins recruit protein phosphatase-1 and inhibitor-2 to the actin cytoskeleton. *The Journal of biological chemistry*, 277(48), pp.46535–46543.

Thompson, R.F. & Langford, G.M., 2002. Myosin superfamily evolutionary history. *The Anatomical record*, 268(3), pp.276–289.

Thusberg, J. & Vihinen, M., 2009. Pathogenic or not? And if so, then how? Studying the effects of missense mutations using bioinformatics methods. *Human mutation*, 30(5), pp.703–714.

Tolarová, M.M. & Cervenka, J., 1998. Classification and birth prevalence of orofacial clefts. *American journal of medical genetics*, 75(2), pp.126–137.

Trinkle-Mulcahy, L. & Lamond, A.I., 2006. Mitotic phosphatases: no longer silent partners. *Current opinion in cell biology*, 18(6), pp.623–631.

Trinkle-Mulcahy, L. et al., 2008. Identifying specific protein interaction partners using quantitative mass spectrometry and bead proteomes. *The Journal of cell biology*, 183(2), pp.223–239.

Trinkle-Mulcahy, L. et al., 1999. Nuclear organisation of NIPP1, a regulatory subunit of protein phosphatase 1 that associates with pre-mRNA splicing factors. *Journal of cell science*, 112 (Pt 2), pp.157–168.

Trinkle-Mulcahy, L. et al., 2006. Repo-Man recruits PP1 gamma to chromatin and is essential for cell viability. *The Journal of cell biology*, 172(5), pp.679–692.

Trinkle-Mulcahy, L. et al., 2003. Time-lapse imaging reveals dynamic relocalization of PP1gamma throughout the mammalian cell cycle. *Molecular biology of the cell*, 14(1), pp.107–117.

Trinkle-Mulcahy, L., Sleeman, J.E. & Lamond, A.I., 2001. Dynamic targeting of protein phosphatase 1 within the nuclei of living mammalian cells. *Journal of cell science*, 114(Pt 23), pp.4219–4228.

Trinkle-Mulcahy, L.C.J.L.Y.W.S.S.A.L.A.I., 2006. *Visualization of intracellular PP1 targeting through transiently and stably expressed fluorescent protein fusions*, Protein Phosphatase Protocols, Ed. G. Moorhead, Humana Press.

Tsukazaki, T. et al., 1998. SARA, a FYVE domain protein that recruits Smad2 to the TGFbeta receptor. *Cell*, 95(6), pp.779–791.

Ulke-Lemée, A. & Macdonald, J.A., 2010. Opportunities to Target Specific Contractile Abnormalities with Smooth Muscle Protein Kinase Inhibitors. *Pharmaceuticals*, 3(6), pp.1739–1760.

Ulke-Lemée, A. et al., 2007. The nuclear PP1 interacting protein ZAP3 (ZAP) is a putative nucleoside kinase that complexes with SAM68, CIA, NF110/45, and HNRNP-G. *Biochimica et biophysica acta*, 1774(10), pp.1339–1350.

Umemoto, S., Bengur, A.R. & Sellers, J.R., 1989. Effect of multiple phosphorylations of smooth muscle and cytoplasmic myosins on movement in an in vitro motility assay. *The Journal of biological chemistry*, 264(3), pp.1431–1436.

Vagnarelli, P. et al., 2006. Condensin and Repo-Man-PP1 co-operate in the regulation of chromosome architecture during mitosis. *Nature cell biology*, 8(10), pp.1133–1142.

Van Dessel, N. et al., 2010. The phosphatase interactor NIPP1 regulates the occupancy of the histone methyltransferase EZH2 at Polycomb targets. *Nucleic acids research*, 38(21), pp.7500–7512.

Van Eynde, A. et al., 2004. The nuclear scaffold protein NIPP1 is essential for early embryonic development and cell proliferation. *Molecular and cellular biology*, 24(13), pp.5863–5874.

Varmuza, S. et al., 1999. Spermiogenesis is impaired in mice bearing a targeted mutation in the protein phosphatase 1cgamma gene. *Developmental biology*, 205(1), pp.98–110.

Vasiliev, J.M. et al., 1970. Effect of colcemid on the locomotory behaviour of fibroblasts. *Journal of embryology and experimental morphology*, 24(3), pp.625–640.

Velasco, G. et al., 2002. Phosphorylation of the regulatory subunit of smooth muscle protein phosphatase 1M at Thr850 induces its dissociation from myosin. *FEBS letters*, 527(1-3), pp.101–104.

Venerando, A., Cesaro, L. & Pinna, L.A., 2017. From phosphoproteins to phosphoproteomes: a historical account. *The FEBS journal*.

Versnel, S.L. et al., 2011. Long-term results after 40 years experience with treatment of rare facial clefts: Part 1--Oblique and paramedian clefts. *Journal of plastic, reconstructive & aesthetic surgery : JPRAS*, 64(10), pp.1334–1343.

Vicente-Manzanares, M. et al., 2009. Non-muscle myosin II takes centre stage in cell adhesion and migration. *Nature reviews. Molecular cell biology*, 10(11), pp.778–790.

Vinogradova, T., Miller, P.M. & Kaverina, I., 2009. Microtubule network asymmetry in motile cells: role of Golgi-derived array. *Cell cycle (Georgetown, Tex.)*, 8(14), pp.2168–2174.

Virshup, D.M. & Shenolikar, S., 2009. From promiscuity to precision: protein phosphatases get a makeover. *Molecular Cell*, 33(5), pp.537–545.

Vreugde, S. et al., 2006. Nuclear myosin VI enhances RNA polymerase II-dependent transcription. *Molecular Cell*, 23(5), pp.749–755.

Wakula, P. et al., 2003. Degeneracy and function of the ubiquitous RVXF motif that mediates binding to protein phosphatase-1. *The Journal of biological chemistry*, 278(21), pp.18817–18823.

Walter, P. & Ron, D., 2011. The unfolded protein response: from stress pathway to homeostatic regulation. *Science (New York, N.Y.)*, 334(6059), pp.1081–1086.

Wang, E.S. et al., 2010. Tetranectin and apolipoprotein A-I in cerebrospinal fluid as potential biomarkers for Parkinson's disease. *Acta neurologica Scandinavica*, 122(5), pp.350–359.

Wang, H. & Brautigan, D.L., 2002. A novel transmembrane Ser/Thr kinase complexes with protein phosphatase-1 and inhibitor-2. *The Journal of biological chemistry*, 277(51), pp.49605–49612.

Wang, Y. et al., 2010. Pseudopodium-enriched atypical kinase 1 regulates the cytoskeleton and cancer progression [corrected]. *Proceedings of the National Academy of Sciences of the United States of America*, 107(24), pp.10920–10925.

Waterman-Storer, C.M. & Salmon, E., 1999. Positive feedback interactions between microtubule and actin dynamics during cell motility. *Current opinion in cell biology*, 11(1), pp.61–67.

Webb, D.J., Brown, C.M. & Horwitz, A.F., 2003. Illuminating adhesion complexes in migrating cells: moving toward a bright future. *Current opinion in cell biology*, 15(5), pp.614–620.

Weiser, D.C., Row, R.H. & Kimelman, D., 2009. Rho-regulated myosin phosphatase establishes the level of protrusive activity required for cell movements during zebrafish gastrulation. *Development (Cambridge, England)*, 136(14), pp.2375–2384.

Westendorf, J.M. et al., 1998. M phase phosphoprotein 10 is a human U3 small nucleolar ribonucleoprotein component. *Molecular biology of the cell*, 9(2), pp.437–449.

Wickham, L. et al., 1999. Mammalian staufen is a double-stranded-RNA- and tubulin-binding protein which localizes to the rough endoplasmic reticulum. *Molecular and cellular biology*, 19(3), pp.2220–2230.

Wilson, N.R. et al., 2016. SPECC1L deficiency results in increased adherens junction stability and reduced cranial neural crest cell delamination. *Scientific reports*, 6, p.17735.

Winsor, B. & Schiebel, E., 1997. Review: an overview of the Saccharomyces cerevisiae microtubule and microfilament cytoskeleton. *Yeast (Chichester, England)*, 13(5), pp.399–434.

Wu, J. et al., 2016. The Fra-1-miR-134-SDS22 feedback loop amplifies ERK/JNK signaling and reduces chemosensitivity in ovarian cancer cells. *Cell death & disease*, 7(9), p.e2384.

Wu, J.Q. et al., 2009. PP1-mediated dephosphorylation of phosphoproteins at mitotic exit is controlled by inhibitor-1 and PP1 phosphorylation. *Nature cell biology*, 11(5), pp.644–651.

Wu, Y. et al., 2005. Localization of myosin phosphatase target subunit and its mutants.

Journal of muscle research and cell motility, 26(2-3), pp.123–134.

Xia, D., Stull, J.T. & Kamm, K.E., 2005. Myosin phosphatase targeting subunit 1 affects cell migration by regulating myosin phosphorylation and actin assembly. *Experimental cell research*, 304(2), pp.506–517.

Yamada, K.M. & Geiger, B., 1997. Molecular interactions in cell adhesion complexes. *Current opinion in cell biology*, 9(1), pp.76–85.

Yamashiro, S. et al., 2008. Myosin phosphatase-targeting subunit 1 regulates mitosis by antagonizing polo-like kinase 1. *Developmental cell*, 14(5), pp.787–797.

Yui, J., Chiu, C.P. & Lansdorp, P.M., 1998. Telomerase activity in candidate stem cells from fetal liver and adult bone marrow. *Blood*, 91(9), pp.3255–3262.

Zhang, Y. et al., 1998. A new logic for DNA engineering using recombination in Escherichia coli. *Nature genetics*, 20(2), pp.123–128.

Zhang, Y. et al., 2004. ARA67/PAT1 functions as a repressor to suppress androgen receptor transactivation. *Molecular and cellular biology*, 24(3), pp.1044–1057.

Zhang, Y. et al., 2015. The tumor suppressor proteins ASPP1 and ASPP2 interact with C-Nap1 and regulate centrosome linker reassembly. *Biochemical and biophysical research communications*, 458(3), pp.494–500.

Zheng, P. et al., 1998. PAT1, a microtubule-interacting protein, recognizes the basolateral sorting signal of amyloid precursor protein. *Proceedings of the National Academy of Sciences of the United States of America*, 95(25), pp.14745–14750.

Zitouni, S. et al., 2014. Polo-like kinases: structural variations lead to multiple functions. *Nature reviews. Molecular cell biology*, 15(7), pp.433–452.